National Library of Canada

Bibliothèque nationale du Canada

Acquisitions and Bibliographic Services Branch

Direction des acquisitions et des services bibliographiques

395 Wellington Street
Ottawa, Ontario
K1A 0N4

395, rue Wellington
Ottawa (Ontario)
K1A 0N4

NOTICE

The quality of this microform is heavily dependent upon the quality of the original thesis submitted for microfilming. Every effort has been made to ensure the highest quality of reproduction possible.

If pages are missing, contact the university which granted the degree.

Some pages may have indistinct print especially if the original pages were typed with a poor typewriter ribbon or if the university sent us an inferior photocopy.

Reproduction in full or in part of this microform is governed by the Canadian Copyright Act, R.S.C. 1970, c. C-30, and subsequent amendments.

AVIS

La qualité de cette microforme dépend grandement de la qualité de la thèse soumise au microfilmage. Nous avons tout fait pour assurer une qualité supérieure de reproduction.

S'il manque des pages, veuillez communiquer avec l'université qui a conféré le grade.

La qualité d'impression de certaines pages peut laisser à désirer, surtout si les pages originales ont été dactylographiées à l'aide d'un ruban usé ou si l'université nous a fait parvenir une photocopie de qualité inférieure.

La reproduction, même partielle, de cette microforme est soumise à la Loi canadienne sur le droit d'auteur, SRC 1970, c. C-30, et ses amendements subséquents.

Canada

UNIVERSITY OF ALBERTA

A KINETIC MODEL FOR SILICIDE FORMATION THROUGH SOLID STATE REACTIONS IN METAL-SILICON DIFFUSION CO[illegible]ES

By

Lin Zhang

A thesis submitted to the Faculty of Graduate Studies and Research in partial fulfillment of the requirements for the degree of **DOCTOR OF PHILOSOPHY**

IN

METALLURGICAL ENGINEERING

DEPARTMENT OF **MINING, METALLURGICAL AND PETROLEUM ENGINEERING**

EDMONTON, ALBERTA

FALL 1993

National Library of Canada

Acquisitions and Bibliographic Services Branch

395 Wellington Street
Ottawa, Ontario
K1A 0N4

Bibliothèque nationale du Canada

Direction des acquisitions et des services bibliographiques

395, rue Wellington
Ottawa (Ontario)
K1A 0N4

Your file Votre référence

Our file Notre référence

The author has granted an irrevocable non-exclusive licence allowing the National Library of Canada to reproduce, loan, distribute or sell copies of his/her thesis by any means and in any form or format, making this thesis available to interested persons.

L'auteur a accordé une licence irrévocable et non exclusive permettant à la Bibliothèque nationale du Canada de reproduire, prêter, distribuer ou vendre des copies de sa thèse de quelque manière et sous quelque forme que ce soit pour mettre des exemplaires de cette thèse à la disposition des personnes intéressées.

The author retains ownership of the copyright in his/her thesis. Neither the thesis nor substantial extracts from it may be printed or otherwise reproduced without his/her permission.

L'auteur conserve la propriété du droit d'auteur qui protège sa thèse. Ni la thèse ni des extraits substantiels de celle-ci ne doivent être imprimés ou autrement reproduits sans son autorisation.

ISBN 0-315-88061-9

Canada

UNIVERSITY OF ALBERTA

RELEASE FORM

NAME OF AUTHOR: **Lin Zhang**

TITLE OF THESIS: **A Kinetic Model for Silicide Formation through Solid State Reactions in Metal-Si Diffusion Couples**

DEGREE: **Doctor of Philosophy**

YEAR THIS DEGREE GRANTED: **Fall 1993**

Permission is hereby granted to the University of Alberta Library to reproduce single copies of this thesis, and to lend or sell such copies for private, scholarly or scientific research purposes only.

The author reserves all other publication and other rights in association with the copyright in the thesis, and except as hereinbefore provided neither the thesis nor any substantial portion thereof may be printed or otherwise reproduced in any material form whatever without the author's prior written permission.

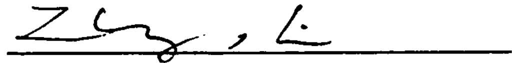

c/o. Mr. Jian Xin
Building 5-2-403, Tuanjiehu Beitoutiao
Beijing, P.R.China

Date: Oct. 1, 1993

UNIVERSITY OF ALBERTA

FACULTY OF GRADUATE STUDIES AND RESEARCH

The undersigned certify that they have read, and recommend to the Faculty of Graduate Studies and Research for acceptance, a thesis entitled **A KINETIC MODEL FOR SILICIDE FORMATION THROUGH SOLID STATE REACTIONS IN METAL-SILICON DIFFUSION COUPLES** submitted by **LIN ZHANG** in partial fulfillment of the requirements for the degree of **DOCTOR OF PHILOSOPHY** in **METALLURGICAL ENGINEERING.**

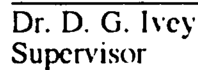

Dr. D. G. Ivey
Supervisor

Dr. M. L. Wayman

Dr. S. A. Bradford

Dr. M. J. Brett

Dr. Y. A. Chang

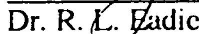

Dr. R. L. Eadie

DATE: Oct. 1, 1993

ABSTRACT

In this study, a kinetic model for silicide formation through solid state reactions in transition metal-Si diffusion couples has been developed The reactive interface in a metal-silicon couple is considered to be a reaction region, and the reaction process is divided into three steps. Several physical quantities have been defined to describe each of these steps, i.e., the diffusion flux of moving reactant to the reaction region (J), the release rate of nonmoving reactant (r) and the formation rate of the growing phase (F). The relationship between these quantities in a given reaction region has been demonstrated by means of a reaction process plot (RPP), which is also developed in this study.

Expressions for free energy degradation rate (FEDR) in a reaction region are derived. It is shown, by using the expressions and an RPP, that in a given reaction region there are always a number of possible reaction processes competing with one another. One of these processes can result in the largest FEDR. Based on this result, a criterion for solid state reactions in metal-Si diffusion couples is proposed, i.e., of all possible reaction processes, the reaction which can result in the largest FEDR will actually occur.

According to the kinetic model and the reaction criterion, the stepped curve in the RPP for a reaction region adjacent to an elemental nonmoving reactant represents the actual reaction path of the release process in the region. Therefore, the silicide formation sequence in the region is predictable if the stepped curve or the RPP for the region is available. A method for calculating relative maximum release (RMR) rates and constructing semiquantitative RPPs (SRPPs) has been proposed. Using this method, calculations of RMR rates have been done for 15 metal-Si systems and a few typical SRPPs have been drawn using the resulting data. Predictions of first silicide formation and multiple phase growth sequence have been done using the SRPPs for these systems. Comparison of the predictions with the experimental results from the literature shows very good agreement, which provides strong support for the kinetic model and the reaction criterion.

Multiple phase sequential growth in thin film Ni-Si couples has been investigated by means of transmission electron microscopy (TEM), energy dispersive x-ray spectroscopy (EDS) and electron diffraction. The observed growth sequence is Ni_2Si and then NiSi. Experimental results from a previous study using thin film Mn-Si couples are also given, which indicates a formation sequence of Mn_3Si followed by MnSi. The results in the two systems provide experimental evidence for the predictions of silicide formation sequences in these systems.

Direct deposition reactions of Ni on Si substrates have also been investigated using TEM, EDX and electron diffraction. The observed silicide formation sequence is $NiSi_2$,

Ni_2Si, then NiSi and Ni-rich solid solution layers. Most of the observed phenomena in this study can be explained by SRPPs and the new kinetic model, which provides additional support for the new model.

ACKNOWLEDGEMENTS

I am deeply grateful to Dr. D. G. Ivey for his supervision, guidance, and encouragement extended throughout the course of this study. Many thanks are also due to Dr. M. L. Wayman and Dr. S. A. Bradford for their valuable comments on Chapter 3. I am also indebted to Dr. M. J. Brett for his advice on the direct deposition reaction experiments.

I am greatly appreciative to the Alberta Microelectronic Center (AMC) for their financial support, and for providing access to their excellent facilities. I would like to acknowledge the staff of AMC, Mr. Graham McKinnon, Mr. Alan Mitchell, Mr. Mike Konevecki, Mr. Yan Loke, Mr. Glen Fitzpatrick and Mr. Doug Bowles, for their invaluable assistance during the specimen preparation (thin film deposition).

I wish to thank Dr. R. F. Egerton, Dr. M. H. Chen, and Mr. J. Malinski who provided access to TEMs. I also acknowledge Ms. Tina Barker, Mr. John Czuroski, Mr. Shiraz Merali and Mr. Bob Konzuk for their help in obtaining supplies.

I am also grateful to the Natural Sciences and Engineering Research Council of Canada for financial assistance.

Finally, I would like to thank my wife, Ms. Ping Jian, for her selfless support and encouragement, as well as assistance in typing the thesis and generating the figures.

TABLE OF CONTENTS

CHAPTER PAGE

1. Introduction 1
2. Literature Review 4
   2.1. Single Phase Growth and Multiple Phase Growth 4
   2.2. Silicide Formation Sequence 7
      2.2.1. Experimental Observations of Silicide Formation Sequences 7
      2.2.2. Prediction of Single Phase Formation Sequences 8
      2.2.3. Explanation of SSA and Amorphous Phase Critical Thickness 11
      2.2.4. Prediction of Multiple Phase Growth Sequence 13
   2.3. Solid State Amorphization 13
   2.4. Direct Deposition Reactions 16
   2.5. Factors Influencing Reaction Kinetics 19
      2.5.1. Diffusion in Thin Film Couples 19
      2.5.2. Impurity Effects 22
      2.5.3. Crystal Structure and Orientation of Substrates 23
   2.6. Theories and Models for Silicide Formation 25
      2.6.1. Silicide Growth Kinetics 25
         2.6.1.1. Diffusion Controlled and Interface Reaction Controlled Processes ... 26
         2.6.1.2. Nucleation Controlled Processes 28
      2.6.2. Kinetic Models for Silicide Formation 30
         2.6.2.1. Kinetics of Layered Growth in Bulk Couples - Kidson Approach ... 30
         2.6.2.2. Competitive Growth Approach 32
         2.6.2.3. Competitive Nucleation Approach 35
      2.6.3. Applications of Thermodynamic Theories to the Studies of Silicides ... 39
3. A Kinetic Model for Silicide Formation 56
   3.1. Computation of Diffusion Fluxes and Release Rates 56
      3.1.1. Basic Equations 56
      3.1.2. Method for Computing Diffusion Flux and Release Rate 58
      3.1.3. Selection of Experimental Data from The Literature 59
   3.2. Calculations and Analysis of Pt_2Si and PtSi Formation in Pt/Si Thin Film Couples ... 60

3.2.1. Simultaneous Growth of Pt_2Si and PtSi 60
3.2.2. Successive Single Phase Growth of Pt_2Si and PtSi 66
3.3. A Kinetic Model For Silicide Formation 68
3.3.1. Assumptions.. 68
3.3.2. Definition and Explanation of Important Physical Quantities............. 69
3.3.3. Relationship Between Release Rate (r) and Diffusion Flux (ΔJ)......... 69
3.3.4. Other Factors Influencing Release Rate 73
3.3.4.1. The Reactants 73
3.3.4.2. Reaction Temperature 74
3.3.4.3. Impurities.. 74
3.3.4.4. Interface Conditions... 75
3.3.4.5. Conditions of the Contracting Phase 75
3.3.5. Relationship between Formation Rate and Release Rate 75
3.3.6. Reaction Process Plot.. 78
3.4. Analysis of Data from Other Experiments.. 79
3.4.1. Calculation of Data from Ex.3.. 79
3.4.2. Calculations of the Data from Ex.4 80
3.4.3. Analysis of Results from Exs.2, 3 and 4..................................... 81
3.4.4. Analysis of Ex.5 82
3.5. Discussion 82
4. Criterion for Silicide Formation in Transition Metal - Si Diffusion Couples 101
4.1. Expression of FEDR for a Reaction Region....................................... 102
4.1.1. Basic Equation for the Rate of Free Energy Change of a System 102
4.1.2. Expression of FEDR for a Reaction Region 104
4.2. Thermodynamic Fluxes and Driving Forces for Silicide Reactions.............. 108
4.2.1. Diffusion Flux and Chemical Potential Difference of a Reaction Region.. 109
4.2.2. Maximum Release Rate and Free Energy Change of Release Process... 112
4.2.2.1. Expression of Maximum Release Rate.......................... 112
4.2.2.2. Expression for Free Energy Change for the Release Process 118
4.2.3. Maximum Formation Rate and Free Energy Change for Formation Process 122
4.2.3.1. Free Energy Change of Formation 122
4.2.3.2. Maximum Formation Rate.. 124

4.3. Criteria for Silicide Formation 126
4.3.1. Driving Force as a Function of Flux 126
4.3.2. Criteria for Silicide Formation 131
4.4. Discussion 135
5. Semiquantitative Reaction Process Plots for Silicide Formation 149
5.1. Relative Maximum Release Rate and Semiquantitative Reaction Process Plots 150
5.2. Results and Predictions 154
5.3. Discussion 161
6. Silicide Formation Sequence Experiments 172
6.1. Experimental Procedure 173
6.1.1. Deposition of Nickel Films 173
6.1.2. Annealing Procedure 173
6.1.3. X-Ray Diffraction Experiments 173
6.1.4. Transmission Electron Microscopy (TEM) 174
6.1.4.1. Specimen Preparation and Equipment 174
6.1.4.2. Thickness Measurement Using TEM Micrographs 174
6.1.4.3. Phase Identification 175
6.2. Experimental Results 176
6.2.1. Multiple Phase Growth in Thin Ni Film-Si Diffusion Couples 176
6.2.2. Direct Deposition Reactions between Ni and Si Substrates 177
6.3. Discussion 178
6.3.1. Critical Diffusion Flux for NiSi Formation 178
6.3.2. Explanation of Silicide Formation Sequence during Direct Deposition Reactions 179
7. Conclusions and Recommendations 197
7.1. Conclusions 197
7.2. Recommendations 198
References 200

LIST OF TABLES

TABLE PAGE

1-1. Si-rich silicides and their properties ... 3

2-1. Comparison of first phase predictions with experimental results from the literature ... 43

2-2. Major diffusers in thin silicide films ... 45

2-3. Apparent activation energies from the literature ... 46

2-4. Summary of Gösele and Tu's analysis of growth kinetics ... 48

3-1. Diffusion flux (Pt) and release rate (Si) ... 85

3-2. Diffusion flux and release rate calculations ... 86

3-3. Key values of diffusion fluxes of Pt in Ex.3 (atoms/cm^2s). ... 87

3-4. Summary of the results from Exs. 2, 3, and 4 ... 88

3-5. Initial diffusion fluxes of Ni and Pt (atoms/cm^2s) ... 89

4-1. Relationship between silicide formation sequences and standard enthalpy change ... 141

5-1. Calculations of relative maximum release rates for 15 metal-Si systems ... 163

5-2. Comparison of predictions of silicide formation ... 167

6-1. Summary of direct deposition reactions ... 182

6-2. Comparison of diffusion fluxes in two experiments ... 183

LIST OF FIGURES

FIGURE PAGE

2-1 Phase sequence in Ni-Si lateral diffusion couples 49
2-2 Schematic view of multiple phase growth in thin film couples 49
2-3 Schematic configurations of thin film Cr-Si diffusion couples 50
2-4 Schematic of formation sequence of nickel silicides 51
2-5 Free energy vs. concentration plot for metastable phase formation (I) 52
2-6 Free energy vs. concentration plot for metastable phase formation (II) 53
2-7 Schematic summary of Gösele and Tu's analysis of growth kinetics 54
2-8 Schematic free energy vs. composition plot for A-B binary system 55
3-1 Schematic of a Type II process 90
3-2 Plot of growth kinetics from Ex.1 90
3-3 Plot of growth kinetics from Ex. 2 91
3-4 Plots of growth kinetics for oxygen doped Pt-Si thin film couple from Ex. 3 91
3-5 Plot of growth kinetics for a $Pt_{90}Cr_{10}$ alloy-Si diffusion couple from Ex. 4 92
3-6 Plot of growth kinetics for a Ni-Si thin film couple from Ex. 5 92
3-7 Schematic plot of regression lines 93
3-8 Reaction process of multiple phase growth of Pt_2Si and PtSi in Ex.1 93
3-9 Schematic of simultaneous growth of Pt_2Si and PtSi 94
3-10 Schematic of second reaction of single phase growth in thin film Pt-Si couple 94
3-11 Schematic showing silicide formation 95
3-12 Schematic plot of the relationship between release rate of Si and diffusion flux of Pt 95
3-13 Schematic plot of r^{Si} vs. J^{Pt} 96
3-14 r^{Si} vs J^{Pt} plot from calculation results of Ex.1 and Ex.2. 96
3-15 Schematic of general r^N vs. J^M plot 97
3-16 r^{Si} vs J^{Pt} plot illustrating the influence of temperature on release rate of Si 97
3-17 Schematic of relationship between formation rate F_{ik} and release rate r_i 98
3-18 Schematic of relationship between F_{ik} and r_i for two phases of ith silicide. 99
3-19 Schematic reaction process plot 100
3-20 Reaction process plot drawn by using the data from Ex.2 as a reference 100
4-1 Schematic transition metal-Si diffusion couple 142
4-2 Schematic transition metal-Si diffusion couple (Si region is divided

into n slabs) 142
4-3 Schematic chemical bond breaking and forming process in a reaction region...... 143
4-4 Schematic energy vs. reaction coordinate plot 144
4-5 Schematic free energy vs. composition plot showing driving forces for reactions 144
4-6 Schematic bonding structure of (100) Si surface. 145
4-7 Schematic distribution of free energy over the reaction region........ 145
4-8 Schematic free energy vs. composition plot showing driving forces for different phases to form 146
4-9 Schematic r vs. ΔJ plot 147
4-10 Schematic F vs. r plot........ 147
4-11 Schematic free energy vs. time plot 148
4-12 Schematic plot showing activation energies for interfacial reactions 148
5-1 Semiquantitative reaction process plot for Mn-Si system........ 169
5-2 Semiquantitative reaction process plot for Co-Si system 169
5-3 Semiquantitative reaction process plots for Ni-Si system........ 170
5-4 Semiquantitative reaction process plots for Ti-Si system 171
6-1 TEM micrograph, SAD pattern and EDX spectrum of Ni_2Si layer........ 184
6-2 Cross-section TEM micrographs from cold substrate samples........ 186
6-3 Schematic summary of multiple phase growth sequence in thin Ni film-Si diffusion couples 186
6-4 Cross-section TEM micrographs from thin film Mn-Si couples 187
6-5 XTEM micrographs from hot substrate specimens (300°C, 0.1 nm/s) 188
6-6 XTEM micrographs from hot substrate specimens (300°C, 2 nm/s) 189
6-7 Plan view of TEM micrograph and SAD pattern from $NiSi_2$........ 190
6-8 SAD pattern from Ni_2Si and $NiSi_2$........ 191
6-9 SAD pattern showing an orientation relationship between $NiSi_2$ and NiSi 192
6-10 XTEM micrographs from hot substrate specimens (250°C, 0.1 nm/s)........ 193
6-11 Micrograph and SAD pattern from polycrystalline Ni_2Si........ 194
6-12 Kinetic plots showing thicknesses of Ni_2Si as a function of annealing time 195
6-13 Semiquantitative reaction process plot for Ni-Si reactions in a reaction region adjacent to Si substrate........ 196

SYMBOLS

Since the symbols in Chapter 2 (Literature Review) are from original papers, some symbols are used for different definitions. In order to avoid confusion, the symbols in Chap.2 and those in other chapters are listed separately. Furthermore, the models which some particular symbols are only used for are indicated in the list for Chap.2.

Symbols in Chapter 2

B_β Constant in parabolic growth equation (Kidson)

C Composition

ΔC Composition difference in a given phase (Gösele and Tu)

D Interdiffusivity of the moving species (Bené)

D^*_β Chemical interdiffusion coefficient with subscript indicating particular phase (Gösele and Tu)

G Gibbs free energy

G_β Constant determined by the compositions of the involved phases (Gösele and Tu)

ΔG Gibbs free energy change

ΔG_c Change in "chemical" free energy due to the formation of a new phase (d'Heurle and Gas)

ΔG^* Activation energy of nucleation (d'Heurle and Gas)

Δg_v Chemical free energy change due to new phase formation (Thompson)

H Constant factor related to the compositions of the equilibrium phases (Gösele and Tu)

$\Delta H'$ Effective heat of formation (Pretorius)

ΔH^o Standard heat of formation (Pretorius)

ΔH_d Deformation energy loss due to the volume change caused by phase transformation (d'Heurle and Gas)

J_{in} Diffusion flux into a reactive interface

J_{out} Diffusion flux out of a reactive interface

ΔJ Difference between the diffusion fluxes into and out of a reactive interface

k_B Boltzmann constant

K Constant in Kidson equation

n_r Number of initial reaction centers on a substrate surface (Losch)

n_s Total number of surface atoms (Losch)

n_c Number of easy mass transport channels (Losch)

r Ratio of diffusion fluxes (Gösele and Tu)

r_1 Critical value of diffusion flux ratio

r_2 Critical value of diffusion flux ratio

ΔT Temperature difference between the liquidus curve and the peritectic (or peritectoid point for the system under consideration (Tsaur *et al*.)

x_{α}^{crit} Critical thickness of an amorphous phase (Gösele and Tu)

x_{β}^{c} Critical thickness of phases with subscript indicating particular phase (Gösele and Tu)

x_{β}^{*} Changeover thickness (Gösele and Tu)

κ_{γ}^{eff} Effective interface reaction barrier (Gösele and Tu)

κ Interfacial mobility

λ Average jump distance of diffusing atoms (Thompson)

$\sigma_{\beta x}$ Interface energy between β phase and a crystalline compound X (Thompson)

$\Delta\sigma$ Increase in surface energy due to new phase formation (d'Heurle and Gas)

Symbols in other Chapters

A Area

c Concentration of moving reactant atoms in a reaction region

C_i Ratio of moving reactant atoms to nonmoving reactant atoms in one formula unit of ith silicide

D Diffusivity of moving reactant

E Activation energy for breaking nonmoving reactant bonds without new bond formation

E' Energy compensated by new bond formation during old bond breaking process

E_{ai} Arrhenius activation energy for ith silicide formation

E_i Energy barrier for a reaction at coherent interface

E_{ik} Activation energy of rearranging a molecule from reaction region to the growing phase

F_{ik} Formation rate of k phase of ith silicide

$F_{ik\ max}$ Maximum formation rate for k phase of ith silicide to form

F_{ik}' Conditional maximum formation rate for k phase

G Gibbs free energy

G_j	Gibbs free energy of jth part of a system
G_R	Free energy of a reaction region
$g_0(c)$	Free energy per molecule of a solution of uniform concentration c
$\Delta G°$	Standard free energy change of reaction
ΔG_{ik}	Free energy change for the formation process
$\overline{\Delta G_{ik}}$	Average free energy change for formation process per molecule
$\Delta G'_{ik}$	Energy barrier for heterogeneous nucleation
$\Delta G'_{ik\ hom}$	Energy barrier for homogeneous nucleation
$\Delta G_{ik\ tot}$	Total driving force in a reaction region
ΔG_{ir}	Free energy change for a release process at the stochiometric composition
ΔG^*_{ir}	Free energy change for a release process which is a function of diffusion flux
d_cG	Free energy change due to energy exchange between different parts of a system
d_eG	Free energy change due to the energy exchange with the environment
d_iG	Free energy change due to changes within a system
dg_{ik}	Free energy change for formation process per unit area of a reaction region
dg_{ir}	Free energy change for release process per unit area of a reaction region
dg^i_R	Free energy change for ith silicide formation per unit area of a reaction region
ΔH^o_{298}	Standard heat of formation
ΔH_d	Elastic strain energy per unit volume induced by nucleation
J_{iLC}	Lower critical diffusion flux for ith silicide to form
J_{iUC}	Upper critical diffusion flux for ith silicide to form
J_{in}	Diffusion flux into reaction region
J_k	Generalized thermodynamic flux
J_{out}	Diffusion flux out of reaction region
ΔJ	Difference between the diffusion fluxes into and out of reaction region
$\underline{k}$	Reaction rate constant in first order chemical reaction rate equation
K	Equilibrium constant
$\bar{k}$	Gradient energy coefficient
k_B	Boltzmann Constant
k_p	Slope of the regression line for parabolic growth kinetic equation
m_i	Number of moving reactant atoms per formula unit of product for ith silicide
N_i	Number density of ith silicide
N^*_i	Number of formula units in a unit area of a single layer of ith silicide

N_V	Number density of the product molecules per unit volume of a reaction region
n_d	Number density of atomic defect positions in a surface layer of nonmoving reactant
n_i	Number of nonmoving reactant atoms (or formula units) per formula unit of product for ith silicide
n_R^i	Number density of ith silicide molecules per unit area reaction region
n^*	Number density of nonmoving reactant atoms per unit area of surface layer
P	Entropy production per unit time
Q_i	Concentration quotient of reactants and product for ith silicide formation
r_i	Release rate for ith silicide formation
r_{ik}	Critical release rate related to the maximum formation rate for k phase formation
r_{ik}'	Conditional critical release rate for k phase formation
r_{imax}	Maximum release rate of nonmoving reactant for ith silicide formation
S	Total entropy of a system
S_j	Entropy of jth part of a system
d_eS	Flow of entropy due to interactions with the exterior
d_iS	Entropy production due to changes within a system
T	Temperature
t	Reaction time
t^*	Time required to initiate growth of a phase
Δt	Time interval
Δt_i	Average interaction time to form a single molecule layer of ith silicide
X_i	Mole fraction of product molecules
X_i^M	Mole fraction of moving reactant
X_i^N	Mole fraction of nonmoving reactant
X_k	Generalized thermodynamic force
x	Thickness
x_c	Interfacial layer (reaction region) thickness corresponding to a minimum interfacial free energy
x_0	Intercept of the regression line for parabolic growth kinetic equation
x_R	Interfacial layer (reaction region) thickness
Δx^*	Observed thickness increase of PtSi
$(\Delta x^*)^T$	True displacement of the PtSi/Si interface
Y	Reaction rate for a reaction at coherent interface

α	Proportionality constant in a linear free energy relationship equation
β	Constant in a linear free energy relationship equation
β'	Temperature independent constant in a linear free energy relationship equation
θ	Contact angle for nucleation
λ	Average jump distance of moving reactant atoms
μ	Chemical potential
μ^o	Standard chemical potential
$\mu_R^M(c)$	Chemical potential of moving reactant in a uniform solution of concentration c
$\mu_R^M(dc/dx)$	Chemical potential due to the contribution of gradient energy
$\Delta\mu_R^{M'}$	Chemical potential difference in a reaction region
ν	Vibration frequency of nonmoving reactant atoms at the surface exposed to a reaction region
σ_{kN}	Surface tension of the interface between k phase and nonmoving reactants
$\Delta\sigma$	Difference in interface energies due to k phase nucleation

ABBREVIATIONS

CBED	Convergent Beam Electron Diffraction
DDR	Direct Deposition Reaction
EDX	Energy Dispersive X-ray spectroscopy
FEDR	Free Energy Degradation Rate
HRTEM	High Resolution Transmission Electron Microscopy
IBM	Ion Beam Mixing
LFER	Linear Free Energy Relationship
M	Moving reactant
ML	Monolayer of atoms
N	Nonmoving reactant
RBS	Rutherford Backscattering Spectrometry
RMR	Relative Maximum Release rate
RPP	Reaction Process Plot
RTA	Rapid Thermal Annealing
SAD	Selected Area Diffraction
SPE	Solid Phase Epitaxy
SOR	Short Range Order
SRPP	Semiquantitative Reaction Process Plot
SSA	Solid State Amorphization
TEM	Transmission Electron Microscopy
UHV	Ultra High Vacuum
VLSI	Very Large Scale Integration
XRD	X-Ray Diffraction
XTEM	Cross-sectional Transmission Electron Microscopy
ZA	Zone Axis

Chapter 1. INTRODUCTION

During the last two decades, transition metal silicides have attracted tremendous interest from scientists around the world. Many silicon-rich silicides have been widely used in very large scale integrated circuit (VLSI) technology and will probably be used in other electronic devices. This is because they have many advantages over other materials, and because they are compatible with existing Si integrated circuit technology [1-9]. In Table 1-1, these silicides are listed in three groups (i.e., near noble metal silicides, refractory metal silicides and semiconducting silicides), depending on their general properties and applications.

For applications to VLSI technology and in electronic devices, thin film silicides grown on Si substrates are required. In many cases, epitaxial thin film silicides are desirable. Various techniques for growing thin film silicides on Si substrates have been developed. Among them, the most basic and a very important one is silicide formation through thermal reaction of thin film metal-Si diffusion couples, since many other techniques, such as rapid thermal annealing (RTA), ion beam mixing (IBM), solid phase epitaxy (SPE), self-aligned silicidation, buried silicide layers, and direct deposition reactions (DDR) etc., are based on thermal reactions. Therefore, kinetic studies of silicide formation through thermal reactions are technologically significant.

Silicide formation kinetics is also of interest from the viewpoint of basic science. When a metal film is deposited onto an atomically clean surface of a Si substrate, the two elements are brought into intimate contact. At elevated temperatures, various physical and chemical processes, such as diffusion, intermixing, and chemical reactions, may take place. One of the main consequences of these processes is silicide formation. Therefore, a mechanistic understanding of these processes is not only an important theoretical foundation for processing control of thin film silicide growth but also a valuable contribution to solid state reaction theories. For instance, the results from reactions at metal-Si interfaces may be good references for the kinetic studies on the reactions at metal-metal or metal-ceramics interfaces.

Thus far, a number of prominent experimental phenomena have been discovered in thin film metal-Si diffusion couples, which include single phase growth, silicide formation sequences, competitive growth, solid state amorphization (SSA), and DDR. These phenomena cannot be explained by conventional theories. For example, the kinetic behavior of single phase growth and competitive growth are in contradiction with classical diffusion reaction theory. The silicide formation sequences and SSA cannot be explained by equilibrium thermodynamics, i.e., whether and when a silicide phase can form is not

predictable from its thermodynamic stability and from the magnitude of free energy change for this phase formation. In order to explain and predict these phenomena, many kinetic models have been proposed [10-28]. Each model, however, is applicable only for some cases but fails in other cases. Thus, the objective of this study is to establish a generalized kinetic model for silicide formation through solid state reactions in thin film metal-Si diffusion couples and to provide experimental support for the mode!.

The thesis is divided into seven chapters. Chap.2 is a brief overview of important experimental phenomena observed in transition metal-Si diffusion couples and of kinetic theories reported in the literature. The main body of the thesis consists of four chapters, i.e., Chaps. 3 to 6. In Chap.3, a kinetic model and a reaction process plot (RPP), demonstrating the relationship between the physical quantities that control the reaction processes, will be developed. In Chap.4, expressions for free energy degradation rate (FEDR) in a reaction region (i.e., a reactive interface in a diffusion couple) are derived. It is shown, by using the expressions and an RPP, that in a given reaction region there are always a number of possible reaction processes competing with one another. One of these processes can result in the largest FEDR. Based on this result, a reaction criterion, the largest FEDR criterion, is proposed for silicide formation in a diffusion couple. Chapter 5 shows semiquantitative calculations of RPPs. The results are used to predict silicide formation sequences in 15 metal-Si systems. The results from a multiple phase sequential growth experiment and the (DDR) experiment are given in Chap.6. The results from the former experiments are compared with predictions from the new model, while the new phenomena observed in the latter experiment are explained using the RPP. In the final chapter, the results from this study will be summarized and recommendations for future work will be provided.

Table 1-1 Si-rich silicides and their properties [3, 4]

Group	Silicide	Resistivity (μΩ-cm)	Schottky Barrier Height (eV)	High Temp. Stability	Applications
near noble metal silicides	$CoSi_2$ $NiSi_2$ PdSi PtSi	low, < 50	greater than half the Si band gap energy, increase with atomic no.	poor	Schottky barrier or ohmic contacts
refractory metal silicides	$TiSi_2$ $ZrSi_2$ VSi_2 $NbSi_2$ $TaSi_2$ $MoSi_2$ WSi_2	low < 100	all have similar values around 0.55	good	1) Schottky barrier contacts 2) gate metallization, interconnects in VLSI
semiconductor silicides	$FeSi_2$ $CrSi_2$ $MnSi_{1.73}$ $ReSi_{1.73}$ $IrSi_{1.73}$	high > 250	various values	variable	promising in applications such as laser detectors, LEDs, fibre communication devices

Chapter 2. LITERATURE REVIEW

Kinetics of silicide formation through solid state reactions in thin film metal-Si diffusion couples has been extensively investigated for more than twenty years. In early studies, some prominent experimental phenomena, i.e., single phase growth, low reaction temperature, sequential formation, and competitive growth, had been found. From classical diffusion reaction theory, single phase growth and sequential formation are unlikely to take place in a bulk diffusion couple. The discovery of these prominent phenomena in thin film couples and the potential applications of single layer Si-rich silicides to integrated circuit technology and other electronic devices have generated strong interest in thin film silicide formation kinetics. Experimental results from early studies have been discussed, in detail, in many review papers [1-9]. A number of kinetic models explaining or predicting the experimental phenomena have been proposed by various research groups [5, 6, 10-15]. During the last few years, with ultra high vacuum (UHV) equipment being used for thin film deposition and with high resolution analytical techniques, such as TEM and high resolution transmission electron microscopy (HRTEM), being used for thin film interface characterization, new experimental phenomena have been observed. These phenomena, including solid state amorphization (SSA), metastable phase formation, room temperature deposition reactions, and different first phase formation, have had a significant impact on kinetic theories and models for thin film silicide formation developed from early studies. A number of new kinetic models and theories have been proposed in order to account for these new experimental results [9, 16-28]. The experimental results from the literature and the kinetic models proposed up to date will be briefly reviewed in this chapter.

2.1. Single Phase Growth and Multiple Phase Growth

As is well known from classical diffusion reaction theory, in a bulk couple, all the phases predicted by the equilibrium phase diagram will be observed to grow simultaneously, apart from some exceptional absences of individual compounds [29-32]. It is found, however, that in a pure (i.e., no impurity contamination) thin film couple, these phases tend to form sequentially, i.e., they grow one by one. Moreover, some phases which can be observed in bulk couples do not show up in thin film couples [1-9, 13, 14, 33-43]. Because of the apparently different growth behavior, the growth process in a bulk couple and that in a thin-film couple are referred to as multiple phase growth and single phase growth, respectively, in a couple of review papers [13, 14]. It is also reported, from

early studies, that when an initial silicide phase grows over a critical thickness, a second silicide starts to form and then the two phases grow simultaneously [37, 44-47]. In some circumstances, it is also found that shortly after the second phase formation, the first phase starts to shrink while the second phase continues growing [45, 46]. When the observations, from the experiments using UHV metal film depositions and well controlled annealing ambience [34, 35, 48], and the results, from the experiments using oxygen doped metal films [49-51], are compared, it is concluded that the simultaneous growth of two phases is due to impurity effects. Later investigations in Co-Si, Rh-Si, and Mn-Si diffusion couples [6, 9, 42-54], however, show that this phenomenon may also be observed in diffusion couples with relatively thick metal films (e.g., about several hundred nanometers for the Co-Si couple). In particular, the lateral diffusion couple experiments, conducted by Zheng *et al*. [55] and Barbour *et al*. [56, 67], successfully demonstrate that initial phase formation and growth mechanisms are the same in both thin film and lateral diffusion couples, and that the reaction sequence, observed in lateral couples, reflects the behavior which would be found in bulk couples in earlier stages of silicide formation. In these experiments, a Si film, 50 nm thick, was deposited onto an Al_2O_3 substrate, followed by deposition of a 120 nm thick Ni island (400×400 μm^2). The samples were subjected to a preanneal and then were heat treated at different temperatures (400 to 800°C) for different periods. Fig.2-1 shows a cross-section of this configuration from one of the annealed samples. It is found, by cross-sectional TEM (XTEM) observation [56, 57], that at the beginning of the reaction, only one phase, i.e. Ni_2Si, is formed and that the second phase, NiSi, does not show up at the Ni_2Si/Si interface until a critical thickness of Ni_2Si is reached. Similarly, the other phases, Ni_3Si_2 and Ni_5Si_2, are only observed after the NiSi and Ni_2Si grow over certain thicknesses respectively. From these experiments, it is well understood that the difference in formation sequence between thin film couples and bulk couples, after the first phase formation, is produced by the source limitation of one component in thin film couple. If the source of one component is not enough for the first phase to grow over its critical thickness, a single phase growth sequence will occur. Actually, the experiments with relatively thick metal films on Si substrates [6, 9, 52-54] already provide clear evidence for this argument. Fig.2-2 shows some results from these experiments, e.g., thick Co and Rh films on Si [6, 52, 54]. These results suggest that the reaction mechanisms for silicide formation would be the same in both thin film couples and bulk couples in the early stages of silicide formation although the formation sequences in these couples appear different from each other. Because of this, single phase sequential growth and multiple phase sequential growth are redefined, here, for the following discussion. Single phase sequential growth means that silicides form in sequence and only

one silicide grows at a time in a given diffusion couple. A multiple phase sequential growth means that after an initial silicide grows over a critical thickness, other silicide(s) start to form sequentially and more than one silicide grows at the same time in a given diffusion couple. (It can be either a bulk couple or a thin film couple or a lateral couple. Additional experimental results on formation sequences will be discussed in the next section).

The experimental phenomena of both single phase growth and multiple phase growth disagree with the statement of classical diffusion reaction theory, i.e., all or most of the equilibrium phases predicted will appear and grow simultaneously in a binary bulk diffusion couple. This is not surprising as classical diffusion processes deal with bulk diffusion couples annealed at high temperatures for long periods. The high temperatures and long anealing times are required because the interface between two components of a bulk couple is not as clean as in thin film couples. As a result of such annealing, the early stages of silicide formation in a bulk couple are "skipped" in these experiments. This can be demonstrated by a comparative experiment of silicide formation in thin film and in bulk Ni-Si couples [42]. In this experiment, the formation sequence in a couple with a 100 nm Ni film on a Si wafer is Ni_2Si at 300°C for 20min., NiSi at 400°C for 20min., and $NiSi_2$ at 800°C for 1h. On the other hand, four silicides, i.e., Ni_5Si_2 (10µm), Ni_2Si (55µm), Ni_3Si_2 (670µm), and NiSi (10µm), are observed simultaneously after annealing a bulk couple at 850°C for 8h. The $NiSi_2$ phase cannot be detected, by a microprobe with a spatial resolution of 1 µm, until a bulk sample is annealed at 750°C for 5 days.

One explanation for the discrepancy between classical theory and experimental results is that all the phases predicted by a phase diagram actually exist but cannot be observed because of the spatial resolution limitation of analytical tools. Tu *et al*. [42, 58] have examined Pd_2Si/Si and NiSi/Si interfaces in Pd-Si and Ni-Si thin film couples respectively, by XTEM lattice imaging techniques. According to the Pd-Si and Ni-Si phase diagrams, Si-rich silicides [59], PdSi and $NiSi_2$, would have appeared at the Pd_2Si/Si and NiSi/Si interfaces if the above argument was true. However, no such evidence is found even at atomic scale resolution (about 0.3 nm).

It has been reported, very recently, that simultaneous occurrence of multiphases is observed in the interfacial reactions of UHV deposited Ti, Hf and Cr thin films with (111) Si, respectively [60, 61]. In these experiments, an amorphous layer is found in all the as-deposited samples of these thin film couples. At lower annealing temperatures, only amorphous layer growth is observed, while at relatively high temperatures, more than one crystalline silicide phase is detected, by HRTEM, at the amorphous phase/Si interface in each type of couple. For instance, Cr_5Si_3 and $CrSi_2$ are found to form side by side at the amorphous phase/Si interface. It should be pointed out, however, that these results do not

provide support for the argument of coexistence of all equilibrium phases, for two reasons. Firstly, from classical diffusion reaction theory, the coexistence of these phases should have a layered configuration (Fig.2-3a), instead of the configuration reported by Ref.[60, 61] (Fig.2-3b). Otherwise, the chemical potential continuity at interfaces, required by the theory [29], cannot be satisfied. Secondly, most of the equilibrium phases, predicted by the respective phase diagrams, do not form even in these experiments, e.g., only HfSi and Hf_5Si_3 are observed in a Hf-Si couple but there are five other phases (i.e., Hf_2Si, Hf_3Si_2, Hf_4Si_3, Hf_5Si_4 and $HfSi_2$ [56]) missing at the interface. Similarly, three other silicides, Cr_3Si, Cr_2Si and Cr_3Si_2, are missing in the Cr-Si couple. Thus far, no experimental evidence for the above argument, that all or most of equilibrium phases coexist at the early stages of silicide formation, has been found. On the other hand, sequential growth of single phase or multiple phases has been widely accepted to be a general phenomenon in both thin film couples and bulk couples in early stages of silicide formation.

2.2. Silicide Formation Sequence

It has been found that the growth of silicides in diffusion couples follows special formation sequences, either single phase growth or multiple phase growth, depending on the type of silicides and the relevant amount of the two components in the thin-film couples [1-3, 6, 9, 13, 14].

2.2.1. Experimental Observations of Silicide Formation Sequences

One typical example for single phase growth is the reaction of thin-film Ni with a Si substrate. According to experimental observations [1-3, 6, 9, 13, 14] (Fig.2-4a), the first phase formed between the metal and Si is Ni_2Si and it grows until all the Ni is exhausted. The second phase, NiSi, then begins to form at the Ni_2Si/Si interface and grows by consuming the Ni_2Si, till all the Ni_2Si completely disappears. The last phase, $NiSi_2$, is formed only at high temperatures ($\geq 750°C$). If the diffusion couple is made of a thin Si film and a Ni substrate, the reactions will follow the other sequence illustrated in Fig.2-4a. The binary phase diagram for the Ni-Si system is shown in Fig.2-4b. Comparing Fig.2-4a with Fig.2-4b, it is evident that one phase, i.e. Ni_3Si_2, which exhibits the most extensive growth in bulk couples [42, 55], is absent.

At present, the most complete multiple phase growth sequence experimentally observed is that in a Ni-Si lateral diffusion couple [55-57], which has been described in Sec.2.1. More investigations using other metal-Si lateral or bulk couples are necessary to

gain more experimental evidence for multiple phase growth sequences, although the cleanliness of the interface in a bulk couple may pose a problem. On the other hand, the initial stage of multiple phase growth, i.e., simultaneous growth of the first two phases, has also been studied by reacting relatively thick or impurity-doped metal films with Si substrates [6, 9, 37, 44-47, 49-54]. In some of these M-Si couples (M represents Ni, Pt, Co etc.), metal atoms are the predominant moving species so that M_2Si forms initially and MSi follows after M_2Si reaches its critical thickness [37, 44-47, 49-52]. In contrast, Si atoms are the major diffuser in Mo-Si couples so that $MoSi_2$ is the first phase to form while Mo_5Si_3 is the second phase [6]. It is believed that the moving species is one of the key factors determining formation sequences [6, 9].

2.2.2. Prediction of Single Phase Formation Sequences

Prediction of silicide formation sequences is a long standing problem for kinetic studies. A number of empirical rules and theoretical models have been proposed to predict and explain the formation sequences [11-28]. Before solid state amorphization (SSA) reactions were found to be a rather general experimental phenomenon in thin film diffusion couples (around 1987), the Walser-Bené rule [10] had been the most frequently referred to empirical rule for predicting first phase nucleation in thin film metal-Si couples. The rule is as follows: "The first compound nucleated in planar binary (thin film) reaction couples is the most stable congruently melting compound adjacent to the lowest temperature eutectic on the bulk equilibrium phase diagram". They reasoned [10, 62] that when a thin film of metal was deposited on Si substrates, a "metallic glass" layer, with a composition near the lowest-temperature eutectic in the binary system, was formed at the interface. Consequently, the nucleation process is actually a process of atomic rearrangement from liquid-like short-range order (SRO) to crystalline SRO. Since a higher energy barrier, associated with the large rearrangement, is required for noncongruent states than for congruent states at the same concentration, the nucleation process would highly favor congruently melting states over noncongruent states. In addition, if the concentration fluctuations driving nucleation are produced by a diffusion mechanism, the first phase that nucleates would be the congruent phase closest in concentration to the initial eutectic composition. According to earlier experimental results, this rule appeared to work in many cases, so that it was very influential for more than ten years. A similar rule is also proposed for first phase nucleation in metal-metal thin film systems [63].

After examining phase diagrams and sequences of phase formation in several metal-silicon systems, Tsaur *et al.* [11] formulated a rule for predicting single phase growth sequence: "The second phase formed is the compound with the smallest ΔT that exists in

the phase diagram between the composition of the first phase and the unreacted element". They defined ΔT as the temperature difference between the liquidus curve and the peritectic (or peritectoid) point for the system under consideration. In addition to the experimental results, this rule is based on the following argument. There exists an interface region between the silicide and pure element. The interfacial region has a width estimated to be $\leq$ 2nm and has a concentration profile with compositions ranging from the silicide to the pure element. Nucleation of compounds within this composition range can occur, but usually only one compound will nucleate and grow to a measurable amount. Phase nucleation is a competitive process due to the variation of concentration in the interfacial region [11]. On the other hand, the larger the ΔT value for a peritectic phase, the larger the compositional difference between the solid peritectic compound and the liquid phase at the peritectic temperature. Therefore, a small difference in composition between the peritectic and liquid phase at the peritectic temperature yields a low-energy barrier for nucleation, because only small compositional fluctuations are required for nucleation. This rule can explain the formation sequences in Pd-Si, Pt-Si, Ni-Si, Co-Si, and some other systems.

The "effective heat of formation" model is proposed by Pretorius to predict single phase growth sequences in metal-Si and metal-metal thin film couples [21-23, 64-66]. In this model, the effective heat of formation, $\Delta H'$, is defined by the expression [21-23]:

$$\Delta H' = \Delta H^o \times \left(\frac{\text{available concentration limiting element}}{\text{compound concentration limiting element}} \right) \qquad (2\text{-}1),$$

where ΔH^o is the standard heat of formation of the silicide in Joules per mole of atoms. When calculating $\Delta H'$ for a given metal-Si binary system, the composition at the lowest eutectic point is taken as the available concentration limiting element, which is based on the argument that the intermixing at the metal-Si interface, during annealing, takes place at concentrations similar to that of the lowest eutectic point. In addition, another condition, i.e., nucleation of a congruent phase is much easier than that of a noncongruent phase, is imposed. Using this condition and the term, $\Delta H'$, an "effective heat of formation" rule for single phase growth sequences is formulated by Pretorius [21, 22]: "The first silicide compound to form during metal-Si interaction is the congruent phase with the most negative effective heat of formation ($\Delta H'$) at the concentration of the lowest temperature eutectic of the binary system. The next phase formed at the interface between the compound and remaining element (Si or metal) is the next congruent phase richer in the unreacted element, which has the most negative effective heat of formation." As can be seen from comparison of this model with the Walser-Bené rule and the rule of Tsaur *et al*.,

the basic considerations about "available concentration limiting element" and "congruent phase nucleation" in this model are the same as those in the other two rules. The only main difference between these rules is that thermodynamic data, ΔH, instead of the information from the equilibrium phase diagram, are used in the effective heat of formation model. If the experimental results from early studies are used, predictions of first phase formation from this model are about 80% successful [21-23, 64-66].

With better analytical techniques being used for characterizing metal-Si interfaces, however, more and more experimental results have shown disagreement with the rules introduced above. These experimental results can be divided into three groups and will be discussed one by one in the following paragraphs.

1) Different initial phases: Both the Walser-Bené rule and the effective heat of formation rule imply that only one phase is the initial phase in a given metal-Si diffusion couple, whereas more and more experiments provide evidence of different first phase formation being possible. A comparison of first phase formation predictions from these two rules with the experimental results from 15 metal-Si systems are shown in Table 2-1. It is evident, from this Table, that about 50% of these systems have more than one initial phase being reported. A typical example is the Ni-Si system in which almost all early studies found Ni_2Si to form first [6, 11, 37, 55-57, 95-97]. However, when a diffusion barrier layer, such as an amorphous layer, α-NiZr [101] or α-NiCr [100], is introduced at the interface between Ni and Si, $NiSi_2$ or NiSi becomes the initial silicide in each respective diffusion couple. One could argue that the Si surface structure is probably changed by contacting the barrier layer, which may affect the first phase formation. Another experiment with an ultrathin SiO_2 layer (about 1.5 nm) as a barrier layer shows that it is not the case. In this experiment, the observed initial phase is $NiSi_2$ [102]. Since the usual oxide removal procedure, i.e., HF etching, can only remove oxide and leave the original SiO_2/Si interface exposed to the surface, the Si surface structures with and without SiO_2 barrier layer should be the same [102]. Therefore, it is believed that the reaction in the experiment with ultrathin SiO_2 barrier should be the same as that in a Ni-Si couple without the barrier layer if the initial Ni diffusion flux can be decreased to the same degree.

2) Solid State Amorphization and Metastable Phase Formation: From the three rules introduced above, all the phases formed should be equilibrium phases from phase diagrams. During the last few years, a number of research groups reported that an amorphous metal-Si alloy layer formed initially and grew before any crystalline phase formed, when a thin film metal-Si diffusion couple was annealed at relatively low temperatures [61, 78, 105, 106, 123-138]. This phenomena is called solid state amorphization. The metal-Si systems which have shown such kinetic behavior include Rh-

Si [123], Ti-Si [78, 124-134], Ni-Si [135, 136], Cr-Si [61], V-Si [78], Zr-Si and Hf-Si [61, 105, 106], and Nb-Si and Ta-Si [137, 138]. In these systems, the amorphous phase is the initial phase when a given system is annealed at low temperatures. Other metastable phases that can form during annealing of thin film couples have also been reported. A well known example is C49 $TiSi_2$ whose formation precedes that of the equilibrium phase C54 $TiSi_2$ [68, 69, 124, 125, 127, 134, 139-143]. Similarly, that the metastable phase, hexagonal $MoSi_2$, grows before tetragonal $MoSi_2$ formation is observed [144]. Some other examples are metastable θ-Ni_2Si [145] and metastable hexagonal NiSi [96, 146] formation on Si (111), respectively, and a metastable $FeSi_2$ phase formation on Si (111) [147].

3) Exceptions to the rules: When the Walser-Bené rule and effective heat of formation rule were proposed, it was pointed out, by the authors, that there existed some exceptions (e.g., Zr_5Si_4 [11] and Mn_5Si_3 [11, 22] were predicted from the rule as the initial phases in Zr-Si and Mn-Si systems) which were not in agreement with the experimental results at that time. No experimental support for these predictions has been found to date. Instead, Mn_3Si [9, 53] or MnSi [40, 41], and $ZrSi_2$ [1-4, 11, 103, 104] or ZrSi [105, 106] have been reported to be the initial phases in each respective system.

2.2.3. Explanation of SSA and Amorphous Phase Critical Thickness

Although the phenomenon of different initial phases has received very little attention, SSA reactions have attracted great interest. Recently, Bené [16] proposed a kinetic model and a criterion for the generation of initial bulk silicide phases (where the term of bulk silicide phase is used, by Bené, to indicate the phases that are large enough to be detected by electron or X-ray diffraction). According to the model [16], the metal-Si interface region, which is at a high free energy state compared to the mixed state, will undergo kinetic transition(s) to structure(s) that maximize the FEDR (locally) after successive small increments of time. In other words, among all phases (stable, metastable or amorphous) whose formation can reduce the local free energy of the metal-Si interface, the one with the largest FEDR will form first. The term, FEDR, is expressed by $-D\Delta G$, where D is the interdiffusivity of the moving species in a given silicide, and ΔG is the free energy change for this phase formation. This model and the largest FEDR criterion are used [16] to explain amorphous phase formation at the beginning of silicide reactions. Hence, although the amorphous phase has a smaller value of $-\Delta G$ than stable silicide phases, it can still form initially if its D is so large that its $-D\Delta G$ is the largest compared to those for other phases. From approximate free energy calculations, Bené [16] also concluded that growth of amorphous phases between Si and Ni, Co, Pd, Pt, Ti, V, Ta, and Hf is possible, but

not with Cr, Mo, and W. Experimentally, amorphous phase formation at the beginning of silicide reactions has been found in Ni-, Ti-, V-, Ta-, Hf-, and Cr-Si systems [61, 78, 105, 106, 123-138] but not in Co-, Pd-, Pt, and Mo-Si systems [72, 107, 127, 130].

Gösele and Tu [19] examined and derived expressions for the critical thickness, x_α^{crit}, of an amorphous phase. There are two different cases depending on the specific form of free energy (G) - versus - composition (C_A) diagrams. In the first case (shown in Fig.2-5(a)), x_α^{crit} is expressed as

$$x_\alpha^{crit} = H_{\gamma\alpha}\Delta C_\alpha^{eq'} D_\alpha / H_\gamma \Delta C_\gamma^{eq'} \kappa_\gamma^{eff} \quad (2\text{-}2),$$

where $\Delta C_\alpha^{eq'}$ and $\Delta C_\gamma^{eq'}$ are indicated in Fig.2-5(b), $H_{\gamma\alpha}$ and H_γ are factors related to the compositions of the equilibrium $A_\gamma B$ and $A_\alpha B$ phases, D_α is the diffusion coefficient in α phase, and κ_γ^{eff} is the effective interface reaction barrier which describes the energy barrier associated with changes in atomic arrangements or effects due to volume changes at the interfaces [12-14, 19]. Gösele and Tu suggested that, in this case, as soon as the amorphous phase reaches the critical thickness, x_α^{crit}, the crystalline phase, $A_\gamma B$ starts to form. Meanwhile, the amorphous layer will continue growing. In the second case (shown in Fig.2-6) the amorphous phase starts to shrink after it reaches x_α^{crit}. The procedure for estimating the x_α^{crit} is developed based on the following concept: At the beginning of the reaction the FEDR for amorphous phase formation is the largest so that it grows first. The FEDR will decrease with phase growth. As soon as the FEDR becomes smaller than that for the crystalline phase to form, the amorphous phase starts to shrink and the crystalline phase grows. The thickness of the amorphous phase at the point where the FEDR for the amorphous phase and that for crystalline phase are equal is the critical thickness, x_α^{crit}. These theoretical results have been used to qualitatively interpret the experimental phenomena of amorphous phase formation and subsequent crystalline phase formation in multilayer diffusion samples [19].

It can be seen, from the above discussion, that a lot of experimental and theoretical work has been done on silicide formation sequences. However, predictions of the formation sequences from various models are not very successful and questions still remain. More details concerning these models and theories are discussed in Sec.2.6.

2.2.4. Prediction of Multiple Phase Growth Sequence

There has been little done on predicting multiple phase growth formation. Very recently, Jan, Chen and Chang [148] predicted the growth of Co_2Si, CoSi, and $CoSi_2$ in thin film Co-Si couples using numerical solutions of diffusion equations and interdiffusion coefficients determined from bulk Co-Si diffusion couples. Quantitative agreement was obtained between the calculated thicknesses of Co_2Si, CoSi and $CoSi_2$ and the data reported in the literature. It is noteworthy that the values of parabolic growth constants of these silicides, experimentally determined from samples annealed at high temperatures (800-1050°C), when extrapolated to lower temperatures, agree quite well with those obtained by Lau *et al.* [47] from thin film couples annealed at these temperatures. Moreover, it is pointed out, by these authors, that the growth sequence of these silicides, according to the order of the parabolic growth constants, is Co_2Si, CoSi, and $CoSi_2$ at low temperatures (430-545°C) and is CoSi, Co_2Si and $CoSi_2$ at high temperatures (>1000°C). The predicted low temperature growth sequence is in agreement with the experimental observations reported in the literature [1-4, 6, 11, 43, 85, 86]. These results provide strong support for the argument that the mechanisms of silicide reactions in both thin film and bulk couples are basically the same, and that the the difference between single phase growth sequence and multiple phase growth sequence is due to reactant source limitation in thin film couples [25].

2.3. Solid State Amorphization

As mentioned above, SSA phenomena have attracted much attention. It has been found, by XTEM or HRTEM, that in many metal-Si systems (including metal-amorphous Si bilayer, metal-Si multilayer, and metal films on single crystal Si), such as Ti-Si [128, 131-134], Ni-Si [135, 136], Hf-Si [61, 105, 106], Zr-Si [105, 106], Ta-Si [137, 138], Nb-Si [137, 138], Mo-Si [132] and Co-Si [132, 135], a very thin amorphous layer is formed during metal film deposition at room temperature. When these couples are annealed, the amorphous phase disappears and a crystalline phase forms in the Mo-Si and Co-Si systems respectively, whereas the amorphous layer grows initially in each of other systems. In the literature amorphous layer growth in the latter cases is referred as to SSA.

More extensive research on SSA reactions has been done in metal-metal systems than in metal-Si systems so that the theoretical and experimental results from metal-metal systems are often used to explain phenomena observed in metal-Si systems. These results will be briefly summarized in the following [149, 150]:

1) The driving force for SSA is a large negative heat of mixing between the two components of a metal-metal bilayer couple, which results in the mixed amorphous alloy having a lower free energy than that of the bilayer structure (i.e., two metals separated by an interface).

2) The reaction advances by a layered growth process. At the beginning of the reaction, the amorphous layer growth is linear in time with the rate proportional to the interface mobility, κ, whereas the layer growth becomes and then remains a parabolic function of time during the latter stages. In other words, when the layer thickness is less than the characteristic length $l \sim D/\kappa$ (D is the interdiffusion coefficient), one has interfacial reaction controlled growth. If the layer thickness is much thicker than l, the growth is diffusion controlled (see section 2.6.1.1. for more details about diffusion controlled and interfacial reaction controlled processes). It has been estimated that l=1.6nm for Ni-Hf couples at 340°C [149]. Typical amorphous growth experiments in metal-metal systems are carried out over time scales of about 10^4s with the layer thicknesses ranging up to 100-200 nm, where there is still no crystalline phase formed. These results suggest that linear growth occurs only at very early stages of SSA so that the atom transport over the growing layer plays the dominant role in controlling glass (i.e., amorphous) growth [149, 150].

3) In near noble metal - refractory metal couples the near noble metal atoms are the major diffusers in the growing glass layers and they have much higher diffusivities than refractory metal atoms.

4) It is believed that metastable glass phase formation prior to the formation of any stable crystalline phases in a given couple is due to kinetic constraint(s) on crystalline phase nucleations [149]. Johnson and Schwarz [151] have suggested possible kinetic constraint(s): The first is the absence of mobility of one component, such as refractory metal atoms in a near noble metal-refractory metal couple. The second factor is the absence of a potentially low energy or coherent interface between the intermetallic compound crystal and parent metals of the diffusion couple. The last factor is the "kinetic interfacial barrier", i.e., the successive atomic rearrangements required to grow an intermetallic compound from an existing interface may require many correlated atomic jumps, which would lead to a small interfacial mobility, κ. According to Johnson [149], experimental support for the original interface between two metals and the grain boundaries to act as preferred nucleation sites of SSA has been obtained.

In metal-Si systems, it is found that some experimental results are very similar to those observed from metal-metal couples, but the others are not. Gibbs free energy versus composition and metastable phase diagrams for the Ti-Si system have been calculated [150], which show that there is a large negative heat of mixing of the components in this

system and that amorphous phase formation is possible over a wide composition range. Experimentally, exothermal SSA is observed in the Ti-Si system and a value of enthalpy change equal to -35 kJ/mol [150], for a Ti-Si multilayer sample with an overall equiatomic composition, is determined using differential scanning calorimetry. Enthalpy change of mixing for many other metal-Si systems has also been calculated [16]. All these systems have a negative value of enthalpy change, which indicates that there exists a thermodynamic driving force for SSA in each respective system. Based on the magnitude of the calculated values, Bené [16] divides these systems into two categories, i.e., those with large negative mixing enthalpy values, in which SSA is favorable and those with small negative mixing enthalpy values, in which SSA is unfavorable. As mentioned in Sec.2.2.3, experimental results from the literature do not agree very well with this classification [61, 78, 105, 106, 123-138]. It seems that the magnitude of mixing enthalpy may not be a proper criterion for SSA, although a negative mixing enthalpy is a necessary condition for SSA.

SSA in metal-Si systems also produces a microscopically uniform flat layer (as in SSA in metal-metal systems), although the critical layer thickness for inducing crystalline phase formation is usually equal to or smaller than 20nm, about 10 to 20 times smaller than that in metal-metal systems. Growth kinetics studies of the glass layers provide different results. The growth kinetics is reported to be diffusion controlled in Ti-Si and Ni-Si systems, respectively, by Holloway and Sinclair [131] and by Ma *et al*. [136]. But, the kinetics is found, by Chen and co-workers [105, 106, 133, 137, 138], to be interfacial reaction controlled in Ti-Si, Zr-Si, Hf-Si, Ta-Si and Nb-Si systems, even at the layer thicknesses of 17nm and 27nm.

It has also been shown that fast diffusion of one component in the amorphous phase may be an important characteristics of SSA in metal-Si systems. In reacted Ti-Si multilayers, Kirkendall voids in the silicon layers indicate that Si is the dominant diffuser [131, 150]. The reaction kinetics for SSA is about five orders of magnitude faster than that for crystalline silicide formation at the same temperature [131], which implies Si diffusion is much faster in the glass layer than in the crystalline silicide layer. During SSA in Ni-Si multilayer samples annealed at 250°C, the diffusion coefficient of Ni is between 2.9×10^{-14} and 4.3×10^{-13} cm^2/s [135], while in a Ni-amorphous Si bilayer annealed at 240°C this coefficient is estimated as being $\approx 10^{-14}$ cm^2/s [136]. According to Holloway and Sinclair [135], these values are about 5 to 70 times larger than that for Ni_2Si (which is the first crystalline phase to form in these experiments) growth at the same temperature. In addition, it is noted that so-called "anomalous diffusion", i.e., one of the two components of a given diffusion couple diffuses much faster in the other, is usually observed in metal-metal systems which exhibit SSA behavior and is believed to be one of possible kinetic

constraints for crystalline phase nucleation [149]. This "anomalous diffusion", in fact, is very common in almost all metal-Si systems when annealed at relative low temperatures. However, only in some of these systems is SSA detected [78, 112, 132, 135], which implies that "anomalous diffusion" may only be a necessary condition rather than a sufficient condition for SSA to occur.

In summary, it is rather widely accepted, at present, that the essential factors that permit SSA are fast diffusion of one component in the other and the existence of a negative value of mixing enthalpy in the binary system under consideration [149-151]. It is believed that the reason SSA can take place is due to kinetic constraints on crystalline phase nucleation [149, 151], although this remains to be confirmed both theoretically and experimentally.

2.4. Direct Deposition Reactions

During the last ten years or so, DDRs between the deposited metal and the Si substrate have been investigated by many groups. The significance of this research is both scientific and technological. Scientifically, it is very interesting to know the mechanism of DDR. There are a number of reports that the reaction between the two components takes place readily even at room temperature, when the first few layers of metal atoms are deposited onto the Si substrate [112, 113, 145, 152-169]. Furthermore, it is found that, in Ni-Si and Co-Si systems, the first silicide formed during DDR is different from that most frequently observed during thermal annealing of thin film couples [145, 152-162]. In other systems, however, such as the Pd-Si [112, 113, 145, 165, 166] and Fe-Si [168, 169] systems, initial silicides are the same for DDR and thermal reaction of thin film couples in a given system. These phenomena cannot be explained by existing theories for silicide formation, or by other theories for solid state reactions. On the technological side, a so-called "template" method, for growing high quality epitaxial Ni or Co disilicide thin film, has been invented, by Tung *et al*. [152] using DDR techniques. In this procedure, a few layers of Ni or Co are deposited onto (111) Si substrates and then the samples are annealed at elevated temperatures (450-550°C) to obtain ultrathin and high quality epitaxial disilicide films [152]. This film serves as a "template" for further silicide film growth, by depositing more metal (Ni or Co) or co-depositing metal with Si onto the "template" followed by annealing. If a conventional solid phase epitaxy technique is used, epitaxial disilicides can only form at high temperatures (≥600°C for $CoSi_2$ and ≥750°C for $NiSi_2$). The resulting films tend to be discontinuous for thicknesses < 100nm [152]. In contrast, the "template" technique can produce continuous epitaxial disilicide layers at relatively low temperatures

with a large range of thicknesses. Therefore, DDRs find important applications in the "template" technique.

In the rest of this section, emphasis will be put on silicide formation sequence during DDR, especially on the first phase formation, because it will be shown later in this thesis that the formation sequence can be explained using a new kinetic model developed in this study.

Experimental observations of DDR in Ni-Si [145, 152-159], Co-Si [145, 156-162], Pt-Si [112, 163, 164], Pd-Si [112, 113, 145, 165, 166], Ti-Si and Sc-Si [167], and Fe-Si [168, 169] systems have been reported. Of these systems Ni-Si and Co-Si are most extensively studied. Recent review papers about the experimental phenomena of DDR in these two systems can be found in Ref. [156-159].

Many experimental results show that epitaxial $NiSi_2$ forms on (111) Si substrates during DDR at room temperature if the Ni thickness is less than three monolayers (ML) [145, 154, 157, 159]. When the Ni thickness is between 3 and 10 ML, either Ni_2Si islands or $NiSi_2$ islands topped by some unreacted Ni are observed [159]. Above 10 ML of Ni, the silicide islands coalesce, the Ni-Si reaction stops, and unreacted Ni starts to accumulate on top of the reacted layer. The initial silicide's identity on (100) Si substrates is still not very clear.

It has been found that an epitaxial $CoSi_2$ layer is grown when 1-4 ML of Co are deposited onto (111) Si substrates at room temperature [156-162]. At more than 5 ML of Co, the surface becomes more Co-rich than the $CoSi_2$ phase. When more than 10 ML of Co is deposited, either unreacted Co or a distorted Co_2Si phase is found at the surface [159].

For the Pt-Si system, the initial phase that formed during DDR at room temperature was reported to be polycrystalline Pt_2Si in Ref.[112] and an amorphous phase with a composition close to either Pt_2Si or PtSi by Ref. [164]. An earlier study provides evidence that Pt_2Si forms initially at 320°C while PtSi forms first at 400°C during DDR [163].

Unlike the Pt-Si system, there is good agreement in studies on Pd-Si systems, i.e., a Pd_2Si layer is grown when the first few monolayers of Pd are deposited onto Si substrates at room temperature [112, 113, 145, 165, 166]. Even if the deposition is carried out with the substrate heated up to 200°C, the initial phase observed is still Pd_2Si [165].

For room temperature DDR in the Ti-Si system, it is reported [167] that when the deposited Ti is less than 1 ML, the reacted Ti-Si regions grow to form a Si-rich phase, which probably corresponds to the interfacial transition region between Si and the silicide phase that forms during further deposition. When 1ML to 4 ML of Ti are deposited a silicide phase with an average composition of TiSi forms. This phase is highly disordered

and inhomogeneous. With further deposition, up to 11 ML, a $TiSi_x$ solid solution phase (5<x<15 at%) forms. This final phase yields to a metal overlayer for 15 ML.

It is observed [168] that when 5 ML of Fe is deposited onto (100) Si substrates at room temperature, the interaction between Fe and Si produces a polycrystalline or an amorphous FeSi silicide film 3 ML thick (0.8nm). This silicide film is uniform and homogeneous. There is some unreacted Fe lying on top of the FeSi film. According to Alvarez *et al*., by selecting an adequate temperature range, it is possible to directly grow a certain phase on the Si substrate [169]. Their results show that when a fixed deposition rate is used, epitaxial FeSi and β-$FeSi_2$ can form as the initial phase when the Si substrate is held at 475°C and 750°C, respectively. This is attributed to the different diffusivities of Si at those temperatures.

It is quite puzzling that DDR can occur at room temperature and that the silicides, such as $NiSi_2$ and $CoSi_2$, which can form only during high temperature annealing in thin film diffusion couple, can form easily at room temperature. These phenomena can be explained using the new model and will be discussed further later. Here, only the effect of latent heat on DDR is discussed.

When metal atoms in vapor phase condense on a surface, latent heat (which basically is the difference in potential energy between metal atoms in vapor phase and those in solid phase) will be released. This energy is usually on the order of a few electron volts per atom. If this energy is directly transferred to one or two Si atoms as soon as a metal atom reaches the Si surface, it is large enough to allow the Si atom(s) break its (their) chemical bonds with the Si substrate and react with the metal atom readily without the help of thermal activation. An alternative form of energy transfer is that the metal atom passes the energy to the Si atoms surrounding it in the form of lattice vibrations and hence increases the temperature of the local crystal lattice, which in turn puts the Si atoms in a thermally activated state. From this point of view, it can be inferred that deposition rate, deposition method (e.g., evaporation and sputter etc.), the type of metal, and substrate temperature will be the main factors that determine silicide formation sequences during DDR. The effects of these factors on the reaction could be quite complex. Faster deposition rates will inject more power (i.e., energy per unit time) into the substrate surface area, which may accelerate the reaction. On the other hand, faster deposition rate means faster supply of metal atoms to the surface. If the reaction rate for a certain silicide formation is not as fast as the metal supply rate, this silicide is kinetically unfavorable. Instead, some other reaction, fast enough to consume the deposited metal atoms, may take place. This inference is in agreement with the result that a small deposition rate in the range of a monolayer per minute favors the room temperature growth of epitaxial $CoSi_2$ [158].

An interesting experimental observation is that Ni_2Si and NiSi can form in a Ti/Ni/Si sample during sputter deposition of Ti on top of Ni film that is previously deposited onto a Si substrate [170]. In this experiment, a thermocouple is attached to the back of a Si wafer. A 12 nm/min deposition rate of Ti is used. After a one minute deposition, Ni_2Si formation is observed. Further deposition results in NiSi growth as well. It is found that the highest substrate temperature is 380°C [170]. Obviously, the silicide reaction occurs because of the elevated substrate temperature which is in the range for conventional furnace annealing. The thermal effect is attributed to the highly energetic secondary electrons that are necessary for sustaining the plasma in the front of the substrate, the latent heat of Ti, and the kinetic energy of Ti and argon ions. The energy borne by these particles is transformed into heat when they arrive at the substrate [170]. It should be pointed out that the kinetic energy of these particles is usually in the range of a few hundred electron volts, i.e., about one hundred times higher than the latent heat of most metals. Therefore, this experiment is only an extreme example showing how the energy borne by free atoms and other particles can be transformed into heat to promote the metal-Si reactions.

2.5. Factors Influencing Reaction Kinetics

The main factors which affect the reaction kinetics of silicide formation are diffusion, impurities, and crystalline defects. They will be discussed in this section.

2.5.1. Diffusion in Thin Film Couples

Theoretical and experimental considerations about special aspects of diffusion in thin films have been reviewed by Balluffi and Blakely [171] and Tu [13]. When studying thin film metal-Si diffusion couples, three topics are of much interest; i.e., identification of the major diffuser, diffusivity of the moving species in the growing phase, and the effects of crystalline defects on diffusion.

Identification of the major diffuser is very important in explaining the complicated phenomena in thin film metal-silicon reactions. For instance, in the example of the simultaneous growth of two phases described above (Fig.2-2), the second phase that formed is CoSi in the Co-Si system but Rh_3Si_2 in the Rh-Si system. This difference is due to Co being the major diffuser in the former case, whereas Si is the major diffuser in the latter case.

The major diffusers in most transition metal silicides are well documented. Table 2-2 shows a summary of major diffusers determined from marker experiments [1-6, 9, 96, 107, 172-183]. It is notable, according to this table, that in V_3Si, Co_2Si, Ni_2Si, Pt_2Si,

Ru_2Si_3, Os_2Si_3, Rh_4Si_5, and most of the disilicides (with the exception of $NiSi_2$ and $CoSi_2$), the majority atoms are the most mobile. This phenomenon is called, by some authors [5, 183], an "ordered Cu_3Au effect". According to these authors [5, 183], the majority atoms constitute a continuous network on which a vacancy can easily migrate. Conversely, the motion of minority atoms requires either the coexistence of two vacancies (minority and majority) or a local destruction of the crystalline lattice. In either case the motion of the minority atoms will be characterized by an activation energy considerably larger than that for the majority atoms.

For monosilicides, such as NiSi, CoSi, PtSi, FeSi, IrSi, etc., there is no general rule for major diffusers. Even the silicides which are isostructural compounds may have different moving species. As an example, NiSi, FeSi, and IrSi all have the FeSi-B20 structure, but, from Table 2-2, metal atoms are the moving species in NiSi while Si is the major diffuser in FeSi and IrSi.

It should be pointed out that for some silicides, such as CoSi, PtSi and Pd_2Si, the identity of moving species is still controversial. Although most previous studies conclude that Si and Pt are the dominant diffusers during CoSi and PtSi growth, respectively, very recent investigations suggest that Co [173] is the major diffuser in CoSi and Si [179] is the moving species in PtSi. As for Pd_2Si, earlier experiments show that both Si and Pd diffuse during Pd_2Si formation. The result from a recent study [181] indicates that Si is the dominant diffuser while Pd will participate in mass transport only when Si motion becomes obstructed.

Experimental determination of diffusivity, D, of moving species is essential for kinetic studies. For example, in the competitive growth model [12-14], diffusivity and the effective interface reaction barrier are crucial kinetic factors in determining whether a phase can grow. If these factors for a given metal-Si couple are known, this model can be practically tested. Data for diffusion activation energies have been reported (Table 2-3). However, except for a few studies [148] in which the diffusivities and activation energies are determined from concentration profiles in the phases under consideration, all studies only provide the data of so-called apparent activation energies. This type of activation energy is obtained by assuming that the silicide growth follows a parabolic law, i.e., $x^2 \approx Dt$, (where x is the thickness of growing phase and t is annealing time) and by determining the slope of the Arrhenius plot, i.e., $\ln(x^2/t)$ versus $1/T$ plot (T is annealing temperature). The activation energy determined by this method may be a combination of activation energies for several processes since the growth of a silicide layer involves processes such as the interfacial reactions, diffusion in the phase under consideration and diffusion in adjacent phases. As such, the application of the apparent activation energy, as a diffusion

activation energy, is reasonable only when the contributions from other processes to the apparent activation energy are negligible compared with that of the diffusion process of interest.

It has been found in early studies that reaction temperatures for thin film couples are much lower than those for bulk couples [1-3, 13, 25, 167]. One of the main reasons for this is that the films generally contain high densities of point defects such as vacancies and low temperature short circuits for diffusion, such as grain boundaries and dislocations. The effects of crystalline defects on diffusion and on the reaction kinetics have been investigated by various groups. Diale *et al.* [173] find that Co atoms diffuse in both the Co layer and CoSi layer, by a vacancy mechanism, during the CoSi growth in a Co-Si thin film couple. These authors also present evidence that some of the Co vacancies in the CoSi layer are annihilated at the Co surface. Comrie and Egan report [180] that Si is the dominant moving species in both polycrystalline and epitaxial Pd_2Si growth and diffusion takes place through a vacancy mechanism. After comparing Ni_2Si formation rates in thin film couples with the values of Ni lattice and grain boundary diffusion coefficients in bulk Ni_2Si, Gas [185] has concluded that Ni_2Si formation in thin film couples is controlled by grain boundary diffusion of Ni in the growing Ni_2Si phase. A similar result is also reported by Olowolafe *et al.* [37]. Corcoran *et al.* find that Si diffusion through the grain boundaries in C54-$TiSi_2$ is the major atomic transport mechanism [141]. Some studies have provided results demonstrating how defects can affect reaction kinetics. For instance, when metal contacts of TiPdAg, MgPdAg, and NiAg to Si are capped with Ta_5O_2, the thermal reactions between the metals and Si are either suppressed or enhanced, depending on the contact system [186]. This is because the capping layer suppresses both the generation and annihilation of vacancies at the free surface of the metal which are necessary to support the reactions. In the experiment of $TiSi_2$ formation just mentioned above, it is found that, in addition to a decrease in the diffusion flux with increasing $TiSi_2$ layer thickness, the diffusion flux also decreases as the $TiSi_2$ grain size grows laterally with annealing time. As a result, a non-parabolic growth behavior is observed [141].

From the discussions in this section, it can be seen that diffusion study can be complicated significantly by the presence of a high density of defects. For example, a self diffusion coefficient measured from a bulk sample is not necessarily the same as that in a thin film sample of the same material. The high density of vacancies in the thin film will result in a smaller activation energy or larger diffusivity for self diffusion because the vacancy concentration is much higher than the equilibrium value. If during thermal reaction, the vacancies are annihilated faster than they are generated, the diffusivity will decrease with annealing time. If the metal is also the major diffuser in the growing silicide,

then both the diffusion of the metal atoms in the silicide and the reaction kinetics will be affected by the diffusivity change in the metal film. Adding impurity effects (please see the next section) complicates the diffusion process even more.

Considering the complexity of diffusion in thin film couples, it seems that the original motivation of diffusion studies, i.e., finding the relation between diffusion and reaction kinetics as well as the formation sequences, is unreachable. Actually, it has been somewhat ignored that the solid state reactions in metal-Si couples take place only at the interfaces between various phases. From this point of view, a knowledge of the major diffuser, its flux at a given interface and the composition of the growing phase at this interface is enough to study the effects of diffusion on silicide reaction kinetics. A simple method for determining the difference in diffusion fluxes, ΔJ ($\Delta J = J_{in} - J_{out}$, where J_{in} and J_{out} are the fluxes into and out of the interface under consideration) at reactive interfaces has been developed in this study. The details of the method will be described in Chap.3. The primary advantage of this method is it allows the diffusion flux, ΔJ (for convenience, ΔJ is referred to as diffusion flux, instead of "difference of diffusion fluxes"), to be estimated without knowing the information about diffusivities, concentration or chemical potential gradients, defect densities, and the change of diffusivities with concentrations and defect densities, etc. In addition, by linking the diffusion flux at a given time with the phase that is growing at the interface at the same time, the relation between diffusion and silicide formation sequences is made evident.

2.5.2. Impurity Effects

Impurities are usually introduced for various reasons, such as impurities incorporated in metal films during deposition, impurities implanted into substrates, and impurities diffused into thin films from the annealing environment.

Impurity effects on silicide formation kinetics have been investigated by a number of groups [6, 35, 45, 49-51, 184, 187-195]. These effects can be divided into two categories. One of these is the effect of impurities on the diffusion of the moving species. The other is the competition between impurity-metal compound formation and silicide formation.

It has been found that impurities can greatly decrease the diffusivity of the moving species. For example, increasing partial pressures of O_2 during Pt depositions causes Pt_2Si growth rates to decrease by up to a factor of 20 and causes changes in the formation sequence [35]. When a Pt-Si couple is annealed in a UHV system, the diffusion coefficient of Pt in this couple is about one order of magnitude higher than that in a Pt-Si couple annealed in a conventional furnace [6]. In another experiment with a Ni-Si thin film

couple, it has been found that oxygen diffuses through the Ni film to form SiO_2 at the silicide/metal interface, which prevents further Ni transport to the reactive interface [49]. A similar situation is also observed in refractory metal-Si thin film couples [187-189], where the difference is that diffusion of the moving species, Si, instead of metal, is blocked by SiO_2 formation at either the refractory metal/Si interface or the refractory metal/silicide interface. Dopants (B, P, and As), which are implanted into Si substrates before metal deposition and thermal annealing, also have significant effects on the diffusivity of moving species. For instance, it is reported that segregation of As and P at the interface slows down Si diffusion which delays silicide growth in Co-Si [190], Ti-Si [191, 192] and W-Si [193] thin film couples, respectively.

The most important consequence of decreasing diffusion flux probably is that the critical thicknesses, required for inducing new phase formation, are decreased. This results in multiple phase growth even in thin film couples. For example, when a Pt-Si couple with an oxygen doped Pt film is annealed, the rapid decrease of diffusion flux induces PtSi formation at the Pt_2Si/Si interface in the presence of unreacted Pt [45, 50, 51]. However, in purer Pt-Si couples, PtSi will not begin to form until all the Pt is consumed. Similar phenomena are also observed in the Ni-Si system [49] and in the Mo-Si system, where Mo_5Si_3 forms at $MoSi_2$/Mo interface. At this point, it should be emphasized that Pt and Ni are the major diffusers in Pt-Si and Ni-Si couples, respectively, while Si is the moving species in Mo-Si couples. The results suggest that there must exist a strong connection between diffusion flux, critical thicknesses and silicide formation sequences.

The second type of impurity effect, i.e., the competition between impurity-metal compound formation and silicide formation, has not been studied as extensively. In one case, the dopant, B, forms a stable tungsten boride compound during annealing of a W-Si thin film couple, which normally forms WSi_2 [192]. The growth of WSi_2 is strongly retarded by the boride formation. In another example, a Si-deficient, oxygen-rich Ti-Si-O sublayer forms at the Ti/$TiSi_2$ interface when a Ti-Si thin film couple with a high oxygen concentration is annealed, by RTA, between 550°C and 600°C [188]. It is found that this Ti-Si-O layer is composed of TiO_x and $TiSi_2$ compounds, which also slow down $TiSi_2$ growth. It seems that this type of impurity effect requires a high impurity content. This high content of impurity is unusual in most metal-Si thin film couples for microelectronic applications, which probably accounts for the lack of documented experimental results.

2.5.3. Crystal Structure and Orientation of Substrates

It should be noted, in Table 2-3, that the apparent activation energies for Ni_2Si, NiSi, PtSi and Pd_2Si formation are different for each respective silicide to grow on different

substrates. It is interesting that the activation energy for the formation of each of these silicides on (100) Si substrates is smaller than that for the same silicide to form on (111) Si [37, 95, 111, 184]. Olowolafe *et al* [37] find that when thin Ni films deposited onto various substrates are annealed from 200°C to 325°C, only Ni_2Si, forms on (100), (111) and polycrystalline Si substrates, while simultaneous growth of two phases, Ni_2Si and NiSi, is observed in Ni-amorphous Si (vacuum deposited) thin film couples. In addition, it is found that the growth rates of Ni_2Si depend on the substrates. On (100), polycrystalline and amorphous Si substrates the rates are similar, which are four times higher than on (111) Si [31]. The slower growth of Ni_2Si on (111) Si is attributed, by the authors, to slower Ni grain boundary diffusion due to the larger grain size of Ni_2Si. Majni *et al* also report that the growth rate of NiSi on (100) Si is significantly higher than on (111) Si [95]. Zheng *et al* (97) find that $NiSi_2$ grows at the expense of NiSi when the $NiSi_2$/NiSi bilayer is in contact with evaporated Si (i.e., a configuration of NiSi/$NiSi_2$/amorphous Si) at 450°C, whereas $NiSi_2$ dissociates into NiSi and Si when the bilayer is in contact with single crystal Si at the same temperature. All these results suggest that the crystalline structure and the orientation of Si substrates have significant effects on silicide formation kinetics. Furthermore, it is well known that Ni and Pt are the major diffusers during Ni-Si and Pt-Si reactions. Therefore, these effects cannot be explained by the possible difference in Si diffusion in crystalline and amorphous substrates.

Very recently, Losch [28] proposed a kinetic model to explain substrate effects on silicide and SiO_2 growth kinetics. This model is based on two assumptions: 1) There is a limited number n_r of initial reaction centers on the substrate surface. This number depends on the surface structure and is generally smaller than the total number n_s of surface atoms. 2) The n_r reaction centers determine, from the very beginning of the interaction, the number n_c of easy mass transport channels, which in turn determine all the later growth processes. It is argued [28] that a reconstructed Si substrate surface is inhomogeneous in terms of the structure of free surface atomic sites, which may result in different reactivities of the surface atomic sites. According to the author, the reaction centers are the Si surface atomic sites with high reactivity and the easy mass transport channels are actually short circuits for diffusion, such as grain boundaries and dislocations. The number n_c depends on the ratio of n_r/n_s, which means that the short circuits will not change during the reaction, as long as they are formed. This model has been used to explain qualitatively some of the observed kinetic behavior in terms of substrate surface structure [28]. The model has two main disadvantages: 1) The method for determining n_r and n_c is unclear. It is questionable that the short circuits for diffusion are exclusively determined by the reactive atomic sites in a few surface layers, especially in those thin film couples where metal atoms are the moving

species. 2) It is unlikely that n_c remains constant during silicide growth if factors such as stress change, grain growth, and point defect density change, are taken into account. In addition, real time observations of the oxidation process of Si by TEM [196, 197] demonstrate that the oxidation reaction on (111) Si substrate takes place one atom layer at a time, which disagrees with the reaction center assumption.

2.6. Theories and Models for Silicide Formation

Many theories and models have been proposed to explain experimental phenomena of transition metal silicide formation in thin film couples or predict silicide formation sequences [5, 6, 10-28]. The theories and the models from early studies have been reviewed by a number of authors [1-9]. In this section these theories and models, together with those from recently published papers [16, 17, 22-28], will be briefly introduced and discussed.

2.6.1. Silicide Growth Kinetics

Kinetic behavior of silicide formation is determined by monitoring the silicide growth process. The most often used techniques in these investigations are Rutherford backscattering spectrometry (RBS) and x-ray diffraction (XRD). During the last few years, XTEM techniques have become more and more popular in the areas of metal/Si interface characterization and silicide growth kinetics investigation. Since this technique has much better spatial resolution and, therefore, is more accurate and reliable, it provides many valuable results for kinetic studies.

Silicide formation kinetics can be classified into three types, i.e. diffusion controlled processes, interface reaction controlled processes, and nucleation controlled processes. The first two types of kinetics are used to describe layered growth processes. These two types of kinetic processes are studied by monitoring the thickness change of the growing silicides with annealing time. If the thickness is a linear function of the time, the growth process is classified as an interface reaction controlled process. If the thickness is a parabolic function of of annealing time, the growth process is called a diffusion controlled process [1-9].

The other type of kinetics is used to explain island growth of silicides. In layered growth processes silicides nucleate almost simultaneously at the entire interface between the metal and Si substrate and then grow in one dimension. However, in an island growth process, silicides nucleate first at some points of the interface and then grow in three

dimensions [5, 7, 9, 20, 41]. Therefore, this type of kinetics is nucleation controlled. Each type of kinetics will be discussed below.

2.6.1.1. Diffusion Controlled and Interface Reaction Controlled Processes

Gösele and Tu [12-14] have derived an expression for silicide growth rate in a thin film metal-Si couple. Similar expressions have also been developed by other researchers [5, 17, 18, 24, 25]. Since Gösele and Tu's expression is the first that introduces the concept of interface reaction barrier (an alternative concept is interface reaction constant) into silicide growth kinetics and has a concise form, only this expression is discussed here. Starting from the assumptions that the silicide layer, β, may be characterized by an essentially constant chemical interdiffusion coefficient D^*_β, a steady state of diffusion fluxes, and compound formation only occurring at the interface, Gösele and Tu [12] derived the following expression for β layer growth rate.

$$\frac{dx_\beta}{dt} = \frac{G_\beta \, \Delta C^{eq}_\beta \, k^{eff}_\beta}{(1 + x_\beta k^{eff}_\beta / D^*_\beta)} \qquad (2\text{-}3),$$

where x_β and t are the silicide layer thickness and annealing time, respectively, k^{eff}_β is a constant and is called the effective interfacial reaction barrier, ΔC^{eq}_β is the difference between the equilibrium concentrations of the diffuser at the two interfaces of the β layer, and G_β is a constant determined by the compositions of the involved phases.

From Eq.(2-3), a changeover thickness x^*_β can be defined by

$$x^*_\beta = \frac{D^*_\beta}{k^{eff}_\beta} \qquad (2\text{-}4).$$

It can be seen that the growth kinetics described by Eq. (2-3) are different below and above the changeover thickness. It follows that

$$\frac{dx_\beta}{dt} \approx G_\beta \Delta C^{eq}_\beta k^{eff}_\beta, \quad \text{or} \quad x_\beta \propto t, \quad \text{for } x_\beta << x^*_\beta \qquad (2\text{-}5);$$

$$\frac{dx_\beta}{dt} \approx G_\beta \Delta C^{eq}_\beta \frac{D^*_\beta}{x_\beta}, \text{ or } \; x_\beta \propto \sqrt{t}, \text{ for } x_\beta >> x^*_\beta \qquad (2\text{-}6).$$

Eq.(2-5) and (2-6) indicate that the growth process is interface reaction controlled when $x_\beta << x^*_\beta$, whereas the growth process is diffusion-controlled when $x_\beta >> x^*_\beta$. According to Gösele and Tu [12-14], whenever planar growth of a compound takes place, it should pass through two stages. Initially, growth will follow interface controlled kinetics. After the layer has grown so that the condition $x_\beta >> x^*_\beta$ is satisfied, the process will change over to diffusion controlled growth kinetics. This theory can explain many cases well, where a thickness against time relationship has been experimentally established, such as WSi_2, $MoSi_2$, $TiSi_2$, etc. For these silicides, when bulk diffusion couples are used, the growth kinetics is diffusion controlled [3]. But, when thin-film couples are used, in most observed cases, the processes for the growth of WSi_2, $MoSi_2$, and $TaSi_2$, etc. are interface controlled [2, 5]. The implication is that the thicknesses of the silicide layers obtained in thin film couples are smaller than the changeover thicknesses for these silicides. More recently, linear time dependence of amorphous MSi alloy (where M is metal) layer growth has been experimentally observed [105, 106, 133, 137, 138].

On the other hand, there exist shortcomings in these types of expressions. First, in most cases, the effective interfacial reaction barrier, or alternatively the interfacial reaction constant, is not experimentally measurable [17, 26] so that the prediction of the kinetic behavior transition from an interfacial controlled process to a diffusion controlled process is impossible. In fact, the growth kinetics for the formation of many silicides in thin film couples, such as Ni_2Si, NiSi, Co_2Si, CoSi, Pt_2Si, PtSi, Pd_2Si, FeSi, IrSi, HfSi, MnSi and RhSi, has been reported to be diffusion controlled [2, 5]. It is not known whether this is because the changeover thickness, x^*_β, is too small to be detected or because there is no interfacial controlled process occurring during silicide growth at all. Secondly, the physical meaning of the effective interfacial reaction barrier is not very clear. According to Gösele and Tu [12], the reaction barrier may arise from the rearrangement of the atoms at the interfaces required for the growth of a compound layer. From investigations of WSi_2, however, it has been found that the so called interface barrier for WSi_2 formation is in fact an oxide layer, which prevents Si atoms from penetrating the interface and therefore delays the WSi_2 reaction [198-200]. It is also reported that the formation of this oxide layer may

be thermodynamically driven and that the layer can even appear at the original clean interface after W film deposition, if the diffusion of oxygen in the metal film is rapid enough [199]. After special techniques, such as ion beam mixing, are used to break down the oxide layer already formed, the growth of WSi_2 is found to follow diffusion controlled kinetic behavior [199-201].

2.6.1.2. Nucleation Controlled Processes

Nucleation controlled processes for silicide formation have been reviewed by d'Heurle and Gas [5, 7, 20]. They use classical nucleation theory to discuss the phenomena encountered in thin film reactions. According to the classical theory of nucleation, the activation energy ΔG^* for a new phase AB forming at an interface between two phases A and B, is proportional to $\frac{(\Delta\sigma)^3}{(\Delta G)^2}$. $\Delta\sigma$ indicates the increase in surface energy, because two interfaces A/AB and AB/B replace the original A/B interface during AB formation; ΔG is the free energy change per unit volume of AB and is given below:

$$\Delta G = \Delta G_c - \Delta H_d \qquad (2\text{-}7).$$

ΔG_c is the change in "chemical" free energy per unit volume of AB due to the formation of the new phase and ΔH_d is the deformation energy term due to the volume change caused by phase transformation. Therefore, ΔG^* can be written as:

$$\Delta G^* \propto \frac{(\Delta\sigma)^3}{(\Delta G_c - \Delta H_d)^2} \qquad (2\text{-}8).$$

According to d'Heurle and Gas [5, 7, 20], in general, when metals and silicon react with one another to form silicides, the absolute value of the ΔG's is large and the ΔG^*'s are then small. As a result, nucleation is so easy and rapid that one cannot isolate it and observe it experimentally. There are, however, two types of silicide reactions whose nucleation processes are rather slow, so that the growth processes of these silicides show an island growth behavior.

One example of these two reactions is rare earth metal (R.E.)-Si reactions to form silicides with a formula $(R.E.)Si_{1.7}$ [202, 203]. In this type of reaction, the silicon atoms are very mobile [182, 204] because they act like interstitials. The silicon sublattice contains 15% vacancies, since the structure is that of AB_2 but the composition is $R.E.Si_{1.7}$. The relatively high mobility of Si atoms allows the growth of silicides at low temperatures

(about 300°C). On the other hand, the metal atoms in the silicides do not become mobile until extremely high temperatures, on the order of 1000°C. Therefore, when the silicides are formed at low temperatures (such as around 300°C), the deformation stress can not be relaxed easily. The result is a large ΔH_d and small $|\Delta G_c - \Delta H_d|$. Consequently, ΔG^* is large and the growth of these silicides is nucleation controlled.

The other type of nucleation controlled reaction is observed in the following silicides: $Mn_{11}Si_{19}$ [41, 53], $NiSi_2$ [5, 7], $ZrSi_2$ [5], Rh_4Si_5 [204], Rh_3Si_4 [204], PdSi [5, 7], $HfSi_2$ [5], $OsSi_2$ [5], and $IrSi_3$ [5]. In this case, ΔG_c is very small and causes ΔG^* to be so large that the growth process becomes nucleation controlled. For example, in the formation of $NiSi_2$ [5, 7], the reaction of Ni with Si results in diffusion controlled formation of Ni_2Si and NiSi at temperatures below 500°C. After total formation of NiSi (no Ni or Ni_2Si remaining), further heating does not cause any other change until about 800°C. Then, the sudden formation of $NiSi_2$ in islands is observed. The islands spread through the whole thickness of the films. In this process, the equation for the reaction is

$$NiSi + Si = NiSi_2 \qquad (2\text{-}9)^*,$$

because the NiSi layer already exists on the Si substrate. Thus, the "chemical" free energy change for this reaction, instead of being the free energy of $NiSi_2$ formation, $\Delta G^f_{NiSi_2}$, should be the difference between $\Delta G^f_{NiSi_2}$ and the free energy of NiSi formation, ΔG^f_{NiSi}, i.e. $\Delta G_c = \Delta G^f_{NiSi_2} - \Delta G^f_{NiSi}$. Since these two quantities of free energy of formation are nearly equal, ΔG_c is close to zero. This causes ΔG^* to be large. At temperature T*, where nucleation occurs, the diffusion coefficients are quite large so that growth of the nuclei is extremely rapid [5, 7]. The theory of nucleation-controlled growth described above can quantitatively explain island growth in the two types of silicide formation quite well, although, according to d'Heurle and Gas [5, 7], more work needs to be done for the model of $R.E.Si_{1.7}$ formation.

---

* Eq.(2-9) is not correct if the fact that Ni is the major diffuser during $NiSi_2$ growth [1-4, 6, 9, 97] is taken into account. The reaction is completed in two steps $2NiSi \rightarrow NiSi_2 + Ni$ at $NiSi/NiSi_2$ the interface and $Ni + 2Si \rightarrow NiSi_2$ at $NiSi_2/Si$ interface. In this case, ΔG_c is positive for the first step. However, d'Heurle and Gas's argument about small ΔG_c and large ΔG^* is correct if it is assumed that Eq.(2-9) is correct.

2.6.2. Kinetic Models for Silicide Formation

According to Thompson [26], two general approaches to analyzing the kinetic constraints on phase selection have been pursued, one based on competitive growth arguments, and the other based on constraints on nucleation. For the convenience of the following discussion these approaches are called the competitive growth approach and the competitive nucleation approach respectively. The kinetic models will be briefly discussed in two groups according to their approaches. Since some basic diffusion theories are involved in the following discussion, this section will start by introducing classical theory governing diffusion reactions in bulk couples.

2.6.2.1. Kinetics of Layered Growth in Bulk Couples – Kidson Approach

Growth kinetics of multiple phase systems in binary bulk couples have been treated by Kidson [29] and Wagner [30] in the 1960's and later by other authors [31, 32]. Since the results from various approaches are very similar, only those derived from Kidson are discussed here. By assuming that the concentrations at the interface are constant and equal to the equilibrium values and by applying Fick's first law and the Boltzmann theorem, Kidson obtained the following expressions for the layer thickness of a growing phase, β, between phases α and γ in an A-B binary bulk couple.

$$x_\beta = B_\beta \sqrt{t} \qquad (2\text{-}10),$$

$$B_\beta = 2\left\{\left(\frac{(DK)_{\gamma\beta} - (DK)_{\beta\gamma}}{C_{\beta\gamma} - C_{\gamma\beta}}\right) - \left(\frac{(DK)_{\beta\alpha} - (DK)_{\alpha\beta}}{C_{\alpha\beta} - C_{\beta\alpha}}\right)\right\}\frac{1}{\sqrt{t}} \qquad (2\text{-}11).$$

Here, x_β and t are the β layer thickness and annealing time, the subscripts $\gamma\beta$ and $\beta\gamma$ represent each side of an interface so that $C_{\beta\gamma}$, $C_{\gamma\beta}$, and $C_{\beta\alpha}$, $C_{\alpha\beta}$ represent the equilibrium concentrations of element A at each side of the β/γ and α/β interfaces respectively. D is the interdiffusion coefficient and K is a constant that implicitly depends on all of the diffusion coefficients in the system since

$$K = \sqrt{t}\frac{\partial}{\partial x} C(x, t, D_\alpha, D_\beta, \ldots D_n) \qquad (2\text{-}12).$$

This is the well known parabolic growth law. Eq.(2-12) suggests that in a multiple phase system, the thickness of any phase, as a function of time, depends only on the eight parameters (D and K) within that phase and its two immediately adjacent phases.

Kidson has discussed the physical meaning of B_β [29]. When $B_\beta > 0$, the rate of formation of the new β phase from the γ phase is larger than the transition of the β phase to the α phase and consequently, the thickness of the β increases with time. When $B_\beta < 0$, the rate of supply of A element from the α to β phase is so fast compared to the flow rate in the β phase that a "pile-up" of excess material occurs resulting in the direct transformation of α to γ. In this case, no β phase would appear in the diffusion region. When $B_\beta = 0$, the situation is similar to $B_\beta < 0$, i.e., again no β phase appears. Therefore, it is possible for some phases to be absent from the diffusion region from a kinetic point of view. Kidson has, however, ruled out these latter two cases, i.e., $B_\beta \leq 0$. The situation where $B_\beta \leq 0$ would imply an infinite chemical potential gradient at the α/γ interface, which is contrary to the thermodynamic requirement that the chemical potential (μ_A) be continuous and monotonic throughout the bulk couple. From these results it is concluded that all equilibrium phases should be present [29-32]. It is found that the parabolic growth law agrees with experimental results when the diffusion region in a bulk couple is sufficiently large [29-32].

However, experimental observations, particularly XTEM and HRTEM observations of the interfaces in thin film couples and lateral diffusion couples, have shown that single phase and multiple phase sequential growth are the general characteristics of diffusion reactions in binary couples (please see Secs.2.1 and 2.2). Therefore, the parabolic growth law itself cannot explain the phenomenon of sequential growth. In addition, Tu [22] also pointed out that, according to the parabolic law, the growth velocity is inversely proportional to the layer thickness. Thus, an existing phase cannot vanish, since the velocity will become extremely large as the thickness approaches zero. But, it is demonstrated by competitive growth experiments that a phase already formed in a thin-film couple does vanish under certain conditions. In the experiment [13, 37], a thin Co layer was deposited onto a CoSi layer, previously formed on a Si substrate. When the specimen (Co/CoSi/Si) was annealed at 460°C, it was found that a Co_2Si layer began to grow at Co/CoSi interface and that the existing CoSi layer, instead of growing, began to shrink so that the configuration of the specimen became Co/Co_2Si/CoSi/Si. Upon further annealing, the growth of Co_2Si dominated at the expense of CoSi and Co. Finally, CoSi vanished leaving a Co/Co_2Si/Si structure . Then, with continued annealing, Co_2Si grew until all the Co was consumed. CoSi then reappeared between Si and Co_2Si, i.e., the configuration of the specimen changed to Co_2Si/CoSi/Si, and CoSi grew by consuming Co_2Si and Si. The same phenomena were also observed when Co was replaced with Ni or Pt [6, 205]. It is obvious that the parabolic growth law cannot explain the disappearance of phases, which have already nucleated and grown.

In general, as is pointed out by Dybkov [17], the coexistence of all or most of equilibrium phases in multiphase binary systems is the exception rather than the rule. According to Gösele and Tu [19] and Dybkov [17], the failure of classical diffusion theories in predicting sequential phase formation occurs because only diffusion processes are taken into account in these theories. In fact, diffusion of reactants is only a necessary but not a sufficient step for a compound layer to grow. This step should be followed by a chemical reaction or an interfacial reaction step [17]. Therefore, Gösele and Tu [19] emphasize that for treating sequential phase formation, interfacial reaction barriers leading to finite reaction constants κ have to be introduced.

2.6.2.2. Competitive Growth Approach

A competitive growth model for silicide formation in thin film couples was proposed first by Gösele and Tu [12-14]. Later, an almost identical model was also developed by d'Heurle and Gas [5] using a slightly different mathematical derivation. More complex models derived from analytical solutions of diffusion equations and interfacial reaction rate equations [18, 24], or from physicochemical considerations of interfacial reactions [17, 25] have also been proposed independently. In spite of the variety of the expressions for silicide growth rates derived from these approaches, all the models share a common feature, i.e., the interfacial reaction constant term or effective interfacial reaction barrier is incorporated into the expressions. Consequently, these models are able to qualitatively explain sequential phase formation in thin film couples. The interfacial reaction constant, according to Dybkov [17], indicates the reactivity of a given solid (such as Si or a silicide) surface, while the effective interfacial reaction barrier, as stated by Gösele and Tu [19], describes the energy barrier associated with changes in atomic arrangements or effects due to volume changes at the interfaces.

Because of the similarity of these models in terms of their basic assumptions, their results, and their explanation of sequential phase formation, only one of them, Gösele and Tu's model, is selected to be briefly reviewed. This model involves both interface reaction controlled and diffusion controlled processes. The flux of A atoms into the $A_\gamma B$ phase, J_γ^A, is given by the following:

$$J_\gamma^A = \frac{\Delta C_\gamma^{eq} k_\gamma^{eff}}{(1 + x_\gamma k_\gamma^{eff}/D_\gamma^*)} \qquad (2\text{-}13).$$

where ΔC_{γ}^{eq}, k_{γ}^{eff} and D_{γ}^{*} have the same meaning as they do in Eq.(2-3) but are for the $A_{\gamma}B$ phase. The flux in $A_{\beta}B$ has a similar expression. According to Gösele and Tu [12], because of the nature of the competitive growth, the growth rate of the two phases, β and γ, should be

$$\frac{dx_{\beta}}{dt} = G_{\beta}J_{\beta}^{A} - G_{\beta\gamma}J_{\gamma}^{A} \qquad (2\text{-}14),$$

$$\frac{dx_{\gamma}}{dt} = G_{\gamma}J_{\gamma}^{A} - G_{\gamma\beta}J_{\beta}^{A} \qquad (2\text{-}15);$$

where G_{β}, G_{γ}, $G_{\beta\gamma}$, and $G_{\gamma\beta}$ are constants determined by the compositions of the related compounds in the diffusion couple. Eq.(2-14) and (2-15) represent the growth conditions of the $A_{\beta}B$ and $A_{\gamma}B$ layers. If $\frac{dx_{\beta}}{dt} > 0$, the $A_{\beta}B$ layer will grow. From Eq.(2-14), this condition can also be expressed as

$$\frac{J_{\beta}^{A}}{J_{\gamma}^{A}} > \frac{G_{\beta\gamma}}{G_{\beta}} = r_1 \qquad (2\text{-}16).$$

Similarly, the growth condition for the $A_{\gamma}B$ layer is

$$\frac{J_{\beta}^{A}}{J_{\gamma}^{A}} < \frac{G_{\gamma}}{G_{\beta\gamma}} = r_2 \qquad (2\text{-}17).$$

In Eq.(2-16) and (2-17), r_1 and r_2 are constants, and it can be proven that

$$r_2 > r_1 \qquad (2\text{-}18).$$

Based on these conditions, Gösele and Tu defined a convenient parameter for single phase growth kinetics, in terms of the flux ratio, i.e.,

$$r = \frac{J_{\beta}^{A}}{J_{\gamma}^{A}} \qquad (2\text{-}19).$$

Applying this parameter, r, combined with Eq.(2-5) and (2-6) (see Sec.2.6.1.1) and Eq.(2-13) (Sec.2.6.2.2), they analyzed and discussed various possibilities related to the thin-film diffusion couples as summarized in Table 2-4 and Fig.2-7. From Table 2-4, it can be seen that r is a factor indicating how the two phases compete with each other to grow. If the thicknesses of the both phases are smaller than their own changeover thicknesses, the competition is between the interfacial reactions for each respective phase (Fig.2-7a). When the layer thickness for one phase is larger that its changeover thickness, but the thickness of the other phase is smaller than its own changeover thickness, the competition is between the diffusion process in the former and the interfacial reaction for the latter (Figs.2-7b and 2-7c). Depending on the r values, the results of competition will be that either one phase grows and the other shrinks or both phases grow at the same time.

In their analysis and explanation of single phase growth kinetics, the most important point is the critical thickness of phases (β and γ), x_β^c and x_γ^c. Below these thicknesses only single phase ($A_\beta B$ or $A_\gamma B$) growth actually occurs, whereas above these critical values simultaneous growth of two phases must result. This point has, in fact, become the basis of all explanations about these unique phenomena in thin-film reactions.

From Table 2-4 and Fig.2-7, it can be seen that single layer growth can be explained as follows. If there is unlimited supply of A and B, sooner or later, $A_\gamma B$ (assuming it forms first) can grow and exceed x_γ^c. At this point, two compounds ($A_\gamma B$ and $A_\beta B$) grow at the same time. If the material supply, for example B, is consumed before $x_\gamma > x_\gamma^c$, the thickening process of $A_\gamma B$ will stop. After a short transition period a new steady-state diffusion situation will develop, which may approximately be described by $J_\gamma^A = 0$. Thus, Eqs.(2-14) and (2-15) change to

$$\frac{dx_\beta}{dt} = G_\beta J_\beta^A > 0 \qquad (2\text{-}20),$$

$$\frac{dx_\gamma}{dt} = -G_{\gamma\beta} J_\beta^A < 0 \qquad (2\text{-}21);$$

which indicate that $A_\beta B$ will form and grow whereas $A_\gamma B$ will shrink. This theory has been used to explain the competitive growth of Co_2Si and CoSi, Ni_2Si and NiSi, as well as Pt_2Si and PtSi. It is successful in proving that an existing phase can vanish due to kinetic

reasons. It can also qualitatively explain some other cases where single phase growth takes place and is helpful in understanding the effects of diffusion on the growth sequence.

There exist some problems with competitive growth models. The first is that no experimental data for the effective interfacial reaction barrier are documented. In most thin film metal-Si systems, it is impossible to determine these constants experimentally because no interfacial reaction controlled process has been observed in these systems. Without knowing the values of these constants, the predictive capability of these models is limited [26]. The second, as stated by Thompson [26] and by Gösele and Tu [12], is that the competitive growth approach does not consider the possibility of metastable phase formation. As a result, these models cannot predict and explain SSA and other metastable phase formation [26]. The third problem is that some results deduced from particular model(s) do not agree with the experimental results in the literature. For example, Tu [13, 14] pointed out, according to Gösele and Tu's model, that only the phase with the fastest growth rate can form. This may not be true. In the Ni-Si lateral diffusion couple experiment (see Fig.2-1 and Sec.2.1), after Ni_2Si and NiSi form, Ni_3Si_2 starts to grow and the interface between Ni_2Si and Ni_3Si_2 moves opposite to the Ni flux. This indicates that $J_{Ni3Si2} \geq J_{Ni2Si}$. From other investigations, Ni_3Si_2 has the largest thickness in bulk couples [40, 42], i.e., Ni_3Si_2 has the fastest growth rate. However, it is not the first phase appearing in the thin-film couple, and it does not appear in the single phase formation sequence. Another example is from Dybkov's model [17]. According to the model, the initial phase (or phases) in a metal-Si system is exclusive and determined only by the interfacial reaction constants of all the phases in that system. This is not in agreement with the experimental results showing different first phase formation (please see Table 2-1).

2.6.2.3. Competitive Nucleation Approach

In this approach, it is considered that phase formation requires nucleation as an initial step [11], so that the silicide formation sequence (or called phase selection by some authors) is determined by nucleation competition among all phases that have a thermodynamic driving force to form. Many researchers have discussed nucleation [5, 7, 10, 11, 16, 20-23, 26, 206]. Based on non-classical heterogeneous nucleation theory, Allen and Sargent [206] have suggested that the following factors should be taken into account in order to model nucleation during interfacial reaction in real systems: 1) The thermodynamic driving forces and the influence of gradient energy contributions (i.e., the free energy increase due to a steep concentration gradient in a nonuniform solution with respect to a uniform solution); 2) interfacial structures, compositions and energies; 3) relative diffusion rate, including the influence of the initially steep concentration (chemical

potential) gradients; 4) elastic distortion energy contributions; 5) prenucleaction state of the interface, including its structure and cleanliness; and 6) the influence of small concentrations of certain elements such as phosphorus. As is pointed out by these authors, obviously, we are a long way from putting together a theory which can incorporate all of these demands. Actually, almost all competitive nucleation models proposed up to date include only one or two of the factors listed above. These approaches will be discussed separately depending on which factor(s) is (are) incorporated in respective model(s).

The influence of gradient energy contribution has been discussed by Allen and Sargent [206]. They emphasized that the gradient energy is comparable to the macroscopic chemical driving force for the interface reaction when a steep concentration gradient exists in a distance of a few atom diameters. Consequently, the contribution of gradient energy to the overall driving force is not negligible. After considering the effects of the original interface in a binary diffusion couple on heterogeneous nucleation, they concluded that non-classical heterogeneous nucleation theory, which incorporates the contribution of gradient energy to the overall energy of the system during nucleation, is applicable to model interfacial reactions in thin film metal-Si couples [206]. However, there is no such model in the literature, as far as the author knows.

The effects of thermodynamic driving force, ΔG_c, interfacial energies, $\Delta\sigma$, and elastic distortion energy, ΔH_d, on nucleation have been examined by d'Heurle and Gas [5, 7, 20] in terms of a nucleation energy barrier. Using classical nucleation theory (i.e., in this theory no gradient energy is taken into account), these authors showed that the nucleation energy barrier, ΔG^*, is a function of ΔG_c, $\Delta\sigma$ and ΔH_d. If $\Delta\sigma$ and ΔH_d were known, the prediction of first phase nucleation could be achieved by comparing the activation energies for various phases to nucleate. The phase with smallest ΔG^* will form first because, from classical nucleation theory [7], the nucleation rate exponentially depends on ΔG^* (i.e., $\exp\{-\Delta G^*/k_BT\}$). This type of model, according to Thompson [26], has limited predictive capability due to its dependence on unknown factors such as $\Delta\sigma$ and ΔH_d. It is also questionable whether this approach can predict metastable phase nucleation in cases where metastable phases are known to form first, even though calculations of the driving force for nucleation indicate no barrier to the formation of stable phases.

The influence of interfacial structures and compositions on nucleation has been incorporated into various models [10, 11, 16, 21-23]. In the Walser and Bené rule [10], Tsaur et al rule [11] and Pretorius model [21, 22], the interfacial composition is a key factor determining which phase will nucleate. Walser and Bené postulate that the original interface in a thin film couple consists of a "metallic glass" due to thin film deposition (which is already observed in many metal-Si systems), and that the "glass" has a

composition near the lowest- temperature eutectic in the binary system (this still needs to be verified experimentally). From this postulation, they expect that the first phase to nucleate should have a composition close to that at the eutectic point. Similar arguments are adopted by Tsaur et al [11] and Prestorius [21, 22]. When developing a new kinetic model for silicide nucleation, Bené [16] pointed out that many metal-metalloid glasses display a significant local preferred ordering around either the metalloid, or around the metal, and this preferred local ordering occurs over significant regions of glass composition. If the ordering also takes place in the metallic glass at the original metal/Si interface in a thin film couple, when crystalline compounds compete with each other to nucleate, the phase with its structure similar to that of the ordered clusters in the glass layer will nucleate first. Whether the amorphous layers at the metal/Si interfaces have the ordered clusters is still open to question, as no experimental evidence has been found. Bené also qualitatively compared the interfacial energies and found that at an interface in a diffusion couple, the total interfacial energy for a new compound with one coherent interface and one incoherent interface is about the same as that for an amorphous phase, but is about half of that for a compound with two incoherent interfaces. Thus, he concluded that the first two phases will preferentially nucleate according to the interfacial energy. The main problems associated with these approaches are: 1) They are only qualitative and, in particular, the actual composition and structure of the amorphous layers are unknown, so that predictions from these models are still empirical. 2) The arguments involving the interfacial concentrations and structures cannot explain why amorphous phase growth, instead of crystalline phase nucleation, takes place at the very beginning of the reactions. 3) These approaches, except Bené's new model, ignore the effects of diffusion on interface compositions and nucleation.

The effects of relative diffusion rates on nucleation have been discussed by Thompson [26]. According to the author, interdiffusion and self-diffusion play important roles in phase selection (i.e., formation sequence). While the relative rates of nucleation are ultimately controlling in phase selection, nucleation is controlled by interdiffusion, and the nucleation rates are controlled, not only by the barriers to nucleation (including chemical free energy change and interfacial energy change, according to nucleation theory), but also by the diffusion required to form critical sized clusters of the product phases. Based on this argument and a number of assumptions, an expression for SSA in a A-B binary couple has been derived as:

$$\frac{D_{B\ in\ \beta}}{D_{A\ in\ \beta}} << \frac{4}{3}\lambda^2 k_B T \frac{\sigma_{\beta x}}{\Delta \bar{g}^2} \quad (2\text{-}22),$$

where β is a limited solid solution of A in B, $D_{B\ in\ \beta}$ and $D_{A\ in\ \beta}$ are the self-diffusion coefficients of B and the diffusivity of A in B, λ is the average jump distance of A atoms, $\sigma_{\beta x}$ is the interface energy between β and a crystalline compound X (for simplicity, it is assumed that there is only one compound in the A-B binary system), $\Delta\bar{g} = \Delta g_v + (\Delta\sigma)\lambda^2$ where Δg_v and $\Delta\sigma$ are the chemical free energy change and interfacial free energy change respectively due to X formation at the interface. This expression indicates that if $D_{B\ in\ \beta} <<$ $D_{A\ in\ \beta}$, or if $\sigma_{\beta x}$ is large and $\Delta\bar{g}$ is small, SSA will occur. This model is qualitatively in agreement with the experimental observations that SSA is usually observed in the binary diffusion couples in which one component has a much larger diffusivity in the other. The advantage of this model is its emphasis on the important roles of diffusion in nucleation and nucleation rates which have been ignored by most competitive nucleation approaches.

Various competitive nucleation models have been briefly reviewed. All these approaches depend, more or less, on some unknown factors, such as interface energies, elastic distortion energies, etc. These models actually imply that phase formation sequences are determined only by nucleation, i.e., the phase nucleating first will grow first. According to competitive growth models [12-14, 17, 19, 24], a phase which already nucleates may disappear due to its kinetic instability. Therefore, a phase that nucleates first may not be the phase that grows first. A good example is Ni-Si deposition reactions, found in Ref. [16] and references therein. In the competitive growth approach, the important role of nucleation in determining phase formation sequences is also ignored. Actually, competition among various phases exists all through the silicide reactions. At the very beginning, there may be only nucleation competition among the phases. As soon as first phase starts to grow, the competition is between the growth rate of the first phase and the nucleation rates of other phases. Therefore, a successful competition approach should be able to describe not only competitive nucleation or competitive growth but also the competition between the nucleation and growth processes. From the discussion above, it is imaginable how difficult it could be to develop such a model. Thus, a different approach may be helpful to improve our understanding of silicide formation processes and the capability of predicting silicide formation sequences. Such a model has been developed during this study and will be discussed in Chapters 3 to 5.

2.6.3. Applications of Thermodynamic Theories to the Studies of Silicide Formation

It has been recognized for years that the first phase to form in a metal-Si couple need not be the most stable phase, in terms of the largest (negative) free energy change of formation [10, 16, 26, 62]. In fact, progress in the area of SSA has shown that a metastable phase can be the first phase to form [61, 105, 106, 128-138, 149-151]. As a result, it is believed that phase selection is mainly determined by kinetics with the free energy playing a secondary role [16]. The "secondary role", according to Bené, means that the evolution of the reaction must be in the direction of decreasing Gibbs free energy, but the free energy is not necessarily a minimum for any state along the reaction path. Therefore, application of thermodynamic theories is mostly limited to determining whether there exists a driving force (i.e., decrease in free energy) for a given reaction and how large it is, if the necessary thermodynamic data are available [5, 7, 14, 20-23, 64-65, 149-151].

As mentioned in Sec.2.3, SSA is driven by a negative heat (or enthalpy change) of mixing between the two components of a diffusion couple [149]. The enthalpy changes of mixing for a number of metal-Si systems have been calculated [16, 150]. The enthalpy change for forming an equiatomic Ti-Si amorphous layer has been experimentally determined as -35 kJ/mole [150]. Again, the thermodynamic driving force is only a necessary condition, since it is found that although all the calculated systems have negative heats of mixing, only in some of them has SSA been observed [61, 78, 105, 106, 128-138].

Another area of kinetic studies involving thermodynamic driving forces, is the nucleation of new phases [5, 7, 20, 26, 149, 206]. In this case, nucleation is driven by the chemical free energy for new phase formation [5, 7, 20, 26, 206] and the gradient energy due to the existence of a steep concentration (or chemical potential) gradient near the reactive interface [206]. According to d'Heurle [7], in a single phase growth sequence, the driving force for a subsequent compound decreases with respect to that for the immediate preceding compound (See Fig.2-8 and the discussion in the next paragraph). As a result, nucleation is likely to become dominating as the driving force decreases, even though the first phase formation may not be nucleation controlled at all, due to the large driving force during the initial reaction. Therefore, the magnitude of the driving forces is an important issue in terms of the nucleation energy barrier and nucleation rate (see Sec.2.6.2).

In examining driving forces, a free energy versus composition plot is usually used as a reference [5, 7, 16, 20, 149-151]. A schematic free energy versus composition plot for A-B binary system is shown in Fig.2-8 [7], which depicts the free energy curves for two solid solutions α and β (assuming very low solubilities) and four compounds A_3B, AB,

AB_2 and AB_3. According to d'Heurle [7], if the first phase to form is AB, the driving force is shown by line IH.When the second phase A_3B forms through the reaction, AB+ 2A → A_3B, the driving force is represented by the line EC and not the line DC. Similarly, if AB_3 nucleates after AB_2 formation, the driving force is line LK, which will result in a nucleation controlled process or may even be too small to allow AB_3 to nucleate. It is obvious, from the example, that a quantitative free energy versus composition plot would be very helpful in determining the driving force for new phase formation. Another point worth mentioning here is that the common tangent between α and H in Fig.2-8 indicates a metastable equilibrium between the chemical potentials of α and AB phases at the α/AB interface during AB growth. This interface will become unstable as soon as A_3B is able to nucleate. This approach has been broadly used in explaining SSA, single phase growth and sequential formation [5, 7, 16, 20, 149-151]. From this approach, it can be seen that the thermodynamic requirement that the chemical potential be continuous and monotonic throughout a diffusion couple, as stated by Kidson (see Sec.2.6.2.1), is still satisfied in the case of single phase growth. Consequently, the coexistence of all equilibrium phases in a diffusion couple is not necessary in order to satisfy such a requirement.

It has already been noted that equilibrium binary metal-Si phase diagrams have been used to predict single phase formation sequences in the Walser-Bené rule [10] and the Tsaur *et al* rule [11]. The basic consideration for these rules, however, is based on kinetic arguments, such as the effects of interface compositions and structures. In addition, the rules are apparently unable to predict metastable phase formation, just as the thermodynamic stability of a phase fails to tell the kinetic stability of the phase, i.e., whether and when it can form.

A very interesting recent trend is the application of the concept of free energy degradation rate (or the rate of free energy change) and a similar concept, effective heat of formation, to kinetic studies. This will be discussed in the rest of this section.

In an attempt to link thermodynamics to kinetics, Pretorius [21-23] formulated an effective heat of formation model (see Sec.2.2.2 and Eq.(2-1)). From the model, the criterion for predicting formation sequence is basically that the phase with the largest (negative) effective heat of formation will grow [21, 22]. The advantage of this approach is that the change in enthalpy with the composition (and hence with the evolution of the reaction) is incorporated into the model. The disadvantages are the following: 1) The term effective concentration, or available concentration limiting element, is not well defined, so that the formation sequence prediction after first phase growth heavily depends on the questionable restriction that the non-congruent phases are relatively unstable (see Sec.2.2.2), but not on the effective heat of formation approach. 2) Since only the heats of

formation for equilibrium phases are used in this model, it also fails to predict metastable phase formation. Even if the heats of formation for metastable phases are used, this model will still fail because the metastable phase may have a similar composition as the stable phase, but a smaller value of heat of formation.

A more advanced model linking thermodynamics to kinetics is the one recently proposed by Bené [16]. After reviewing the work being done on other systems, such as dendrite nucleation and growth, and snowflake generation, Bené pointed out that these systems change their shape as a function of size because the new metastable shape allows a more rapid decrease in the system energy. The metastable shape of these systems can be analogous to the metastable chemical structure that forms in metal-Si couples. As a result, Bené proposed a criterion for silicide nucleation, i.e., maximum FEDR or the largest FEDR. According to the criterion, at the beginning of the reaction, the phase whose formation results in the maximum FEDR grows first. When the growth of a new phase reduces the energy of the system faster than continued growth of the first phase, the new phase will start to nucleate [16]. The criterion has been used by some other groups [19, 90]. This criterion appears to be logical since the largest FEDR implies that under given kinetic conditions the free energy of the reactive interface and surrounding region is a minimum relative to all energy states accessible by other reactions. The state determined by the largest FEDR criterion is stable in terms of minimum free energy at given kinetic conditions and time. There are some disadvantages in Bené's criterion. 1) This criterion (and the expression) is only qualitative so that it is not applicable to actual prediction of formation sequences. 2) The expression for FEDR, i.e., $-D\Delta G$, is only applicable to diffusion controlled growth processes but not to nucleation processes and interfacial controlled reaction. As mentioned in Sec.2.6.2.3, first phase formation may be a competition between nucleation of all possible phases. After this, the competition becomes that between the growth of the existing phase and the nucleation of other possible phases. As a result, this expression cannot be practically used to determine formation sequence.

From the discussion above, it can be seen that the concept that the free energy changes with the advance of the diffusion reaction, has been used, more or less, by many researchers [7, 16, 19, 20, 21-23, 61-66, 90]. It should be pointed out that since free energy in a diffusion couple must change with annealing time, the free energy change or the FEDR can also reflect the kinetic characteristics of the changing system. Therefore, the study of FEDR and its role in determining formation sequences is definitely significant to the kinetic studies of silicide formation.

In this literature review, the experimental phenomena of silicide formation, the theories and models for reaction kinetics and the applications of thermodynamic theories in the

related studies have been discussed. It is noted that many kinetic theories and models have been proposed. Some of them can qualitatively explain many of the experimental phenomena quite well. The main disadvantages are: 1) They have limited capability of predicting silicide formation sequences because of their dependence on unknown kinetic factors, such as interface reaction barrier and interface energy. 2) The focus of most models is concentrated on first phase formation. Single phase formation sequence and, particularly, multiple phase formation sequences have not been given sufficient consideration. 3) The competitive growth approach and competitive nucleation approach both only work well in some cases but fail in other cases, probably because the real reaction process involves competition among nucleation rates and growth rates of all possible phases instead of only between growth rates or only between nucleation rates. Therefore, development of a new kinetic model, which is able to explain the experimental phenomena and predict both single phase formation sequences and multiple phase formation sequence, is still necessary.

Table 2-1 Comparison of first phase predictions with experimental results from the literature.

First Phases Predicted from W-B Rule[a] [10]	First Phases Predicted from EHF Rule[b] [22]	First Phases Observed in Experiments	References
$TiSi_2$	$TiSi_2$	$TiSi_2$	[6, 11, 67-69]
		TiSi	[3, 70-73]
		Ti_5Si_3	[3]
VSi_2	VSi_2	VSi_2	[6, 11, 74-77]
		V_3Si	[4, 77]
$CrSi_2$	$CrSi_2$	$CrSi_2$	[6, 11, 67, 78-81]
Mn_5Si_3	Mn_5Si_3	Mn_3Si	[9, 53]
		MnSi	[40, 41]
FeSi	FeSi	FeSi	[6, 11, 82-84]
Co_2Si	Co_2Si	Co_2Si	[1-4, 6, 11, 43, 85, 86]
		CoSi	[4, 78, 87, 88]
		$CoSi_x$	[89, 90]
		$CoSi_2$	[91-94]
Ni_2Si	Ni_2Si	Ni_2Si	[6, 11, 37, 55-57, 95-97]
		NiSi	[98-100]
		$NiSi_2$	[101, 102]
Zr_5Si_4	$ZrSi_2$	$ZrSi_2$	[1-4, 10, 11, 103, 104]
		ZrSi	[105, 106]
$NbSi_2$	$NbSi_2$	$NbSi_2$	[6, 10]
$MoSi_2$	$MoSi_2$	$MoSi_2$	[6, 10, 67, 107-109]
		Mo_5Si_3 and Mo_3Si	[110]
Pd_2Si	Pd_2Si	Pd_2Si	[1-6, 67, 111-113]
HfSi		HfSi	[6, 114, 115]

Table 2-1 continued

First Phases Predicted from W-B Rule[a] [10]	First Phases Predicted from EHF Rule[b] [22]	First Phases Observed in Experiments	References
$TaSi_2$	$TaSi_2$	$TaSi_2$	[6, 116, 117]
WSi_2	WSi_2	WSi_2	[6, 118-120]
Pt_2Si	Pt_2Si	Pt_2Si	[1-6, 33-35, 44, 45, 50, 112]
		PtSi	[121, 122]

[a] W-B rule indicates the Walser-Bené rule.

[b] EHF rule indicates the effective heat of formation rule.

Table 2-2 Major diffusers in thin silicide films [1-6, 9, 96, 107, 172-183]

Silicide	Diffuser	Marker	Silicide	Diffuser	Marker
$TiSi_2$	Si	Xe, Si	RhSi	Si	Ar
V_3Si	V	Xe	Rh_4Si_5	Si	d
VSi_2	Si	Xe, c	Rh_3Si_4	Si	d
$CrSi_2$	Si	Xe, Si	Pd_2Si	Pd and Si	O, W
FeSi	Si	Xe	PdSi	Pd and Si	W
Co_2Si	Co	W, Si, Xe	$TbSi_{1.7}$	Si	c, Kr, Ar
CoSi	Si, Co	Ta	$ErSi_{1.7}$	Si	c, Kr, Ar
$CoSi_2$	Si, Co		HfSi	Si	Ar, Zr
Ni_2Si	Ni	Xe, Si	$TaSi_2$	Si	Nb
NiSi	Ni	Xe	WSi_2	Si	c, Mo, Ge
$NiSi_2$	Ni	Xe	Os_2Si_3	Si	c
$YSi_{1.7}$	Si	Tb, Er, Kr	IrSi	Si	Co, Rh
$ZrSi_2$	Si	Si	$IrSi_{1.75}$	Si	Co, Rh
$NbSi_2$	Si	c, V	Pt_2Si	Pt	Si
$MoSi_2$	Si	c	PtSi	Pt, Si	Si, Ti, Co, Ni
Rh_2Si_3	Si	W			

c: By analogy from isomorphous silicide studied in the same investigation.

d: Deduced from oxidation experiments.

Table 2-3 Apparent activation energies from the literature

Metal	Silicide	E_A (eV/atom)	Reference	Comments
Ti	TiSi	1.8	[4]	
	$TiSi_2$	1.8	[72]	
V	V_3Si	2.0	[117]	
	VSi_2	[illegible]7	[117]	
Cr	$CrSi_2$		[80]	
Mn	MnSi	1.9	[7, 41, 53]	
Fe	Fe[illegible]	[illegible].36	[84]	
	β-$FeSi_2$	2.6	[84]	
Co	Co_2Si	1.5	[4, 96]	
	CoSi	1.9	[4, 96]	
	Co_2Si	1.45	[148]	bulk couple
	CoSi	1.66	[148]	bulk couple
	$CoSi_2$	1.97	[148]	bulk couple
Ni	Ni_2Si	1.5	[3, 96]	
	NiSi	1.4-1.65	[3, 96]	
	Ni_2Si	1.3	[37]	on polycrystal Si
		1.5	[37]	on (100) Si
		1.6	[37]	on (111) Si
	NiSi	1.23	[95]	on (100) Si
		1.83	[95]	on (111) Si
Mo	Mo_3Si	3.3	[117]	
	Mo_5Si_3	3.7	[117]	
	$MoSi_2$	2.2, 2.4	[4, 108, 117]	
Rh	RhSi	1.95	[3]	
Pd	Pd_2Si	0.9	[111]	on amorphous Si
		0.95	[111]	on (100)Si
		1.05	[111]	on (111) Si

Table 2-3 continued

Metal	Silicide	E_A (eV/atom)	Reference	Comments
Hf	HfSi	2.5	[3]	
	$HfSi_2$	3.5	[115]	on amorphous Si
W	W_5Si_3	3.7	[117]	
	WSi_2	2.2, 3.0	[3, 117]	
Ir	IrSi	1.9	[3, 4]	
Pt	Pt_2Si	1.3, 1.5	[3, 4, 35]	
	PtSi	1.5, 1.6	[3, 4, 35]	
	PtSi	1.45	[184]	on (100) Si
		1.60	[184]	on (111) Si

Table 2-4 Summary of Gösele and Tu's analysis of growth kinetics

	Fig. 2-7a	Fig. 2-7b	Fig. 2-7c
	$x_\beta << x^*_\beta$, $x_\gamma << x^*_\gamma$	$x_\beta << x^*_\beta$, $x_\gamma >> x^*_\gamma$	$x_\beta >> x^*_\beta$, $x_\gamma << x^*_\gamma$
$r = \frac{J_\beta}{J_\gamma}$	$\frac{\Delta C^{eq}_\beta K^{eff}_\beta}{\Delta C^{eq}_\gamma K^{eff}_\gamma}$	$\frac{\Delta C^{eq}_\beta K^{eff}_\beta x_\gamma}{\Delta C^{eq}_\gamma D^*_\gamma}$	$\frac{\Delta C^{eq}_\beta D^*_\beta}{\Delta C^{eq}_\gamma K^{eff}_\gamma x_\beta}$
case I $r < r_1$	$A_\beta B$ shrinks $A_\gamma B$ grows	$A_\beta B$ shrinks, $A_\gamma B$ grows, until $r_1 \leq r$	$A_\beta B$ shrinks, $A_\gamma B$ grows, until $r_1 \leq r$
case II $r_1 < r < r_2$	$A_\beta B$ and $A_\gamma B$ grow	$A_\beta B$ and $A_\gamma B$ grow simultaneously until $r_2 = r$	$A_\beta B$ and $A_\gamma B$ grow simultaneously until $r_1 = r$
case III $r_2 < r$	$A_\beta B$ grows $A_\gamma B$ shrinks	$A_\beta B$ grows, $A_\gamma B$ shrinks, until $r \leq r_2$	$A_\beta B$ grows, $A_\gamma B$ shrinks, until $r \leq r_2$

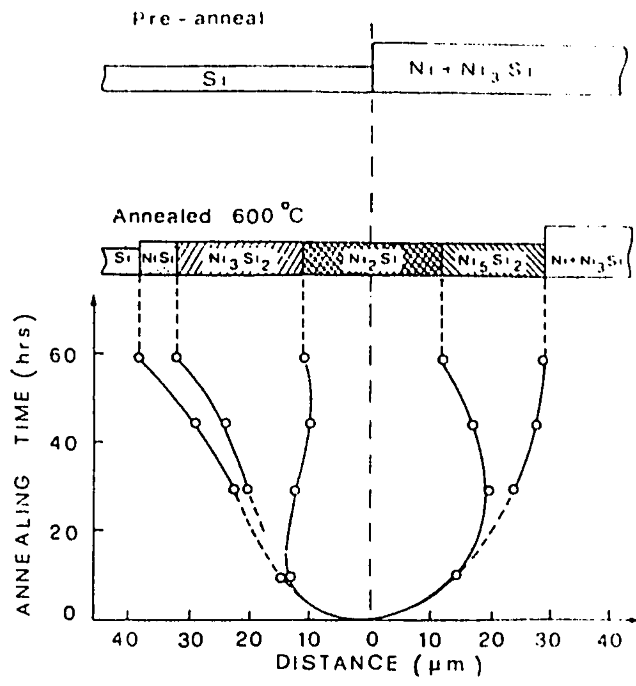

Fig.2-1 Plot of the length of the individual phases vs annealing time at 600°C, showing the phase sequence in the lateral diffusion couples [55].

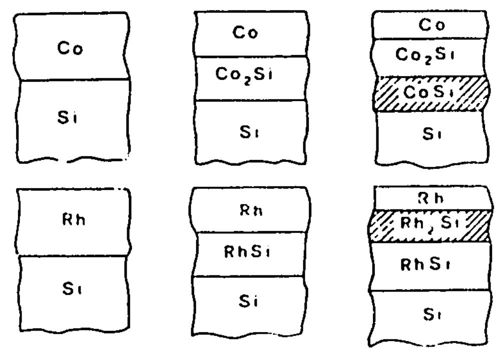

Fig.2-2 Schematic view of multiple phase growth in thin film couples with relatively thick metal films on Si substrates [6].

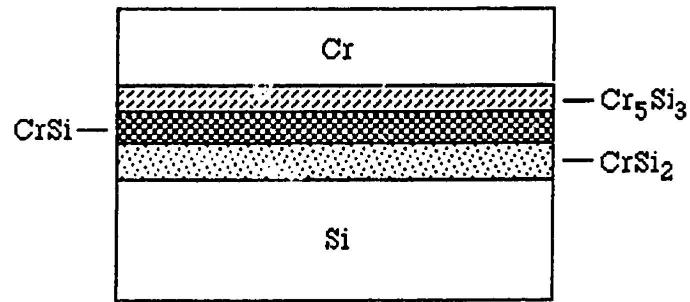

(a)

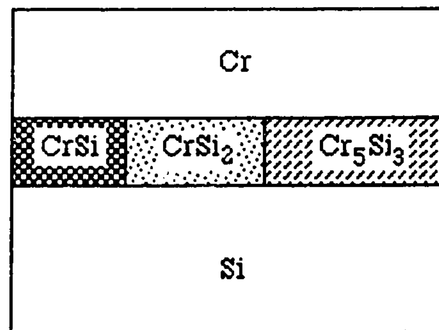

(b)

Fig.2-3 Schematic configurations of thin film Cr-Si diffusion couples. (a) Layered multiple phase growth according to classical diffusion theory. (b) Simultaneous occurrence of multiphases reported in Ref.[61].

Fig.2-4a Schematic of formation sequence of nickel silicides [2].

Fig.2-4b Binary Ni-Si phase diagram [3].

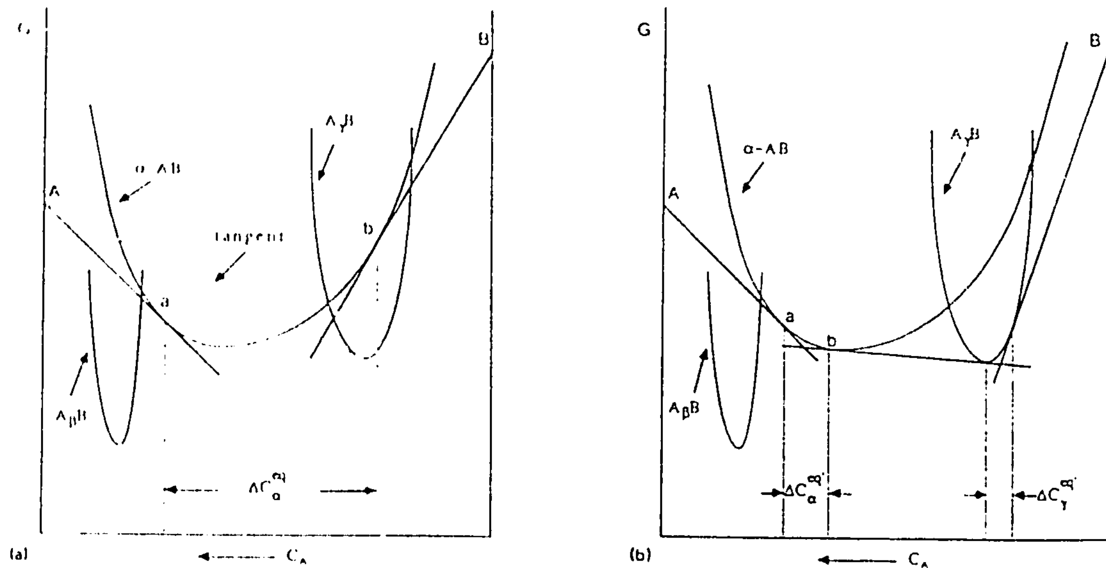

Fig.2-5 Gibbs' free energy G as a function of concentration C_A of component A in a binary system forming one metastable phase α-AB and two equilibrium compound phases $A_\beta B$ and $A_\gamma B$. (a) α-AB is assumed to be the first phase to grow and cross the dotted tangent on the second growing compound $A_\gamma B$. ΔC_α^{eq} indicates the concentration change in α-AB in the diffusion couple assuming local thermodynamic equilibrium at the interfaces. (b) Same as (a), but now it is assumed that $A_\gamma B$ grows simultaneously with the amorphous phase which had formed first [19].

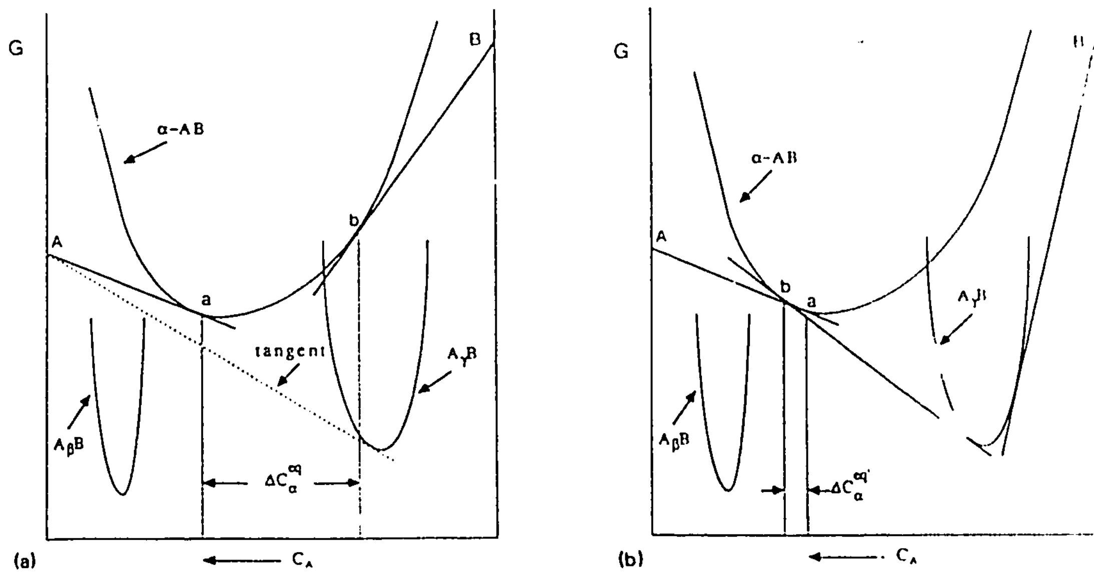

Fig.2-6 (a) Same as Fig.2-5a, but now the G curve of the amorphous phase does not cross the dotted tangent on the second growing phase $A_\gamma B$. The amorphous phase is assumed to start to grow first. (b) Same as (a), but now the second growing phase $A_\gamma B$ has been introduced which leads to a concentration reversal across the amorphous layer as compared to (a) [19].

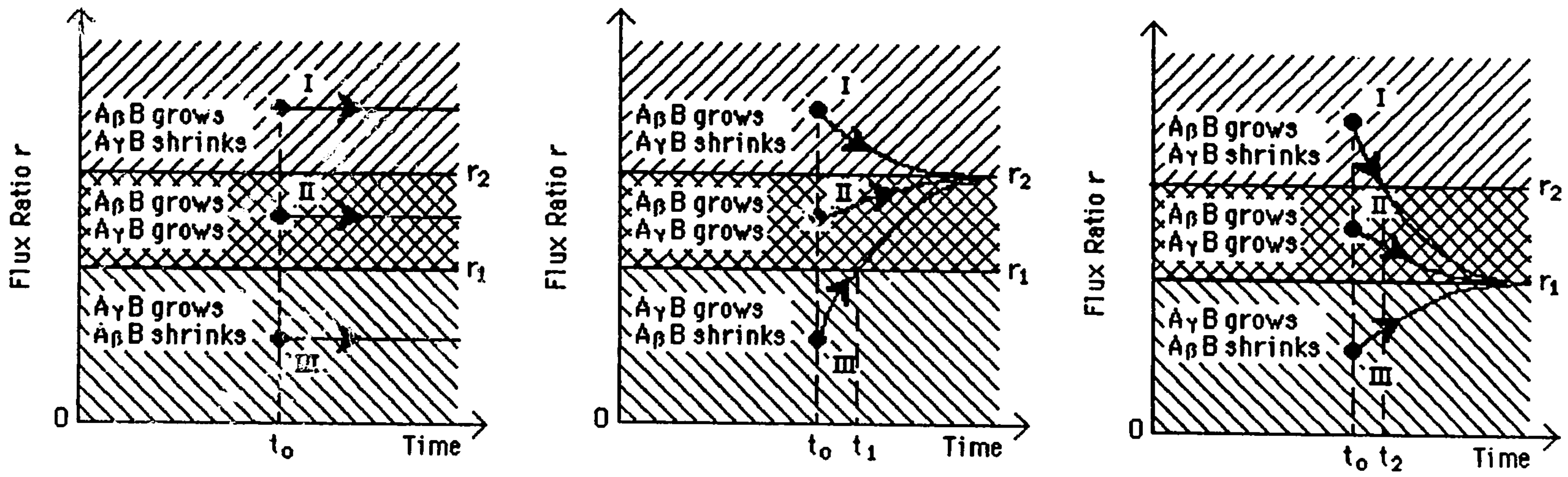

Fig.2-7 Schematic of growth/shrinkage behavior vs time. (a) It is assumed that the transport across both layers ($A_\beta B$ and $A_\gamma B$) is interface reaction controlled, $x_\beta << x_\beta^*$ and $x_\gamma << x_\gamma^*$. The flux ratio is independent of the layer thicknesses and is determined by κ_β^{eff} and κ_γ^{eff}. (b) It is assumed that transport across the $A_\gamma B$ layer is diffusion controlled, whereas transport across the $A_\beta B$ layer is interface controlled. At time $t = t_1$, in case III, the growing $A_\gamma B$ layer has reached its critical thickness x_γ^c. (c) It is assumed that transport across the $A_\beta B$ layer is diffusion controlled, whereas transport across $A_\gamma B$ layer is interfacial controlled. At time $t = t_2$, in case I, the growing $A_\beta B$ layer has reached its critical thickness x_β^c [12].

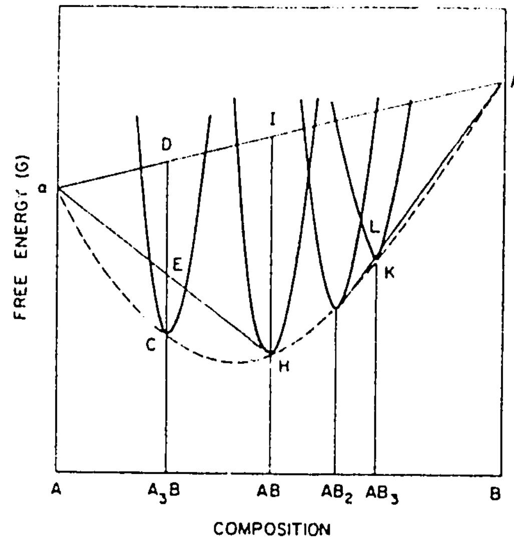

Fig.2-8 Schematic free energy versus composition plot for A-B binary system depicting the free energy curves for two solid solutions α and β (assuming very low solubilities) and four compounds A_3B, AB, AB_2 and AB_3 [7].

Chapter 3. A KINETIC MODEL FOR SILICIDE FORMATION

In this chapter a kinetic model for silicide formation in transition metal-Si diffusion couples is developed using an approach different from competitive growth and competitive nucleation approaches (see Sec.2.6). First, a simple method, which uses numerical calculations to estimate diffusion fluxes into reactive interfaces during silicide formation processes, has been developed. It is found, from the analysis of calculated diffusion fluxes, from experiments from five different published papers [34, 44, 51, 95, 121], that the formation of a new silicide or the growth sequence is not only determined by diffusion fluxes in the diffusion region, but also determined by some other variables. New physical quantities, then, are defined to describe these variables and these are incorporated into the model. The relationships among these physical quantities are examined and mathematical expressions for these relations are developed. The relationships among these quantities are demonstrated by means of a reaction process plot, which is also developed in this study. Finally, the model is used to explain the kinetic behavior during silicide formation in thin film metal-Si diffusion couples.

3.1. Computation of Diffusion Fluxes and Release Rates

3.1.1. Basic Equations

Silicide formation through thermal reaction of thin film diffusion couples is a process of phase transformation induced or manipulated by solid state diffusion. There are two basic types of processes. One of these is characterized by a diffusion couple in which both components are diffusers and is referred to as a "Type I" process here. A "Type II" process is one in which the diffusion of one component is slow when compared with the other component. As a result, only one diffuser (major diffuser) is generally considered in this type of process. In the following discussions the major diffuser will be referred to as the moving reactant while the other reactant is referred to as the non-moving reactant. Thin film silicide reactions usually occur at temperatures below half of the lowest eutectic temperature in the binary phase diagram for a given diffusion couple. As such, Type II processes are more common in silicide reactions and will be examined exclusively here.

A Type II process is shown schematically in Fig.3-1. It is assumed that the reaction occurs at the interface (for consistency, the interface is called a reaction region (R region) in this section and the definition can be found in section 3.3.1) between nonmoving reactant and growing silicide.

$$m_i M + n_i N \rightarrow M_p N_q \qquad (3\text{-}1),$$

where M and N represent the moving reactant and non-moving reactant respectively; $p = m_i$ and $q = n_i$ indicate the number of moving reactant and nonmoving reactant atoms (or formula units, i.e., f.u.) per unit formula of product (M_pN_q or abbreviated as i for ith silicide) respectively. In practice, M could be metal atoms (e.g., in near noble metal-Si diffusion couples) or Si atoms (as in refractory metal-Si diffusion couples). N could be Si atoms (in near noble metal-Si diffusion couples), metal atoms (in refractory metal-Si diffusion couples) or silicide "molecules."

As shown in Fig.3-1, the growth rate of i is $\frac{dx_i}{dt}$, and $\Delta J = J_{in} - J_{out}$ represents the difference between the diffusion fluxes of M into (J_{in}, which is equal to J_S^M in Fig.3-1) and out of (J_{out}, which is equal to J_N^M in Fig.3-1) the reaction region. For convenience, ΔJ will be referred to as the diffusion flux instead of the difference between diffusion fluxes, J_{in} and J_{out}. According to diffusion theory, an equation, expressing the relation between the growth rate, $\frac{dx_i}{dt}$, and the diffusion flux, ΔJ, can be written by assuming a mass balance between the moving reactant atoms supplied and consumed.

$$m_i N_i \frac{dx_i}{dt} = \Delta J \qquad (3\text{-}2),$$

where N_i is the number density of ith silicide (f.u./cm^3) and ($N_i \frac{dx_i}{dt}$) is the formula units of ith silicide that form per unit area and unit time. This quantity can be defined as the formation rate, F_{ik} (f.u./cm^{2}s), and hence

$$m_i F_{ik} = \Delta J \qquad (3\text{-}3).$$

The nonmoving reactant is also consumed during the reaction (Fig.3-1), because the nonmoving reactant (e.g., N atoms or "molecules") exposed to the R region is released from its lattice into the region by interaction between M atoms and N "molecules". r_i is defined as the release rate of N atoms into a unit area of R region per unit time.

$$n_i N_i \frac{dx_i}{dt} = n_i F_{ik} = r_i \qquad (3\text{-}4).$$

The physical meaning of release rate and formation rate will be further discussed later. It should be pointed out that, in these equations and the following equations, the subscripts indicate products or the reactions which form these products and the superscripts will be used to indicate reactants whenever necessary, unless otherwise specified.

A special case of a Type II process, which can be described by these equations, is one where the nonmoving reactant is silicon. In this case, the reaction is

$$m_iM + n_iSi \rightarrow M_pSi_q \qquad (3\text{-}5).$$

If the diffusion flux of M atoms in the Si substrate is negligible compared with the flux of M in the new phase, ΔJ in Eqs.(3-2) and (3-3) can be replaced by J_{in}.

From Eqs.(3-2) and (3-4), it is evident that if the growth rate of the new phase, $(\frac{dx_i}{dt})$, is given, the diffusion flux and the release rate (ΔJ and r) can be evaluated. Fortunately, growth data are available from silicide formation experiments. $\frac{dx}{dt}$ can be expressed numerically by $\frac{x_{j+1} - x_j}{t_{j+1} - t_j}$ if the time interval ($\Delta t = t_{j+1} - t_j$) is small enough (where x_{j+1} and x_j are the thicknesses of new phase at time t_{j+1} and t_j, respectively). Therefore, Eqs.(3-2) and (3-4) can be rewritten as

$$m_iN_i\frac{x_{j+1} - x_j}{t_{j+1} - t_j} = \Delta J \qquad (3\text{-}6),$$

$$n_iN_i\frac{x_{j+1} - x_j}{t_{j+1} - t_j} = r_i \qquad (3\text{-}7).$$

These two equations are the basic equations for calculating diffusion fluxes and release rates.

3.1.2. Method for Computing Diffusion Flux and Release Rate

Data for analysis were taken from published results (e.g., Figs.3-2 to 3-6). Linear regression was used to curve fit the data.

$$x = x_0 + k_p\sqrt{t} \qquad (3\text{-}8),$$

where x_o is the intercept and k_p is the slope of the regression line. In all cases parabolic growth was assumed, although this is not a necessary condition for the analysis. The square of the correlation coefficient was greater than 0.95 in most cases, although in a few instances values as low as 0.85 were obtained. It should be noted, however, that in these instances a poorer fit was obtained for linear growth.

Once x_0 and k_p are determined and an appropriate time interval is set, t_j and x_j values can be calculated. The resulting values of x_j and t_j are inserted into Eqs.(3-6) or (3-7) to calculate diffusion fluxes and release rates of reactants at time $t=t_j$. All these calculations, including linear regression analysis, are done with Lotus 123 software on a PC microcomputer.

An x_0 value in Eq.(3-8) larger than zero (e.g., Fig.3-7) indicates that before annealing starts at the temperature of interest or before the defined $t=0$ condition, a new phase has already been formed. This is practically possible, since during heating of the sample phase formation may occur. In this case, the starting diffusion flux should be considered as the one calculated at point $x = x_0$ and $t = 0$. If $x_0 < 0$, then the reaction has an incubation period which, in single phase growth processes, usually is the time required for the growth of a previous phase to be completed. Therefore, the calculated starting diffusion flux and release rate have to begin from the point $x = k_p\sqrt{t^*} + x_0 = 0$, where t^* is the time required to initiate growth of the phase of interest.

3.1.3. Selection of Experimental Data from The Literature

Experimental data from the literature were selected according to several requirements:

i) The experimental data had to be presented in the form of growth kinetics, e.g., x vs $\sqrt{t}$.

ii) Each system must have been well characterized, providing information such as the major diffuser, silicide number densities, etc.

iii) Experiments showing typical phenomena in thin film metal-Si reaction processes, such as successive single phase growth, different first phase formation and multiple phase growth, were chosen.

According to the requirements above, five experiments were selected [34, 44, 51, 95, 121]. The kinetic curves for these experiments are shown in Figs.3-2 to 3-6. In order to avoid confusion in discussing the various experiments, the experiments are designated as follows: Ex.1 for Muta and Shinoda [44] (Fig.3-2); Ex.2 for Canali *et al.* [34] (Fig.3-3); Ex.3 for Nava *et al.* [51] (Fig.3-4); Ex.4 for Tu *et al.* [121] (Fig.3-5); Ex.5 for Majni *et al.* [95] (Fig.3-6).

When the basic equations for the numerical calculations of diffusion flux and release rates were derived, only one reaction region in a diffusion couple was considered. In practice, reaction processes may be more complex. Reactions often occur in more than one reaction region at the same time, so that observed growth rates of the products are not always the same as their true growth rates. This effect has to be accounted for in any growth calculations.

3.2. Calculations and Analysis of Pt_2Si and PtSi Formation in Pt/Si Thin Film Couples

In this section Ex.1 and Ex.2 are analyzed using the equations described in the previous section.

3.2.1. Simultaneous Growth of Pt_2Si and PtSi

Ex.1 was conducted using diffusion couples with electron beam evaporated Pt films on n-type <111> Si wafers [44]. The samples were annealed in flowing hydrogen. It was found that the reaction proceeded as follows: Pt-Si, Pt-Pt_2Si-Si, Pt-Pt_2Si-PtSi-Si, and Pt_2Si-PtSi-Si [44]. According to the definition in Sec.2.1, this is a multiple phase sequential growth process. The process is shown schematically in Fig.3-8. Fig.3-8a shows the sample configuration before annealing; Fig.3-8b shows the initial stage of annealing, i.e. single phase growth of Pt_2Si; Fig.3-8c shows the main stage of annealing, i.e. simultaneous growth of Pt_2Si and PtSi. It is well known that Pt is the major diffuser in both the Pt_2Si and PtSi phases [2, 6]. Therefore, Pt_2Si formation in the initial stage (Fig.3-8b) takes place at the Pt_2Si/Si interface according to

$$2Pt + Si \rightarrow Pt_2Si \qquad (3\text{-}9),$$

whereas Pt_2Si formation in the main stage (Fig.3-8c) takes place at the Pt_2Si/PtSi interface.

$$Pt + PtSi \rightarrow Pt_2Si \qquad (3\text{-}10).$$

At the same time, PtSi formation in the main stage occurs at the PtSi/Si interface and the reaction should be

$$Pt + Si \rightarrow PtSi \qquad (3\text{-}11).$$

Since the reported experimental data were from the main stage of annealing, caution must be taken when evaluating diffusion fluxes.

The observed change in layer thicknesses with time is illustrated in Fig.3-9. In order to differentiate between the thickness of Pt_2Si and that of PtSi, x_j and x_{j+1} are used here to indicate the thicknesses of Pt_2Si at time t_j and t_{j+1} ($t_{j+1} = t_j + \Delta t$) and x_j^* and x_{j+1}^* are used for PtSi. As shown in Fig.3-9a, during period Δt, the observed thickness increase, Δx, of Pt_2Si is

$$\Delta x = x_{j+1} - x_j \qquad (3\text{-}12),$$

which is also the true thickness increase of Pt_2Si. However, for PtSi, the observed thickness increase is not the same as the true displacement of the PtSi/Si interface. According to Fig.3-9b, the observed thickness increase of PtSi, Δx^*, is

$$\Delta x^* = x_{j+1}^* - x_j^* \qquad (3\text{-}13).$$

Δx^* is not the true displacement of the PtSi/Si interface, because a part of PtSi has been consumed by Pt_2Si formation (Eq.(3-10)) and has not been included in the observed thickness x_{j+1}^*. If the missing part is labeled as $\Delta x''$, the true displacement of the PtSi/Si interface is

$$(\Delta x^*)^T = \Delta x^* + \Delta x'' \qquad (3\text{-}14).$$

$\Delta x''$ can be obtained from the following equation:

$$n_{Pt2Si}^{Si} N_{Pt2Si} \frac{\Delta x}{\Delta t} = n_{PtSi}^{Si} N_{PtSi} \frac{\Delta x''}{\Delta t} \qquad (3\text{-}15);$$

where n_{Pt2Si}^{Si} and n_{PtSi}^{Si} are the numbers of Si atoms per formula unit of Pt_2Si and PtSi respectively; N_{Pt2Si} and N_{PtSi} are the number densities of Pt_2Si and PtSi respectively; \F(Δx , Δt) and $\frac{\Delta x''}{\Delta t}$ are the growth rate of Pt_2Si and the contracting rate of PtSi respectively. Since $n_{PtSi}^{Si} = n_{Pt2Si}^{Si} = 1$, Eq.(3-15) becomes

$$\Delta x" = \frac{N_{Pt2Si}}{N_{PtSi}} \Delta x \qquad (3\text{-}16).$$

By inserting Eq.(3-16) into Eq.(3-14), one obtains the true displacement of the PtSi/Si interface as

$$(\Delta x^*)^T = \Delta x^* + \frac{N_{Pt2Si}}{N_{PtSi}} \Delta x \qquad (3\text{-}17).$$

The difference in diffusion fluxes at time t_j, i.e., $\Delta J^{Pt}(t_j) = J^{Pt}_{Pt2Si} - J^{Pt}_{PtSi}$, can be calculated from Eq.(3-6) by letting the growing silicide (i) be Pt_2Si and nonmoving reactant (N) be PtSi and by inserting $m^{Pt}_{Pt2Si} = 1$ and $N_{Pt2Si} = 2.118 \times 10^{22}$ f.u./cm^3 [3]:

$$2.118 \times 10^{22} \frac{x_{j+1} - x_j}{t_{j+1} - t_j} = \Delta J^{Pt}(t_j) \qquad (3\text{-}18).$$

Similarly, the release rate of PtSi at the Pt_2Si/PtSi interface can be calculated from the following equations (derived from Eq.(3-7)):

$$2.118 \times 10^{22} \frac{x_{j+1} - x_j}{t_{j+1} - t_j} = r^{PtSi}_{Pt2Si}(t_j) \qquad (3\text{-}19).$$

From Eqs.(3-6) and (3-17), the equation for evaluating the Pt diffusion flux to the PtSi/Si interface (J^{Pt}_{PtSi}) can be derived by letting PtSi be the growing silicide (i) in Eq.(3-6) and by letting the true displacement of the PtSi/Si interface, $(\Delta x^*)^T$, be equal to $(x_{j+1} - x_j)$ in Eq.(3-6), i.e.,

$$m^{Pt}_{PtSi} \left\{ N_{PtSi} \frac{x^*_{j+1} - x^*_j}{t_{j+1} - t_j} + N_{Pt2Si} \frac{x_{j+1} - x_j}{t_{j+1} - t_j} \right\} = J^{Pt}_{PtSi}(t_j) \qquad (3\text{-}20),$$

where $m^{Pt}_{PtSi} = 1$ and $N_{PtSi} = 3.342 \times 10^{22}$ formula units/cm^3 [3]. This yields

$$3.342 \times 10^{22} \frac{x^*_{j+1} - x^*_j}{t_{j+1} - t_j} + 2.118 \times 10^{22} \frac{x_{j+1} - x_j}{t_{j+1} - t_j} = J^{Pt}_{PtSi}(t_j) \quad (3\text{-}21).$$

The equations for computing Si release rate at the PtSi/Si interface can be obtained in a similar manner:

$$3.342 \times 10^{22} \frac{x^*_{j+1} - x^*_j}{t_{j+1} - t_j} + 2.118 \times 10^{22} \frac{x_{j+1} - x_j}{t_{j+1} - t_j} = r^{Si}_{PtSi}(t_j) \quad (3\text{-}22).$$

The total Pt diffusion flux through Pt_2Si into the Pt_2Si/PtSi interface can be evaluated as

$$J^{Pt}_{tot} = J^{Pt}_{Pt2Si} = \Delta J^{Pt} + J^{Pt}_{PtSi} \quad (3\text{-}23).$$

This equation implies that the flux out of the Pt_2Si/PtSi interface, J^{Pt}_{PtSi}, is equal to the flux into the PtSi/Si interface, J^{Pt}_{Si}. To a first approximation, this assumption is reasonable considering that the thickness of the silicide film is less than 1 μm. Eq.(3-23) is valid for $t \geq t^*$, where t^* is the time for PtSi formation to start. When $t < t^*$, $J^{Pt}_{PtSi} = 0$ and ΔJ^{Pt} is not applicable for describing the supply rate of Pt to Pt_2Si/Si interface because the reaction there is defined by Eq.(3-9). Since knowledge of the initial flux, $J^{Pt}_{tot}(t = 0)$, is necessary for this study, the following procedure is used to evaluate the value of $J^{Pt}_{tot}(t = 0)$. The total flux of Pt through Pt_2Si at time $t > t^*$, $J^{Pt}_{tot}(t > t^*)$, can be obtained from Eq.(3-23). Assuming that, at this time, PtSi formation has not begun and only Pt_2Si formation occurs at the Pt_2Si/Si interface, this reaction can be described by Eq.(3-6) as

$$J^{Pt}_{tot}(t > t^*) = m^{Pt}_{Pt2Si} N_{Pt2Si} \frac{x_{j+1} - x_j}{t_{j+1} - t_j} \quad (3\text{-}24).$$

Because this reaction supposedly follows a parabolic growth behavior, the change in thickness of Pt_2Si with time should satisfy the relation described by Eq.(3-8). Inserting Eq.(3-8) into Eq.(3-24), one obtains

$$J_{tot}^{Pt}(t > t^*) = m_{Pt2Si}^{Pt}\ N_{Pt2Si}\frac{k_p(\sqrt{t_{j+1}} - \sqrt{t_j})}{t_{j+1} - t_j}$$

or

$$J_{tot}^{Pt}(t > t^*) = m_{Pt2Si}^{Pt}\ N_{Pt2Si}\frac{k_p}{\sqrt{t_{j+1}} + \sqrt{t_j}} \quad (3\text{-}25).$$

From Eq.(3-25), k_p can be evaluated because J_{tot}^{Pt} $(t > t^*)$ is known. The total starting diffusion flux of Pt can then be calculated from the following equation:

$$J_{tot}^{Pt}(t_0 = 0) = m_{Pt2Si}^{Pt}\ N_{Pt2Si}\frac{k_p}{\sqrt{t_1} + \sqrt{t_0}}$$

$$= m_{Pt2Si}^{Pt}\ N_{Pt2Si}\frac{k_p}{\sqrt{\Delta t}} \quad (3\text{-}26),$$

where $t_1 = t_0 + \Delta t$, and $\Delta t > 0$. Table 3-1 lists the total diffusion flux of Pt to the Pt_2Si/Si interface ($J_{tot}^{Pt}(t = 0)$) and the release rate of Si ($r_{Pt2Si}^{Si}(t = 0)$). Because this is the initial stage of annealing (Fig.3-8b) and only one phase (Pt_2Si) is forming, the total flux of Pt to the Pt_2Si/Si interface (reaction region) is equal to the diffusion flux of Pt in the Pt_2Si phase, i.e.

$$J_{tot}^{Pt} = J_{Pt2Si}^{Pt} \quad (3\text{-}27).$$

Also, the total release rate of Si is given below:

$$r_{tot}^{Si} = r_{Pt2Si}^{Si} \quad (3\text{-}28).$$

In Table 3-2, the key values of diffusion fluxes and release rates at $t = t^*$, when PtSi starts to form, are listed. These results include the total diffusion flux of Pt to the $Pt_2Si/PtSi$ interface (J_{tot}^{Pt} $(t = t^*)$), the total release rate of Si ($r_{tot}^{Si}(t = t^*)$), the difference in diffusion fluxes of Pt at the $Pt_2Si/PtSi$ interface ($\Delta J^{Pt}(t = t^*)$), the release rate of PtSi for Pt_2Si formation ($r_{Pt2Si}^{PtSi}(t = t^*)$), the diffusion flux of Pt into the PtSi/Si interface for PtSi formation ($J_{PtSi}^{Pt}(t = t^*)$) and the release rate of Si for PtSi formation ($r_{PtSi}^{Si}(t = t^*)$). At t

=t*, multiple phase growth just begins (Fig.3-8c) and two phases grow together so that the following relations among these quantities are applicable:

$$J^{Pt}_{tot} = J^{Pt}_{Pt2Si} = \Delta J^{Pt} + J^{Pt}_{PtSi} \qquad (3\text{-}23),$$

$$r^{Si}_{tot} = r^{Si}_{PtSi} \qquad (3\text{-}29).$$

Three important points are apparent from the calculation results.

1) The calculations show that diffusion fluxes (J^{Pt}_{PtSi} and ΔJ^{Pt}) decrease with increasing silicide thickness and the release rates of Si and PtSi decrease accordingly. This indicates that the amount of nonmoving reactant (Si or PtSi) involved in the reactions is a variable instead of constant.

2) Although the diffusion fluxes and release rates may continue decreasing by more than an order of magnitude, the ratios of release rates of Si and PtSi to the diffusion flux remain constant for a given reaction.

3) At 300°C and t = 0 the total diffusion flux of Pt to the Pt_2Si/Si interface (J\S(Pt,tot) = J^{Pt}_{Pt2Si}) is 6.6 × 10^{15} (atoms/cm^2s) and the corresponding consumption rate of Si is 3.3 × 10^{15} atoms/cm^2s (Table 3-1). At the same temperature and t = t*, however, the total diffusion flux of Pt to the Pt_2Si/Si reaction region ($J^{Pt}_{tot} = J^{Pt}_{Pt2Si}$) decreases to 4.5 × 10^{15} atoms/cm^2s and the corresponding total release rate of Si is 2.6 × 10^{15} atoms/cm^2s (Table 3-2). Obviously, the ratio of release rate of Si to total diffusion flux of Pt has changed from

$$\frac{r^{Si}_{tot}(t = 0)}{\Delta J^{Pt}_{tot}(t = 0)} = 0.5$$

to

$$\frac{r^{Si}_{tot}(t = t^*)}{\Delta J^{Pt}_{tot}(t = t^*)} = 0.58.$$

Once the second R region (the Pt_2Si/PtSi interface) is separated from the first R region (the PtSi/Si interface), the ratio for the first R region becomes

$$\frac{r^{Si}_{PtSi}(t)}{J^{Pt}_{PtSi}(t)} = 1.$$

A similar situation occurs in the samples annealed at 400°C and 500°C (Table 3-1 and 3-2). This indicates that the ratio of release rate of N to diffusion flux of M may change during the reaction process and that new phase formation coincides with this ratio change.

3.2.2. Successive Single Phase Growth of Pt_2Si and PtSi

Data from Ex. 2 and Fig.3-3 were used for this analysis [34]. In this experiment, 270 nm thick Pt films were deposited on n-type <111> and <100> silicon wafers by sputtering. The samples were then annealed in vacuum (10^{-6} torr) at 323°C. The reaction process was a single phase sequential growth process as follows: Pt-Si, Pt-Pt_2Si-Si, Pt_2Si-Si, Pt_2Si-PtSi-Si, PtSi-Si [34]. In this case, the process was made up of two successive reactions. The first reaction can be described by Eq.(3-9) because it is the same as the reaction in the initial stage of simultaneous growth of Pt_2Si and PtSi discussed in Sec.3.2.1. The reaction is a Type II process and diffusion fluxes as well as release rates can be calculated using Eqs.(3-6) and (3-7), by letting Pt_2Si be the growing silicide (i), and inserting $m^{Pt}_{Pt2Si} = 2$, $n^{Si}_{Pt2Si} = 1$ and $N_{Pt2Si} = 2.118 \times 10^{22}$ atoms/cm²s into those equations.

After the first reaction is completed, the second reaction occurs by two steps as shown in Fig.2-10. The first step occurs at the Pt_2Si/PtSi interface, where Pt_2Si decomposes according to

$$Pt_2Si \rightarrow PtSi + Pt \qquad (3\text{-}30).$$

Pt, produced from Pt_2Si decomposition, then diffuses through the growing PtSi phase to the PtSi/Si interface and reacts with Si to form PtSi (recall Eq.(3-11)).

$$Pt + Si \rightarrow PtSi$$

The second step is a Type II process. However, if Eq.(3-6) and (3-7) are to be used to calculate diffusion flux and release rate, a modifying factor has to be introduced due to the effect of the first step on the whole process. The decomposition of every Pt_2Si "molecule" will lead to the formation of two PtSi "molecules", one of them formed through a Type II process. Therefore, when Eqs.(3-6) and (3-7) are used for the calculation of diffusion flux

in the second step, the observed thickness increase of PtSi, $x_{j+1} - x_j$, should be divided by a factor of 2, i.e.

$$m^{Pt}_{PtSi}\ N_{PtSi}\frac{x_{j+1} - x_j}{2(t_{j+1} - t_j)} = J^{Pt}_{PtSi}(t_j) \qquad (3\text{-}31),$$

$$n^{Si}_{PtSi}\ N_{PtSi}\frac{x_{j+1} - x_j}{2(t_{j+1} - t_j)} = r^{Si}_{PtSi}(t_j) \qquad (3\text{-}32).$$

Following the procedure described in Sec.3.1.2. and using Eqs.(3-31) and (3-32), the diffusion flux of Pt to the PtSi/Si interface, J^{Pt}_{PtSi}, and the release rate of Si, r^{Si}_{PtSi}, can be computed numerically. The calculated starting Pt flux to the Pt_2Si/Si interface, $J^{Pt}_{Pt2Si}(t = 0)$, is 4.7 × 10^{15} atoms/cm^{2}s and the ending flux is about 3.2 × 10^{14} atoms/cm^{2}s, whereas the starting Pt flux to the PtSi/Si interface, $J^{Pt}_{PtSi}(t^* = 2842\ s)$, is 9.5 × 10^{13} atoms/cm^{2}s.

Several points are apparent:

1) The Si release rate decreases with a decrease in Pt diffusion flux.

2) The ratio of Pt diffusion flux to Si release rate remains constant during each reaction. A ratio change does not occur until Pt_2Si formation is completed in this experiment.

3) Comparison of the results from the two experiments indicates that the Pt initial flux for PtSi formation in Ex.1 is about 2.6 × 10^{15} atoms/cm^{2}s, whereas the flux in Ex.2 is 9.5 × 10^{13} atoms/cm^{2}s. The former is about 26 times higher than the latter. On the other hand, the total Pt flux when PtSi starts to form in Ex.1 is 4.5 × 10^{15} atoms/cm^{2}s and is comparable to that of Pt (4.7 × 10^{15}atoms/cm^{2}s) when Pt_2Si starts to form in Ex.2. This fact shows that the onset of change in the $\{(r^{Si}_i)/J^{Pt}\}$ ratio is not controlled by the diffusion flux (J^{Pt}).

The above results indicate that Si release rate is a variable. This variable can change with Pt diffusion flux, but is not exclusively controlled by diffusion flux. To summarize the discussion above, the following equation can be written:

$$\frac{r^{Si}}{J^{Pt}} = C_i \quad \text{if} \quad J^{Pt}_{i\ LC} < J^{Pt} < J^{Pt}_{i\ UC} \qquad (3\text{-}33),$$

where r^{Si} is the release rate of Si, J^{Pt} is the diffusion flux into the reaction region and C_i is the ratio of Si to Pt atoms in one formula unit of ith silicide, i.e.

$$C_i = \frac{n_i^{Si}}{m_i^{Pt}} \quad (3\text{-}34).$$

J_{iLC}^{Pt} and J_{iUC}^{Pt} are the lower and upper critical values for Pt diffusion flux respectively. Thus, Eq.(3-33) indicates that when the diffusion flux in a reaction region is between $J_{i\,LC}^{Pt}$ and $J_{i\,UC}^{Pt}$, the ratio of release rate to diffusion flux is constant (C_i). When the diffusion flux into a reaction region is $J^{Pt} < J_{i\,LC}^{Pt}$ or $J^{Pt} > J_{i\,UC}^{Pt}$, the ratio will change.

3.3. A Kinetic Model For Silicide Formation

3.3.1. Assumptions

i) The phase boundary between the growing phase (the product) and the contracting phase (the nonmoving reactant) is assumed to be the reaction region (Fig.3-11).

ii) During the reaction, one of the reactants diffuses through the growing phase to arrive at the R region and is considered to be a moving reactant (M). The other reactant (i.e., the element or compound which makes up the contracting phase) is considered to be a nonmoving reactant (N) due to its low diffusivity in the growing phase. The reaction process can be divided into three steps. Step 1: The M atoms diffuse through the growing phase into the reaction region. Step 2: The M atoms in the R region interact with the N atoms which are exposed to this region. The interaction between these two reactants causes the N atoms to be released from their own lattice into the R region, forming product "molecules" with the M atoms at the same time. The "molecules" have similar composition and chemical bonding as the growing phase. Step 3: The "molecules" rearrange themselves on the lattice of the growing phase.

There is support for the above assumptions from experimental observations. Firstly, all experimental results, including those from XTEM and HRTEM observations to date, suggest that thin film silicide growth takes place through the advance of the reactive interfaces toward the contracting phase, i.e., the reactions only occur at the interfaces. Secondly, as is well known, the interfaces or phase boundaries, except coherent or semi-coherent interfaces, are usually a few atomic layers thick, poorly ordered, and non-uniform

in chemical composition. In particular, the interface is sandwiched between two phases (Fig.3-11), whose chemical compositions and crystalline structures are quite different. In such a configuration, the reaction must take place by the release of N atoms at one side and "crystallization" of new silicide (the product) on the other side of the interface region. In addition, diffusion is a necessary first step to induce the reaction by transporting moving reactant into the interface region. Therefore, it is reasonable to assume a three step process for silicide formation in a diffusion couple.

3.3.2. Definition and Explanation of Important Physical Quantities

Three physical quantities control the reaction process. These are the diffusion flux of M (ΔJ) into the R region, the release rate of N (r) and the formation rate of growing phase (F). Diffusion flux determines the supply rate of M to the R region; release rate determines the supply rate of nonmoving reactant to the region and the reaction rate for forming product "molecules" and formation rate determines the velocity of rearranging the "molecules" from the R region to the crystal lattice of the growing phase. The relationship between release rate r and diffusion flux ΔJ determines which silicide compound will form while the relationship between formation rate F and r determines which phase (i.e., metastable or stable phase) of the silicide will grow.

3.3.3. Relationship Between Release Rate (r) and Diffusion Flux (ΔJ)

In Sec.3.2.2., Eq.(3-33) which expresses the relationship between release rate and diffusion flux, was derived based on results from Ex.1 and Ex.2. To better understand the physical meaning of the relationship and r^{Si}, consider an experiment in which a single layer of Pt atoms is deposited on an atomically clean surface of bulk silicon crystal. An intermixing process between the Pt and the Si atoms will occur due to the interaction between them. Several types of "molecules" with different compositions and different structures may be formed during this process. Each of these requires a certain time to complete its own formation process, because the chemical bonds of Si atoms on the top surface have to be broken or rearranged before or during formation. The required time can be considered as an average interaction time (Δt_i) to form a single molecule layer. (Experimental evidence can be found in Refs. [145] and [160]. Gibson and co-workers [145] reported that a 5 min period was required for four monolayers of Pd on Si to form Pd_2Si at room temperature. Pirri *et al.* [160] reported a Co-Si chemical bond formation process for Co on Si at room temperature.) For example, there are C_1, C_2, ...C_i,...C_n different "molecules" that can form, where C_i represents the ith molecule and its composition (recall Eq.(3-34)),

$$C_i = \frac{n_i^{Si}}{m_i^{Pt}} \tag{3-34}$$

The corresponding average interaction times for these molecule layers are Δt_1, $\Delta t_2, \ldots \Delta t_i, \ldots \Delta t_n$ respectively. The difference in release rates between different "molecules" will be determined mainly by the difference between the average interaction times. This is because when molecule C_i is formed, the number of molecule layers formed per unit time should be $\frac{1}{\Delta t_i}$. If the number of formula units in a unit area of a single layer C_i is N_i^*, [illegible]ase rate of Si for molecule C_i is

$$r_i^{Si} = \frac{n_i^{Si} \cdot N_i^*}{\Delta t_i} \tag{3-35}$$

From Eqs.(3-34) and (3-35),

$$r_i^{Si} = \frac{n_i^{Si} \cdot N_i^*}{\Delta t_i} = C_i \frac{m_i^{Pt} \cdot N_i^*}{\Delta t_i} \tag{3-36}$$

where $(m_i^{Pt} \cdot N_i^*)/\Delta t_i$ is the number of Pt atoms combined into molecule C_i per unit area per unit time. In a metal-Si couple, Pt atoms are transported to the Si surface by diffusion. When the diffusion flux of Pt is just equal to $(m_i^{Pt} \cdot N_i^*)/\Delta t_i$, one obtains

$$r_i^{Si} = C_i \frac{m_i^{Pt} \cdot N_i^*}{\Delta t_i} = C_i J^{Pt} \tag{3-37}$$

Eq.(3-37) gives a critical value of diffusion flux, J_{UC}^{Pt}. Beyond this value, i.e., for any $J^{Pt} > J_{UC}^{Pt}$, Eq.(3-37) becomes

$$r_i^{Si} = C_i \frac{m_i^{Pt} \cdot N_i^*}{\Delta t_i} < C_i J^{Pt} \qquad (3\text{-}38),$$

since the number of Pt atoms which are combined into C_i "molecules" per unit area per unit time cannot be more than $(m_i^{Pt} \cdot N_i^*)/\Delta t_i$. This is determined by the average interaction time Δt_i. Consequently, as long as $J^{Pt} > J_{iUC}^{Pt}$, r_i^{Si} will be constant. On the other hand, if $J^{Pt} < J_{iUC}^{Pt}$, which means the transportation rate of Pt is less than the capability of C_i "molecules" to consume Pt atoms, the formation process of C_i becomes "diffusion controlled," i.e., as soon as a Pt atom is transported into the interface it is combined into "molecules". In this case, Eq.(3-37) becomes

$$r_i^{Si} = C_i J^{Pt} < C_i \frac{m_i^{Pt} \cdot N_i^*}{\Delta t_i} \qquad (3\text{-}39),$$

which indicates that the release rate, r_i^{Si}, will vary linearly with J^{Pt}. Both of these situations ($J^{Pt} > J_{iUC}^{Pt}$ and $J^{Pt} < J_{iUC}^{Pt}$) can be clearly shown in a plot of r^{Si} vs. J^{Pt}, which is plotted on a log scale (Fig.3-12). Therefore, Eq.(3-37) defines the maximum value of Si release rate. For a given reaction, the maximum r_i^{Si} can be written as

$$r_{i\,max}^{Si} = C_i \frac{m_i^{Pt} \cdot N_i^*}{\Delta t_i} = C_i J_{iUC}^{Pt} \qquad (3\text{-}40),$$

where $r_{i\,max}^{Si}$ and J_{iUC}^{Pt} represent the maximum r_i^{Si} and the upper critical value of J^{Pt} respectively. Eqs.(3-38) and (3-39) can also be rewritten as

$$r_i^{Si} = r_{i\,max}^{Si} \quad \text{if} \quad J^{Pt} \geq J_{iUC}^{Pt} \qquad (3\text{-}41);$$

$$r_i^{Si} = C_i J^{Pt} \quad \text{if} \quad J^{Pt} < J_{iUC}^{Pt} \qquad (3\text{-}42).$$

Eqs.(3-40) to (3-42) are general forms of the relation between r^{Si} and J^{Pt} for all possible Pt-Si "molecules" (or silicides). When all the r^{Si} vs. J^{Pt} curves are plotted in one diagram, the relationship between r^{Si} and J^{Pt} over a broad range of diffusion fluxes can be determined. Fig.3-13 illustrates one of these plots in which each dashed line represents a possible "molecule" (silicide), so that each r^{Si} vs. J^{Pt} curve can be fitted onto the plot depending on the composition of the mixture. A stepped curve can then be drawn for all these r^{Si} vs. J^{Pt} curves. It is evident that the area below the stepped curve includes all possible release rates for different silicides and the area above the stepped curve represents non-viable release rates. As a result, the stepped curve represents the largest release rates available at any value of diffusion flux, J^{Pt}. For a given flux, e.g., J_0^{Pt} (Fig.3-13), there are a number of possible silicides and, therefore, a number of possible release rates of Si. These release rates can be shown by the intersections of a vertical line through J_0^{Pt} with all the r^{Si} vs. J^{Pt} curves (Fig.3-13). The release rate which will actually occur is expected to be the largest one, i.e. r_4^{Si}, as shown in Fig.3-13. This is because the occurrence of the largest release rate will result in the largest FEDR (see Chap.4).

Experimental evidence for the above is apparent if r^{Si} vs. J^{Pt} curves are drawn using the data from Ex.1 and Ex.2 (Fig.3-14). The curve for Ex.2 (dashed line) is discontinuous because the Pt source was used up before J^{Pt} became low enough to initiate a new type of molecule. According to this figure if there is enough Pt supply, the same continuous curve as the solid curve (for Ex.1) in Fig.3-14 will be found for Ex.2. Since many other transition metal-Si systems have shown similar behavior as the Pt-Si system in both single phase sequential growth and multiple phase sequential growth processes, one can conclude that for a Type II process of silicide formation in a transition metal-Si system, the system has a tendency to let its release rate of N be as high as possible at a given diffusion flux of M. Consequently, the stepped curve in Fig.3-13 represents the path by which r^{Si} changes with J^{Pt} in the R region, which is adjacent to Si. A critical flux is represented by the top of each step (Fig.3-13). This flux is the upper critical flux, J_{iUC}^{Pt}, which has been defined in Eq.(3-40). There is also a lower critical flux for each step. It can be determined by its neighboring J_{iUC}^{Pt}, i.e.,

$$J_{iLC}^{Pt} = \frac{C_{i+1} \cdot J_{(i+1)UC}^{Pt}}{C_i} \qquad (3\text{-}43).$$

Therefore, the stepped curve can be expressed as

$$\frac{r^{Si}}{J^{Pt}} = C_i\,, \quad \text{if} \quad \frac{C_{i+1}\cdot J^{Pt}_{(i+1)UC}}{C_i} < J^{Pt} < J^{Pt}_{iUC} \qquad (3\text{-}44),$$

and

$$J^{Pt}_{iUC} = \frac{m_i^{Pt}\cdot N_i^*}{\Delta t_i} = \frac{r^{Si}_{i\,max}}{C_i} \qquad (3\text{-}40).$$

Eq.(3-44) is the same as Eq.(3-33) which was derived from experimental results.

3.3.4. Other Factors Influencing Release Rate

3.3.4.1. The Reactants

It is easy to understand that for different reactants, the type and the strength of the interaction between them should be different. For example, in Ex.1, there are two reactions taking place at the same time but at different R regions. At the PtSi/Si reaction region, the two reactants are Pt and Si whereas at the Pt_2Si/PtSi reaction region, the two reactants are Pt and PtSi. The interaction between Pt and Si is different from that between Pt and PtSi. As a result, the corresponding average interaction time, Δt_i's, are also different and the Si release rate may differ from that of PtSi. Therefore, every pair of reactants should have its own release rate curve. A plot of r^{Si} vs. J^{Pt} can be generalized as the plot of N release rate vs. diffusion flux of M, i.e. r^N vs. J^M as shown in Fig.3-15. This type of plot includes all possible combinations of reactants for silicide formation, since N indicates any nonmoving reactant and M represents any moving reactant. Eqs.(3-41) and (3-42) can also be generalized as

$$r_i^N = r^N_{i\,max} \quad \text{if} \quad \Delta J^M \geq J_{iUC} \qquad (3\text{-}45),$$

$$r_i^N = C_i\,\Delta J^M \quad \text{if} \quad \Delta J^M < J_{iUC} \qquad (3\text{-}46).$$

3.3.4.2. Reaction Temperature

The release rate of N is expected to increase with increasing reaction temperature, since the phonon energy increases, thereby increasing the likelihood of breaking chemical bonds. An example from Ex.1 is shown in Fig.3-16.

3.3.4.3. Impurities

Impurities are always present in silicide reactions. Generally, there are three sources of impurities, i.e. impurities intentionally doped in the Si substrate, impurities incorporated into the metal film during deposition and impurities diffused into the metal film from the annealing environment. Because impurities present in the Si substrate or other nonmoving reactant lattices can either weaken or strengthen the chemical bonds of the nonmoving reactant, the release rate of N will either increase or decrease with increasing impurity content. It should be emphasized that impurities must be present in the lattice of the N or at least in the front of the R region to affect the release rate. According to this point of view, only dopant atoms and impurities which exist in the metal film or the environment before annealing, but diffuse into the R region or substrate during annealing, affect the release rate.

The influence of impurities on release rate can be used to explain why simultaneous growth of Pt_2Si and PtSi was obtained in Ex.1 but not in Ex.2. Both release rate curves of Ex.1 and Ex.2 are put together in Fig.3-14. This figure shows that the release rate of Si for PtSi reaction has been decreased significantly in Ex.2. The following differences are apparent when comparing the conditions of samples in these two experiments: 1) The doping level is about 10^{16} atoms/cm^3 in Ex.1 compared with about 10^{15} atoms/cm^3 in Ex.2 (These values were estimated from reported resistivity values). 2) Segregation effects were not reported in Ex.1, but Al segregation was observed in an area adjacent to the reaction region in Ex.2. The presence of Al in Ex.2 is mainly caused by sputter deposition. It is likely that Al is absent in Ex.1. 3) Samples were annealed in flowing hydrogen in Ex.1 and in vacuum (10^{-6} torr) in Ex.2. Which of the above impurities (dopant, Al or H) is responsible is not clear yet. According to one study of Si oxidation, when phosphorous (an n-type dopant in Si) concentration in Si was increased, the oxidation rate of Si at low temperatures (700-900°C) was correspondingly increased [207]. Therefore, it is quite possible that the lower doping level is the reason for the lower release rate in Ex.2.

Recently, the effect of impurities on silicide formation kinetics have been investigated by different groups. Dopants (B, P, As) and oxygen are reported to delay silicide formation in Ti-Si, Mo-Si, W-Si and Co-Si systems [184, 187-195].

3.3.4.4. Interface Conditions

Interface conditions include impurity segregation, the preparation procedure of the interface and the types of interfaces, such as incoherent, coherent or semi-coherent interfaces, etc.

3.3.4.5. Conditions of the Contracting Phase

The conditions of the contracting phase include the type of the chemical bonding, the composition, the crystal structure, the orientation, the type and concentration of crystal defects and stress levels in the region near the reaction region.

3.3.5. Relationship between Formation Rate and Release Rate

Formation rate of the growing phase, F, is a physical quantity that describes the formation velocity of the growing phase from the product "molecules" which are formed during the nonmoving reactant release process. In some ways, the formation process of the growing silicide phase is similar to crystal growth from a liquid, in which the observed growth rate is determined by the velocity of an interfacial process that transfers atoms or "molecules" from disordered liquid phase into a well-ordered solid phase. In a silicide formation process, the observed F is determined by the velocity of an interfacial process that transfers "molecules" from a poorly ordered solid interface region into a well-ordered phase. However, the important difference here is that the "molecules" are formed by another interfacial process, i.e., a nonmoving reactant release process. If these two processes proceed at the same velocity, no excess "molecules" can accumulate in the interface region and hence the reaction and the interface region are stable. If the formation process is slower than the release process, the accumulation of excess "molecules" may induce another reaction or another phase to form, in order to maintain a stable interface. Recently, the formation of metastable phases and amorphous phases during thermal reaction of metal-Si thin film couples has been reported by many groups [96, 105, 106, 123-147, 149, 150]. It seems that these phenomena can be explained by the velocity difference between the release process and the formation process.

According to Assumption 2 in Sec.3.3.1, the formation rate, F_{ik} (the subscripts i and k indicate ith silicide and kth phase of the silicide in a given system, respectively), should be a function of release rate r_i, but not exclusively controlled by r_i. This relationship is demonstrated in Fig.3-17 and is expressed as

$$F_{ik} = \frac{r_i}{n_i} \qquad \text{if} \qquad r_i < r_{ik} \qquad (3\text{-}47),$$

$$F_{ik} = F_{ik\,max} \quad \text{if} \quad r_i \geq r_{ik} \qquad (3\text{-}48),$$

where n_i is the number of N atoms per formula unit of ith silicide and r_{ik} is a critical release rate related to the maximum formation rate, $F_{ik\,max}$, for k phase formation. When the release rate is low, F_{ik} is a linear function of r_i. If r_i is equal to or higher than the critical value r_{ik}, F_{ik} reaches the maximum value an becomes constant. The maximum formation rate, $F_{ik\,max}$, is determined by the energy barrier (see Chap.4) for the formation process of the growing phase k. The energy barrier is that which must be overcome when the chemical bonds and the molecule coordination and compositions in the R region are adjusted to those in the k phase. Therefore, $F_{ik\,max}$ is independent of release rate r_i. During ith silicide formation, if a release rate, r_i, for ith silicide is smaller than the critical release rate, r_{ik} (see Fig.3-17), no excess "molecules" will accumulate in the R region. Otherwise, excess "molecules" may pile up in this region so that some phase other than the k phase of the silicide will grow. At the initial stage of k phase formation, however, the nucleation of the phase has not been accounted for. In a formation rate versus release rate plot (i.e., F vs. r plot, such as Fig.3-17), the horizontal line labeled as $F_{ik'}$ indicates a formation rate that is equal to the nucleation rate of k phase. Since nucleation is a necessary condition for a phase to grow in most cases, $F_{ik'}$ represents an upper limit for F_{ik}. The term, $F_{ik'}$ can be called the conditional maximum formation rate for k phase. Correspondingly, the release rate $r_{ik'}$ is a conditional critical release rate

$$F_{ik} = F_{ik'} = \frac{r_{ik'}}{n_i} \qquad \text{if} \quad r_i \geq r_{ik'} \qquad (3\text{-}49),$$

$$F_{ik} = \frac{r_i}{n_i} \qquad \text{if} \quad r_i < r_{ik'} \qquad (3\text{-}50)$$

If at the very beginning of the reaction, the release rate r_i is smaller than $r_{ik'}$, the k phase will nucleate. Otherwise, another phase of ith silicide may nucleate first.

The maximum formation rate, $F_{ik\,max}$, is expected to be a material property related to the crystalline structure, chemical bonds and composition of the k phase. In particular, the energy barrier of the formation process may change with crystalline orientation of the k phase, since the atomic processes of rearranging "molecules" from R region to k phase may not be the same for different crystalline orientations. Consequently, there might exist some "preferred growth orientations" in which the growth energy barrier is smaller than in other orientations. In addition to these factors just mentioned above, the conditional maximum

formation rate, $F_{ik'}$, is also controlled by two other factors, i.e., the difference between interfacial energies, $\Delta\sigma$, and the strain energy, ΔH_d (see Sec.2.6). As a result, a nucleus tends to form in the orientations with smaller $\Delta\sigma$ and ΔH_d values, and hence, there exist some "preferred nucleation orientations." In general, the "preferred growth" and "preferred nucleation" orientations may not be the same. The arguments given above are supported by experimental results. Two types of $NiSi_2$ orientations, i.e., type-B and type-A orientations are observed when epitaxial $NiSi_2$ films are grown on (111) Si [157, 159]. If epitaxial growth is obtained by room temperature Ni deposition followed by thermal annealing, it is found that type-B $NiSi_2$ nucleates during Ni deposition while type-A $NiSi_2$ grows faster during annealing. Tung and co-workers proposed [152, 157, 159] that the nucleation of type-B $NiSi_2$ at room temperature was due to kinetic and energetic advantages, and that the formation of type-A $NiSi_2$ was due to a kinetic advantage in its growth.

When the ith silicide has more than one possible form, e.g., two phases, one is the stable phase (designated as k=1) and the other is a metastable phase (designated as k=2), the relationship between release rate and formation rate is shown for three possible cases in F vs r plot (Fig.3-18). In the first case (Fig.3-18a), both $F_{i1\,max}$ and $F_{i1'}$ are larger than $F_{i2\,max}$ and $F_{i2'}$. When $r_{i2'} \leq r_i \leq r_{i1'}$, the stable phase will nucleate and grow first because of its larger formation rate. When r_i decreases as the reaction proceeds and becomes smaller than $r_{i2'}$, the metastable phase cannot form either, because the stable phase growth will result in the largest FEDR (see Chap.4). In most silicide reactions stable phase formation is observed as the initial phase, and the relation between F_{ik} and r_i relations for all these reactions can be described by Fig.3-18a. In the second case (Fig.3-18b), both $F_{i2\,max}$ and $F_{i2'}$ are larger than $F_{i1\,max}$ and $F_{i1'}$. If at the beginning of the reaction, $r_{i1'} \leq r_i \leq r_{i2'}$, the metastable phase will nucleate and grow first. When r_i becomes smaller than $r_{i1'}$, the stable phase starts to nucleate and grow at the interface between the nonmoving reactant and the metastable phase (phase 2). SSA (see Sec.2.3.) may belong to this case because amorphous phase formation will have a smaller $\Delta\sigma$ [16] and growth barrier energy and hence a larger $F_{ik\,max}$ and $F_{ik'}$. The last case (Fig.3-18c) is similar to the second one, except $F_{i1'}$ becomes smaller than $F_{i2\,max}$ and $F_{i2'}$ under some conditions, such as certain substrate orientations. This can be used to explain why only stable Ni_2Si, NiSi and $MoSi_2$ phases are observed in most studies using Ni-Si and Mo-Si thin film couples, but metastable phases, i.e., θ-Ni_2Si, hexagonal NiSi and $MoSi_2$ are observed to grow on (111) Si substrates, respectively [96, 144-146]. It should be pointed out that there is also a critical thickness, which is determined by the critical release rate $r_{i1'}$, for metastable phase growth in the last two cases. If one component of the diffusion couple is completely consumed before the metastable phase reaches its critical thickness, then only the

metastable phase of ith silicide can be observed. Otherwise, the coexistence of metastable phase and stable phase should be observed, when the stable phase starts to grow.

For convenience, in the following discussion an additional term, i.e., consumption rate of reactants, is introduced. The consumption rate is the number of reactant atoms or reactant formula units transformed into a growing phase per unit area per unit time (atoms/cm^{2}s). Therefore, the moving reactant consumption rate and the nonmoving reactant consumption rate can be expressed in terms of their formation rates as mF and nF respectively.

3.3.6. Reaction Process Plot

A reaction process plot (RPP) for a reaction between a moving reactant M and a nonmoving reactant N is shown in Fig.3-19. The vertical axis indicates both the release rate, r, and the consumption rate, nF, of N. The horizontal axis indicates both the diffusion flux, J, and the consumption rate, mF, of M. The dashed lines represent the compositions (C_i) for all possible silicides that can form in the R region and represent the corresponding nF vs. mF lines for these silicides. The solid lines represent the r vs. J curves for the same silicides. The dashed lines overlap with the inclined segments of r vs. J curves. For a given silicide, e.g., C_2, the end of dashed line and the cross on the solid line indicate two conditional maximum consumption rates, $r_{21'}=n_2F_{21'}$ and $r_{22'}=n_2F_{22'}$, for phase 1 and phase 2, respectively. If C_2 has more than two phases, more crosses should be introduced, with each cross representing a particular $n_iF_{ik'}$ of k phase. The same is applicable to silicides C_1 and C_3. For simplicity, however, it is assumed that these silicides only form as stable phases. In addition, the maximum consumption rates ($n_iF_{ik\,max}$) for all four phases, i.e., C_1 and C_3, phase 1 and 2 of C_2, are not shown in this figure.

At a given diffusion flux, J_0, all possible reactions in the reaction region can be found by drawing a vertical line at J_0. The intersection of the ith inclined line with the vertical line indicates the release rate, r_i, for ith silicide formation. As mentioned in Sec.3.3.3, the largest release rate, r_2 in this case (Fig.3-19), is expected to take place. The same intersection also indicates that $r_2 = n_2F_{21} > n_2F_{22'}$, where n_2 is the number of N atoms per formula unit of silicide 2 (C_2). According to the argument in Sec.3.3.5, phase 1 of the silicide will grow. With a decrease of diffusion flux, the release rate r_2 decreases and passes the critical value, $r_{22'}$, at some point. If phase 1 is the stable form of C_2, this phase will continue growing. If, however, phase 2 is the stable phase, it will start to nucleate and grow at the interface between the nonmoving reactant and phase 1. When the diffusion flux decreases and passes the critical diffusion flux, J_{3UC}, silicide 3 (C_3) will start to form. By using this plot, the reaction process can be described clearly. It should be emphasized,

however, that only a single RPP is necessary for this type of analysis if the N and the M are the same during these reactions and the R region under consideration is the one adjacent to the nonmoving reactant. Otherwise, other RPPs should be used. Furthermore, if a quantitative reaction process plot for a transition metal-Si system is available, the silicide formation sequence of the system is predictable (see Chap.5).

3.4. Analysis of Data from Other Experiments

3.4.1. Calculation of Data from Ex.3.

The specimens in this experiment were prepared by depositing Pt films on Si wafers, implanting oxygen into the Pt film and then annealing [51]. The doped oxygen concentrations in each sample are listed in Table 3-3. The kinetics data are plotted in Fig.3-4.

Calculations from linear sections of Fig.3-4 were done by using the same procedure as in Sec.3.2. Estimates for other nonlinear sections of the curves, were conducted by directly inserting the data measured from the figures (x_j and t_j) into Eqs.(3-6) and (3-7). The important data points are listed in Table 3-3.

In this table, $t-t_0$ indicates the time for Pt_2Si formation to begin; t_1 is the time at which each curve begins to deviate from linear behavior; and t_2 is the time for PtSi formation to begin. The $J^{Pt}_{Pt_2Si}(t-t_2)$ data are calculated by directly inserting the measured data from Fig.3-4. The data corresponding to $J^{Pt}_{Pt_2Si}(t-t_0)$, $J^{Pt}_{Pt_2Si}(t-t_1)$ and $J^{Pt}_{PtSi}(t-t_2)$ are deduced from the prediction equations of those regression lines. From this table, it is evident that oxygen concentration does not affect $J^{Pt}_{Pt_2Si}(t-t_0)$, $J^{Pt}_{Pt_2Si}(t-t_1)$, and $J^{Pt}_{PtSi}(t-t_2)$ significantly. The flux, $J^{Pt}_{Pt_2Si}(t-t_2)$, seems to decrease with increasing oxygen concentration. The error in these data may be rather large, however, due to the difficulty of direct measurement from the experimental curves. Thus, this relation still needs to be verified by further experiment.

The times, t_1, at which the kinetic curves started to deviate from a linear relation, are different for different specimens. However, the values of $J^{Pt}_{Pt_2Si}(t-t_1)$ for all these samples are almost the same. At this time, the reason for this behavior is not clear. There may be two possibilities:

1) When $t > t_1$, the curves deviate from straight lines, which indicates that the mechanism of oxygen effect on Pt diffusion may have changed. As soon as the annealing

process passes through this point ($t = t_1$), the Pt flux decreases faster than before, inducing PtSi formation.

2) Since the data for $t = t_1$ and the initial flux for PtSi formation J^{Pt}_{PtSi} in Table 3-3 show the same behavior, there may be a special relationship between these two sets of data. All the data used for regression of PtSi formation are from the reaction period when Pt_2Si decomposes. During this period, the process is the type described by Eqs.(3-11) and (3-30) in Secs.3.2.1 and 3.2.2 so that the observed flux in this period is double the true diffusion flux. The difficulty in exactly evaluating the flux is that, in this case, the partial Pt supply may still come through long distance diffusion from the Pt film. The exact value of J^{Pt}_{PtSi} and the exact time ($t = t_2$) for PtSi initiation is not known at this time. It is estimated that the true value of $J^{Pt}_{PtSi}(t=t_2)$ in Table 3-3 should be between 1×10^{14} and 2×10^{14} atoms/cm^{2}s. By comparing this value with that for $J^{Pt}_{Pt_2Si}(t=t_1)$, it implies that t_1 may be the time when PtSi started to form (i.e., $t_1=t_2$). The decrease in Pt_2Si growth rate may then be due to most of the Pt being consumed by PtSi formation. As the total diffusion flux into the silicide layers decreases, less and less Pt is available and hence less and less Pt_2Si is formed.

Either of these two possibilities requires further proof. At this point, the best estimate is that the true $J^{Pt}_{PtSi}(t=t_2)$ is between 1×10^{14} and 2×10^{14} atoms/cm^{2}s and the true $t=t_2$ is between the observed values of t_1 and t_2.

3.4.2. Calculations of the Data from Ex.4

The samples in Ex.4 were diffusion couples with $Pt_{90}Cr_{10}$ alloy films on Si wafers [121]. The alloy was prepared by co-deposition using dual electron guns in an evaporator at 10^{-7} torr onto bare <100> oriented, n-type Si wafers, with a resistivity of 10 Ω-cm. The samples were annealed in a quartz tube furnace filled with purified He gas. In this experiment, only PtSi single phase formation was observed [51]. It is significant because Pt_2Si is the first phase to form in both a single phase and a multiple phase sequential growth processes in most other experiments.

The diffusion flux of Pt and consumption rates of Pt and Si were evaluated from the data of this experiment and the same procedure as that used in Sec.3.2.

The starting Pt flux, $J^{Pt}_{PtSi}(t=t_0)$ (where t_0 is the time when PtSi starts to form), for this reaction at 300°C is only 8×10^{13} atoms/cm^{2}s. Comparing this value with that of Ex.1

(2.6×10^{15} atoms/cm^{2}s), $J^{Pt}_{PtSi}(t=t_0)$ in Ex.4 is about 30 times smaller than that in Ex.1. The authors attributed the slow diffusion of Pt to the alloying effect [121].

At 320°C the starting Pt flux ($J^{Pt}_{PtSi}(t=t_0)$) is 2.8×10^{14} atoms/cm^{2}s. This value is quite close to that in Ex.2 ($J^{Pt}_{PtSi}(t=t_0) = 9.5 \times 10^{13}$), considering that some difference may be caused by different experimental procedures.

3.4.3. Analysis of Results from Exs.2, 3 and 4

Table 3-4 lists a summary of the results in Exs.2, 3 and 4, including the condition of Pt film, doping levels, starting diffusion fluxes for Pt_2Si ($J^{Pt}_{Pt_2Si}$) and PtSi (J^{Pt}_{PtSi}) formation and corresponding annealing times and temperatures.

From this table, the following facts are support for the proposed model:

1) All the initial fluxes for PtSi formation are almost the same, although the times (t_2) required for each sample to decrease its diffusion flux to this value, are generally different.

2) The time t_2 becomes longer and longer with decreasing oxygen content in the Pt film, which indicates that the higher the oxygen content in the Pt film, the faster the decrease in diffusion flux.

3) The initial fluxes are independent of the conditions of the Pt film, such as oxygen concentration and alloy composition and thus independent of the diffusivity of Pt in the film.

These facts can only be explained by a critical flux for PtSi formation that is determined by the maximum Si release rate ($r^{Si}_{PtSi\ max}$) (see Sec.3.3.3.).

The silicon wafers used in these experiments have similar doping levels (the type of dopants are unknown). Recall that in Ex.1, the Pt flux at the beginning of PtSi formation, J^{Pt}_{PtSi}, is 2.6×10^{15} atoms/cm^{2}s and the doping level in that silicon wafer is one order of magnitude higher than those in Ex.2 and Ex.4. Since the initial flux is determined by the maximum release rate of Si, a higher initial flux implies a higher maximum release rate of Si. This fact suggests that the doping level has an essential effect on the release rate of Si, which provides additional support for the new model.

From the suggested model, the formation sequence can be explained.

1) With the calculated data from Ex.2 as a reference, an RPP can be drawn as shown in Fig.3-20. In this figure, solid lines show the relationships between diffusion flux and release rate and between the consumption rates of Pt and Si in the R region. From Table 3-4, the starting diffusion fluxes at $t = t_0$ in Ex.3 are 1.4 to 1.7×10^{15} atoms/cm^{2}s. When

these values are plotted in this reaction process plot, they fall in the region where Pt_2Si formation should occur (as indicated by dashed vertical lines in Fig.3-20). When the diffusion fluxes of 1 to 2 × 10^{14} for Ex.3 and 2.8 × 10^{14} for Ex.4 are plotted in Fig.3-20 (as indicated by crosses), these values are close to the critical diffusion flux for PtSi formation. According to the suggested model, it is natural for the PtSi formation to start in Ex.4 without previous formation of Pt_2Si and for PtSi formation to replace Pt_2Si formation in the reaction region in Ex.3.

2) From Table 3-4, t_2 = 6500s for Ex.2, i.e., it takes 6500s for this sample to decrease its diffusion flux to the critical value (2 × 10^{14} atoms/cm^{2}s). But, in this experiment, the Pt film is completely consumed in t ≈ 2500s, when the diffusion flux is about 3.2×10^{14} atoms/cm^{2}s. This is indicated in Fig.3-20 by the broken line. That is why, in Ex.2, only successive single phase growth is observed. However, in Ex.3, the diffusion fluxes decrease much faster than that in Ex.2 so that before the Pt film is consumed (such as samples with 0.11 at% oxygen) or just about consumed (such as samples with 0.33% oxygen), the diffusion fluxes have already reached the critical value. As a result, simultaneous growth of two phases is observed.

From the discussion above, the modified model can explain different and complex reaction processes. The calculations, as well as analysis from different experiments, have shown strong support for this model.

3.4.4. Analysis of Ex.5

Ni diffusion flux calculations were done for Ni_2Si and NiSi formation. These reactions are also typical single layer growth processes like those discussed in Sec.3.2.2. They can be explained in a similar manner to that discussed above. Table 3-5 lists the initial fluxes of Ni for Ni_2Si and NiSi formation and those of Pt for Pt_2Si and PtSi formation. It is noteworthy that the starting diffusion fluxes of Ni in Ni_2Si and NiSi are smaller than those for Pt in PtSi and Pt_2Si. This may indicate that the maximum release rates of Si for both Ni_2Si and NiSi are smaller than those for Pt_2Si and PtSi. According to the authors, the growth rates of both Ni_2Si and NiSi on (111) Si (this experiment) are slower than those on (100) [95]. Thus, the lower release rates may be due to crystal orientation. The effect of different reactants (Pt and Ni) cannot, however, be ruled out, as yet. Further experiments are required.

3.5. Discussion

In this chapter, a simple method has been developed to estimate diffusion fluxes into reactive interfaces during silicide formation in transition metal-Si diffusion couples. Since

silicide reactions in these diffusion couples take place only at the reactive interfaces, a knowledge of the diffusion fluxes into these interfaces is usually enough for the purpose of studying the effects of diffusion on the reaction kinetics. In order to use the method, the only information required is the identity of the major diffuser and the growing silicide phase, a set of growth kinetic data, and the number density of the silicide phase. This method can be used to estimate diffusion fluxes for the reaction processes with other types of growth kinetics, in addition to those of linear or parabolic growth. This is because a proper relation between the growing phase thickness and the annealing time can be obtained by using linear regression to curve fit the kinetic data. Therefore, the method is applicable to the reaction processes showing complex kinetic behavior, such as the exponential dependence of growing layer thickness on reaction time [207] and non-parabolic growth behavior caused by additional diffusion changes due to lateral grain growth of the product [141]. From the calculations and analysis of diffusion fluxes in this chapter, it can be seen that the method, when combined with an RPP, is capable of determining the newly defined physical quantity, maximum release rate, r_{imax}, for a given silicide from experimental data of growth kinetics. This information is essential for developing the new model in this study.

The model proposed here has used an approach completely different from both competitive nucleation and competitive growth approaches (see Sec.2.6). An interfacial reaction during silicide formation is divided into three steps. In particular, it is implied, by the assumptions of the model, that prior to nucleation and growth of a silicide, "molecules" of this silicide have been formed in a R region (i.e., the reactive interface) by the release process. The analysis of growth kinetic data from five experiments has shown that the physical quantity, release rate of N r_i, does exist and it can be demonstrated by the steps of an r vs. J plot from a multiple phase sequential growth experiment. The steps in the r versus J indicate the maximum release rates which are independent of diffusion fluxes and are one of the controlling factors of silicide formation sequence. Unfortunately, a quantitative analysis showing the effect of formation rate on silicide reactions is not available at this time due to the lack of kinetic data. But, the significance of formation rate becomes evident since a formation rate versus release rate plot is capable of explaining such kinetic behaviors as SSA and metastable phase formation (see Sec.3.3.5 and Fig.3-18).

Another point distinguishing this model from others is that the new model is able to show all possible processes, which compete with each other, in one diagram, i.e., the reaction process plot. These competitions include those among release processes of different silicides, those among nucleations of different phases, those among growth processes and those between growth and nucleation processes. Moreover, it is possible to

obtain a quantitative RPP, if the maximum release rates and the conditional maximum formation rates can be determined experimentally. Such an RPP would be useful to predict silicide formation sequences for practical processing and also provide a test of the model.

Table 3-1. Diffusion flux (Pt) and release rate (Si) calculations at time t = 0 (atoms/cm^{2}s).

Temperature (°C)	$J^{Pt}_{tot}(t=0) = J^{Pt}_{Pt_2Si}$ ($\times 10^{15}$)	$r^{Si}_{tot}(t=0) = r^{Si}_{Pt_2Si}$ ($\times 10^{15}$)
300	6.6	3.3
400	36	18
500	170	85

Table 3-2. Diffusion flux and release rate calculations: Rates of reactants at time t = t* (atoms/cm²s).

Temperature (°C)	J^{Pt}_{tot} (× 10^{15})	r^{Si}_{tot} (× 10^{15})	$\Delta J^{Pt}_{Pt_2Si}$ (× 10^{15})	$r^{PtSi}_{Pt_2Si}$ (× 10^{15})	J^{Pt}_{PtSi} (× 10^{15})	r^{Si}_{PtSi} (× 10^{15})
300	4.5	2.6	1.9	1.9	2.6	2.6
400	27	17	10	10	17	17
500	140	97	43	43	97	97

Table 3-3. Key values of diffusion fluxes of Pt in Ex.3 (atoms/cm^{2}s).

Specimen Number	Oxygen Concentration (at%)	$J^{Pt}_{Pt_2Si}$ $(t = t_0)$ $(\times 10^{15})$	$J^{Pt}_{Pt_2Si}$ $(t = t_1)$ $(\times 10^{14})$	$J^{Pt}_{Pt_2Si}$ $(t = t_2)$ $(\times 10^{13})$	J^{Pt}_{PtSi} $(t = t_2)$ $(\times 10^{14})$
No.169	0.33	1.7	2.0	−1.5 [a]	3.0
		$t_0 \approx 0$	$t_1 = 1200s$		$t_2 = 2000s$
No.170	0.18	1.4	2.5	1.1	3.0
		$t_0 \approx 0$	$t_1 = 2400s$		$t_2 = 2600s$
No.171	0.11	1.4	2.0	3.6	2.0
		$t_0 \approx 0$	$t_1 = 2900s$		$t_2 = 3700s$

[a] The negative value is a result of Pt_2Si decomposing while PtSi starts to form. The data for diffusion flux calculations in this case are obtained directly from the non-linear portion of the kinetic plot in Fig.3-4a and not from regression analysis.

Table 3-4. Summary of the results from Exs. 2, 3, and 4 (diffusion fluxes in units of atoms/cm^{2}s).

Experiments	Pt Film Condition	Doping Level ($\times 10^{15}$) [a]	Initial Flux, $J^{Pt}_{Pt_2Si}$ ($\times 10^{15}$)	Initial Flux, J^{Pt}_{PtSi} ($\times 10^{14}$)
Ex.2 (323°C)	oxygen concentration < 0.1 at%	≈ 1.0	4.7 $t_0 \approx 0$	~ 1, (2) [b] (t_2 = 6500s) [b]
Ex.3 (315°C)	oxygen concentration 0.11 at%	unknown	1.7 $t_0 \approx 0$	1~ 2 t_2=2900s to 3700s
Ex.3 (315°C)	oxygen concentration 0.18 at%	unknown	1.4 $t_0 \approx 0$	1~ 2 t_2=2400s to 2600s
Ex.3 (315°C)	oxygen concentration 0.33 at%	unknown	1.5 $t_0 \approx 0$	1~ 2 t_2=1200s to 2000s
Ex.4 (320°C)	$Pt_{90}Cr_{10}$ alloy film was used	≈ 1.0	No Pt_2Si was formed	2.8 $t_2 \approx 0$

[a] The unit of doping level is atoms/cm^3.

[b] The value in parentheses indicate that if the diffusion flux for Pt_2Si in Ex.2 decreases from its starting value to 2×10^{14}, it will take about 6500s.

Table 3-5. Initial diffusion fluxes of Ni and Pt (atoms/cm^2s)

Temperature (°C)	$J^{Ni}_{Ni_2Si}(t = 0)$ ($\times 10^{15}$)	$J^{Ni}_{NiSi}(t = t_0)$ ($\times 10^{15}$)	$J^{Pt}_{Pt_2Si}(t = 0)$ ($\times 10^{15}$)	$J^{Pt}_{PtSi}(t = t_0)$ ($\times 10^{15}$)
323			4.7	0.095
330	1.6	0.036		
350	2.5	0.089		

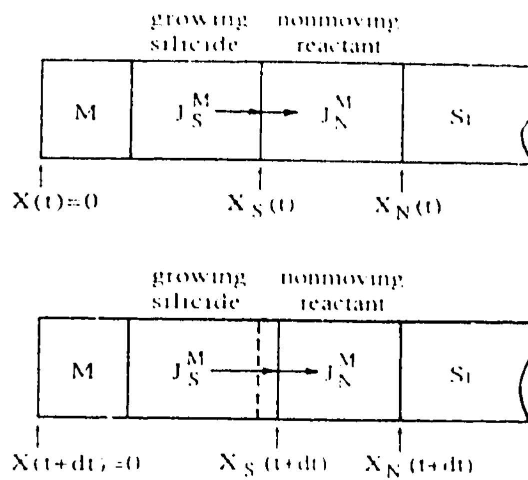

Fig.3-1 Schematic of a Type II process. M is the moving reactant; x, x_i, and x_N are positions of surface, growing silicide/nonmoving reactant interface, and nonmoving reactant/Si interface, respectively. During reaction, the silicide grows at the expense of nonmoving reactant so that $x_i(t+dt) = x_i(t) + dx_i$, and the growth rate is dx_i/dt.

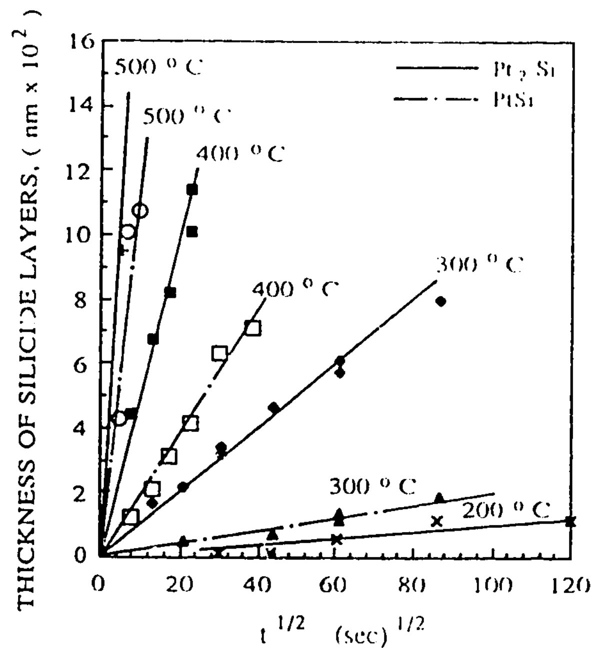

Fig.3-2 Plot of growth kinetics from Ex.1 [44]. Thickness is plotted as a function of square root of annealing time for different temperatures.

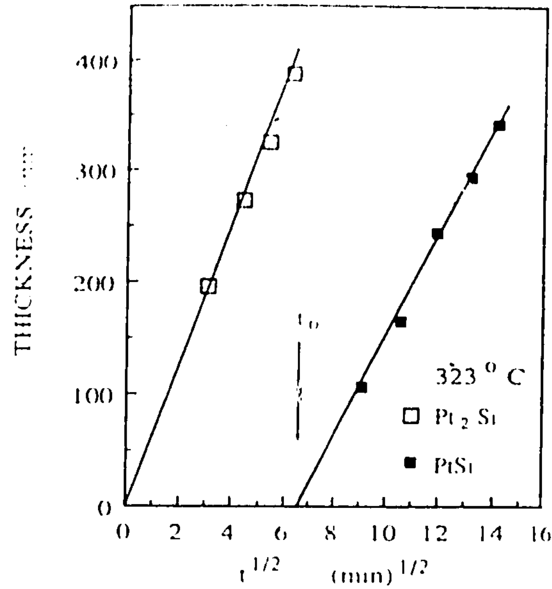

Fig.3-3 Plot of growth kinetics of a Pt-Si thin film diffusion couple from Ex. 2 [34].

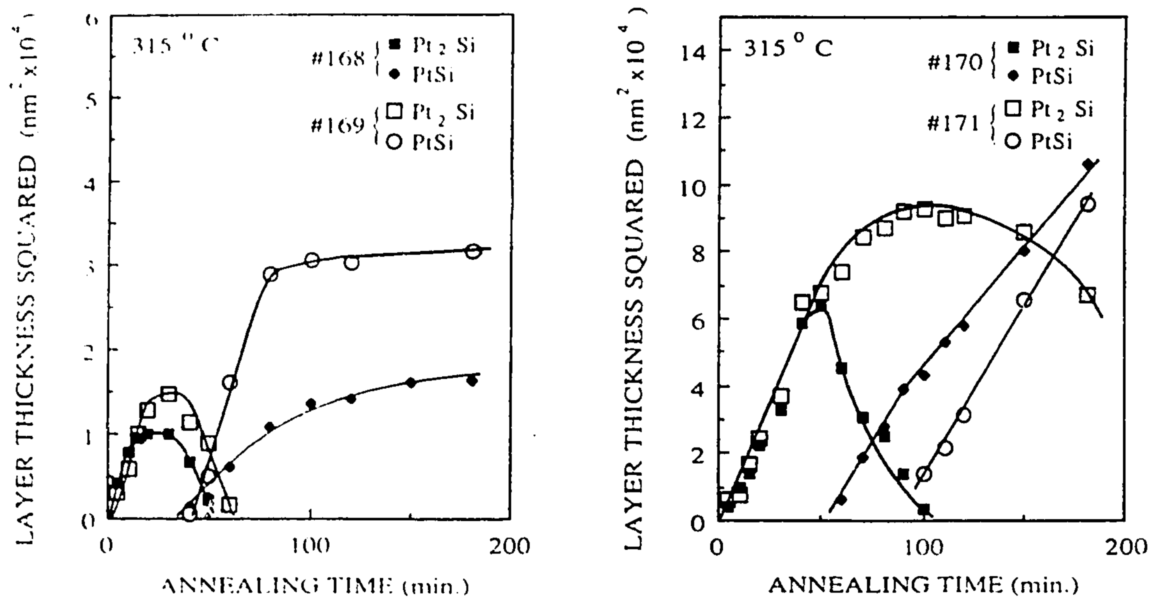

Fig.3-4 Plots of growth kinetics for a oxygen doped Pt-Si thin film diffusion couple from Ex. 3 [51].

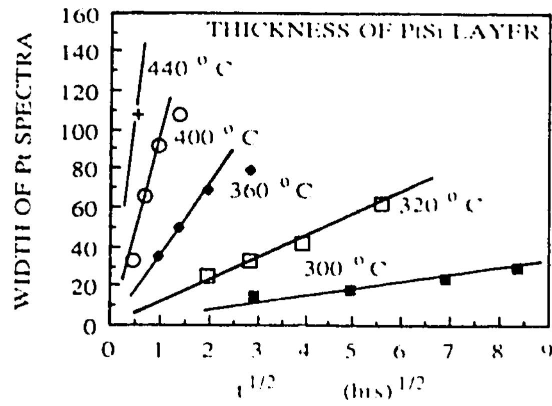

Fig.3-5 Plot of growth kinetics for a $Pt_{90}Cr_{10}$ alloy-Si diffusion couple from Ex. 4 [121].

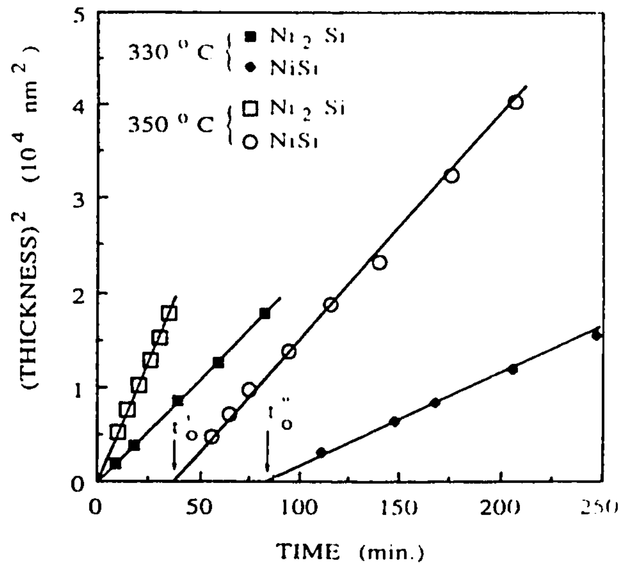

Fig.3-6 Plot of growth kinetics for a Ni-Si thin film diffusion couple from Ex. 5 [95].

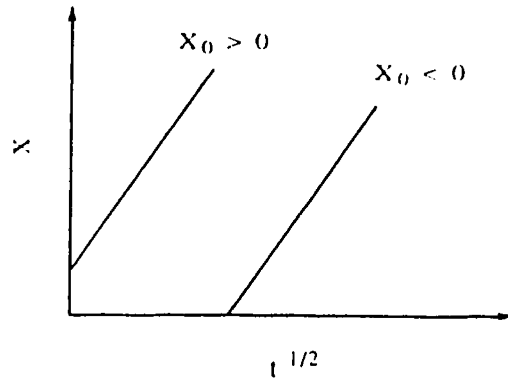

Fig.3-7 Schematic plot of regression lines with prediction equation $x = x_0 + k_p\sqrt{t}$. The top line indicates a regression line with $x_0 > 0$, and the bottom line indicates a regression line with $x_0 < 0$.

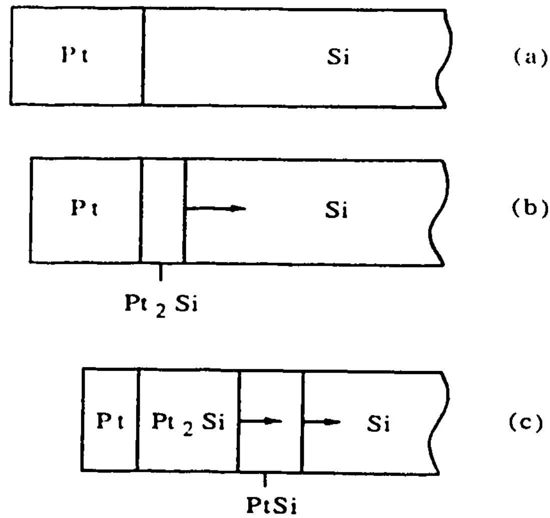

Fig.3-8 Reaction process of multiple phase growth of Pt_2Si and PtSi in Ex.1. (a) As deposited state. (b) Initial stage of the reaction. (c) Main stage of reaction. The arrows indicate the direction of growth of new phases. Not to scale.

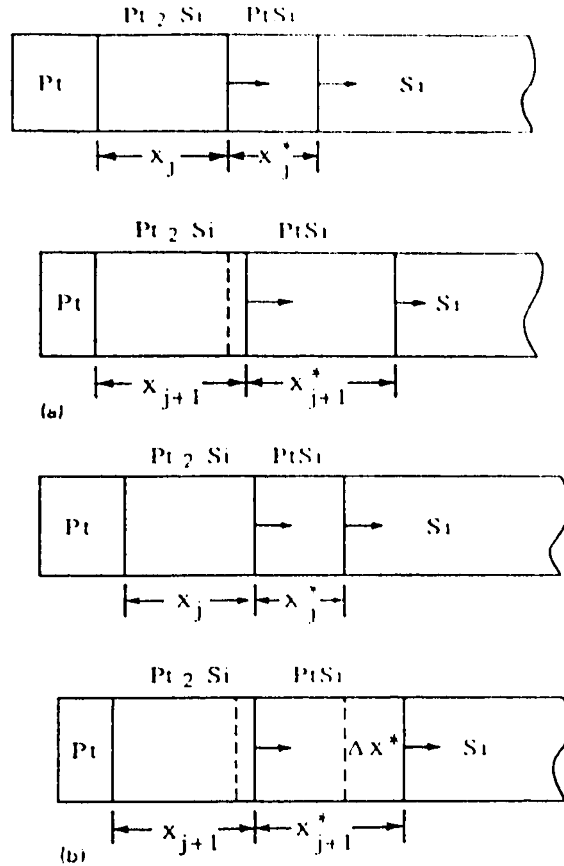

Fig.3-9 a) Schematic of simultaneous growth of Pt_2Si and PtSi. The observed thickness increase in Pt_2Si is $\Delta x = x_{j+1} - x_j$ which is also the true growth of Pt_2Si. The arrows in the figure indicate the direction of interface movement. b) Schematic showing thickness increase of PtSi during simultaneous growth of Pt_2Si and PtSi. The observed thickness increase is $\Delta x^* = x^*_{j+1} - x^*_j$ which is not equal to the true displacement of the PtSi/Si interface. The arrows in the figure indicate the direction of interface movement.

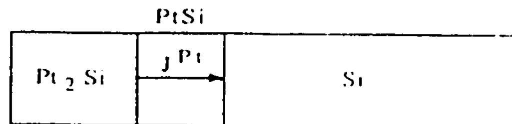

Fig.3-10 Schematic of second reaction of single phase growth in thin film Pt-Si diffusion couple. Step 1, Pt_2Si decomposes at Pt_2Si/PtSi interface. Step 2, decomposed Pt diffuses to the PtSi/Si interface and reacts with Si.

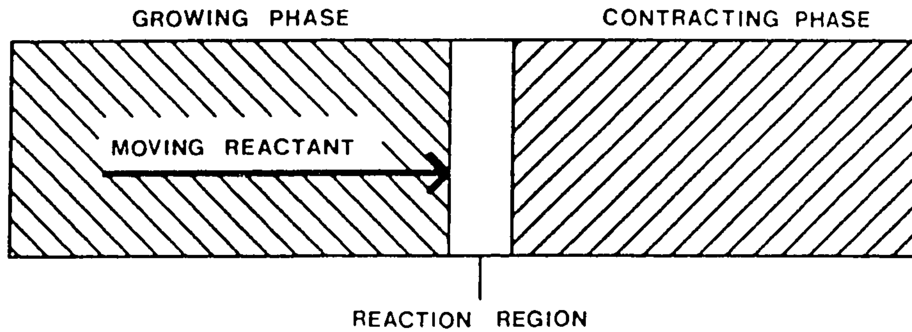

Fig.3-11 Schematic showing silicide formation. The interface region between the growing phase and the contracting phase is assumed to be the reaction region (not to scale).

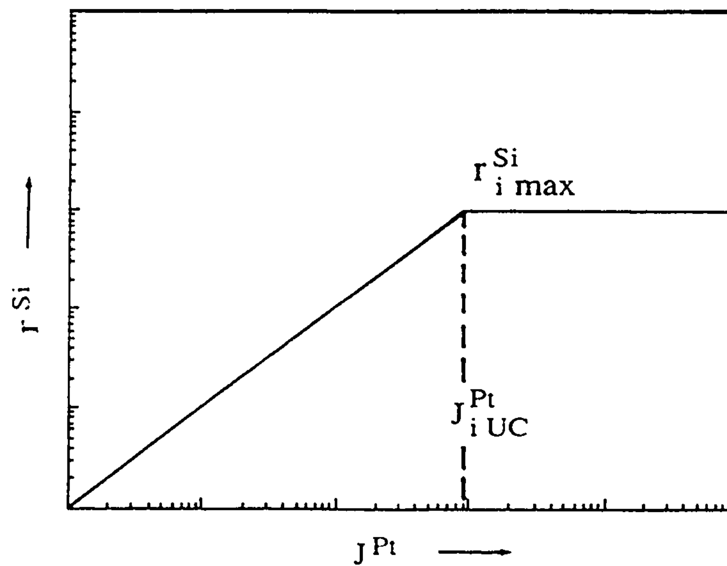

Fig.3-12 Schematic plot of r^{Si} vs J^{Pt} to show the relationship between release rate of Si and diffusion flux of Pt.

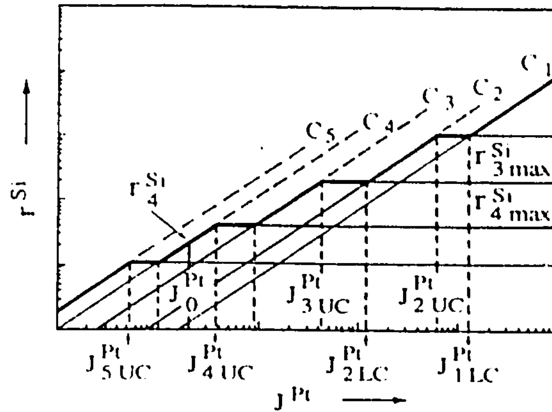

Fig.3-13 Schematic plot of r^{Si} vs J^{Pt} in which each dashed line represents a possible "molecule" (silicide). The plot is drawn by fitting each r^{Si} vs. J^{Pt} curve of given silicides onto the dashed lines depending on the composition of the molecule. A stepped curve can then be drawn for all these r^{Si} vs. J^{Pt} curves. The stepped curve represents the largest release rates available at any value of diffusion flux, J^{Pt}.

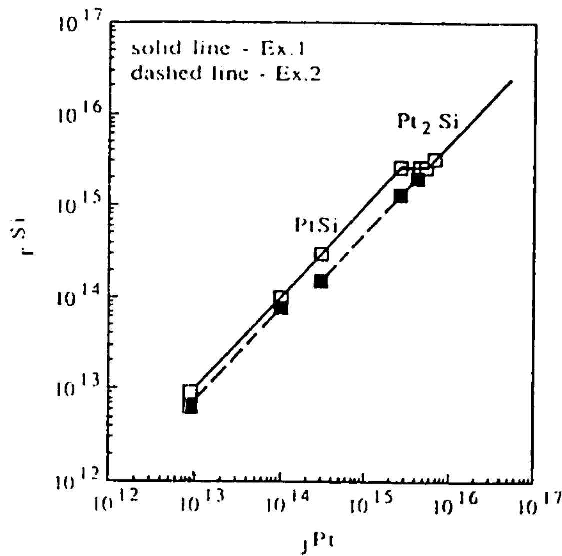

Fig.3-14 A r^{Si} vs J^{Pt} plot from calculation results of Ex.1 and Ex.2.

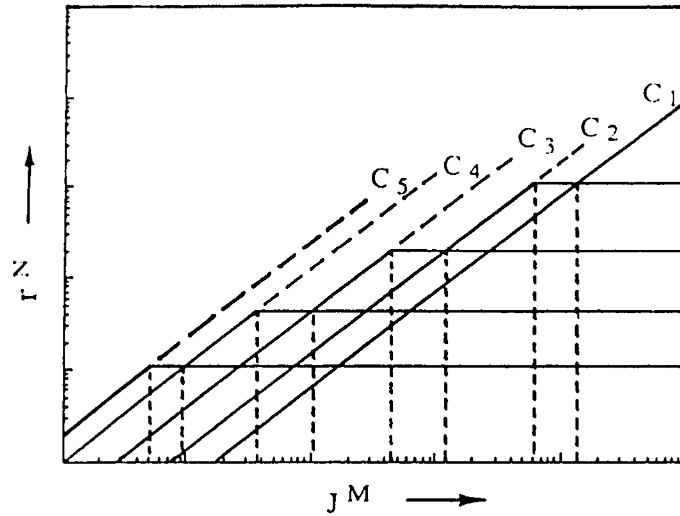

Fig.3-15 A schematic of general r^N vs J^M plot. Superscripts N and M indicate nonmoving reactant and moving reactant respectively.

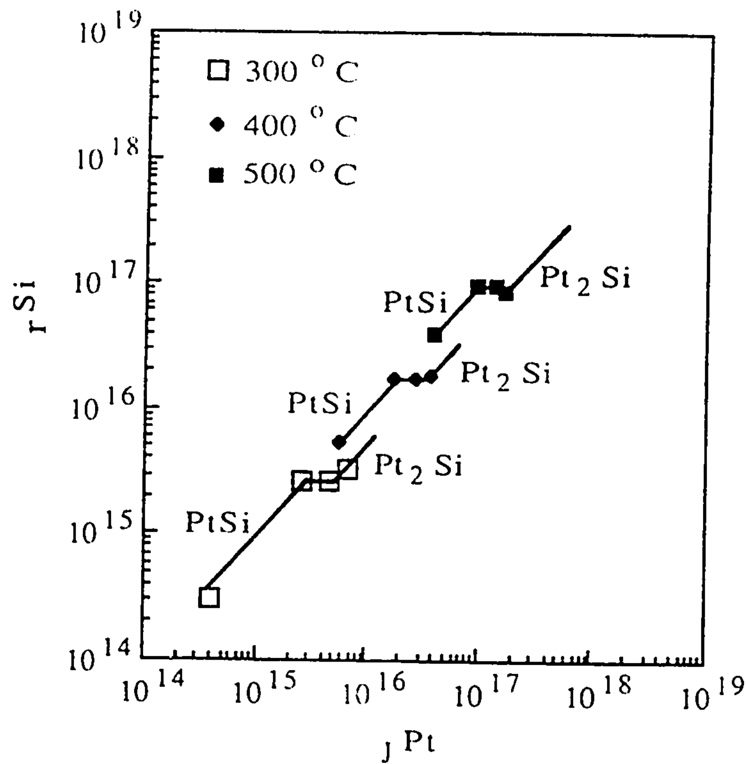

Fig.3-16 A r^{Si} vs J^{Pt} plot from calculation results of Ex.1 to illustrate the influence of temperature on release rate of Si.

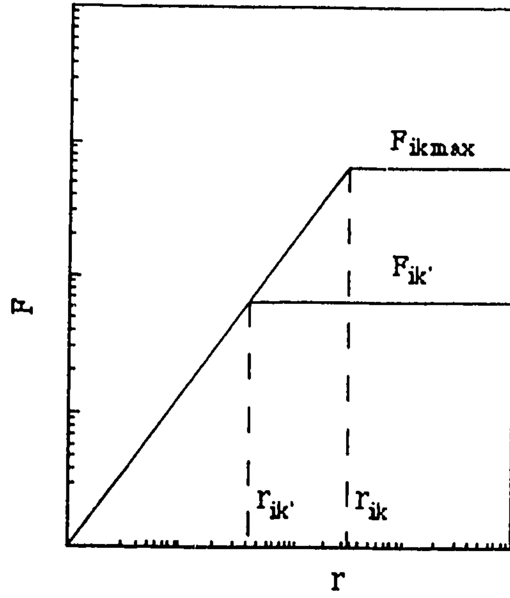

Fig.3-17 Schematic of relationship between formation rate F_{ik} and release rate r_i.

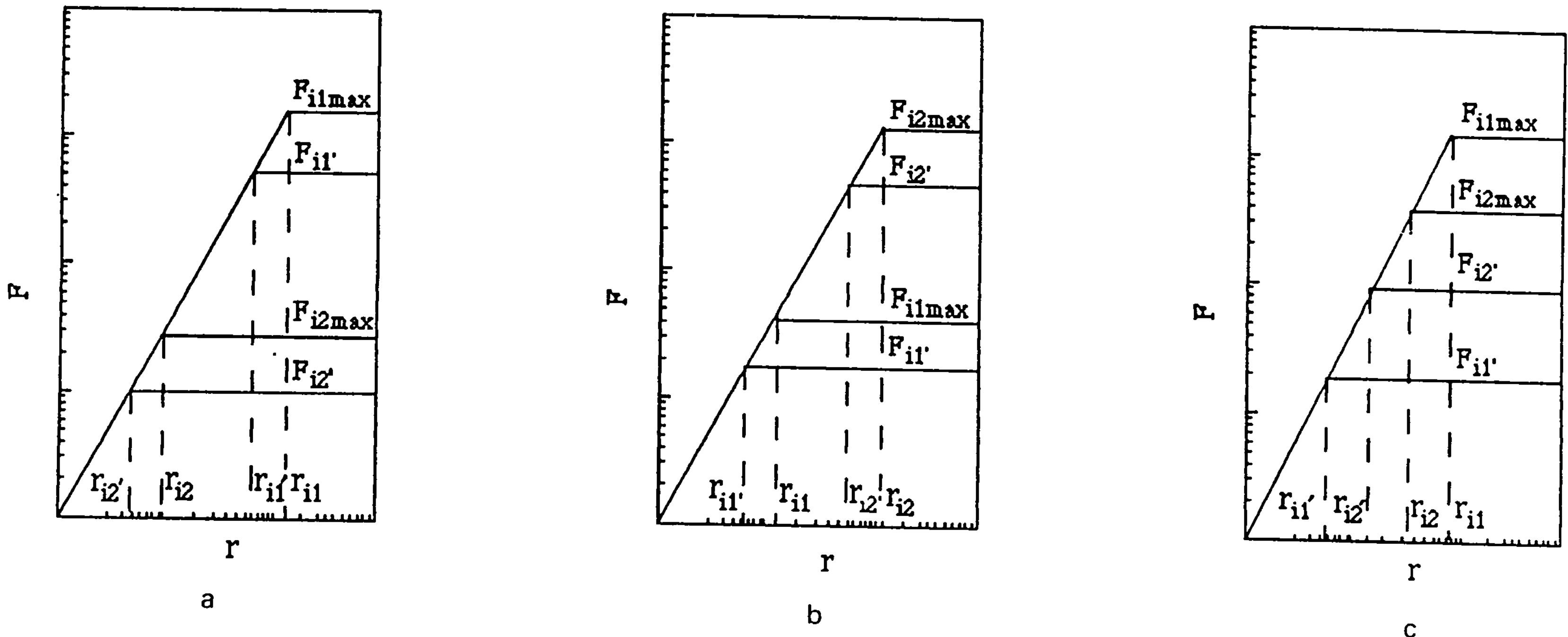

Fig.3-18 Schematic of relationship between formation rate F_{ik} and release rate r_i for two phases of ith silicide. Phase 1 (k = 1) is a stable phase and phase 2 (k = 2) is a metastable phase. $F_{ik\,max}$ indicates maximum formation rate of k phase while $F_{ik'}$ represents conditional maximum formation rate due to kinetic constraints on nucleation.

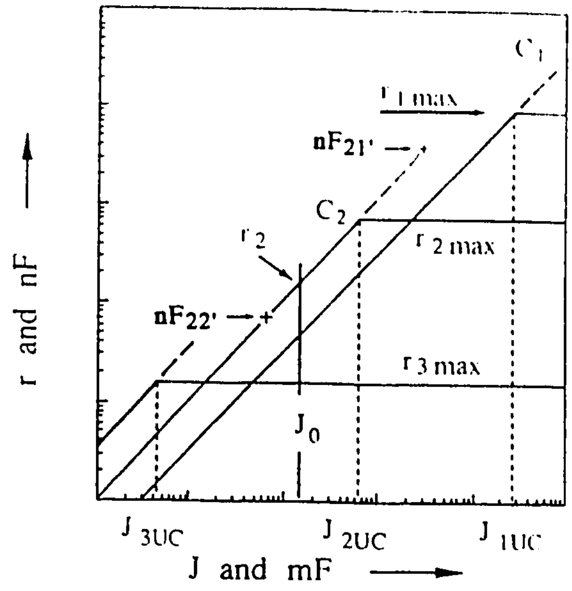

Fig.3-19 A schematic reaction process plot. J_0 is a given diffusion flux. J_{iUC} indicates the critical values of diffusion flux. r_2 is the largest release rate at given diffusion flux J_0. $n_2F_{21'}$ and $n_2F_{22'}$ represent the conditional maximum consumption rates for phase 1 and 2 of silicide 2 (C_2) respectively.

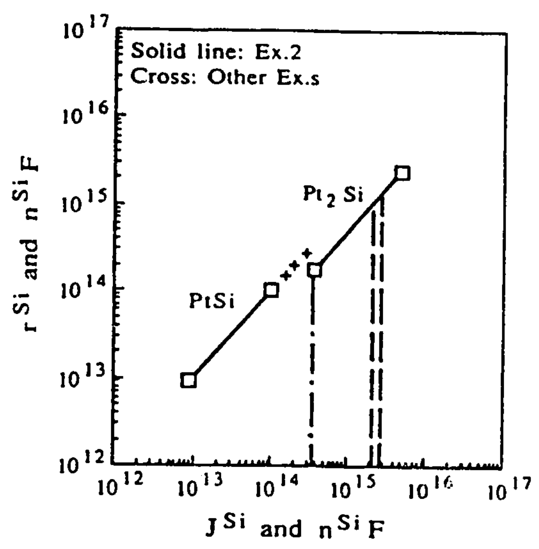

Fig.3-20 Reaction process plot drawn by using the data from Ex.2 as a reference. The dashed vertical lines indicate the starting diffusion fluxes $J^{Pt}(t=0)$ of Ex.3. The broken line indicates the flux at which the Pt supply is completely consumed in Ex.2. Crosses indicate the initial flux for PtSi formation for Ex. 3 and Ex.4.

Chapter 4. Criterion for Silicide Formation in Transition Metal-Si Diffusion Couples

In Sec.3.3.3 and 3.3.5 the term, the largest FEDR, was used to explain why at a given diffusion flux in an R region, the largest release rate is expected to occur and at a given release rate, the largest formation rate will take place. In this Chapter, expressions for FEDR will be derived. Using these expressions and an RPP, it will be shown that the largest release rate and the largest formation rate will result in the largest FEDR. Based on these results, criteria for silicide formation in transition metal-Si diffusion couples are proposed.

As was already pointed out in Sec.2.6, the term, free energy degradation rate, was first used by Bené [16] in his criterion for solid state silicide nucleation, i.e., the maximum FEDR. A little later, the concept of maximum FEDR was adopted by Gösele and Tu [19] in their criterion for critical thickness of an amorphous phase. A similar concept is also accepted and used by other authors [90]. According to Bené [16], the term FEDR means the rate of free energy change with time, and particularly, the change is in a direction which decreases the value of the system's free energy. There may be some concern about the terminology of FEDR, since it deals with the subject of thermodynamics of irreversible processes (TIP), as the system of interest is not in thermodynamic equilibrium and a change in state occurs at a finite rate [208]. It appears, at first glance, that a free energy degradation rate is not a valid concept in TIP. This is because the only general criterion of irreversibility is given by the entropy production (per unit time) according to the expression, $d_iS/dt > 0$ (where d_iS/dt is the entropy production per unit time due to changes inside the system) [209-211]. Actually, as is pointed out by Prigogine [209], other criteria of irreversibility, similar to d_iS/dt, exist for some particular cases, such as changes in state at constant temperature and volume or at constant temperature and pressure, to which the thermodynamic function Helmoholtz free energy and Gibbs free energy (G) are applicable. Examples using rate of free energy change dG/dt to discuss chemical reactions in an ideal gas at constant temperature and pressure can also been found in the literature [211]. Therefore, the criterion, $d_iG/dt < 0$, is applicable to irreversible processes during which the temperature and pressure are constant. In textbooks on thermodynamics, such as Ref.[208], the term $T(d_iS/dt)$ (where T is temperature) is referred to as the rate of energy dissipation. Since $T(d_iS/dt)$ and d_iG/dt can be used for different systems, d_iG/dt should have another "name". Therefore, if the term of FEDR due to Bené is used to indicate d_iG/dt, the Gibbs free energy decrease per unit time due to changes within the system, it should not cause any confusion. This definition will be used throughout the thesis.

4.1. Expression of FEDR for a Reaction Region

4.1.1. Basic Equation for the Rate of Free Energy Change of a System

From TIP theory, entropy has the following properties [209-211]:

1) The entropy of the system is an extensive property. If a system consists of n parts, the total entropy of the system S is

$$S = \sum_{j=1}^{n} S_j \qquad (4\text{-}1),$$

where S_j is the entropy of jth part. By differentiating Eq.(4-1) with respect to time one obtains

$$\frac{dS}{dt} = \sum_{j=1}^{n} \frac{dS_j}{dt} \qquad (4\text{-}2).$$

The entropy change per unit time in the system is equal to a sum of the changes in each part.

2) The entropy change for a system can be split into two parts, i.e.,

$$dS = d_eS + d_iS \qquad (4\text{-}3),$$

where d_eS denotes the flow of entropy due to interactions with the exterior, and d_iS represents the entropy production due to changes within the system. When the rate of entropy change is of interest, it can be expressed as

$$\frac{dS}{dt} = \frac{d_eS}{dt} + \frac{d_iS}{dt} \qquad (4\text{-}4).$$

It is the entropy production per unit time, d_iS/dt, that provides a general criterion of irreversibility for TIP, i.e., for a reversible process in the system,

$$\frac{d_iS}{dt} = 0 \qquad (4\text{-}5),$$

For an irreversible process in the system,

$$\frac{d_iS}{dt} > 0 \qquad (4\text{-}6).$$

The same is true when the jth part of the system (see Eqs.(4-1) and (4-2)) is under consideration, i.e.,

$$\frac{dS_j}{dt} = \frac{d_eS_j}{dt} + \frac{d_iS_j}{dt} \qquad (4\text{-}7),$$

and

$$\frac{d_iS_j}{dt} \geq 0 \qquad (4\text{-}8).$$

d_eS_j/dt is the flow of entropy due to the interactions of the jth part with the other parts and the exterior of the system. d_iS_j/dt is the entropy production per unit time due to the changes within the jth part.

It is easy to show that Gibbs free energy has similar properties as those of entropy, so that one has the following equations,

$$\frac{dG}{dt} = \sum_{j=1}^{n} \frac{dG_j}{dt} \qquad (4\text{-}9),$$

$$\frac{dG_j}{dt} = \frac{d_eG_j}{dt} + \frac{d_iG_j}{dt} \qquad (4\text{-}10),$$

$$\frac{d_iG_j}{dt} \leq 0 \qquad (4\text{-}11).$$

The last equation is a criterion of irreversibility for a system at constant temperature and pressure.

In TIP, an analytical expression of so called local entropy production per unit time, $(d_iS/dt)/V$ (entropy production per unit time and unit volume), has been given as [208]

$$\frac{d_iS}{dt}\frac{1}{V} = \sum_{k} J_k X_k \qquad (4\text{-}12),$$

where J_k is the generalized thermodynamic flux, such as heat flux, diffusion flux, and chemical reaction rate, while X_k is generalized thermodynamic force. An expression

similar to Eq.(4-12) should also exist for (d_iG/dt) if the four assumptions [210] for deriving the equation are applicable to the system of interest. The assumptions are the following:

1) The system is isothermal (T = constant).

2) The system is at mechanical equilibrium (no mass flow) and is not subject to external fields.

3) The concentration gradients are not too high in the sense that the composition variables do not vary appreciably within distances of the order of the mean free path. This restriction implies, in particular, the absence of interfaces inside the volume V.

4) The system is subject to time-independent boundary conditions.

However, the third assumption [210] cannot be satisfied if the R region or reactive interface is considered as a part of the system (e.g. a diffusion couple). The point is that if the entropy production of the interface region is to be investigated, the contribution of concentration gradient to (d_iS/dt) still has to be incorporated into the expression. A generalized expression for such systems is not available at this time (to the knowledge of the author), so that the expression of d_iG/dt for a R region has to be treated as an individual case.

Also, it should be mentioned that Bené [16] and Gösele and Tu [19] have already given the expressions of dG/dt according to their models respectively. These expressions are, however, obviously not applicable to the model proposed by this study. This is because the reaction process is considered as a three step process in the new model and each step has its own contribution to the total d_iG/dt in the R region, which cannot be expressed by either Bené's formula [16] or that of Gösele and Tu [19]. Therefore, an expression for FEDR applicable to this model can only be derived from Eqs.(4-9) to (4-11) and the assumptions of the model.

4.1.2 Expression of FEDR for a Reaction Region

The assumptions for the following derivations are:

1) Silicide formation in a diffusion couple occurs at constant temperature and pressure. 2) The diffusion couple is a closed system, i.e., there is only energy exchange between the system and the surroundings and there is no matter exchange. 3) There is no external force or potential field, such as an electrical field, acting on the system. The energy exchange is only due to heat flow.

For a metal-Si system with metal atoms being the moving reactant (the derivation is also applicable to the cases of Si atoms being the moving reactant, but it is more convenient to

describe the concept when the moving reactant is specified), which is schematically shown in Fig.4-1, the free energy of the system at time t can be expressed as

$$G = G_{MS} + G_R + G_{Si} \quad (4\text{-}13),$$

where G_{Si}, G_R and G_{MS} are the free energies of the Si, the reaction region (R, the silicide/Si interface), and the region including both the metal and the silicide phase (MS), respectively. From Eqs.(4-9) and (4-13), the rate of free energy change in the system is a sum of contributions from the three parts, i.e.,

$$\frac{dG}{dt} = \frac{dG_{Si}}{dt} + \frac{dG_R}{dt} + \frac{dG_{MS}}{dt} \quad (4\text{-}14).$$

The term dG_{MS}/dt in Eq.(4-14) can be split into three parts,

$$\frac{dG_{MS}}{dt} = \frac{d_eG_{MS}}{dt} + \frac{d_cG_{MS}}{dt} + \frac{d_iG_{MS}}{dt} \quad (4\text{-}15),$$

where the d_eG_{MS}/dt denotes the free energy change rate due to the energy exchange of region MS with the environment. The d_cG_{MS}/dt is due to the energy and matter exchange between the the MS region and the R region, such as metal flux into the R region and the silicide molecule flux out of the R region. The last term d_iG_{MS}/dt is due to the diffusion of metal atoms in MS region. Therefore, Eq.(4-15) has the same form as Eq.(4-10) if the first two terms are combined so that the resulting term indicates the contributions due to energy and matter exchanges with neighboring parts of the system and due to energy exchange with the exterior of the system. But the three term expression in Eq.(4-15) is preferred because it is more useful in the following discussion. The same is true for Eqs.(4-16) and (4-17).

The term, dG_R/dt in Eq.(4-14) can be split into four parts,

$$\frac{dG_R}{dt} = \frac{d_eG_R}{dt} + \frac{d_{c1}G_R}{dt} + \frac{d_{c2}G_R}{dt} + \frac{d_iG_R}{dt} \quad (4\text{-}16),$$

where d_eG_R/dt is due to the energy exchange of the R region with the exterior. $d_{c1}G_R/dt$ and $d_{c2}G_R/dt$ are due to the matter and energy exchange of the R region with the MS region and the Si phase respectively. The term d_iG_R/dt is due to the three step process occurring

in the R region and will be discussed in detail later. The last term in Eq.(4-14) can be expressed as

$$\frac{dG_{Si}}{dt} = \frac{d_eG_{Si}}{dt} + \frac{d_cG_{Si}}{dt} + \frac{d_iG_{Si}}{dt} \quad (4\text{-}17),$$

where d_eG_{Si}/dt, d_cG_{Si}/dt and d_iG_{Si}/dt represent the free energy changes per unit time due to energy exchange of Si phase with the exterior, the matter and energy exchange of Si phase with the R region and the diffusion of metal in Si.

It can be shown, by the method used by Prigogine in Chap.2 of Ref. [209], that $(d_cG_{MS}/dt) = -(d_{c1}G_R/dt)$ and $(d_{c2}G_R/dt) = -(d_cG_{Si}/dt)$. As a result, one obtains, by inserting Eqs.(4-15) to (4-17) into Eq.(4-14),

$$\frac{dG}{dt} = \frac{d_eG}{dt} + \frac{d_iG_{MS}}{dt} + \frac{d_iG_R}{dt} + \frac{d_iG_{Si}}{dt} \quad (4\text{-}18).$$

The first term in the right hand side of the equation is a sum of three terms, i.e., (d_eG_{MS}/dt), (d_eG_R/dt) and (d_eG_{Si}/dt), which indicates the total contribution due to the energy exchange of the system with the exterior. From Eq.(4-11), it is clear that the necessary and sufficient conditions for the irreversible process to occur in each part of the system are

$$\frac{d_iG_{MS}}{dt} < 0, \ \frac{d_iG_R}{dt} < 0, \ \text{and} \ \frac{d_iG_{Si}}{dt} < 0 \quad (4\text{-}19)$$

which also satisfy the following condition

$$\frac{d_iG}{dt} = \frac{d_iG_{MS}}{dt} + \frac{d_iG_R}{dt} + \frac{d_iG_{Si}}{dt} < 0 \quad (4\text{-}20).$$

According to Eqs.(4-18) to (4-20), it is evident that a knowledge of FEDR due to changes in the R region is sufficient for examining the silicide formation which takes place only at the reactive interface in a diffusion couple.

It is noted that in TIP theory, d_iS/dt is usually used to describe entropy production at a fixed spatial location. The R region under consideration of this study, however, is moving during silicide formation. Therefore, how the d_iG_R/dt of an R region is related to the changes (reactions) in a particular location of the diffusion couple should be explained. In Fig.4-2, the diffusion couple shown in Fig.4-1 is redrawn with the Si part divided into n

slabs. Each slab has the same width as the R region. If the free energy change in each of the slabs is observed by a monitor fixed on the diffusion couple, it is obvious that the FEDR, d_iG_l/dt, due to the lth slab being transformed from Si to silicide can only occur at the time t_l when R region reaches this slab. Using this approach, the FEDR of the reaction, d_iG_l/dt, can be examined one slab at a time, which can be quite tedious. An alternative approach is to monitor the R region and observe the FEDR of the R region only. It appears that d_iG_R/dt is the FEDR of a fixed location (the R region) during the reaction period. Actually, the observed value d_iG_R/dt at the instant t_l is equal to d_iG_l/dt due to the changes in the lth slab. In the following discussion, the latter approach and the term, FEDR of the R region, d_iG_R/dt, will be used in the context described above.

As is assumed in the kinetic model (Sec.2.3.1), the reaction process in the reactive interface can be divided into three steps. In step 1, M atoms diffuse from one side of the R region (adjacent to growing silicide) to the other side of the region. (In the assumption, step 1 includes diffusion through the growing phase. Here, as is shown above, when only the FEDR for R region is examined, it is not necessary to consider the diffusion process occurring in other parts of the system.). In step 2, N atoms are released from the surface of their own lattice and form product "molecules" with the M atoms at the same time. In step 3, the "molecules" are rearranged onto the lattice of the growing siiicide. The three steps include all possible changes in the R region. Therefore, the FEDR per unit area of R region can be expressed as

$$\frac{dg_R^i}{dt} = \frac{1}{A}\frac{d_iG_R^i}{dt} = J_{in}\Delta\mu_{R'}^M + r_i\Delta G_{ir}^* + F_{ik}\Delta G_{ik} \qquad (4\text{-}21),$$

where dg_R^i/dt is the FEDR for ith silicide formation per unit area of R region (Joules/cm^{2}s). J_{in} is the diffusion flux of M atoms (atoms/cm^{2}s). (It is expected that the diffusion flux in the R region, J, is equal to the flux into the region from the growing silicide, J_{in}. See discussion in Sec.4.2.1.) r_i and F_{ik} are the release rate of N atoms (atoms/cm^{2}s) and the formation rate of the growing phase (f.u./cm^{2}s) for k phase of ith silicide, respectively. $\Delta\mu_{R'}^M$, ΔG_{ir}^*, and ΔG_{ik} are the driving forces for these processes to occur, and they are the

difference in chemical potential of M atoms in the R region (Joules/atom), the free energy change for the release process per N atom and the free energy change for the formation process per formula unit of product. The first term in the right hand side of Eq.(4-21) can be divided into two terms, i.e., $\Delta J\Delta\mu_{R'}^M$ and $J_{out}\Delta\mu_{R'}^M$.

$$\frac{dg_R^i}{dt} = \Delta J \Delta\mu_{R'}^M + J_{out}\Delta\mu_{R'}^M + r_i \Delta G_{ir}^* + F_{ik}\Delta G_{ik} \quad \text{(4-21a)},$$

where $\Delta J = J_{in} - J_{out}$ is the flux of M consumed by the release and formation processes while J_{out} is the flux of M that flows through the R region but is not involved in reactions in the region. In the following discussion in this chapter, the competitions between reactions in terms of FEDR are to be examined. Since the competitions are the main concerns of the study and since the term, $J_{out}\Delta\mu_{R'}^M$, does not contribute to the FEDR for release and formation processes, this term may be neglected for the purpose of this study. Therefore, Eq.(4-21b) will be used to replace Eq.(4-21) in the following discussions.

$$\frac{dg_R^i}{dt} = \Delta J \Delta\mu_{R'}^M + r_i \Delta G_{ir}^* + F_{ik}\Delta G_{ik} \quad \text{(4-21b)}.$$

Also, in cases where $J_{in} >> J_{out}$ so that $J_{in} \approx \Delta J$, Eq.(4-21b) will also be used.

In Eq.(4-21b) the FEDR for the R region is expressed as a sum of three contributions with each part being a product of a flux and a force, which appears similar to the expression of local entropy production (Eq.(4-12)) in TIP theory. In the following section, these fluxes and forces will be discussed and the differences between Eq.(4-12) and (4-21b) will be pointed out.

4.2. Thermodynamic Fluxes and Driving Forces for Silicide Reactions

According to assumption 2 of the kinetic model (Sec.2.3.1), N atoms are released and form product "molecules" during the release process. The composition and chemical bonds of the "molecules" are similar to those of the growing phase. The assumption implies that the "molecules" constitute the interface between the growing silicide and the nonmoving reactant phase. It is also implied that step 2 and step 3 of the reaction take place at different locations of the R region, i.e., the release process occurs at the side adjacent to N while step 3, the formation process, occurs at the other side of the region. For convenience, the side for step 2 to occur is called the N surface, while the side for step 3 to occur is called the growing phase surface in the following discussion.

There are two characteristics of the R region that are crucial to the derivation of thermodynamic fluxes and driving forces for the three step process proposed by the new model. In the first, the structure of the R region is poorly ordered or disordered and some

chemical bonds of "molecules" are not satisfied. This is mainly because the release of N atoms can be considered as an individual event, i.e., the release of one atom is independent of the release of others (Some exceptions will be discussed when the concentration of product "molecules" at the surface of the N lattice is considered. See Sec.4.2.2.2.). In the second, the composition is nonuniform throughout the region. It is expected that a relatively steep concentration gradient exists over the small width of the region ($\leq$ 2 nm). The growing silicide surface has a concentration of M equal to that in the growing silicide while the N lattice surface is somewhat N rich, compared to the growing silicide. It will be seen that the energies arising from both the interfacial structure and the concentration gradient of R region contribute to the fluxes and the driving forces.

4.2.1. Diffusion Flux and Chemical Potential Difference of a Reaction Region

The thermodynamic flux and the driving force for step 1 of silicide formation are diffusion flux and the chemical potential difference of M between the two sides of the R region. Tu [13] has discussed the effect of concentration gradient on diffusion flux. The general expression for diffusion flux as a function of chemical potential gradient is [13]:

$$J = \frac{2Dc}{\lambda} \sinh\left(\frac{-\lambda(\partial\mu/\partial x)}{2k_BT}\right) \quad (4\text{-}22),$$

where D, c, λ and $\partial\mu/\partial x$ are the diffusivity, concentration, average jump distance, and chemical potential gradient of the moving species, respectively. For the condition where $(-\lambda(\partial\mu/\partial x)/k_BT) \ll 1$, J is a linear function of $\partial\mu/\partial x$, i.e.,

$$J = \frac{Dc}{k_BT}\left(-\frac{\partial\mu}{\partial x}\right) \quad (4\text{-}23).$$

If $\mu = \mu^o + k_BT \ln c$, then one obtains the usual form of Fick's first law by inserting the expression for μ into Eq.(4-23),

$$J = -D\frac{\partial c}{\partial x} \quad (4\text{-}24).$$

When a large concentration gradient, such as that at an interface region, exists, the condition $(-\lambda(\partial\mu/\partial x)/k_BT) \ll 1$ cannot be satisfied. In this case, the diffusion flux should be larger and be expressed by Eq.(4-22). In practice, however, it is expected that the diffusion flux in the R region is limited by the diffusion of the moving species in the growing silicide adjacent to the region and actually is equal to the diffusion flux from the

silicide into the R region (i.e., $J = J_{in}$). Similarly, the flux out of R region, J_{out} is limited by diffusion in the N lattice, so that the flux ΔJ can be determined by examining J_{in} and J_{out} in the two phases, respectively.

In order to derive the expression for $\Delta\mu_R^M$, the chemical potential difference in a R region, the expression for the free energy of an interface given by Cahn and Hilliard [212] can be used. According to the authors, the free energy, G_R, (The subscript R is added to indicate that this is the free energy of the R region in the following discussion. In the original Cahn and Hilliard equations, F and f are used instead of G and g, respectively.) can be expressed as

$$G_R = AN_V \int \left[g_0(c) + \bar{k}(dc/dx)^2 \right] dx \qquad (4\text{-}25).$$

The first term in the integrand is the free energy per molecule of a solution of uniform concentration c. The second term in the integrand is the gradient energy per molecule, i.e., the free energy due to the existence of a large concentration gradient (dc/dx) in a small volume of nonuniform solution. $\bar{k}$ is the gradient energy coefficient. A and N_V in the equation are the area of the interface region under consideration and the number density of the "molecules" per unit volume of the region, respectively. From Eq.(4-25), the free energy per molecule is the sum of the two terms in the integrand,

$$g(c) = g_0(c) + \bar{k}\,(dc/dx)^2 \qquad (4\text{-}26),$$

where $g_0(c)$ can be expressed as a sum of chemical potentials of its constituents, i.e.,

$$g_0(c) = m_i\mu_R^M(c) + n_i\mu_R^N(c) \qquad (4\text{-}27).$$

$\mu_R^M(c)$ and $\mu_R^N(c)$ in this equation are the chemical potentials per M and N atoms (or per f.u.) in a solution of uniform concentration c. Combining Eqs.(4-26) and (4-27) and applying partial derivatives to the resulting equation, according to the definition of chemical potential, one obtains

$$\mu_{R'}^{M} = \left[\frac{\partial g(c)}{\partial m}\right]_{T.P.n.} = \frac{\partial}{\partial m}\left[g_0(c) + \bar{k}(dc/dx)^2 \right]_{T.P.n.}$$

$$= \mu_R^M(c) + \mu_R^M(dc/dx) \qquad (4\text{-}28).$$

This equation denotes that the chemical potential per M atom ($\mu_{R'}^{M}$) in a small volume of nonuniform solution is a sum of two contributions (where the subscript R' is used to differentiate $\mu_{R'}^{M}$ from $\mu_R^M(c)$). One part is $\mu_R^M(c)$, the chemical potential in a uniform solution of concentration c. The second part is $\mu_R^M(dc/dx)$, the chemical potential due to the contribution of "gradient energy," which is an extra term and is usually negligible when the composition gradient is small. Similarly, the chemical potential per N atom $\mu_{R'}^{N}$ in the solution can be expressed as

$$\mu_{R'}^{N} = \mu_R^N(c) + \mu_R^N(dc/dx) \qquad (4\text{-}29),$$

where $\mu_R^N(c)$ and $\mu_R^N(dc/dx)$ have the same meanings as $\mu_R^M(c)$ and $\mu_R^M(dc/dx)$, but are for N atoms. The chemical potential gradient across the R region, therefore, can be derived from Eq.(4-28) and given by the following:

$$\frac{d\mu_{R'}^{M}}{dx} = \frac{d\mu_R^M(c)}{dx} + \frac{d\mu_R^M(dc/dx)}{dx} \qquad (4\text{-}30).$$

Since the diffusion distance, i.e., the thickness of the interface x_R, is so small that the gradient can be approximately expressed as $(\Delta\mu_{R'}^{M}/x_R)$,

$$\Delta\mu_{R'}^{M} = x_R \frac{\Delta\mu_{R'}^{M}}{x_R} = \Delta\mu_R^M(c) + \Delta\mu_R^M(dc/dx) \qquad (4\text{-}31).$$

Eq.(4-31) is the expression for the chemical potential difference in the R region, which indicates that the driving force consists of two parts, i.e., the chemical potential differences due to the composition difference and due to the "gradient energy" difference between the two sides of the region. It should be mentioned here that TIP theory has not given a general treatment for the cases where a large concentration gradient exists in the solution.

The generalized expression of entropy production per unit time (Eq.(4-12)) is valid only when a large concentration gradient is absent. In other words, the contribution of the concentration gradient to the driving force of diffusion is neglected in that equation.

4.2.2. Maximum Release Rate and Free Energy Change of Release Process

4.2.2.1. Expression of Maximum Release Rate

The expression of release rate as a function of diffusion flux, ΔJ, has been given in Sec.3.3.4.1,

$$r_i = r_{imax} \qquad \text{if } \Delta J \geq J_{iUC} \qquad (3\text{-}45),$$

$$r_i = C_i \Delta J \qquad \text{if } \Delta J < J_{iUC} \qquad (3\text{-}46).$$

In this section, the expression for r_{imax} will be derived. In order to do so, Eqs.(3-45) and (3-46) are combined when $\Delta J = J_{iUC}$ so that

$$C_i = \frac{r_{imax}}{J_{iUC}} \qquad (4\text{-}32).$$

Inserting Eq.(4-32) into Eq.(3-46) yields

$$r_i = C_i \Delta J = r_{imax} \frac{\Delta J}{J_{iUC}} \qquad (4\text{-}33).$$

This equation appears similar to the common first order reaction rate equation in chemical kinetics, e.g., $-(d[A]/dt) = \underline{k}[A]$, since r_i, r_{imax} and $\Delta J/J_{iUC}$ are analogous to the reaction rate $[-(d[A]/dt)]$, reaction rate constant $\underline{k}$, and concentration of reactant A [A]. Because of the analogy between Eq.(4-33) and the reaction rate equation, the so-called linear free energy relationship (LFER) approach [213-216], widely used in chemical kinetics to find the relation between rate constant and standard free energy change of the reaction or other property changes of the system under consideration, may also be used for examining the expression for r_{imax}. During early development of this method, an LFER was an empirical linear equation relating the reaction rate constant $\underline{k}$ to the standard free energy change ΔG^o or equilibrium constant K of a series of reactions as follows:

$$\log \underline{k} = \alpha \log K + \beta$$
$$= \alpha\left(-\frac{\Delta G^{o}}{k_B T}\right) + \beta \qquad (4\text{-}34).$$

All reactions or all compounds that behave similarly (i.e., their $\Delta G°$ and experimentally determined $\underline{k}$ values can fit the same empirical LFER equation) are classified into one category. The similar behavior is interpreted as those processes having the same reaction mechanism. Further development of this method broadens its applicability to correlating the changes of any property measured on any ensemble of similar chemical processes and systems [212]. This method is useful to classify chemical systems and processes and explain reaction mechanisms by relating the parameters of a particular LFER, such as α and β in Eq.(4-34), to microscopic theory. Thus far, there are already numerous cases in which LFERs as described in Eq.(4-34) are observed [213-215]. It is very attractive to apply the LFER method to examine the relationship between r_{imax} and free energy change of the release processes for silicide formation. Quantitative analysis, however, is impossible at this time, because r_{imax}, is a new physical quantity just introduced by the kinetic model and, as such, there is not enough experimental data for estimating r_{imax}. A qualitative analysis from experimental results in the literature is summarized in Table 4-1. In the table, the silicides that form through multiple phase growth processes in five metal-Si couples are listed in the order of formation sequence. That is, the initial silicide is listed first in each system. The next is the second silicide that forms at the interface between the first silicide and the nonmoving reactant (Si or refractory metal depending on which diffusion couple is used). The third is the silicide that forms at the interface between the second silicide and the nonmoving reactant. According to the reaction process plot (Sec.2.4.), the multiple phase formation sequence in a given metal-Si couple depends on the values of r_{imax} for these silicides; e.g., in Mn-Si system, the formation sequence is Mn_3Si, MnSi, and $MnSi_{1.73}$, because $r_{Mn3Si\ max} > r_{MnSi\ max} > r_{MnSi1.73\ max}$. Therefore, the formation sequence for each system indicates the order of maximum release rates in that system with the initial silicide having the largest r_{imax}. The right column of Table 4-1 shows the standard enthalpy changes of silicide formation per mole of N atoms. It is evident that there does exist a relationship between the enthalpy changes and the formation sequences and, hence, a relationship between the enthalpy changes and the maximum release rates for each metal-Si system. r_{imax} for different silicides, formed in a given metal-Si couple, decreases as the standard enthalpy changes per mole of N atoms for each corresponding silicide reaction decreases. (An exception is that Ni_3Si_2, which has the second largest enthalpy change per mole Si atoms in the Ni-Si system, cannot form before

NiSi which has a smaller enthalpy change. The reason for this will be discussed in Secs.4.2.2.2 and 4.4.) Furthermore, considering that entropy change during a solid state reaction is much smaller than enthalpy change for the reaction, the enthalpy changes listed in Table 4-1 can be replaced by standard free energy change per mole N atoms (ΔG^{o}_{ir}) without significant effects on the relationship.

From the results of a lateral Ni-Si couple annealed at 450°C [56], it is known that NiSi does not form until the initial silicide Ni_2Si reaches a thickness of 2 μm. From Eq.(3-2) and parabolic growth law, it can be shown that $J \propto 1/x$, i.e., the diffusion flux of Ni into the R region is proportional to the reciprocal of the Ni_2Si thickness. Therefore, the critical flux, $J_{NiSi\ UC}$, for NiSi formation is about 10^{-4} smaller than that for initiating Ni_2Si formation, which indicates, according to Eq.(4-32), that $r_{Ni2Si} \approx 10^4 r_{NiSi\ max}$. On the other hand, $(\Delta G^{o}_{Ni2Si} - \Delta G^{o}_{NiSi})/RT \approx (\Delta H^{o}_{298\ Ni2Si} - \Delta H^{o}_{298\ NiSi})/RT$ is only 10.4 at 450°C. From this example and Table 4-1, it is likely that r_{imax} is exponentially dependent on standard free energy change for ith silicide formation and, hence, it is likely that there exist linear free energy relationships correlating the r_{imax} to the ΔG^{o}_{ir} for solid state reactions in transition metal-Si systems according to the following equation,

$$\ln(r_{imax}) = -\frac{\alpha}{k_B T}\Delta G^{o}_{ir} + \beta \qquad (4\text{-}35).$$

The LFER for each system may not be the same, i.e., α and β may vary from system to system. To confirm this point further and to obtain quantitative LFERs, many more experiments for determining r_{imax} from multiple phase growth processes in metal-Si couples are required.

In the following discussion, an expression for r_{imax} will be derived from microscopic considerations. This expression will be compared with the LFERs in order to provide experimental support for the expression on one hand and to explain the constants in Eq.(4-35) on the other hand.

Consider a surface of an N (e.g., Si or a refractory metal) crystal lattice that is exposed to an R region in a metal-Si diffusion couple. The N atoms in the surface layer and the M atoms in the R region come into intimate contact, which makes chemical reaction between these atoms possible. If an N atom (or molecule) sitting on the surface has a vibration frequency ν, the frequency for the atom to jump away from the surface into the R region is equal to ν multiplied by a Boltzmann factor, $\exp\{-E_a/k_B T\}$. Only those vibrations with energy higher than the activation energy, E_{ai}, can free the atom from the bound state at the

surface. Therefore, the maximum release rate of N for ith silicide formation in this reaction region can be expressed as

$$r_{imax} = n^* \nu \exp\left[-\frac{E_{ai}}{k_B T}\right] \qquad (4\text{-}36),$$

where n* is the number density of N atoms per unit area of surface layer (atoms/cm^2). The activation energy E_{ai} for the ith silicide formation can be obtained by determining r_{imax} at various temperatures experimentally and by drawing an Arrhenius plot. The activation energy is referred to as the Arrhenius activation energy throughout the thesis. It has been noted that the Arrhenius activation energy E_{ai} is smaller than the energy required to break the chemical bonds of N atoms, which is a very common phenomenon in chemical reactions. According to chemical kinetic theories of rate constant, this is because the simultaneous formation of a new chemical bond compensates for the breaking of the old bond [217]. This point will be considered in deriving an expression for E_{ai}. Fig.4-3 shows schematically the release process in a part of an R region adjacent to a Si lattice (a similar drawing can show the same argument for any other nonmoving reactant lattice). When metal atom A arrives at the Si surface by diffusion (Fig.4-3a; for simplicity, the "molecules" in the R region are drawn as if they are in an ordered structure), it will start to interact with Si atoms surrounding it as indicated by the arrows. Fig.4-3b shows that when the bonds between Si atoms are being broken, new metal-Si bonds are forming, i.e., the two processes proceed at the same time. The bond breaking process absorbs energy while the bond forming process releases energy. As soon as the Si bonds are broken completely, the metal-Si bonds are formed although the bond structure is not exactly same as that in the growing silicide lattice. This will be adjusted during the process following bond breaking. Therefore, the energy release due to metal-Si bond formation is only partially completed. Further energy release will continue as the bond structure adjusts. As a result, the energy required for breaking Si bonds is partially compensated by the energy released due to the formation of new bonds. This can be schematically shown in Fig.4-4. State 1 and state 2 labeled in the figure correspond to that shown in Figs.4-3a and 4-3b, respectively. State 2 is called the "saddle point" in chemical kinetic theory of rate constants [217]. State 3 indicates the energy for the silicide molecule that forms during the process. State 4 at the peak of the solid curve represents the saddle point if no new bonds form during the Si bond breaking process. The energy difference between state 2 and state 1 is the Arrhenius activation energy E_{ai}. The energy difference between state 1 and state 3 is the thermodynamic driving force for the reaction. The energy difference between state 1

and state 4, E, is the activation energy for breaking Si bonds without new metal-Si bond formation, while the difference between state 4 and state 2, E', is the energy compensated by new bond formation during the Si bond breaking process. Therefore, E_{ai} is made up of two parts, i.e.,

$$E_{ai} = E - E' \quad (4\text{-}37).$$

For a given reaction, E' is proportional to the thermodynamic driving force for the release process ΔG_{ir},

$$-E' = \alpha' \Delta G_{ir} \quad (4\text{-}37a).$$

α' in this equation is the proportionality constant. Inserting Eqs.(4-37) and (4-37a) into Eq.(4-36) yields

$$r_{imax} = n^* \nu \exp\left[-\frac{\alpha' \Delta G_{ir} + E}{k_B T}\right] \quad (4\text{-}38).$$

From Eq.(4-38), one has

$$\ln(r_{imax}) = \ln(n^* \nu) - \frac{\alpha' \Delta G_{ir}}{k_B T} - \frac{E}{k_B T} \quad (4\text{-}39).$$

This equation is similar to Eq.(4-35) if the term β in that equation can be split into two terms, i.e.,

$$\beta = \beta' - \frac{E}{k_B T} \quad (4\text{-}40),$$

β' is a constant independent of temperature. α and β in Eq.(4-35) can be obtained by plotting $\ln(r_{imax})$ vs. ΔG^{o}_{ir} for the various silicides at constant reaction temperature. If this is done at several temperatures, E and β' can then be determined from Eq.(4-40) by plotting β vs. 1/T. Combining Eqs.(4-40) and (4-35), one obtains

$$\ln(r_{imax}) = \beta' - \frac{\alpha\Delta G^{o}_{ir}}{k_BT} - \frac{E}{k_BT} \quad (4\text{-}41).$$

The similarity between Eqs.(4-39) and (4-41) indicates experimental support for Eq.(4-38) derived from microscopic considerations. On the other hand, the similarity also suggests that an empirical LFER equation for a given metal-Si system, if available, can be explained by the microscopic mechanism.

At this point, it should be mentioned that the only difference between Eqs.(4-39) and (4-41) is that the standard free energy change ΔG^{o}_{ir} is used in the latter while the free energy change ΔG_{ir} is used in the former, indicating the possible effect of reactant and product concentrations. During analysis of the experimental results by the LFER approach in the preceding discussion, concentration effects were not taken into account, due to the lack of experimental data. As a result, the concentration term is not incorporated into Eqs.(4-35) and (4-41). Instead, it is implicitly included in the constant β', which is easily seen when the concentration term, $(\ln Q_i)/n_i$ in ΔG_{ir} of Eqs.(4-38) and (4-39), is taken out according to (Q_i is concentration quotient of reactants and product for ith silicide formation):

$$\Delta G_{ir} = \Delta G^{o}_{ir} + \frac{k_BT\ln Q_i}{n_i} \quad (4\text{-}42).$$

A question arising from this is which equation, Eq.(4-39) or Eq.(4-41), reflects the actual LFER when the terms, $(\ln Q_i)/n_i$, for various silicides in a given metal-Si system are significantly different from one another. This problem can only be solved by fitting the two equations and examining the goodness of fit for each equation. The one with better fit should be chosen (the methods for fitting LFER equations and analyzing the goodness of fit have been discussed in detail in Ref.[213]). In the following discussion, however, only Eqs.(4-38) and (4-39) are used for the expression of r_{imax}, because they have the advantage of showing explicitly and clearly the concentration effect on both free energy change ΔG_{ir} and maximum release rate r_{imax}.

If an LFER equation in the form of Eq.(4-39) is obtained from analyzing experimental data of multiple phase growth in a given metal-Si system, the equation can provide the following information: 1) The activation energy E, the vibration frequency ν and n^* are the same for all reactions that fit the equation. This is not surprising since in all the reactions the reactants are the same. In particular, the nonmoving reactant is the same and the factors, E, ν and n^* are the properties of the reactant. However, E may change with crystalline orientation if N is a single crystal (such as a Si wafer). 2) $\ln(r_{imax})$ is linearly

dependent on the free energy change for ith silicide formation, ΔG_{ir}, because according to Eq.(4-38), the energy released during the period of breaking chemical bonds of one N atom is proportional to the thermodynamic driving force, ΔG_{ir}, per N atom. In other words, a larger driving force results in a larger energy release for the bond breaking process and, hence, a smaller Arrhenius activation energy. This relationship reflects the unique character of silicide formation in metal-Si couples.

4.2.2.2. Expression for Free Energy Change for the Release Process

The driving force for the release process is the free energy difference between state 1 and state 3 shown in Figs.4-3 and 4-4, i.e., the state, when M atoms arrive at the N surface and intermix with N atoms (state 1), and the state, when the N atoms are released into R region forming silicide "molecules" with the M atoms. Theoretically, the driving force per molecule can be expressed by the chemical potential of each component,

$$\Delta G_{ir} = \mu_R^i - m_i \mu_{NS}^M - n_i \mu_{NS}^N \qquad (4\text{-}43),$$

where μ_R^i is the chemical potential of the product molecule in the R region. μ_{NS}^M and μ_{NS}^N are the chemical potentials of the M atoms and the N atoms at the N surface (indicated by the subscript NS). The last two chemical potentials are not practically measurable, which makes Eq.(4-43) inappropriate for estimating the driving force in practice. An alternative approach is to use Eq.(4-42) as the expression of the driving force for the release process. It can be shown, using a Gibbs free energy versus composition plot, that this is a reasonable approximation. In Fig.4-5, the curve represents schematically the free energy of a silicide MSi and the straight line indicates the free energy of an ideal M-Si mixture at various compositions (where M represents the metal in the system). The free energy difference between points A and B is the standard free energy change $\Delta G^o_{MSi\ r} = G_B - G_A$, where G_B and G_A are the free energy of pure MSi and the ideal M-Si mixture respectively at the same composition as that of MSi. If the free energy change of mixing is considered, the free energy of M-Si solution should be indicated, for example, by point C. Similarly, when the concentration of MSi at the N surface is taken into account (see discussion about Q_i below), the free energy for MSi is lowered to, say, point D. As a result, the free energy change for transforming the M-Si solution into a MSi silicide (not pure MSi) is $\Delta G_{MSi\ r} = G_D - G_C$, which is equal to the $\Delta G_{MSi\ r}$ expressed by Eq.(4-42). Two more factors still have to be considered. As is shown in Fig.4-3a, when metal atoms arrive at the Si surface,

part of their chemical bonds is not satisfied while the chemical bonds of Si atoms are distorted by the intermixing. Furthermore, the concentration gradient between the surface Si layer and its neighboring layers is very large. These cause the free energy of this layer to be higher than that for the uniform bulk M-Si solution. The difference in free energies of the Si surface layer and a M-Si solution of the same composition is $\Delta G_{MSi\ s} = G_E - G_C$, which is equivalent to an interfacial energy in terms of dangling or distorted bonds and a concentration gradient. When $\Delta G_{MSi\ s}$ is added, the free energy of the Si surface layer is indicated by point E. Similarly, the newly formed "molecules" in the R region are not in a uniform solution either, which has been discussed in Sec.4.2.1. Therefore, the free energy of the "molecules" in the R region should be higher than that at point D and are, for example, represented by point F, i.e., the energy difference $G_F - G_D$ is the interface energy of the R region. Consequently, the actual free energy change for the release process should be $G_F - G_E$, which can also be expressed by Eq.(4-43). However, since G_E is unknown, $G_F - G_E$ can be estimated from $\Delta G_{MSi\ r} = G_D - G_C$ (i.e., using Eq.(4-42)), although some error will be introduced. It may be expected that in most cases the error would be less than ten per cent of actual driving force values, which is a reasonable approximation.

The concentration effect has been mentioned in the preceding discussion. The expression for the concentration quotient is derived in the following. To find a suitable formula for Q for an interfacial reaction in a metal-Si diffusion couple, one has to reasonably define the concentration of reactants and products for such a reaction. In step 2 of the silicide formation process, there is the release of N atoms and formation of silicide "molecules". If, as a first order approximation, only the interaction between nearest neighbor atoms is responsible for the reaction, then only a single atomic layer of N and those M atoms which are the nearest neighbors to the N atoms in this layer can react at once. The N atoms next to the N surface layer cannot be released until the N atoms in the surface layer are removed. Thus, the physical picture for the release process can be described. The reaction occurs in two-dimensional space, defined by the surface atomic layer of N lattice. The N atoms in this space are fixed on a two-dimensional net and the M atoms are mobile. When the M atoms are brought, by the diffusion, into intimate contact with N atoms in this net, reaction between these atoms will occur. During the same period when the silicide "molecules" are formed, the chemical bonds, between the N atoms in the net and those in the next layer, are broken, i.e., these silicide atoms are removed from the surface of the N lattice. A new two-dimensional net of N is then exposed to the reaction region and so on. There are, however, some spots in the previous net where the formed silicide "molecules" may not be removed as quickly as most of the other "molecules", i.e., some of the product "molecules" will stay on the two-dimensional net (or on the surface of

N lattice) longer than other "molecules". This is shown schematically in Fig.4-6. If a two dimensional net is not a perfectly flat crystalline plane, e.g., an N atom is sitting on top of this plane (atom A on a (001) plane of Si in Fig.4-6), then the chemical bonding state for the atoms (B and C atoms in Fig.4-6) next to this atom will be different from other atoms in the same plane. It is obvious that B and C atoms each have three bonds, but all other atoms on the surface have only two bonds each, which means the activation energy, E, for removing atoms B and C is larger than for other atoms. As a result, although the B and C atoms may already react with M atoms to form silicide "molecules", they cannot be removed from the surface as fast as other N atoms. In other words, their release is dependent on A atom removal. Similarly, other defects, such as steps, kinks, vacancies, and dislocation intersections with the surface, can produce the same effect. Thus, in step 2 of the reaction, the N atom release process proceeds one layer at a time without significant movement of defects such as steps, kinks and dislocations. This physical picture does have experimental support. Recently, Ross and Jibson [196, 197] reported that oxidation of silicon (<111> oriented wafers) occurred one monolayer at a time with bilayer steps not moving during the process.

Based on this physical picture, the concentrations of reactants and product in the two-dimensional reaction space can be easily derived. The net number of N atoms which can be released is

$$N^N = n^* - n_d \qquad (4\text{-}44),$$

where n^* indicates the number density of N atoms in a perfect surface layer and n_d is the number density of atomic defect positions in the surface layer. n_d is equal to the number density of product "molecule" which cannot be removed promptly due to the presence of these defects. N^N is the number density of N atoms that can be released promptly during the release process. The number of M atoms which can react with the N^N atoms to form ith silicide is

$$N^M = \frac{m_i}{n_i} (n^* - n_d) \qquad (4\text{-}45),$$

where m_i and n_i have the same meanings as before. In Eqs.(4-44) and (4-45), because $n_d << n^*$, $N^N \approx n^*$ and $N^M \approx (m_i/n_i)n^*$. Using the two equations, the mole fractions of N and M reactants and product (X_i^N, X_i^M and X_i, respectively, with X_i indicating product molecule concentration on the two-dimensional net) can be expressed as follows:

$$X_i^N = \frac{n^*}{\{n^* + \frac{m_i}{n_i} n^* + n_d\}} \quad (4\text{-}46),$$

or

$$X_i^N = \frac{n^*}{\{n^* + \frac{m_i}{n_i} n^*\}}$$

since $n_d << n^*$. Similarly,

$$X_i^M = \frac{\frac{m_i}{n_i} n^*}{\{n^* + \frac{m_i}{n_i} n^*\}} \quad (4\text{-}47);$$

$$X_i = \frac{n_d}{\{n^* + \frac{m_i}{n_i} n^*\}} \quad (4\text{-}48).$$

From Eqs.(4-46) to (4-48), Q_i for the reaction is

$$Q_i = \frac{X_i}{(X_i^N)^{n_i} (X_i^M)^{m_i}} \quad (4\text{-}49),$$

or

$$Q_i = \{\frac{n_d}{n^*[1 + (m_i/n_i)]}\} \times \{(\frac{1}{1 + (m_i/n_i)})^{n_i} \times (\frac{1}{1 + (n_i/m_i)})^{m_i}\}^{-1}$$

where n_d/n^* is the concentration of the defects in the surface. By inserting this equation into Eq.(4-42), ΔG_{ir} in Eq.(4-42) can be expressed simply as

$$\Delta G_{ir} = \Delta G_i^o + \frac{k_B T}{n_i} \ln\{(X_i)/[(X_i^N)^{n_i}(X_i^M)^{m_i}]\} \quad (4\text{-}50).$$

This equation is useful when a comparison of driving forces for different silicides to form is required. From this equation, the comparison is based on the free energy change per non-moving reactant atom (or per mole) which is released. Therefore, a silicide with more than one N atom in its molecule (or formula unit) may have a smaller ΔG_{ir} because n_i >1 (note, ΔG_{ir}^o in Eq.(4-42) and (4-50) is already defined as the standard free energy

change per N atoms and it is equal to the standard free energy change per f.u. divided by n_i). For example, $\Delta H^{o}_{i\,298}$ for NiSi and Ni_3Si_2 are -85.7 and -223.6 kJ per mole formula unit respectively [218]. If $(n_d/n^*)=10^{-6}$, and the reaction occurs at 300°C, then the calculated ΔG_{ir}'s, using Eq.(4-50), for NiSi and Ni_3Si_2 are -148.2 and -138.9 kJ/mol. It is seen that Ni_3Si_2 has a larger negative value of ΔH^{o}_{298}, but a smaller ΔG_{ir}. Experimentally, it has been found that the first silicide to form in almost all transition metal-Si systems are those only containing one N atom per formula unit. A silicide molecule with more than one non-moving reactant atom has a lower likelihood of forming because its formation requires more non-moving reactant atoms to *be released at the same time*. This phenomenon has been considered in Eqs.(4-38), (4-42) and (4-50) by expressing the E and ΔG_{ir} as an activation energy and a free energy change for releasing one N atom.

4.2.3. Maximum Formation Rate and Free Energy Change for Formation Process

4.2.3.1. Free Energy Change of Formation

The driving force for formation, i.e., the process of rearranging product "molecules" on the surface of a growing phase k, is the difference in free energies between the product "molecules" in the k phase and those on the surface of the k phase. The driving force can be expressed by an equation similar to that used by Cahn and Hilliard [212]:

$$\Delta G_{ik} = m_i\mu^{M}_{ik} + n_i\mu^{N}_{ik} - g_0(c) - \bar{k}\,(dc/dx)^2 \qquad (4\text{-}51),$$

where the last two terms have the same meanings as those in Eqs.(4-25) to (4-27) in Sec.4.2.1. μ^{M}_{ik} and μ^{N}_{ik} are the chemical potentials per M and N atoms in the k phase, respectively. Inserting Eq.(4-27) into Eq.(4-51) yields

$$\Delta G_{ik} = m_i\mu^{M}_{ik} + n_i\mu^{N}_{ik} - m_i\mu^{M}_{R}(c) - n_i\mu^{N}_{R}(c) - \bar{k}\,(dc/dx)^2$$

or

$$\Delta G_{ik} = \Delta g - \bar{k}\,(dc/dx)^2 \qquad (4\text{-}52).$$

$m_i\mu^{M}_{R}(c)$ and $n_i\mu^{N}_{R}(c)$, as defined in Eq.(4-27), are the chemical potentials per M and N atoms in a uniform solution of composition c in the R region. As a result, Δg in Eq.(4-52)

is the free energy difference per molecule due to the differences in structures and compositions between the "molecules" in the growing phase and those in the R region. The value of ΔG_{ik} can be estimated from the surface tension, σ_{kN}, of the interface between the k phase and the nonmoving reactant phase (which is the R region during k phase growth). According to Cahn and Hilliard,

$$\sigma_{kN} = \frac{-\Delta G_{ik\ tot}}{A} = -N_V \int \left[\Delta g - \bar{K}(dc/dx)^2\right] dx \qquad (4\text{-}53).$$

The minus sign in this equation is used because the terms in the integrand are arranged in such a way that ΔG_{ik} is negative when deriving Eqs.(4-51) and (4-52), but the surface tension σ_{kN} should have a positive value. The term $\Delta G_{ik\ tot}$ in Eq.(4-53) is the total driving force in area A of the reaction region, and N_V is the number density of "molecules" per unit area of the reaction region. From this equation, the average driving force per molecule, $\overline{\Delta G_{ik}}$, can be obtained by

$$\overline{\Delta G_{ik}} = \frac{-\sigma_{kN}}{x_R N_V} = \frac{1}{x_R} \int \left[\Delta g - \bar{K}(dc/dx)^2\right] dx \qquad (4\text{-}54),$$

where x_R is the thickness of the interface. Cahn and Hilliard [212] have proposed an optical method to measure x_R for metal samples. By using HRTEM, the x_R is also measurable for other crystalline samples. Therefore, the average driving force per molecule for formation can be determined if σ_{kN} is available. At this point, it should be mentioned that Eqs.(4-52) and (4-54) cannot be obtained from TIP theory since the driving force involvs in an interfacial process and contains a "gradient energy" term due to the existence of a large concentration gradient.

Fig.4-7 shows schematically how the free energy is distributed over the R region. In the figure, G_N represents the free energy of N phase. G_E, G_F and G_D have the same meaning as that shown in Fig.4-5, i.e., the free energies of N surface, R region and the growing phase (k), respectively. The NS region is the N surface layer. When M atoms diffuse to the N surface, some intermixing occurs and the free energy is lowered from G_N to G_E. The R region in the figure is the reaction region. As soon as N atoms are released into this region and form new "molecules", free energy, $G_F - G_E$, is released. The GS region is the surface of growing phase k. The "molecules" are driven to the region to crystallize by the energy difference, $G_D - G_F$, which is equal to the interface energy per

"molecule". As the reactions proceed, the R region and hence the free energy distributions over the region will move together to the right of the figure, leaving crystalline silicide, i.e., the k phase, behind.

As is discussed in Sec.3.3.5, there may be more than one phase for a given silicide. In this case, the driving forces for different phases of the silicide are not the same. This is schematically shown in a Gibbs free energy versus composition plot (Fig.4-8). There are, for example, two possible phases for the ith silicide, the stable phase (indicated as i1) and the metastable phase (indicated as i2). In the figure, G_F is the free energy of "molecules" in the R region, G_{i1} and G_{i2} (i.e., $G_{ik} = m_i\mu_{ik}^M + n_i\mu_{ik}^N$) are the energies of "molecules" in stable and metastable phases, respectively. Therefore, the driving forces for the two phases are $\Delta G_{i1} = G_{i1} - G_F$ and $\Delta G_{i2} = G_{i2} - G_F$. The stable phase has a larger driving force. An interesting conclusion that may be drawn from this result is that if the free energy G_{i2} for a metastable phase is equal to or larger than G_F, there is no driving force for this phase formation. This conclusion can be used to explain why a large heat of mixing for a metal-Si system does not guarantee amorphous phase formation. In this case, the heat of mixing is considered as the thermodynamic driving force for SSA (See Sec.2.3 [16, 152, 153]), i.e., the enthalpy of the amorphous phase, H_{am}, can be approximately taken as G_{i2} in Fig.4-8. From the standpoint of the conclusion above, no matter how large the heat of mixing is, there is no driving force for amorphous phase to form, as long as $H_{am} \approx G_{i2} \geq G_F$. As a result, a crystalline phase, rather than an amorphous phase, will grow.

4.2.3.2. Maximum Formation Rate

Unlike what happens to the maximum release rate, experimental results to date do not provide support for a linear free energy relationship between the maximum formation rate and the driving force for the formation process. Instead, it is reported in the literature that in some metal-Si systems, metastable phases, particularly, amorphous phases grow before the stable phase can form. This means that these metastable phases have larger $F_{ik\,max}$. According to the discussion in the last section, the driving forces for metastable phases are definitely smaller than those for stable phases in each respective system. It is also noted that in most silicide reactions, no metastable phase formation is observed. Therefore, an expression, like Eq.(4-38) for r_{imax}, cannot be expected for F_{ikmax}. This makes the expression for $F_{ik\,max}$ quite simple, i.e.,

$$F_{ik\,max} = n_R^i \nu_i \exp\left[-\frac{E_{ik}}{k_B T} \right] \qquad (4\text{-}55),$$

where ν_i and n_R^i are the vibration frequency and number density (f.u./cm^2) of ith silicide "molecules" per unit area of reaction region, and E_{ik} is the activation energy of rearranging a molecule from reaction region to the growing phase. E_{ik} is the energy required for adjusting the bond structure and the coordinations of the "molecules" in the R region to that of the growing phase. It is conceivable that as less adjustment is required, E_{ik} becomes smaller. For example, the amorphous phase has the most open and least ordered structure compared with crystalline phases of a given silicide. In addition, its structure may also be closest to that of the R region. Therefore, it may have the smallest E_{ik}. As a result, the amorphous phase may have the largest $F_{ik\,max}$. Also, if a crystalline phase has a complex structure which is significantly different from that of R region, E_{ik} for this phase will be large. Consequently, this phase will have a small $F_{ik\,max}$.

In practice, the conditional maximum formation rate, $F_{ik'}$, may be more significant, since nucleation is the first step for a phase to grow. From Eq.(4-55), $F_{ik'}$ can be derived easily as follows:

$$F_{ik'} = F_{ik\,max} \exp\left[-\frac{\Delta G'_{ik}}{k_B T}\right] \quad (4\text{-}56).$$

$\exp[-\Delta G'_{ik}/k_B T]$ in Eq.(4-56) is the Boltzmann factor for k phase nucleation. $\Delta G'_{ik}$ is the energy barrier for heterogeneous nucleation. According to classical nucleation theory, one has

$$\Delta G'_{ik} = \Delta G'_{ik\ hom} \times \frac{2 - 3\cos\theta + \cos^3\theta}{4} \quad (4\text{-}57),$$

if a nucleus in the shape of spherical cap is assumed. θ is the contact angle and $\Delta G'_{ik\,hom}$ is the energy barrier for homogeneous nucleation.

$$\Delta G'_{ik\ hom} = \frac{16\pi}{3} \frac{(\Delta\sigma)^3}{(N_{ik}\Delta G_{ik} + \Delta H_d)^2} \quad (4\text{-}58),$$

where $\Delta\sigma$ is the difference in interface energies due to k phase nucleation and N_{ik} is the number density of "molecules" per unit volume of k phase. ΔH_d is the elastic strain energy per unit volume, which is induced by nucleation. Eqs.(4-57) and (4-58) are the same as those given by classical nucleation theory except that the driving force, ΔG_{ik}, the free

energy difference between the k phase and the R region per unit volume, is different from that used in classical nucleation theory, i.e., ΔG_c the chemical free energy change per unit volume. Actually, ΔG_c includes all the free energy changes in the three step process because an interfacial reaction in a diffusion couple is usually considered as one step process. This concept is applicable to the case where the interface between a growing phase and a contracting phase (made up of the nonmoving reactant atoms or "molecules") is coherent or semicoherent, which will be discussed in Sec.4.4. In other cases where the interface has a thickness of a few atomic or molecule layers, it is unlikely that the chemical reaction between reactant atoms and the transformation of the same atoms from the interfacial region into the growing phase can occur at the same time. Therefore, using ΔG_{ik} to describe the driving force for the formation process is more reasonable.

Recall Eqs.(3-49) and (3-50),

$$F_{ik} = F_{ik'} = \frac{r_{ik'}}{n_i} \quad \text{if} \quad r \geq r_{ik'} \qquad (3\text{-}49),$$

$$F_{ik} = \frac{r_i}{n_i} \quad \text{if} \quad r < r_{ik'} \qquad (3\text{-}50),$$

where r_i and $r_{ik'}$ are the release rate for ith silicide to form and critical release rate corresponding to $F_{ik'}$, respectively. By combining Eqs.(3-49), (3-50) and (4-56), the formation rate can be expressed as a function of release rate and activation energies for formation and nucleation, i.e.,

$$F_{ik} = \frac{r_i}{r_{ik'}} F_{ik\,max} \exp\left[-\frac{\Delta G'_{ik}}{k_B T}\right] \quad \text{if} \quad r < r_{ik'}$$

$$F_{ik} = F_{ik\,max} \exp\left[-\frac{\Delta G'_{ik}}{k_B T}\right] \quad \text{if} \quad r \geq r_{ik'} \qquad (4\text{-}59)$$

4.3. Criteria for Silicide Formation

4.3.1. Driving Force as a Function of Flux

In Sec.4.2, the expressions for the driving forces, i.e., $\Delta\mu_{R'}^{M}$, ΔG_{ir}, and ΔG_{ik} for moving reactant diffusion, nonmoving reactant release and k phase growth, are given in Eqs.(4-31), (4-42) and (4-52), respectively. It is conceivable that the driving forces will

change as the reactions proceed. Since the reactions are induced by diffusion and since smaller diffusion flux means less matter involved in the reactions, the driving forces may decrease corresponding to the change in diffusion flux. In this section, the changes in driving forces will be examined. Recalling Eqs.(4-33), (4-38), and (4-42), and combining them together yields the following;

$$r_i = n^* \nu \frac{\Delta J}{J_{iUC}} \exp\left[-\frac{E + \alpha \Delta G_{ir}}{k_B T}\right]$$

$$= n^* \nu \exp\left[-\frac{E + \alpha \Delta G_{ir}}{k_B T} + \ln\left(\frac{\Delta J}{J_{iUC}}\right)\right] \qquad (4\text{-}60).$$

From Eq.(4-60), a new free energy term, ΔG^*_{ir}, is defined such that the term $\ln(\Delta J/J_{iUC})$ is combined with ΔG_{ir} by means of Eq.(4-50),

$$\alpha \Delta G^*_{ir} = \alpha \Delta G_{ir} - k_B T \ln(\Delta J/J_{iUC})$$

$$= \alpha \Delta G^o_i + \frac{\alpha k_B T}{n_i} \ln\{(X^i_i)/[(X^N_i)^{n_i} (\Delta J/J_{iUC})^{n_i/\alpha} (X^M_i)^{m_i}]\}$$

so that
$$\Delta G^*_{ir} = \Delta G^o_i + \frac{k_B T}{n_i} \ln\{(X^i_i)/[(X^N_i)^{n_i} (\Delta J/J_{iUC})^{n_i/\alpha} (X^M_i)^{m_i}]\} \qquad (4\text{-}61).$$

When $\Delta J \geq J_{iUC}$, from Eq.(4-33) and (3-45), $\Delta J/J_{iUC} = 1$ so that $\Delta G^*_{ir} = \Delta G_{ir}$. When $\Delta J < J_{iUC}$, ΔG^*_{ir} is greater than ΔG_{ir} (i.e., $-\Delta G^*_{ir} < -\Delta G_{ir}$), and as ΔJ decreases, ΔG^*_{ir} increases. Eq.(4-60) can be expressed in terms of ΔG^*_{ir}, i.e.,

$$r_i = n^* \nu \ \exp\{-\frac{E + \alpha \Delta G^*_{ir}}{k_B T}\} \qquad (4\text{-}62).$$

According to the derivation of Eqs.(4-38), (4-39) and (4-61), and the arguments in Sec.4.2.2.1, ΔG^*_{ir} is the driving force for the release process and is a function of diffusion

flux. The change in ΔG^*_{ir} can be understood better by considering the concentration effect.

When the diffusion flux decreases, the number of M atoms arriving at the N surface during a given time interval becomes less and less. Since the number of atoms per unit area of N surface is fixed, the concentration of M atoms at the N surface decreases. Consequently, the energy released during the period for breaking chemical bonds of N atoms (i.e., E', see Sec.4.2.2.1) is shared by more N atoms, so that the energy release per N atom, i.e., ($-\alpha\Delta G^*_{ir}$) becomes smaller. From this viewpoint, Eq.(4-62) can be interpreted as follows.

The release rate, r_i, decreases as the driving force decreases due to the change in moving reactant concentration.

Unlike ΔG^*_{ir}, the driving force for the formation process, ΔG_{ik}, does not decrease continuously, because of its unique character. According to Cahn and Hilliard [212], the thickness of an interface is not an independent variable once the temperature and pressure of the system are specified. Thus, under the conditions used in this chapter, i.e., the system is at constant temperature and pressure, the interfacial layer (reaction region) thickness x_R is a constant, x_c, corresponding to a minimum interfacial free energy. As a result, any change in x_R would increase the interfacial free energy and the interface would act in such a way that the minimum energy state is recovered. During a release process, $r_i > 0$, so that x_R will increase. The interfacial free energy as a function of thickness x_R is

$$-\Delta G_{ik\ tot} = -AN_V \int_0^{x_R} \left[\Delta g - \bar{k}(dc/dx)^2 \right] dx \qquad (4\text{-}63),$$

where the 0 indicates the origin at one side of reaction region and x_R is the thickness of the region. A and N_V are the area and molecule number density per unit volume of R region. The rate of interfacial free energy change with respect to x_R at constant temperature and pressure is

$$\left[\frac{d(-\Delta G_{ik\ tot})}{dx_R}\right]_{T.P.} = -AN_V \left[\Delta g - \bar{k}(dc/dx)^2 \right] \qquad (4\text{-}64),$$

where $[\Delta g - \bar{k}\,(dc/dx)^2]$ is an implicit function of x_R. Since the interfacial free energy ($-\Delta G_{ik\ tot}$) is a minimum at $x_R = x_c$, the derivative on the left hand side of Eq.(4-64) should be equal to zero at the thickness x_c and be larger than zero when $x_R > x_c$. Therefore,

$$\Delta g - \bar{k}\,(dc/dx)^2 = 0 \quad \text{at } x_R = x_c$$
$$\Delta g - \bar{k}\,(dc/dx)^2 > 0 \quad \text{if } x_R > x_c \qquad (4\text{-}65).$$

During silicide reactions, when $r_i > 0$, more and more product "molecules" are formed in the R region, which tends to increase the thickness of the region, i.e., $x_R > x_c$. When $r_i = 0$, $x_R = x_c$. From Eq.(4-52) and (4-54),

$$\Delta G_{ik} = \Delta g - \bar{k}\,(dc/dx)^2 \qquad (4\text{-}52),$$

$$\overline{\Delta G_{ik}} = \frac{-\sigma_{kN}}{x_R N_V} \qquad (4\text{-}54).$$

One obtains, then,

$$\Delta G_{ik} = \Delta g - \bar{k}\,(dc/dx)^2 \approx \overline{\Delta G_{ik}} \qquad \text{if } r_i > 0,$$

and

$$\Delta G_{ik} = \Delta g - \bar{k}\,(dc/dx)^2 = 0 \qquad \text{if } r_i = 0 \qquad (4\text{-}66).$$

From Eq.(4-66), it can be seen that during a silicide reaction, as long as newly formed silicide "molecules" are released into the R region, they will be driven out of the region by the thermodynamic force ΔG_{ik} and rearranged on the growing k phase. Once the diffusion of M atoms stops, i.e., $\Delta J = 0$, so that $r_i = C_i \Delta J = 0$, the driving force will also vanish.

An analytical expression for the chemical potential difference, $\Delta\mu^M_{R'}$, i.e., the driving force for diffusion, as a function of diffusion flux has not been developed during this study. But some general tendencies of changes in $\Delta\mu^M_{R'}$ corresponding to flux J can be qualitatively discussed. The magnitude of $\Delta\mu^M_{R'}$ is mainly determined by the chemical potential difference between a growing silicide phase and a nonmoving reactant phase and by the M concentration at the N surface. Therefore, $\Delta\mu^M_{R'}$ does not change (decrease) significantly during a reaction for a given silicide phase. But, $\Delta\mu^M_{R'}$ usually decreases with the formation of each new silicide. For example, in a near noble metal-Si diffusion couple, the most frequently observed first silicide to form is M_2Si (where M represents Ni, Pt, Pd,

and Co etc.), which is followed by MSi and then by MSi_2 (for Ni-Si and Co-Si systems only). Obviously, the chemical potentials of metal atoms are smaller in the silicide with lower concentration of metal. Therefore, each time a more Si-rich silicide forms, the $\Delta\mu^M_{R'}$ at the growing phase/Si interface becomes smaller than it was prior to the new silicide growth. When the system reaches thermodynamic equilibrium, both ΔJ and $\Delta\mu^M_{R'}$ are equal to zero, because the chemical potentials of M are equal to the same value throughout the system. It is also noteworthy that if the system is not in an equilibrium state while $\Delta J \approx 0$, such as a system held at room temperature, $\Delta\mu^M_{R'}$ still has a non zero value. Therefore, this driving force is different from ΔG^*_{ir} and ΔG_{ik} for release and formation processes. These two forces vanish whenever diffusion stops.

From Eq.(4-21b), the FEDR per unit area of reaction region, dg^i_R/dt, is

$$\frac{dg^i_R}{dt} = \Delta J \Delta\mu^M_{R'} + r_i \Delta G^*_{ir} + F_{ik}\Delta G_{ik} \qquad (4\text{-}21b),$$

The expressions for $\Delta\mu^M_{R'}$, F_{ik}, r_i, ΔG^*_{ir} and ΔG_{ik} are given by Eqs.(4-31), (4-59), (4-62), (4-61) and (4-66) respectively. There are two essential conclusions that can be drawn from these equations and the preceding discussions in this chapter. Firstly, with the advance of a reaction in a given R region, a decrease in diffusion flux ΔJ with time will result in a corresponding decrease in the release rate and formation rate, while the driving force for the release process will also decrease (or ΔG^*_{ir} or increases). The driving forces for diffusion and formation processes, i.e., $\Delta\mu^M_{R'}$ and ΔG_{ik}, are almost constant for a given phase to form. Therefore, the total FEDR in the R region will continuously decrease with time. Secondly, when thermodynamic equilibrium is established in a given system (e.g., a Si-richest phase on Si substrate), all the fluxes ΔJ, r, and F and all driving forces go to zero so that $dg^i_R/dt = 0$. These two conclusions are in agreement with the general results from TIP theory, i.e.,

$$\frac{dP}{dt} \leq 0 \qquad (4\text{-}67),$$

where $P = d_iS/dt$ is the entropy production per unit time. Eq.(4-67) indicates that if a system is at a stationary state (according to TIP, a thermodynamic equilibrium state is considered as a special case of a stationary state), the time variation of the entropy production (dP/dt) is equal to zero. At this state, entropy production per unit time is a minimum. In particular, when a stationary state is the thermodynamic equilibrium state, $d_iS/dt = 0$. It certainly satisfies Eq.(4-67). When the system is away from stationary state, the time variation of the entropy production, dP/dt, is smaller than zero, which means the system is in an irreversible process in which the entropy production decreases with time. The two conclusions mentioned above can be expressed as

$$\frac{d}{dt}\left[\frac{d_iG_R^i}{dt}\right]_{T.P.} = A\,\frac{d}{dt}\left[\frac{d_ig_R^i}{dt}\right]_{T.P.} \geq 0 \qquad (4\text{-}68).$$

The sign $\geq$ is used because $d_iG_R^i/dt$ has a negative value for irreversible processes. $d_iG_R^i/dt$ and A in this equation represent the FEDR in the whole reaction region and the area of the region respectively. This equation is significant because it indicates that when the solid state reactions in a diffusion couple advance toward thermodynamic equilibrium, the FEDR for each R region increases (i.e., $-d_iG_R^i/dt$ decreases) with time. However, both Eq. (4-67) and Eq.(4-68) do not specify how the entropy production per unit time decreases and the free energy degradation rate increases with time. In the following section, it will be shown that in an R region and at a given diffusion flux (ΔJ), there are always some reactions (release and formation processes) that may result in the largest FEDR in the region. From these results, the criteria for silicide formation are proposed.

4.3.2. Criteria for Silicide Formation

From Eq.(4-21b) the FEDR for the release process, dg_{ir}/dt, can be expressed as the follows:

$$\frac{dg_{ir}}{dt} = r_i\Delta G_{ir}^{*} \qquad (4\text{-}69).$$

Inserting Eq.(4-62) to Eq.(4-69) yields,

$$\frac{dg_{ir}}{dt} = n^*v \ \exp\{-\frac{E + \Delta G_i^*}{kT}\}\Delta G_i^* \qquad (4\text{-}70).$$

If in a R region, there are three possible release rates and they have the relationship, $r_2 > r_1 > r_3$ at ΔJ_0, as shown in Fig.4-9, one obtains $|\Delta G_2^*| > |\Delta G_1^*| > |\Delta G_3^*|$ by applying Eq.(4-62) (n^*, v, and E are the same for all reactions in a reaction region Sec.4.2.2.1). Inserting these results into Eq.(4-70), gives

$$\frac{dg_{2r}}{dt} < \frac{dg_{1r}}{dt} < \frac{dg_{3r}}{dt}$$

or

$$\left|\frac{dg_{2r}}{dt}\right| > \left|\frac{dg_{1r}}{dt}\right| > \left|\frac{dg_{3r}}{dt}\right| \qquad (4\text{-}71),$$

which indicates that the largest release rate (r_2) will cause the largest FEDR.

From Eq.(4-21b) the FEDR for the formation process, dg_{ik}/dt, can be expressed as

$$\frac{dg_{ik}}{dt} = F_{ik}\Delta G_{ik} \qquad (4\text{-}72).$$

Fig.4-10 shows schematically a formation rate versus release rate plot for three phases of ith silicide. There are two possible cases to consider. In the first case, phase 1 in the figure is stable while phases 2 and 3 are metastable. The relationship among the driving forces for the three phases to form is $\Delta G_{i1} < \Delta G_{i2} < \Delta G_{i3}$. At a given release rate, r_0, it can be seen, from Fig.4-10, that $F_{i1} > F_{i2}' > F_{i3}'$, i.e., the formation rate of phase 1 is larger than the conditional maximum formation rates (nucleation rates) of the other two phases. Applying Eq.(4-72) to each process, one has the following relationship

$$F_{i1}\Delta G_{i1} < F_{i2}\Delta G_{i2} < F_{i3}\Delta G_{i3}$$

or

$$\left|\frac{dg_{i1}}{dt}\right| > \left|\frac{dg_{i2}}{dt}\right| > \left|\frac{dg_{i3}}{dt}\right| \qquad (4\text{-}73),$$

which means the growth of phase 1 will cause the largest FEDR in all the possible processes. When the release rate decreases and passes a critical release rate r_{i2}', $F_{i1} = F_{i2}' > F_{i3}'$. Even in this case, Eq.(4-73) is still valid because phase 1 has the largest driving

force. Therefore, the formation of stable phase will result in the largest FEDR throughout the process of ith silicide formation.

In case 2, phase 2 in Fig.4-10 is stable and $\Delta G_{i2} < \Delta G_{i1} < \Delta G_{i3}$. According to Fig.4-10, at r_0, one has $F_{i1} > F_{i2'} > F_{i3'}$. If F_{i1} is significantly larger than $F_{i2'}$, the relationship between the FEDRs for these processes is

$$F_{i1}\Delta G_{i1} < F_{i2}\Delta G_{i2} < F_{i3}\Delta G_{i3} \qquad (4\text{-}74).$$

This is because the driving force for the stable phase (phase 2) is usually only a few times larger than that for the metastable phase (see discussion in Sec.4.2.3.1 and Fig.4-8), while F_{i1} is much larger than $F_{i2'}$. When the release rate decreases, at some point, $F_{i1}\Delta G_{i1} = F_{i2'}\Delta G_{i2}$. After this point, the relationship expressed by Eq.(4-74) will change to

$$F_{i2}\Delta G_{i2} < F_{i1}\Delta G_{i1} < F_{i3}\Delta G_{i3} \qquad (4\text{-}75).$$

In case 2, therefore, the metastable phase (k=1) will induce the largest FEDR when its formation rate is much larger than that for stable phase. As soon as Eq.(4-75) is satisfied due to the decrease of release rate, stable phase formation will result in the largest FEDR. Similarly, the case when phase 3 in Fig.4-10 is stable while the other two are metastable phases can be explained as above.

If ith silicide has the largest release rate in a R region and k phase growth of this silicide induces the largest FEDR in all possible formation processes, the total FEDR due to the formation of k phase of ith silicide in the R region is also the largest one compared to all other reactions, i.e.,

$$\left|\frac{dg_R^i}{dt}\right| > \left\{ \left|\frac{dg_R^1}{dt}\right|, \left|\frac{dg_R^2}{dt}\right| \ldots \left|\frac{dg_R^j}{dt}\right| \ldots \right\} \quad j = 1, 2, 3\ldots \text{ and } j \neq i \qquad (4\text{-}76).$$

Thus far, the largest FEDR for the diffusion process has not been examined. Although competitive diffusion processes do exist in bulk and thin film diffusion, the competition in a R region is neglegible for three reasons. Firstly, the concentration gradient in the region is much larger than that in other diffusion regions. Secondly, the interface structure is more open than those of other solid phases. Thirdly, the diffusion distance is rather short, only a few atom layers thick. As a result, diffusion in this region is very fast. It is expected that the diffusion flux in the R region, J, is determined by the diffusion flux

(J_{in}) from the growing phase into the R region through the growing phase. Therefore, $J_{in}\Delta\mu_R^M$, represents the largest FEDR for diffusion in R region. For the purpose of comparing the FEDRs of all possible reactions, the FEDR due to diffusion in the R region can be expressed by $\Delta J\Delta\mu_R^M$, which is actually the same for all possible reactions. (also see Eqs.(4-21), (4-21a) and (4-21b) and discussion therein).

The discussion above can be briefly summarized as follows. At a given diffusion flux, the largest release rate for ith silicide formation will result in the largest FEDR among all possible release processes. When this release rate occurs, the formation of phase k will cause the largest FEDR among all possible formation processes for the ith silicide, if F_{ik} is much larger than other possible phases, or if the k phase has the largest driving force when formation rates of two or more phases are the same. Consequently, the simultaneous occurrence of the release of ith silicide "molecules" and the growth of phase k will result in the largest FEDR in the R region. It is also worth mentioning that if the reactions in an R region adjacent to N advance along the stepped curve of the reaction process plot for the R region, the FEDR of the region will remain the largest at any point of the reaction path.

What, then, are the implications of the largest FEDR in terms of the silicide formation sequence? The significance of the largest FEDR can be shown by Fig.(4-11), the free energy versus time plot. In this figure, the curves represent the possible paths of free energy changes for a given system. Curve 1 indicates the path of the largest FEDR. It is obvious that at the time instants just past the tangent points P3 and P2 respectively, the slope of the tangent for curve 1 has a larger negative value than those for the other curves. Since the slope of each curve corresponds to the FEDR at a certain time, the largest FEDR means that no curve which deviates from curve 1 can have a free energy value lower than those of curve 1. Therefore, curve 1 represents the lowest free energy states of the system at any given time, which can be referred to as relative minimum free energy states. When a system advances along a path of the largest FEDR, it can decrease its free energy in the fastest way and hence keep itself at the relative minimum free energy state until it reaches the "absolute" minimum free energy state, i.e., the equilibrium state. Since at any time along the path, the relative minimum free energy state is the most stable one compared with all other possible states, the largest FEDR path is compatible with the system's final state, i.e., the equilibrium state. Also, it is not contradictory to the general results of TIP theory that are expressed in Eqs.(4-67) and (4-68), as long as the slope of the curve, or the FEDR, continuously increases and [illegible] zero when the system reaches the equilibrium

state. Therefore, it is reasonable to consider the largest FEDR path to be the most favorable path for irreversible processes.

From the results, a criterion for solid state reactions in metal-Si diffusion couples is proposed: During silicide reaction in a reaction region of a metal-Si diffusion couple, there are always a number of possible reactions competing with one another. The reactions which can result in the largest FEDR will actually occur. The criterion is referred to as the largest FEDR criterion.

When the criterion is applied to the release process, it can be translated to a simple kinetic criterion: Among all possible release processes at any diffusion flux, the one with the largest release rate will actually take place.

For formation processes at a given release rate of ith silicide, the phase with the largest $(-F_{ik}\Delta G_{ik})$ will form.

4.4 Discussion

In the preceding sections, the kinetic factors and thermodynamic factors which control the solid state reactions in transition metal-Si diffusion couples have been closely examined by means of the TIP theory, a chemical kinetic approach (LFER) and Cahn and Hilliard's approach to interfacial free energy. The main results are summarized in the following.

From basic principles of TIP theory (Eqs.(4-1) to (4-8)), it has been shown (Sec.4.1.2) that the free energy change due to silicide formation in a diffusion couple can be determined by examining the free energy change of the R region that is between the growing silicide and the nonmoving reactant phase. The free energy degradation rate per unit area of a given R region can be expressed (Eqs.(4-21), (4-21a) and (4-21b)) as a sum of the three contributions, each corresponding to one of the three steps, i.e., moving reactant diffusion, nonmoving reactant release and the product molecule crystallization. Each term is a product of a thermodynamic flux and a driving force. These fluxes and driving forces are examined individually. Analysis of experimental results using the LFER method suggests that a linear relationship between $\ln(r_{imax})$ and free energy changes for the reactions is likely (Sec.4.2.2.1). Based on this analysis, an expression for r_{imax} (Eq.(4-38)), exponentially dependent on the free energy change for the reaction and on the activation energy for breaking chemical bonds of nonmoving reactant, has been derived. A microscopic mechanism is assumed, i.e., the process for breaking chemical bonds of N atoms and that for forming new bonds of product molecule take place at the same time (the assumption is actually included in assumption 2 for the kinetic model). It is shown, by using a schematic plot (Fig.4-5), that the driving force for the release process can be

approximately expressed by Eq.(4-42) (Sec.4.2.2.2), so that the value of the driving force can be estimated if the defect density of nonmoving reactant surface (Eq.4-50) is available. For a formation process, the conditional maximum formation rate, $F_{ik'}$, is probably of more practical importance. $F_{ik'}$ is exponentially dependent on two contributions to the activation energy (Eqs.(4-55) to (4-56)), one for nucleation and the other for rearranging product "molecules" from the R region onto the crystalline lattice of the growing phase. The expression for $\Delta G'_{ik}$ (Eqs.(4-57) and (4-58)), the activation energy for the ik phase nucleation, is basically the same as that given by classical heterogeneous nucleation theory, except that the definitions of the driving force are different. The driving force, ΔG_{ik}, for the formation process (Eq.(4-52)), is derived based on assumption 2 of the new kinetic model and Cahn and Hilliard's expression for interfacial free energy. Its value can be approximated from the surface tension σ_{kN} of the same interface by Eq.(4-54). In particular, it has been shown (Sec.4.3.1.) that the driving force ΔG_{ik} is related to the release rate (Eq.(4-66)). With $r_i>0$, ΔG_{ik} is almost a constant, while for $r_i=0$, $\Delta G_{ik}=0$. This is because the interface intends to remain a specific thickness that corresponds to a minimum interfacial free energy at constant temperature and pressure. An expression for ΔG^*_{ir}, the driving force for the release process, is also given by Eq.(4-61). From this equation, $\Delta G^*_{ir} = \Delta G_{ir}$, when the flux is equal to or larger than J_{iUC}, and ΔG^*_{ir} increases if the diffusion flux decreases. By qualitatively analyzing the trend of all these fluxes (J, r and F) and forces ($\Delta\mu^M_{R'}$, ΔG^*_{ir}, and ΔG_{ik}) changing with time, it is known that the FEDR of the R region will increase with the time (see Eq.(4-68). This analysis is not based on mathematical derivation, but is only from qualitative analysis as discussed in Sec.4.3.1. This result shows that the expressions for FEDR in the R region are in agreement with the general results from TIP theory (Eq.(4-67)). From this point of view, it is further shown that in an R region, there always exists a reaction that will result in the largest FEDR in this region (Sec.4.3.2). Moreover, it is shown, by a schematic free energy versus time plot (strict mathematical derivation would be ideal, but is not available at this time and is beyond the scope of this study), at any instant of time, that the largest FEDR leads the system to a relative minimum free energy state that is most stable compared with any other energy state at the instant. Therefore, a criterion for silicide reaction is proposed.

In the following paragraphs, the results from this chapter and Chap.3, will be applied to discuss some practical problems.

According to the release process proposed in the last section, the stepped curve in an r vs. J plot indicates the path of release processes in a reaction region. Since it represents the

largest release rate at any given diffusion flux, the curve can be used to predict silicide formation sequence in this region. It can be predicted, theoretically, that any silicide in the equilibrium phase diagram of a metal-Si diffusion couple can form first if the release rate for this reaction is on the stepped curve of the r vs. J plot, and if the initial diffusion flux is between J_{LC} and J_{UC}, the lower and upper critical fluxes respectively for this silicide. On the other hand, if none of the release rates for a silicide to form are on the stepped curve, the silicide is unlikely to form through direct metal-Si reaction. Furthermore, it is also possible to predict when and which new silicide will form in a diffusion couple, providing r vs. J plots for this couple are available. The diffusion flux continuously decreases as the first silicide grows. Whenever the diffusion flux reaches a critical value, J_{UC}, a new reaction with its own release rate related to this J_{UC} is initiated and a new silicide starts to grow. The predictions of the initial silicides and multiple phase growth sequences in fifteen metal-Si systems will be discussed in Chap.5.

At present, quantitative calculations of r versus J plots cannot be achieved because of the unknown factors, E and α, in Eq.(4-38). Since these two factors are also important in studying the microscopic mechanism of the release process, it is worth determining these factors by means of the LFER method. As discussed in Sec.4.2.2.1, this can be done by obtaining experimental data of the maximum release rates of a multiple phase growth process in a metal-Si diffusion couple of interest and by fitting these data to a linear equation between $\ln(r_{imax})$ and ΔG_{ir} or ΔG^{o}_{ir} using a least squares method. In order to obtain good fit, the experiments should be carried out under carefully controlled conditions since a number of other factors can affect the maximum release rates, such as impurities, surface preparation, annealing environment and substrate orientation. Once E and α are determined, they can be used to estimate the $\ln(r_{imax})$ values for those silicides whose release rates are not on the experimentally determined stepped curve of the r vs J plot. If the calculated results also show that the release rates of these silicides cannot appear on the stepped curve, then all these reactions belong to the same group and have the same reaction mechanism. Otherwise, they may not be same type of reactions. For example, in the Ni-Si system, Ni_3Si_2 has a larger $(-\Delta H^{o}_{298}) \cong (-\Delta G^{o})$ than NiSi, but it cannot form before NiSi.

In Sec.4.2.2.2, it has been shown that when concentration effect is taken into account, the ΔG_{ir} for Ni_3Si_2 could be smaller than that for NiSi. This is one way to explain the phenomenon, i.e., the empirical LFER equation for Ni-Si system may fit ΔG_{ir} better than ΔG^{o}_{ir}. There is another possible explanation. If the constant α in Eq.(4-38) for Ni_3Si_2 is smaller than that for other reactions, the Arrhenius activation energy for Ni_3Si_2 will be

higher, so that it cannot form before NiSi. This suggests that the chemical bond formation process for Ni_3Si_2 may be different from that for other silicides. From this example, it can be seen that LFER is a useful tool for classifying reactions and investigating reaction mechanism.

According to the criterion for formation processes in the last section, the formation of a phase can be predicted using an F vs r plot (Fig.4-10) and the data for ΔG_{ik}. At the present time, however, the capability of the prediction is limited because very little is known about actual F vs r plots and the driving force for the formation process, ΔG_{ik}. Therefore, the criterion and other results for formation processes from the preceding sections can only be used to explain qualitatively, the experimental phenomena reported in the literature at this time.

From assumption 2 of the kinetic model and the expressions for r_{imax} and $F_{ik'}$, the release process occurs at the surface of the N lattice while the formation process takes place at the surface of the growing silicide. The energy change as a function of reaction coordinate can be schematically shown by the solid curve in Fig.4-12. The numbers 1, 2, and 3 indicate the energy states before and after the release process, and after the formation process. The energy differences between state 4 and 1 and between 5 and 2 are the activation energies for the release and formation processes respectively. This curve is not valid for the silicide reactions occurring at a coherent or semicoherent interfaces, where the release and formation processes actually take place at once. Therefore, the reaction rate (in order to differentiate it from the terms release rate and formation rate, the term reaction rate is used to discuss the rate of this reaction and a capital letter Y is used to indicate it) is expressed as the following

$$Y = n^* \nu \frac{\Delta J}{J_{iUC}} \exp\left[- \frac{\alpha \Delta G_i + E_i + \Delta G'_{ik}}{k_B T} \right] \qquad (4\text{-}77).$$

$\Delta J/J_{iuc}$, n^*, ν and α have the same meanings as defined before, $\Delta G_i = \alpha \Delta G_{ir} + \Delta G_{ik}$ is the total free energy change of the reaction, and $\Delta G'_{ik}$ is the energy barrier for nucleation but is small now because of the low interface energy at the coherent interface. The term E_i is a sum of two contributions, i.e., the energy barrier for breaking nonmoving reactant bonds and the energy barrier for adjusting the bond structure of the product "molecules" into that of the growing phase lattice. The latter may be even higher than that for the three step process, because, at a coherent interface, the adjustment and hence the movement of atoms are restricted due to the coherency requirement. In addition, it is likely that the strain energy is higher in this case and it will increase as the reaction preceeds, which will also

contribute to activation energy, E_i. As a result, E_i will be significantly larger than either E for release process or $E_{ik}+\Delta G'_{ik}$ for the formation process in a three step reaction. This is shown by the dashed curve in Fig.4-12. Numbers 1 and 3 indicate the energy states before and after the reaction. The difference between 6 and 1 represents E_i. Consequently, Y will much smaller than the release rate and the formation rate in a three step reaction for the same silicide forming at an incoherent interface. The argument above provides a good kinetic explanation of why solid phase epitaxy usually cannot occur at relatively low temperatures. The argument can also explain why small lattice constant misfit is only a necessary condition for epitaxial growth but not a sufficient condition. This is because in some crystal orientations, although the misfit is small enough, so that strain energy due to lattice distortion is small, the activation energy for adjusting the bond structure is rather large, which may prevent epitaxial growth from occurring.

The FEDRs due to the formation process have been discussed in Sec.4.3.2. In case 2, i.e., F_{i1} for metastable phase formation larger than F_{i2} for stable phase growth, requires more attention. Although $F_{i1}\Delta G_{i1}<F_{i2}\Delta G_{i2}$ indicates that the formation of phase 1 will lead to a larger FEDR than the formation of phase 2, it is not the largest FEDR. If the formation process occurs according to the proposed largest FEDR criterion, theoretically, the FEDR for this process should be

$$\frac{dg_{i2}}{dt} = (\frac{r_o}{n_i} - F_{i2'})\Delta G_{i1} + F_{i2'}\Delta G_{i2} \quad (4\text{-}78),$$

where r_o is shown in Fig.4-10, $(r_o/n_i)=F_{i1}$ is the intersection of the vertical dashed line, representing r_o, with the formation rate curve of phase 1. It can be reasoned that Eq.(4-78) is valid because each molecule transformed from R region into phase 2 will result in more free energy decrease than that into phase 1. But the number of "molecules" that can be transformed into phase 2 per unit time and unit area is limited and is only equal to $F_{i2'}$. As a result, the other "molecules" will form phase 1 at a rate of $\{(r_o/n_i) - F_{i2'}\}$. If phase 3 in Fig.4-10 also has a larger negative free energy (ΔG_{i3}) than phase 1 has, one more term for phase 3 should be added to Eq.(4-78) and the first term should be modified correspondingly. It is inferred, from Eq.(4-78), that although phase 1 formation may be overwhelming when F_{i1} is a few orders of magnitude larger than $F_{i2'}$, the simultaneous formation of phase 2 together with phase 1 is still likely. Because of the difference in the formation rate, phase 2 can only exist as small domains in phase 1. With a decrease in release rate, F_{i1} becomes closer to $F_{i2'}$, while the formation rate for phase 2 remains the same. Consequently, more and more domains of phase 2 appear until F_{i1} passes $F_{i2'}$. If

the structure of phase 1 can be preserved for examination by high resolution analytical techniques, these small domains of phase 2 should be observed. In particular, when phase 1 is amorphous, this inference may be confirmed if small crystalline particles can be observed at temperatures far below the crystallization temperature of this material. Experimental evidence of this inference would also verify the proposed criterion.

Table 4-1. Relationship between silicide formation sequences and standard enthalpy changes per mole nonmoving reactant atoms

System	Silicide	Nonmoving Reactant[b]	$-\Delta H^{o}_{298}$ kJ/mol[c]
Mn-Si	Mn_3Si	Si	137.1
	$MnSi$		97.0
	$MnSi_{1.73}$		44.5
Co-Si	Co_2Si	Si	115.4
	$CoSi$		100.3
	$CoSi_2$		51.4
Ni-Si	Ni_2Si	Si	148.4
	(Ni_3Si_2)[d]		111.8
	$NiSi$		85.7
	$NiSi_2$		43.6
Pt-Si	Pt_2Si	Si	213.2
	$PtSi$		168.0
Mo-Si	$MoSi_2$	Mo	108.7
	Mo_5Si_3		56.0
	Mo_3Si		33.4

[a] The formation sequences listed in the table are observed in multiple phase sequential growth experiment. $MnSi_{1.73}$ and Mo_3Si formation are not observed in each respective experiment due to metal source limitations.

[b] See discussion about nonmoving reactants in Chap.5.

[c] Data for ΔH^{o}_{298} are from Ref.[218]. The data listed in the table is obtained by dividing ΔH^{o}_{298} for a given silicide by the number of nonmoving reactant atoms per formula unit of the silicide.

[d] It has been found that the formation of Ni_3Si_2 does not occur before NiSi formation, which is an exception of the relationship shown in this table. See the discussion in Secs.4.2.2.2 and 4.4 for the explanation.

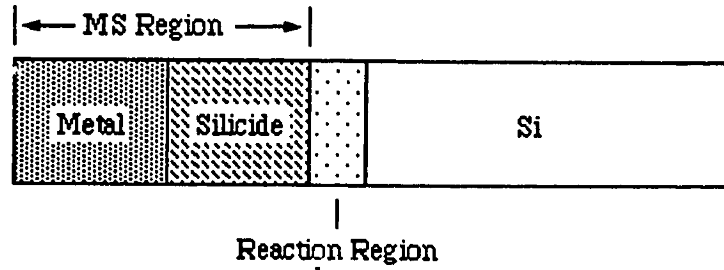

Fig.4-1 A schematic transition metal-Si diffusion couple divided into three regions, i.e., MS region, reaction region and Si region. Not to scale.

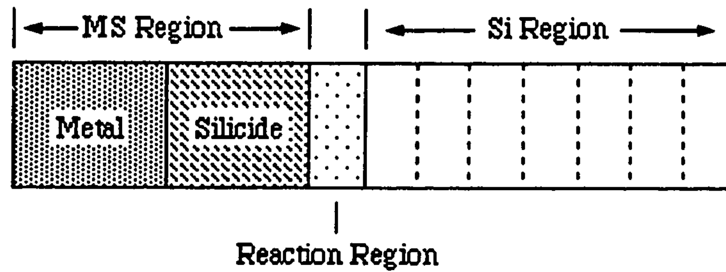

Fig.4-2 Schematic metal-Si diffusion same as above, but Si region is divided into n slabs for explaining the meaning of FEDR in a reaction region. Each slab has the same thickness as reaction region.

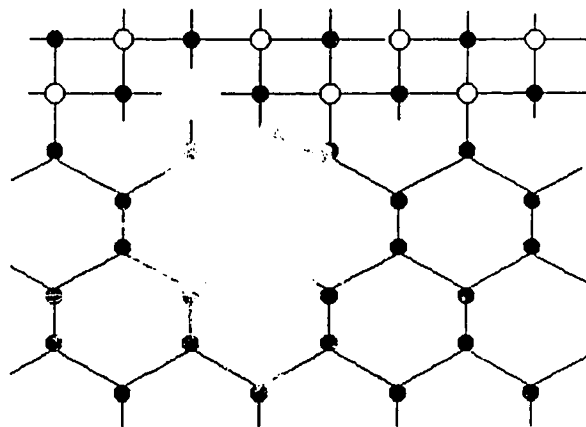

(a)

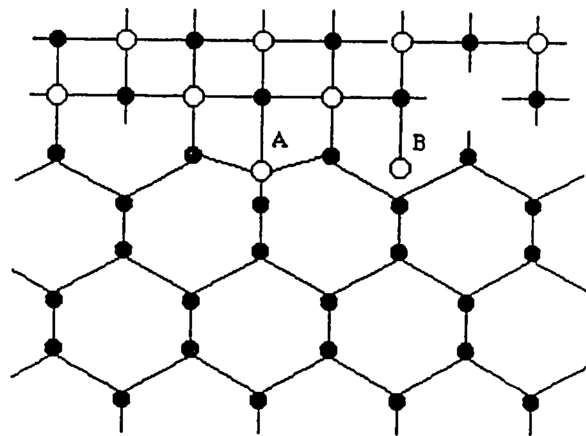

(b)

Fig.4-3 Schematic chemical bond breaking and forming process in a reaction region. Closed circles and open circles represent Si and metal atoms, respectively. (a) Metal atom A just arrives at Si surface and interacts with surrounding Si atoms. (b) Si-Si bond breaking and A-Si bond forming occur at the same time.

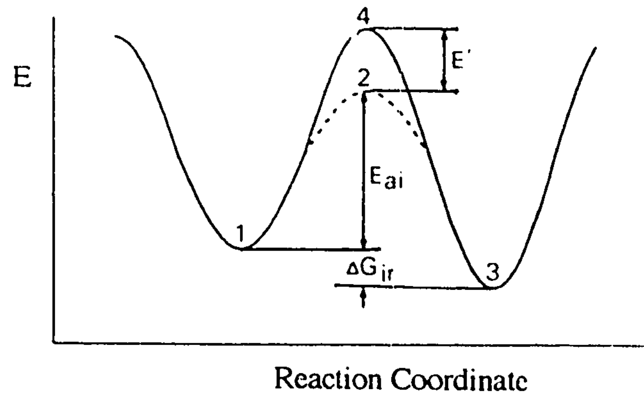

Fig.4-4 Schematic energy vs. reaction coordinate plot showing that the energy required for breaking Si bonds is partially compensated by the energy released due to new bond formation.

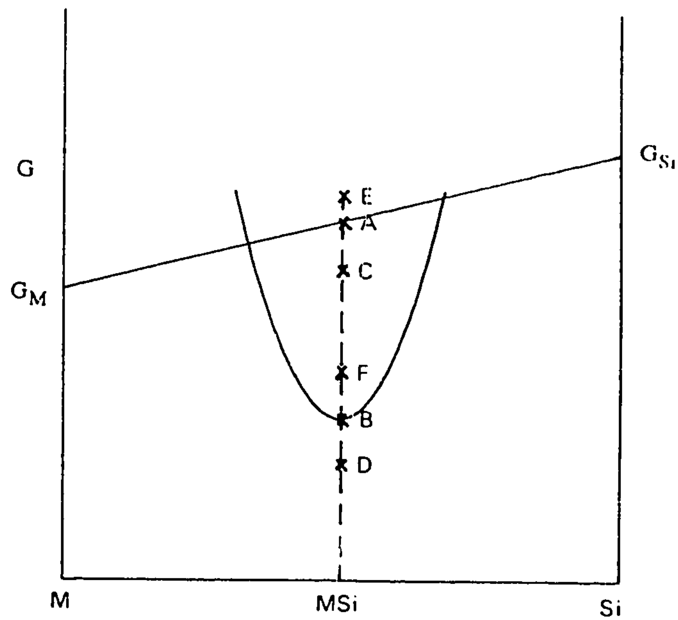

Fig.4-5 Schematic free energy vs composition plot. Points A, B, C, D, E and F represent free energy values G_A, G_B, G_C, G_D, G_E and G_F, respectively.

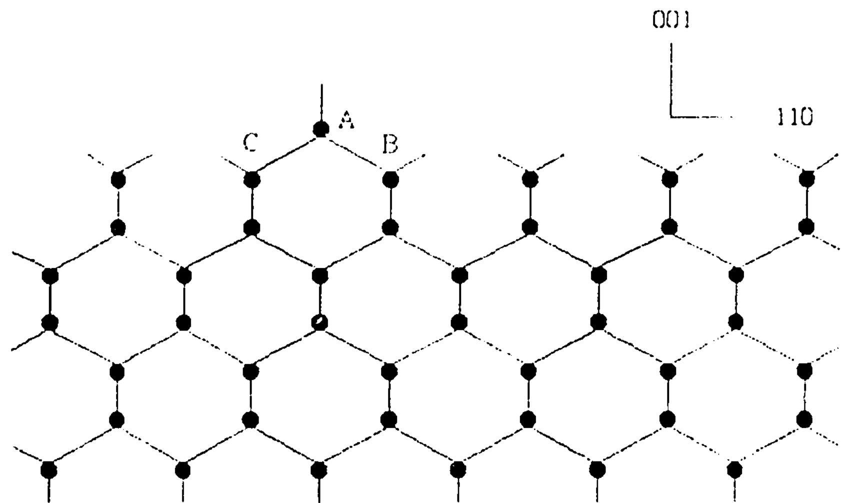

Fig.4-6 Schematic bonding structure of (100) Si surface. Each inclined line represents one bond while each vertical line indicates two bonds. All surface atoms have two unsatisfied bonds but atoms B and C have only one unsatisfied bond.

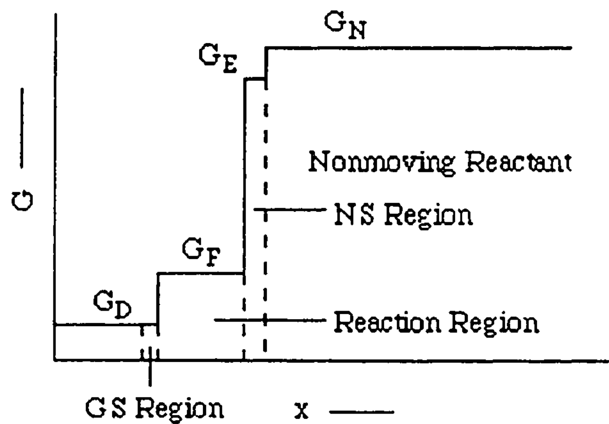

Fig.4-7 A schematic distribution of free energy over the reaction region. G_N, G_E, G_F and G_D are the free energies of nonmoving reactant phase, N surface, reaction region and growing silicide, respectively. With the advance of reactions, the free energy distribution curve moves to the right of the figure together with the reaction region.

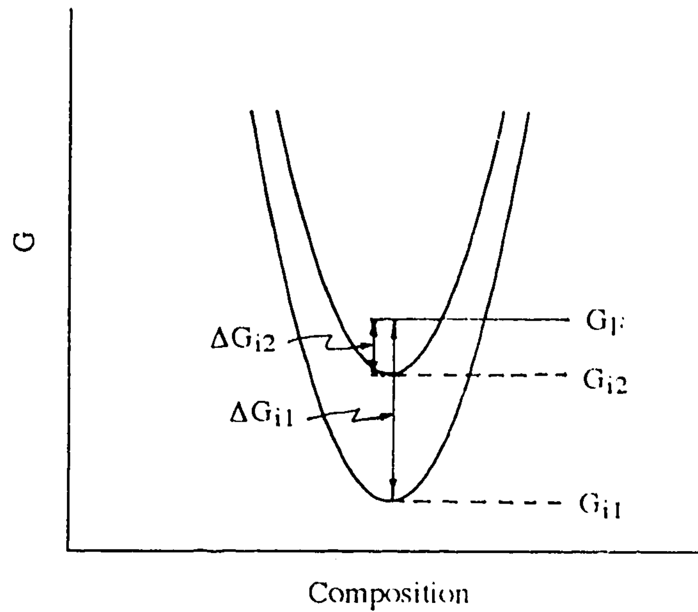

Fig.4-8 Schematic free energy vs composition plot. G_{i1} and G_{i2} indicate the free energies of stable phase and metastable phase of ith silicide respectively. G_{I} represents the free energy of ith silicide molecule at the reaction region (reactive interface). ΔG_{i1} and ΔG_{i2} are the driving forces for phases 1 and 2 to form respectively. The stable phase has a larger driving force.

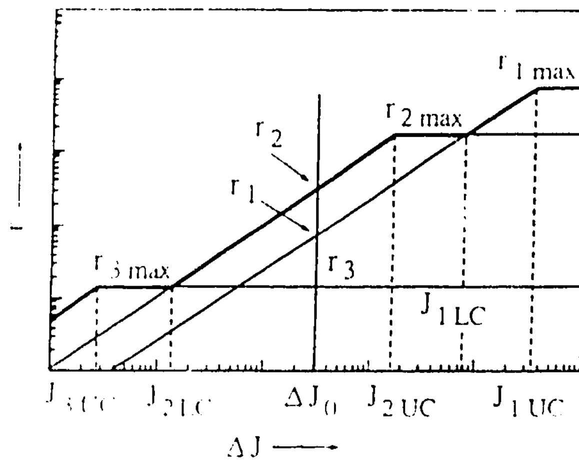

Fig 4-9 Schematic r vs ΔJ plot showing that at given diffusion flux ΔJ_0, $r_2 > r_1 > r_3$.

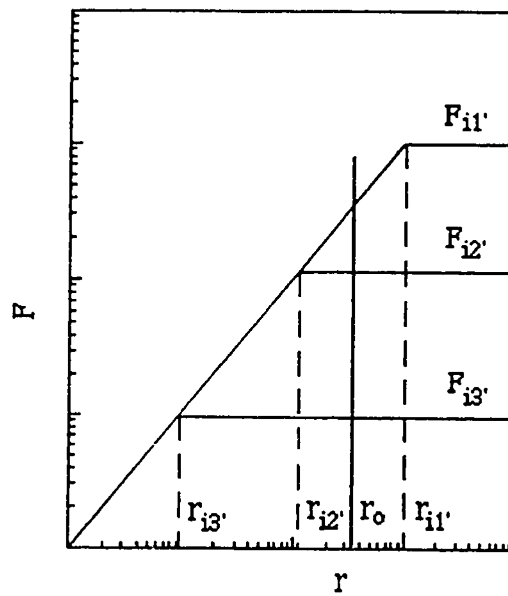

Fig.4-10 Schematic F vs r plot. $F_{ik'}$ represents conditional maximum formation rate for phase k of ith silicide. $r_{ik'}$ indicates the critical release rate corresponding to the $F_{ik'}$.

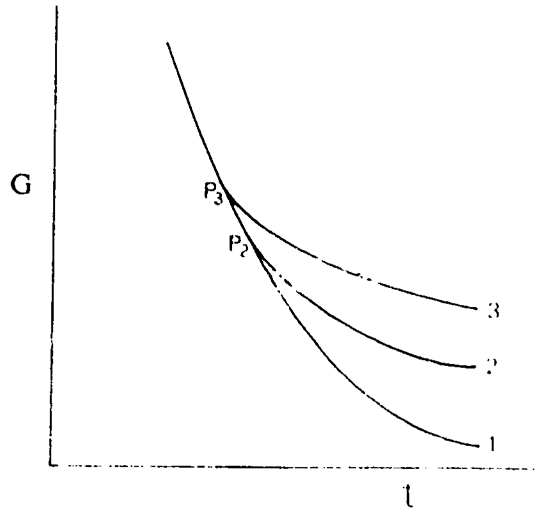

Fig.4-11 Schematic free energy vs time plot. Curve 1 represents the reaction path with the largest FEDR. Points 2 and 3 are tangent points where curves 2 and 3 start to deviate from curve 1 respectively.

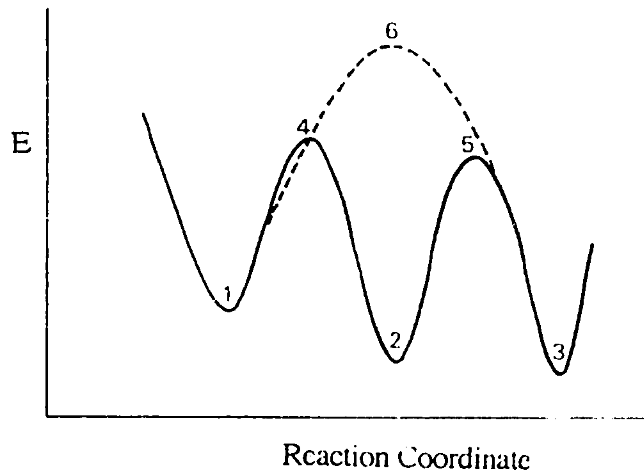

Fig.4-12 Schematic plot showing activation energies for interfacial reactions taking place at coherent and incoherent interfaces respectively. Numbers 1, 2 and 3 indicate the energies corresponding to the states before and after N release, and after formation, respectively, for a three step process at a incoherent interface. The free energy differences between state 4 and 1 and between 5 and 2 are the activation energies for release and formation processes respectively. The energy difference between state 6 and 1 is the activation energy for the reaction occurring at a coherent interface.

Chapter 5 Semiquantitative Reaction Process Plots for Silicide Formation and Prediction of Silicide Formation Sequence

In Chap.3, a reaction process plot (RPP), combining a release rate versus diffusion flux plot (r vs. ΔJ plot) with a formation rate versus release rate plot (F vs. r plot) has been developed to demonstrate the relationship between ΔJ, r_i and F_{ik} during solid state reactions in an R region in a metal-Si diffusion couple. From these plots (RPP, r vs ΔJ, and F vs. r plots), it can be seen that silicide formation in a diffusion couple is a complex process. There always exist various competitions, such as those among possible release processes and those among possible nucleation and growth processes. From both a technological and theoretical point of view, it is desirable to be able to predict the results of the competitions, i.e., to predict the silicide formation sequences under given experimental conditions. According to the criteria of silicide formation proposed in Chap.4, of all possible release rates at a given diffusion flux, the largest release rate, indicated by the release rate on the stepped curve on the RPP (and the r vs. ΔJ plot) for the reaction region of interest, will actually take place. Since the silicide "molecules" are formed during the release process, what type of silicide compounds will form in the R region is determined by the release process. Therefore, the stepped curve on the RPP or the r vs. ΔJ plot for the R region can be used to predict what type of silicide compound will form under given experimental conditions. In addition, according to the same criteria in Chap.4, of all possible formation rates (F_{ik}) at a given release rate, the one which has the largest ($-F_{ik}\Delta G_{ik}$), i.e., which can result in the largest FEDR, will actually occur. Since the silicide "molecules" that are produced by the release process are rearranged into one of the possible phases of this silicide during the formation process, the form (i.e., stable or metastable phase) this silicide will take is determined by the formation process. Therefore, a knowledge of the RPP or F vs. r plot for the system under consideration and of the ΔG_{ik} values for all possible phases of this silicide is sufficient to predict what form of the silicide will grow.

From Eqs.(3-45) to (3-49) in Secs.3.3.4 and 3.3.5, an r vs ΔJ plot and an F vs. r plot for a given metal-Si system can be constructed if the maximum release rates (r_{imax}) and the conditional maximum formation rates (F_{ik}') are known, respectively. As discussed in Sec.4.2.3, F_{ik}' depends on a number of factors, such as E_{ik}, ΔG_{ik}, and $\Delta\sigma$ (Eqs.(4-55) to (4-58)), which vary from phase to phase, so that calculation and comparison of F_{ik} values for various phases of a given silicide are not available without the appropriate data. At the present time, since very little is known about these factors, quantitative or semiquantitative calculations of F vs. r plots are not viable, so that the plots are mainly used to qualitatively explain the experimental phenomena of metastable phase formation.

From Eq.(4-38), r_{imax} also depends on a number of factors, i.e., E, α, n*, ν and ΔG_{ir}. Quantitative calculations of r_{imax} cannot be done either because there is not enough information about E and α available at the present time. According to the derivation of Eq.(4-38), however, the factors, E, α, n* and ν, are the same for reactions in the same reaction region of a diffusion couple, which implies that r_{imax} is exponentially dependent on ΔG_{ir}. As a result, relative values of maximum release rates for these reactions can be calculated. In this chapter, a method for calculating relative maximum release rates (RMR rates) and constructing semiquantitative reaction process plots (SRPPs) from the RMR rates has been proposed. Calculations of RMR rates have been done for 15 metal-Si systems and a few typical SRPps have been drawn from the resulting data. The results and the discussion demonstrate that RMR rate calculations and SRPps can be used to successfully predict and explain silicide reaction phenomena in the 15 systems.

5.1 Relative Maximum Release Rate and Semiquantitative Reaction Process Plots

The following procedure is used to calculate RMR rates: As a reasonable approximation, ΔG^o_{ir} values are replaced by ΔH^o_{i298} values, i.e., standard enthalpies of formation per mole N atoms (or per mole formula unit), which are available for most silicides. An arbitrary value, 1 at/cm^{2}s, is then assigned to the maximum release rate of the silicide (for convenience this release rate is labeled as r_{1max}) which has the smallest negative value of ΔH^o_{i298} (ΔG^o_{ir}). Finally, all other maximum release rates are calculated relative to r_{1max} according to the following equation (obtained from Eq.(4-38)):

$$\frac{r_{imax}}{r_{1max}} = \exp\{-\frac{\Delta G_{ir} - \Delta G_{1r}}{RT}\} \qquad (5\text{-}1),$$

where ΔG_{ir} and ΔG_{1r} in Eq.(5-1) can be replaced directly by ΔH^o_{i298} and $\Delta H^o_{1\,298}$, respectively, if the concentration effect (or the defect concentration effect) is neglected. When the concentration effect is taken into account, the terms, ΔG_{ir} and ΔG_{1r}, can be calculated by using Eq.(4-50) and replacing ΔG^o_{ir} in Eq.(4-50) with ΔH^o_{i298}. It should be mentioned that in Eq.(5-1), the constant α in Eq.(4-38) is assumed to be unity, which will not affect the order of the calculated RMR rates, i.e., if $r_{2max} > r_{1max}$, a different α value cannot change it to $r_{1max} < r_{2max}$. Since the following discussion is focused on the

prediction of silicide formation based on the order of the calculated RMR rate, the discussion is valid even if other α values are used.

The RMR rates calculated by the procedure described above can be used to construct a semiquantitative plot (SRPP). First, a group of straight lines are drawn on a log scale plot with the slope of each line equal to the composition (i.e., n_i/m_i) of a particular silicide in the metal-Si system. A group of horizontal lines are then drawn with each corresponding to the RMR rate value of a silicide. Each horizontal line is drawn starting from the right side of the plot until it connects with the inclined line which represents the same silicide. These two connected lines make up an r vs J curve. Finally, a stepped curve can be drawn along the outside border of these r vs J curves. It represents the largest release rate at any diffusion flux. The plot is completed by labeling RMR rates and the critical diffusion fluxes, i.e., J_{iUC}'s and J_{iLC}'s.

The RMR rates for 15 metal-Si systems have been calculated and the results have been listed in Table 5-1. Several typical SRPP are also constructed, based on the calculations, and are shown in Figs.5-1 to 5-4. Before discussing, in the next section, these results and plots, and examining how well these results agree with those from experiments reported in the literature, several important points related to the data listed in Table 1 have to be addressed.

1) There still are many other metal-Si systems which form silicides. Since, in these systems, either the standard heats of formation or the major diffusers are not available at this time, no calculations have been done for them.

2) In Table 5-1, all known silicides [3] in each system, whether or not their heats of formation are available, are listed according to their compositions with the silicides richest in non-moving reactant at the top of each group.

3) The temperatures used in the calculations are selected from the experimental temperature ranges reported in the literature [2, 3, 6]. Temperatures, other than those used in Table 5-1, can also be used for the calculations as long as the reaction, at these temperatures, is still a type II reaction (see definition in Sec.3.1.1) and the non-moving reactant remains the same as that listed in Table 5-1. Calculations using different temperatures may result in different RMR rates. In some cases, this will change the relationship for the maximum release rates in a given metal-Si system, i.e., if the maximum release rate of one silicide is larger than that of another silicide in the same system, then a large temperature change may reverse this order. The discussion related to whether a silicide can form through direct metal-Si reaction (also see the following paragraphs) in the next section, therefore, will be applicable only for the temperature ranges in which the relationships of RMR rates are the same as those listed in Table 5-1.

4) In Table 5-1, non-moving reactants in the 15 systems have been listed, based on both reported marker experiments in the literature [9] and the fact that, in most silicide reactions, metal atoms are major diffusers in near noble metal-Si diffusion couples whereas silicon atoms are the major diffusers in refractory metal-Si diffusion couples. On the other hand, d'Heurle and Gas [5, 183] have pointed out that the majority atoms are the most mobile in most disilicides (with the exception of $NiSi_2$ and $CoSi_2$) and in the following silicides: V_3Si, Co_2Si, Ni_2Si, Pt_2Si, Ru_2Si_3, Os_2Si_3, and Rh_4Si_5. This phenomenon is referred to as the "ordered Cu_3Au effect". Thus, there may be more than one non-moving reactant for different reactions in a diffusion couple. Nevertheless, calculations for all reactions in one diffusion couple using the non-moving reactant given in Table 5-1 are still significant for the following reasons:

First of all, according to the kinetic model, if more than one silicide grows simultaneously in a diffusion couple, there will exist the same number of R regions (i.e., reactive interfaces), one for each silicide. Reactants in a given R region will not be the same as those in other regions. For example, when two silicides, Ni_2Si and NiSi, are growing at the same time in a Ni-Si diffusion couple, the moving reactant and the non-moving reactant in the Ni_2Si/NiSi reaction region are Ni and NiSi respectively, while in the NiSi/Si reaction region they are Ni and Si respectively. Thus there are different reaction process plots for the two regions. The plot for Ni_2Si/NiSi reaction region is that of r^{NiSi} vs J^{Ni}, while the other plot is drawn with r^{Si} vs J^{Ni} (the superscript for release rate indicates the non-moving reactant while that for diffusion flux indicates the moving reactant). In the calculations, only the reactions occurring in the reaction region adjacent to an elemental non-moving reactant are considered because these results are useful in explaining the controversial problem of "first phase formation" and in predicting multiple phase growth sequences. Calculations for other reaction process plots can be done by following the same method and by replacing the non-moving reactant used in this table with an appropriate non-moving reactant.

Secondly, the formation of most silicides (except the first phase) in thin film diffusion couples, reported in the literature, is not through direct metal-Si reactions which can be described by Eq.(3-1):

$$m_iM + n_iSi \rightarrow M_pSi_q \qquad (3\text{-}1).$$

Instead, after the first phase is formed and one reactant is completely consumed, any new silicide must form either through the decomposition of the previously formed silicide or through reaction between the previously formed silicide and the other reactant. The

calculations in Table 5-1, assuming that the non-moving reactants listed remain immobile compared with the other reactant, will show *whether a silicide can form through direct metal-Si reaction and under what conditions this kind of reaction can occur.* This information is valuable in both theoretical research and technical applications.

5) The units for E and ΔG in Eqs.(4-38) and (4-50) are eV per N atoms (or formula unit, depending on whether N is an element or a compound). These units are converted to Joules per mole N atoms (or formula units). The standard heats of formation in Table 5-1 are calculated, from the original data [218], by dividing the given ΔH^{o}_{i298} (per mole formula unit of ith silicide) by n_i, the number of N atoms per formula unit of the corresponding silicide. It should be mentioned that, for some metal-Si systems, the thermodynamic data provided by Samsonov and Vinitskii [218] are significantly different from those given by other sources [3]. In some cases, e.g., Pt-Si and Pd-Si systems, the data used here have larger negative values (more than twice those provided by Nicolet and Lau [3]). Since the data from both sources are of the same order, e.g., Pt_2Si has a larger negative value of ΔH^{o}_{298} than PtSi in both cases, the RMR rates calculated from the two sets of data have a similar relationship. This difference in thermodynamic data will not affect the following discussion. In other cases, such as the Ti-Si system, however, ΔH^{o}_{298} for TiSi has a larger negative value than that for $TiSi_2$ in one data set [218], while the reverse occurs for the other set of data [3]. Such differences in the thermodynamic data will result in different conclusions about whether $TiSi_2$ can be formed through direct Ti-Si reaction and whether it can be the first phase to form. In these cases, the correct conclusion can only be drawn from careful experiments.

6) Columns r* and r in Table 5-1 list the values of RMR rates calculated with and without taking into account the defect concentration (which is related to the concentration of product "molecules" on the surface of N lattice and is incorporated into in the concentration quotient term in Eqs.(4-49) and (4-50). See Sec.4.2.2.2.), respectively. To calculate r*, a surface defect concentration $\frac{n_d}{n^*} = 10^{-6}$ is assumed and inserted into Eqs.(4-49), (4-50) and (5-1). It should be noted that the actual value of r* for each silicide is larger than that of the corresponding r, but, in some cases, r* appears to be smaller than the corresponding r in Table 5-1. This is because the r and r* values are calculated *relative to the smallest r and r* in the group*, respectively, and a reference value of 1 at/cm²s is arbitrarily assigned to both the smallest r and r*.

7) It has been mentioned that the stepped curve in a reaction process plot represents the largest maximum release rates available at any given diffusion flux. It is also known that if several release rates may occur, the one which will actually occur is the largest one. Therefore, if, in a SRPP, none of the release rates for a silicide to form are on the stepped curve, e.g., those of Mn_5Si_3 in Fig.5-1, the silicide is unlikely to form through direct metal-Si reaction. It should be pointed out that in the SRPPs (e.g., Figs.5-1 to 5-4) no nF vs mF lines, like those shown in Fig.3-19, are drawn because values for conditional maximum release rates, F_{ik}', are not available at this time.

As mentioned at the beginning of this chapter, which silicide forms is determined by step 2, and which form this silicide takes is determined by step 3. Therefore, the following discussion using Table 5-1 and SRPPwill be limited to which silicide can form through direct metal-Si reaction.

5.2 Results and Predictions

A reaction process plot, drawn from the data of column r in Table 5-1, for the Mn-Si system is shown in Fig.5-1. Obviously, the release rates of Si for Mn_5Si_3 are always below those on the stepped curve in this plot, which means that Mn_5Si_3 cannot form through direct Mn-Si reaction. From this figure it can be predicted that if the starting diffusion flux, J_0, for Mn-Si reaction satisfies $J_0 > J_{Mn3Si\ LC}$, the first phase to form is Mn_3Si. With decreasing diffusion flux, the next phase to form is MnSi as soon as J passes the critical value of $J_{MnSi\ UC}$. If the initial flux, J_0, is between $J_{MnSi\ LC}$ and $J_{MnSi\ UC}$, the first phase to form is MnSi. The former prediction agrees with previous experimental results [53] and the latter prediction agrees with that of Eizenberg and Tu [41]. According to the Walser-Bené rule [10], Mn_5Si_3 should be the first phase to form in the Mn-Si system. However, no experimental support for their prediction has been found.

In Fig.5-2, a SRPP for the Co-Si system is drawn using the data from column r in Table 5-1. This plot is very simple. All three silicides can be formed by direct Co-Si reaction and, hence, any one of them can be initial silicide as long as the diffusion flux reaches a proper value. In addition, when Co_2Si forms initially in a bulk diffusion couple or a couple with a thick metal film on a Si substrate, the next phase to form is CoSi which is followed by $CoSi_2$. These silicides then grow simultaneously. Experimental results reported in the literature strongly support this prediction. Co_2Si [1-4, 6, 11, 43, 85, 86], CoSi [4, 78, 87, 88] and $CoSi_2$ [91-94] have all been reported to be initial silicides, respectively. Simultaneous growth of Co_2Si and CoSi (with CoSi forming shortly after Co_2Si) has also been observed [47, 52].

Fig.5-3a and 5-3b illustrate SRPPs for the Ni-Si system with Fig.5-3a drawn using data from r and Fig.5-3b from r* in Table 5-1, respectively. It is very interesting to note that, in Fig.5-3a, only the release rates for Ni_3Si do not show up on the stepped curve. This indicates that all other nickel silicides can be formed by direct Ni-Si reactions. However, when the defect concentration (which is related to the concentration of product "molecules" at the surface of N lattice and is incorporated into the concentration quotient term in Eq.(4-50). in Sec.4.2.2.2) is taken into account, according to Fig.5-3b, other silicides, such as Ni_5Si_2 and Ni_3Si_2, are unable to form through direct Ni-Si reactions. This result is meaningful because it indicates the significance of defects, which exist on crystal surfaces and are introduced by surface preparation, on reaction kinetics. It has been reported, by many researchers [6, 11, 37, 55-57, 95-97], that Ni_2Si is the first silicide to form. Recent studies also provide experimental evidence for NiSi [98-100] and $NiSi_2$ [101, 102] forming initially when a diffusion barrier is introduced in the diffusion couples. In some cases, it has also been found that when the diffusion flux is dramatically decreased due to impurity effects in the Ni film, shortly after Ni_2Si formation, NiSi starts to form and these two phases grow simultaneously [49]. In addition, multiple phase sequential growth of Ni_2Si, NiSi and $NiSi_2$ has been observed in lateral diffusion couples [55-57] and in bulk diffusion couples [42]. Thus far, no evidence for Ni_3Si_2 and Ni_5Si_2 formation through direct Ni-Si reaction has been found either in thin film diffusion couples or in lateral diffusion couples.

According to the data for the Pd-Si system in Table 5-1, the SRPP for the Pd-Si reaction region should be quite similar to that for Co-Si (Fig.5-2), which means that all three silicides can form through direct Pd-Si reactions if suitable diffusion fluxes are available. All experimental results, up to date, show that Pd_2Si is the first phase to form [1-6, 67, 111-113].

SRPP for the Pt-Si system, if drawn from data of r and r* respectively, will look similar to those of the Ni-Si system (Fig.5-3a and 5-3b). Again, the important effect of surface defect concentration on the reaction kinetics can be seen. The r data in Table 5-1 indicate that Pt_3Si and Pt_6Si_5 cannot form through direct Pt-Si reaction, but the RMR rate of Pt_7Si_3 is the same as that for Pt_2Si. After accounting for surface defects (the data listed in column r* of Table 5-1), the RMR rate of Pt_7Si_3 becomes much smaller than that for Pt_2Si, so that in this system only Pt_2Si and PtSi can grow through direct Pt-Si reaction. Experimental results strongly support the results from r*. Thus far, initial Pt_2Si formation has been frequently reported [1-6, 33-35, 44, 45, 50, 112]. Under certain conditions, i.e., a Pt-Cr or a Pt-W alloy film on a Si substrate, initial PtSi formation is also reported [121, 122]. In other cases (such as oxygen doped Pt films on Si) [44, 45, 50, 51], Pt_2Si forms

first followed by PtSi formation and then simultaneous growth of both phases. However, there is no evidence for Pt_6Si_5, Pt_7Si_3 and other platinum silicides forming through direct Pt-Si reactions.

It is noteworthy that the five systems discussed above have an important common thread, i.e., they have Si as the non-moving reactant. Therefore, comparison of calculated and experimental results from different systems may provide additional support for the kinetic model and more clues concerning the potential applications of reaction process plots. From Table 5-1, it is apparent that the silicides, Ni_2Si, Co_2Si, Pt_2Si, and Mn_3Si, have the largest maximum release rates in each corresponding system. This result can be used to explain why these silicides have been most often reported as the initial silicides in their respective systems. It is well known that deposition of metal films will introduce so many defects into the resulting films that the diffusion flux from the film to the metal-Si interface, at the beginning of the thermal reaction, will be greatly enhanced. According to the reaction process plots (e.g., Fig.5-1 to 5-3), large diffusion fluxes will cause silicides with large release rates to form. Considering that many techniques used for thin film deposition are quite standardized, it is not surprising that the films deposited by various groups will have similar defect concentrations and, hence, produce similar diffusion fluxes. In addition, from Table 5-1 and Figs.5-1 to 5-3, it is obvious that diffusion fluxes required for a particular silicide to form can vary by a few orders of magnitude so that even if the diffusion fluxes differ from group to group by 1 or 2 orders of magnitude, the same results can be observed. Ni_2Si and Co_2Si, etc., for example, form first, as long as the starting diffusion flux is larger than the lower critical value for these silicides to form.

Comparison of the ratios, $r_{Co2Si\ max} / r_{CoSi\ max}$, $r_{Ni2Si\ max} / r_{NiSi\ max}$, $r_{Pt2Si\ max} / r_{PtSi\ max}$, $r_{Mn3Si\ max} / r_{MnSi\ max}$, and $r_{Pd2Si\ max} / r_{PdSi\ max}$, indicates that the ratio for cobalt silicides is the smallest by about one order of magnitude. This tends to support the observation that CoSi formation and simultaneous growth of Co_2Si and CoSi are more frequently reported in early studies than those occurring in other systems. It is easy to understand, according to reaction process plots, that the small ratio of $r_{Co2Si\ max} / r_{CoSi\ max}$ implies that only a small change in starting diffusion flux (about one order of magnitude) may result in the formation of a different first phase. In contrast, silicides, such as NiSi and PtSi, can be observed to form initially only when diffusion barriers, e.g., alloy films, are used [91-94, 98-102, 121, 122], because a significant decrease in initial diffusion fluxes is required. The small ratio for cobalt silicides also implies that if Co_2Si is the first phase to form, it only grows a limited amount before the diffusion flux reaches the critical value for CoSi formation. From the experimental results of Lau *et al* [47], the critical Co_2Si thickness for initiating CoSi growth is a few hundred nm when the sample is

annealed at 433°C. In contrast, the critical Ni_2Si thickness for initiating NiSi formation in a lateral diffusion couple is about 2 μm after annealing at 450°C for 12 hours [56, 57] and about 20 μm after annealing at 600°C for 10 hours [55]. In particular, in order to observe simultaneous growth of Pt_2Si and PtSi, and simultaneous growth of Ni_2Si and NiSi in thin film couples, a certain amount of impurity (oxygen) has to be introduced into the metal films to accelerate the decrease in diffusion flux, so that PtSi or NiSi formation can be initiated before the metal films are completely consumed. The qualitative agreement of the RMR rate data with the experimental results lends strong support for the kinetic model and the reaction process plots.

From Fig.5-4a, the SRP plot for the Ti-Si system drawn from the data of column r in Table 5-1, it is unlikely that $TiSi_2$ will form through direct Ti-Si reaction. As mentioned earlier, however, if the value of ΔH^o_{298} for TiSi from Ref.3 is used, $\Delta G^o_{TiSi} \approx \Delta H^o_{TiSi298}$ = -131.7 kJ/mol, and the value of RMR rate is $r_{TiSi\ max}$ = 11.2 at/cm^{2}s, which is slightly lower than that of $TiSi_2$. Fig.5-4b shows a SRPP of Ti-Si system with the $r_{TiSi\ max}$ replaced by the new value. This plot indicates that $TiSi_2$ may also grow through direct Ti-Si reaction. Although many experimental results reported in the literature [3, 70-73] indicate that TiSi forms initially, there are a few investigations in which $TiSi_2$ is found to be the first crystalline silicide [67-69]. It is possible that $TiSi_2$ has a little larger negative value of ΔH^o_{298} than TiSi, although further experimental measurement is needed for clarification.

In early studies, it has also been found that Ti_5Si_3 could form first [3]. As discussed in Sec.2.3, SSA (solid state amorphization) in the Ti-Si system has been investigated by a number of groups [124-131, 133, 134]. It is reported that an amorphous layer, up to a few nm in thickness, can grow by a diffusion controlled process, during low temperature annealing (≤ 450°C) of a thin Ti film and single crystal Si couple [124, 126, 127]. When annealed at about 500°C, crystalline silicide begins to form at the interface between the amorphous layer and Si [124, 126]. It is noteworthy that some groups [124-126] reported that the amorphous layer had a composition approximately equal to that of the monosilicide, i.e., TiSi, and that the first crystalline silicide was TiSi. This is quite similar to observed reactions in bilayers of thin Ti film and amorphous Si films [128-130]. Experimental results from other researchers [127, 131, 132] indicate that the amorphous layer had a composition of $TiSi_2$ and the first crystalline phase was the C49 disilicide, which is a metastable form of $TiSi_2$. A significant feature of these results is that the amorphous layer and the first crystalline phase to form have similar or even the same compositions. This information implies that the controlling factor in the selection of the silicide to be formed is

not the same as that for the phase that subsequently grows. This is a strong support for the new model, because it has been inferred (see the beginning of this chapter), from the model, that release rate determines which silicide will form and the formation rate determines what fc'm this silicide will take.

From Table 5-1, it is evident that the SRPP for the V-Si system, from the data of column r and of column r* respectively, should be quite similar to those for Ni-Si. V_5Si_3 formation through direct V-Si reaction becomes impossible while other silicides, such as VSi_2, V_2Si and V_3Si, can form initially. Thus far, the most frequently reported first silicide to form in the V-Si system is VSi_2 [4, 6, 11, 74-77]. In the cases where Si substrates contain oxygen, V_3Si forms first [4, 77]. An amorphous V-Si phase forms initially in a-Si/V/a-Si (where a-Si represents the amorphous silicon film) layered films [78]. The composition of the amorphous phase is unknown. The crystalline phase that follows the amorphous phase is VSi_2 too.

The SRPP for the Cr-Si system, according to the calculations in Table 5-1, will be similar to that for the Co-Si system (Fig.5-2). The four phases, $CrSi_2$, CrSi, Cr_5Si_3 and Cr_3Si, all can grow through direct Cr-Si reactions and can all form initially. The experimental results, up till now, indicate that $CrSi_2$ forms first whether Cr films are deposited on crystalline Si, amorphous Si or a Pd layer which is on top of a Si substrate [6, 11, 67, 78-81].

The data for the Fe-Si system listed in Table 5-1 show that the SRPP of this system looks similar to that for the Co-Si system. As a result, $FeSi_2$, FeSi, Fe_5Si_3, and Fe_3Si all may form through direct Fe-Si reactions. It has been reported that FeSi forms initially when a thin Fe film and Si diffusion couple is annealed [6, 11, 82-84].

The calculations for the Zr-Si system indicate the important role of surface defect concentration again. From the data of column r, Zr_5Si_4 has the largest maximum release rate of Zr so that Zr_6Si_5, ZrSi, and $ZrSi_2$ cannot form through direct Zr-Si reactions. For a large diffusion flux of Si, the first phase to form can only be Zr_5Si_4. Prediction from the Walser and Bené rule also indicates that this phase will form initially. However, when defect effects are taken into account, only Zr_5Si_3 and Zr_6Si_5 cannot grow through direct Zr-Si reactions, whereas $ZrSi_2$ and ZrSi have the largest and the second largest maximum release rates respectively in this system. This result is in agreement with experiments in which $ZrSi_2$ [1-4, 10, 11, 103, 104] and ZrSi [105, 106] are observed to be the initial silicides, respectively. It is also reported that an amorphous Zr-Si phase forms when thin Zr film -Si diffusion couples are annealed at relatively low temperatures. The composition of the amorphous phase is unknown, but the first crystalline silicide that forms at the amorphous/Si interface is ZrSi [105, 106].

SRPP drawn for the Nb-Si, Mo-Si, and W-Si systems will be very similar to that for Co-Si. $NbSi_2$, Nb_5Si_3, Nb_3Si, Nb_4Si, $MoSi_2$ Mo_5Si_3, Mo_3Si, WSi_2, W_3Si_2 and W_5Si_3, can all form through direct metal-Si reactions. It has been found that $NbSi_2$, $MoSi_2$, and WSi_2 are the first phases formed during annealing of Nb-Si, Mo-Si, and W-Si thin film diffusion couples, respectively [6, 10, 67, 107-109, 118-120]. When an oxygen doped Mo/Si diffusion couple is annealed, a second silicide, Mo_5Si_3, begins growing shortly after the first phase ($MoSi_2$) forms, and they grow together [6]. In some other cases, e.g., in a Mo-Si bilayer, Mo_3Si or Mo_5Si_3 formation through direct Mo-Si reactions is also reported [108,110]. These results are consistent with predictions from the SRPP.

The SRPP for the last two systems, Hf-Si and Ta-Si, will be similar to that for Ni-Si (Fig. 5-3), i.e., all the silicides with their RMR rates listed in Table 5-1 can form through direct M-Si reactions (M represents Hf and Ta respectively), if the defect effect is not taken into account. Otherwise, some of these silicides, e.g., Hf_5Si_3 and Ta_5Si_3, may not form through this type of reaction. Thus far, only $TaSi_2$ has been observed when thin film diffusion couples consisting of c-Si/Ta, c-Si/a-Si/Ta, c-Si/Ta/a-Si (where c-Si and a-Si indicate crystalline and amorphous Si respectively) are annealed [6, 11, 116, 117]. HfSi is the first phase formed during annealing of Hf-Si diffusion couples [6, 11, 114, 115]. When a deposited Hf and Si bilayer is annealed, simultaneous growth of HfSi and $HfSi_2$ has also been observed [115]. These results agree with the predictions from the SRPP quite well.

At this point, it should be pointed out that, for the last ten metal-Si systems discussed above, the most frequently reported first phases, i.e. VSi_2, $CrSi_2$, $ZrSi_2$, $NbSi_2$, $MoSi_2$, $TaSi_2$ and WSi_2, have the largest maximum release rates in their respective systems (see Table 5-1). The other first phases, FeSi and HfSi, have the second largest maximum release rates in their respective systems (Table 5-1). The Ti-Si system is still debatable because of the variability in reported heats of formation for TiSi and $TiSi_2$. It is evident from Table 5-1 that the maximum release rates of Pd_2Si and FeSi, which are two of the three silicides observed as first phases, with the second largest maximum release rates in their systems, are very close to the largest maximum release rates in their own systems.

A comparison of the predictions from the calculations in Table 5-1 with the experimental results reported in the literature has been made and the results are listed in Table 5-2. The first column shows the observed first phases to form. Whenever more than one first phase is reported, the most frequently observed one is indicated by bold letters. In the second column of the table, the results of observed multiple phase growth are given, with the initial phase listed first in each respective system (the second phase to form is next and so on). The third column of Table 5-2 lists the predicted silicides that can

form through direct metal-Si reactions and can appear on the stepped curves of the RPP for each respective system. Using the information in this column, one can predict both first phase formation and multiple phase growth sequences. As mentioned at the beginning of the chapter, each of the predicted silicides in the third column of Table 5-2 can form initially in their respective systems, provided the conditions for the calculations (see Sec.5.1) are satisfied and the initial diffusion fluxes fall in the required ranges. Comparison of the first column with the third column shows very good agreement between the predictions and the experimental results in the Mn-Si, Co-Si, Ni-Si, Pt-Si, Ti-Si, V-Si and Mo-Si systems. For most of the silicides not observed as first phases in each respective system, it can be reasoned that the starting diffusion fluxes required for them to form initially may be too small compared with experimental diffusion fluxes. Therefore, without introducing a diffusion barrier to decrease the initial fluxes to the required critical value, it is impossible to observe the predicted results. It has already been noted that $FeSi_2$ and Pd_3Si have the largest RMR rates in their own systems, but are not observed to form initially. This can be attributed to the fact that the original diffusion flux is smaller than the lower critical diffusion flux, J_{iLC}, for those silicides to form. From the third column of Table 5-2, it can also be predicted that all silicides listed in the column for a given metal-Si system include all phases that will appear during multiple phase growth through direct metal-Si reactions. For example, using the SRPPs for Mn-Si and Ni-Si systems (Fig. 5-1 and 5-2), it is predicted that, after the first silicides, Mn_3Si and Ni_2Si respectively, grow larger than their critical thicknesses, the second silicides that can form should be MnSi and NiSi only. The phases, i.e., Mn_5Si_3 and Ni_3Si_2 that are located, in Mn-Si and Ni-Si phase diagrams respectively, between the first and the second silicides, should be bypassed. By comparing the second column with the third column (Table 5-2), one can find good agreement between predicted and experimental results in the Mn-Si, Co-Si, Ni-Si, Pt-Si and Mo-Si systems. For those phases not appearing in multiple phase growth situations, and for those systems in which multiple phase growth has not been observed in thin film couples, there is a logical reason, i.e., the required critical fluxes are so small that the corresponding critical thicknesses for initializing these silicides are too large. As a result, the formation of these silicides cannot be observed before one of the reactants is completely consumed.

It should be emphasized, as pointed out in the previous section, that these results are valid only when the conditions for these calculations are satisfied. The reactions must be type II reactions and the moving reactant and non-moving reactants must be the same as those indicated in Table 5-1. Otherwise, the predictions from the calculations may fail. Thus, some phases listed in the third column of Table 5-2 may not be the first phase to form at all, because their maximum release rates are so small (by at least 5 order of

magnitudes) that corresponding critical fluxes for the reactions are smaller than the diffusion flux of the other reactant. In this case, moving reactant and non-moving reactant are exchanged and, of course, the previous calculations are no longer applicable.

5.3. Discussion

In the last section, it has been seen that the predictions for silicide formation from SRPP agree with the experimental results from 15 metal-Si systems very well, which provides strong support to the new kinetic model and the criteria of silicide formation proposed from this study. In particular, since the calculations of RMR rates are based on Eq.(4-38), the reported results show favorable evidence for this equation and the microscopic mechanism from which the equation is derived. As mentioned in Sec.4.2.2.1, Eq.(4-38), after being rearranged, has a form very similar to an empirical LFER equation (Eqs.(4-39) and (4-41)), which suggests that the assumption of the release process and the microscopic mechanism for deriving Eq.(4-38) can be further verified by obtaining empirical LFER equations for various metal-Si systems from experiments of multiple phase sequential growth. The resulting equation can also provide quantitative values of E and α, the activation energy for breaking chemical bonds of nonmoving reactant and the proportionality coefficient of the LFER equation (Sec.4.2.2.1).

It has been mentioned in the preceding sections that the predictions here are for the first silicides to form and for multiple phase sequential growth at the R region adjacent to an elemental nonmoving reactant. There are basically two other types of silicide reactions not discussed in this chapter. One type is those reactions, in a multiple phase growth situation, which occur in the reaction regions other than that already discussed above. In this case, the procedure for calculating RMR rates and constructing RSP of these R regions is almost same as that described in Sec.5.1. The main difference is only that the moving and nonmoving reactants may vary from one region to another. Therefore, the predictions of silicide formation at a given R region can be done by obtaining and using SRPP for the region. The other type of reaction is that in a single phase sequential growth situation which take place after one component of a thin film couple is completely consumed by the initial silicide. In this case, as mentioned in point 4 of Sec.5.1, any new silicide must form either through the decomposition of the previous formed silicide or through reaction between the previously formed silicide and the other component. In the latter situation, the SRPP for the reaction region can still be constructed by using the same method as described in Sec.5.1. In the former situation, the reaction actually takes place at two reaction regions. For example, Ni_2Si decomposes to form NiSi according to

$$Ni_2Si \rightarrow NiSi + Ni \qquad (5\text{-}2a),$$

$$Ni + Si \rightarrow NiSi \qquad (5\text{-}2b).$$

The reaction described by Eq.(5-2a) occurs at $Ni_2Si/NiSi$ interface while that described by Eq.(5-2b) takes place at NiSi/Si interface with Ni diffusing through NiSi phase. Again, the latter reaction can be examined using an SRPP constructed by the same procedure as that mentioned above. But the reaction at $Ni_2Si/NiSi$ interface is different from all the reactions discussed above, i.e., it is not a type II reaction. It is evident that in this reaction the moving species is a product (Ni) instead of a reactant and it diffuses away from the reaction region. Besides, there is only one reactant (Ni_2Si in this particular case) which is decomposing. Therefore, the model proposed in this study is not applicable to this reaction. In order to predict this type of silicide reaction, a different kinetic model is required, which is beyond the scope of this study and is left for future studies.

The cases where amorphous phases are reported to form initially are not listed in Table 5-2. As mentioned in the previous sections, according to the model, which silicide forms is mainly determined by release rate, whereas which form the silicide takes is determined by formation rate. The calculations in Table 5-1 are for the RMR rates, and hence, predictions based on these calculations can only indicate what silicide will form and not which phase. Whether the silicide is amorphous, or some other metastable phase, is not determinable from these calculations. This problem may be solved by using formation rate calculations if the required activation energy, driving force, and interfacial energy change values for k phase formation, i.e., E_{ik}, ΔG_{ik} and $\Delta\sigma$ in Eqs.(4-55) to (4-57) respectively, are available.

Table 5-1. Calculations of relative maximum release rates for 15 metal-Si systems

System	Silicide	Temperature ℃	Nonmovig Reactant	ΔH^o kJ/mol[a]	r^b atoms/cm^{2}s	r^{*b} atoms/cm^{2}s
Mn-Si	$MnSi_{1.73}$	380	Si	44.5	1	1
	MnSi			97.0	1.60×10^4	5.89×10^6
	Mn_5Si_3			76.9	3.96×10^2	6.97
	Mn_5Si_2					
	Mn_3Si			137.1	2.60×10^7	8.17×10^9
	Mn_9Si_2					
	Mn_6Si					
Co-Si	$CoSi_2$	350	Si	51.4		1
	CoSi			100.3	$1.2[illegible] \times 10^4$	1.35×10^7
	Co_2Si			115.4	2.32×10^5	2.19×10^8
	Co_3Si					
Ni-Si	$NiSi_2$	300	Si	43.6	1	1
	NiSi			85.7	6.93×10^3	7.38×10^6
	Ni_3Si_2			111.8	1.67×10^6	1.04×10^6
	Ni_2Si			148.4	3.63×10^9	3.42×10^{12}
	Ni_5Si_2			150.5	5.63×10^9	2.74×10^9
	$Ni_{31}Si_{12}$					
	Ni_3Si			140.0	$6.[illegible] \times 10^8$	5.63×10^{11}
Pd-Si	PdSi	300	Si	142.1	1	1
	Pd_2Si			239.5	7.64×10^8	6.78×10^8
	Pd_9Si_4					
	Pd_3Si			251.6	9.74×10^9	8.30×10^9
	Pd_4Si					
	Pd_9Si_2					
	Pd_5Si					

Table 5-1 continued

System	Silicide	Temperature °C	Nonmovig Reactant	ΔH^o kJ/mol[a]	r^b atoms/cm^{2}s	r^{*b} atoms/cm^{2}s
Pt-Si	$PtSi$	300	Si	168.0	1	1
	Pt_6Si_5			167.2	[illegible].84	6.82×10^{-6}
	Pt_2Si			213.2	1.31×10^4	1.16×10^4
	Pt_7Si_3			213.2	1.31×10^4	0.51
	$Pt_{12}Si_5$					
	Pt_5Si_2					
	Pt_3Si			211.5	9.22×10^3	7.86×10^3
	Pt_4Si					
Ti-Si	Ti_3Si	500	Ti			
	Ti_5Si_3			116.2	1	1
	Ti_5Si_4					
	$TiSi$			163.9[c]	1.67×10^3	1.37×10^8
	$TiSi_2$			135.0	18.7	1.37×10^6
V-Si	V_3Si	600	V	38.9	1	1
	V_2Si			77.3	2.01×10^2	1.83×10^3
	V_5Si_3			80.3	3.00×10^2	34.6
	V_5Si_4					
	V_6Si_5					
	VSi_2			313.5	2.76×10^{16}	2.35×10^{20}
Cr-Si	Cr_3Si	400	Cr	46.0	1	1
	Cr_2Si					
	Cr_5Si_3			65.2	31.1	3.59
	Cr_3Si_2					
	$CrSi$			79.4	3.95×10^2	3.80×10^6
	$CrSi_2$			122.9	9.39×10^5	8.00×10^9
Fe-Si	Fe_3Si	450	Fe	31.2	1	1
	$Fe_{11}Si_5$					
	Fe_2Si					
	Fe_5Si_3			48.8	18.8	2.2

Table 5-1 continued

System	Silicide	Temperature °C	Nonmovig Reactant	ΔH° kJ/mol[a]	r[b] atoms/cm^{2}s	r*[b] atoms/cm^{2}s
	$FeSi$			73.6	1.15×10^3	1.11×10^7
	$FeSi_2$			81.1	4.03×10^3	3.44×10^7
Zr-Si	Zr_4Si	700	Zr	54.3	1	1
	Zr_3Si					
	Zr_2Si			104.5	4.95×10^2	1.31×10^4
	Zr_5Si_3			115.4	1.90×10^3	6.44×10^2
	Zr_3Si_2			128.2	9.26×10^3	2.00×10^4
	Zr_4Si_3					
	Zr_5Si_4			163.3	7.09×10^5	2.05×10^5
	Zr_6Si_5			142.8	5.65×10^4	9.92×10^3
	$ZrSi$			154.7	2.45×10^5	6.85×10^9
	$ZrSi_2$			158.8	4.10×10^5	1.01×10^{10}
Nb-Si	Nb_4Si	650	Nb	21.9	1	1
	Nb_3Si			44.0[d]	17.7	52.2
	Nb_5Si_3			97.0	1.77×10^4	6.02×10^3
	$NbSi_2$			137.9	3.70×10^6	9.18×10^{10}
Mo-Si	Mo_3Si	525	Mo	33.4	1	1
	Mo_5Si_3			56.0	30.1	3.47
	Mo_3Si_2					
	$MoSi_2$			108.7	8.46×10^4	7.21×10^8
Hf-Si	Hf_2Si	550	Hf	94.1	1	1
	Hf_5Si_3			112.4	14.5	0.19
	Hf_3Si_2					
	Hf_4Si_3					
	Hf_5Si_4					
	$HfSi$			142.1	1.13×10^3	1.20×10^6
	$HfSi_2$			225.7	2.30×10^8	2.17×10^{11}

Table 5-1 continued

System	Silicide	Temperature °C	Nonmovig Reactant	ΔH^o kJ/mol[a]	r^b atoms/cm^{2}s	r^{*b} atoms/cm^{2}s
Ta-Si	$Ta_{4.5}Si$	650	Ta	32.0	1	1
	Ta_3Si			51.6	12.9	53.3
	Ta_2Si			62.7	55.1	2.06×10^3
	Ta_5Si_3			66.9	95.0	45.3
	$TaSi_2$			119.1	8.63×10^4	3.01×10^9
W-Si	W_3Si	550	W			
	W_5Si_3			38.9	1	1
	W_3Si_2			41.8	1.53	9.76
	WSi_2			92.8	2.66×10^3	1.94×10^8

[a] The values listed in this column are the standard heat of formation per nonmoving reactant atom. The original values of ΔH° are obtained from Ref.[218] except those specified.

[b] r* and r values are calculated with and without taking into account the activity quotient in Eq.(10), respectively.

[c] ΔH° value for TiSi, from Ref.[3], is 131.7 kJ/mol.

[d] This value is from Ref.[3].

Table 5-2. Comparison of predictions of silicide formation with experimental results from the literature

Observed first silicide to form	Observed multiple phase formation	Predicted from this Model	RMR rates[b] atoms/cm^{2}s
Mn_3Si	Mn_3Si	Mn_3Si	8.17×10^9
MnSi	MnSi	MnSi	5.89×10^6
		$MnSi_{1.73}$	1
Co_2Si	Co_2Si	Co_2Si	2.19×10^8
CoSi	CoSi	CoSi	1.35×10^7
$CoSi_2$		$CoSi_2$	1
Ni_2Si	Ni_2Si	Ni_2Si	3.42×10^{12}
NiSi	NiSi	NiSi	7.38×10^6
$NiSi_2$		$NiSi_2$	1
Pd_2Si	N/A[c]	Pd_3Si	8.3×10^9
		Pd_2Si	6.78×10^8
		PdSi	1
Pt_2Si	Pt_2Si	Pt_2Si	1.16×10^4
PtSi	PtSi	PtSi	1
$TiSi_2$	N/A	$TiSi_2$	1.37×10^6
TiSi		TiSi	(9.32×10^5)[d]
Ti_5Si_3		Ti_5Si_3	1
VSi_2	N/A	VSi_2	2.35×10^{20}
		V_2Si	1.83×10^3
V_3Si		V_3Si	1
$CrSi_2$	N/A	$CrSi_2$	8.00×10^9
		CrSi	3.80×10^6
		Cr_5Si_3	3.59
		Cr_3Si	1
FeSi	N/A	$FeSi_2$	3.44×10^7
		FeSi	1.11×10^7
		Fe_5Si_3	2.2
		Fe_3Si	1

Table 5-2 continued

Observed first silicide to form	Observed multiple phase formation	Predicted from this Model	RMR rates[b] atoms/cm^{2}s
$ZrSi_2$	N/A	$ZrSi_2$	1.01×10^{10}
$ZrSi$		$ZrSi$	6.85×10^{9}
		Zr_5Si_4	2.05×10^{5}
		Zr_3Si_2	2.00×10^{4}
		Zr_2Si	1.31×10^{4}
		Zr_4Si	1
$NbSi_2$	N/A	$NbSi_2$	9.18×10^{10}
		Nb_5Si_3	6.02×10^{3}
		Nb_3Si	52.2
		Nb_4Si	1
$MoSi_2$	$MoSi_2$	$MoSi_2$	7.21×10^{8}
Mo_5Si_3 and Mo_3Si	Mo_5Si_3	Mo_5Si_3	3.47
		Mo_3Si	1
$HfSi$	N/A	$HfSi_2$	2.17×10^{11}
		$HfSi$	1.20×10^{6}
		Hf_2Si	1
$TaSi_2$	N/A	$TaSi_2$	3.01×10^{9}
		Ta_2Si	2.06×10^{3}
		Ta_3Si	53.3
		$Ta_{4.5}Si$	1
WSi_2	N/A	WSi_2	1.98×10^{8}
		W_3Si_2	9.76
		W_5Si_3	1

The phases in bold letters are the most frequently observed as initial phases.

The RMR rates listed here are from column r* in Table 5-1.

N/A indicates that multiple phase sequential growth through direct metal-Si reaction has not been reported in the literature.

This RMR rate calculated using the data from Ref.[3], i.e., $\Delta H^{\circ}=-131.7$ kJ/mol.

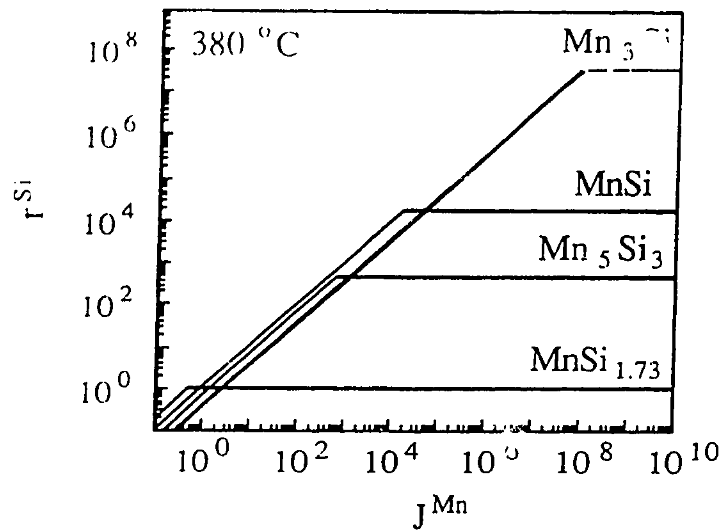

Fig.5-1 SRPP for Mn-Si system. The plot is drawn using the data from column r in Table 5-1.

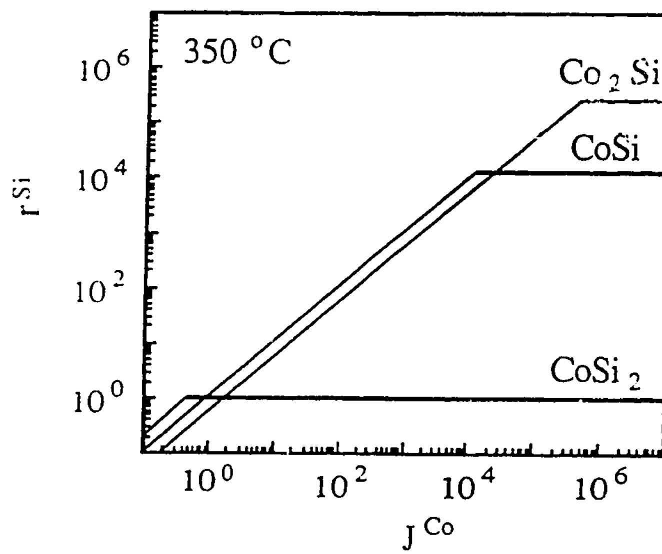

Fig.5-2 SRPP for Co-Si system. The plot is drawn using the data from column r in Table 5-1.

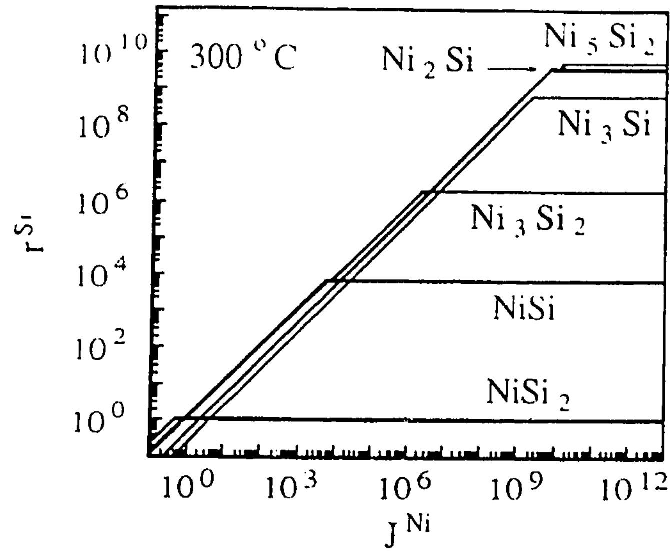

(a)

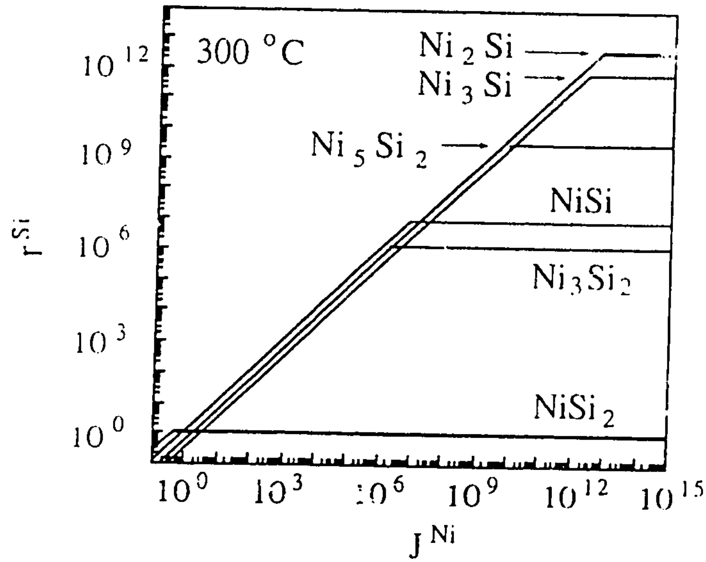

(b)

Fig.5-3 SRPPs for Ni-Si system drawn using the data from columns r (a) and r* (b) in Table 5-1. The inclined segments for $Ni_5Si_2$and Ni_3Si_2 are not drawn in order to avoid cluttering the diagram.

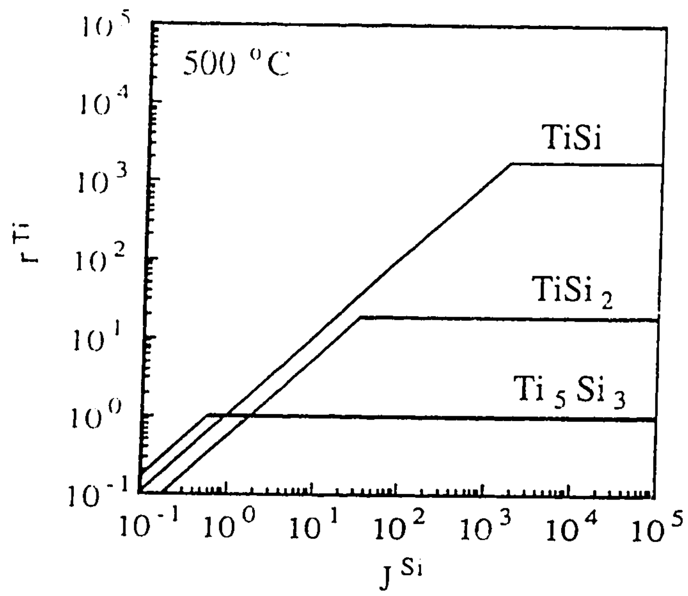

(a)

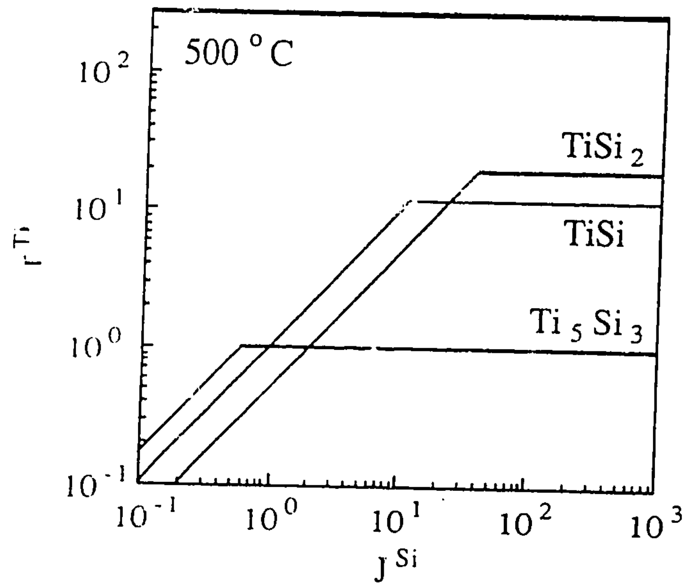

(b)

Fig.5-4 SRPP for Ti-Si system. Fig.5-4a and 5-4b are calculated using the data (ΔH^{o}_{298}) from Ref.[218] and Ref.[3], respectively.

Chapter 6 Silicide Formation Sequence Experiments

From the last chapter, it can be seen that the predictions of silicide formation from the new kinetic model and the reaction criteria are in good agreement with experimental results reported in the literature. The purpose of the experimental work in this study is to provide further experimental support for the model. The experimental work can be divided into two parts. Part one is the observation of the multiple phase growth sequence in thin Ni film-Si diffusion couples. In this experiment, a thin Ni film is deposited on a Si substrate at room temperature and the couple is then annealed at 300°C for various time periods. For convenience, the samples with Ni films deposited at room temperature are called "cold substrate samples." Part two of the experiments is the investigation of silicide formation sequence during direct deposition reactions in which Ni is deposited onto heated Si substrates. The samples used in these experiments are called "hot substrate samples."

The purpose of part one is quite straightfoward, i.e., to compare the experimental observations with the predicted silicide formation sequence. The original experimental design for part two is based on the following considerations. According to the kinetic model (Chap.3) and the reaction criteria (Chap.4), any silicide in a given metal-Si system can be the first silicide to form, as long as the release rates for forming the silicide are on the stepped curve of the RPP plot for this system and the initial diffusion flux is in the required range (see Secs.4.4 and 5.2). During a direct deposition reaction, the diffusion flux of Ni can be controlled by adjusting the Ni deposition rate, which is possible at least for the initial stage of the reaction. From Sec.3.4.4, the critical diffusion flux for initiating NiSi formation is about 5×10^{13} to 1×10^{14} atoms/cm^{2}s at about 330°C. The deposition rate is chosen to match this value so that either Ni_2Si or NiSi is expected to form initially, when Ni is deposited onto a Si substrate held at 300°C. However, it is found, as will be seen in this chapter, that the initial silicide is $NiSi_2$ at all deposition rates used in this experiment. Furthermore, a literature survey [142, 154, 157, 159] shows that when the deposited Ni layer is thinner than 3 monolayers, even room temperature deposition will produce $NiSi_2$ as the initial silicide, which cannot be explained by other models and theories. These results were unexpected by the original experiment design. Therefore, further investigation on the silicide formation sequence during deposition reactions at elevated temperatures was carried out and it is found that the sequence is $NiSi_2$, Ni_2Si and NiSi. Besides, it is also found that if the latent heat release, due to the condensation of metal atoms from the vapor phase onto the Si surface, is taken into account, this phenomenon, i.e., $NiSi_2$ forming initially, can be explained very well by the new kinetic model, providing additional support for the model. These results and subsequent discussion will be given in the following sections.

6.1 Experimental Procedure

6.1.1. Deposition of Nickel Films

Nickel was deposited onto Si wafers by electron beam (e-beam) evaporation. <100> oriented, single crystal silicon wafers (n-type with a doping level between 5×10^{12} and 1×10^{13} cm^{-3}), obtained from the Alberta Microelectronic Center, and high purity nickel (99.9%), obtained from Cerac Ltd., were used to prepare the samples. Before loading into the deposition chamber, the Si wafers were dipped in a 10:1 buffered HF solution for 1 minute to remove the oxide, rinsed in deionized water and dried with high purity nitrogen.

For Ni deposition on cold substrates, the chamber was pumped down to a base pressure better than 2×10^{-7} torr. The deposition rate of Ni was controlled to between 2 and 3 nm/s. The pressure during deposition was kept at about 1×10^{-6} torr. The nominal thickness of deposited Ni films was 100 nm.

For preparing hot substrate samples, after the base pressure had reached 3 to 4×10^{-7} torr, the heating lamps in the chamber were turned on until the substrates reached the desired temperature. A thermocouple was attached to a separate Si wafer located near the sample wafers to monitor the substrate temperature. Two temperatures, 300°C and 250°C, were used. The deposition rates, ranging from about 0.1 nm/s to about 6 nm/s, were controlled by adjusting the electron gun current. The chamber pressure during deposition was between 1 and 2×10^{-6} torr. Four deposited nominal Ni film thicknesses, i.e., approximately 3, 5, 10 and 30 nm, were chosen.

6.1.2. Annealing Procedure

For part one of the experiments, the cold substrate samples (i.e., Si wafer with Ni films) were cleaved, using a diamond knife, into 1cm × 1cm pieces and loaded individually into a BioRad RC2400 Alloying Furnace. Annealing was done in flowing nitrogen (purified nitrogen, 99.97%) at 300°C for 5, 10, 20, 40, and 120 min. The samples can be heated to 300°C in 55 seconds and cooled from 300°C to 200°C in two and one-half min. and from 300°C to 100° in eight and one-half min.

6.1.3. X-Ray Diffraction Experiments

Prior to transmission electron microscopy (TEM) analysis, all specimens were characterized by x-ray diffraction with Cu-K_{α} radiation. The x-ray diffractometer is comprised of a Rigaku-Denki D-F3 generator, a Philips PW1380 goniometer, a Philips PW1965/20/30 proportional counter, a PM8000/06/07 chart recorder and a PW/1370/00/01/60/61 circuit panel. The obtained x-ray spectra were identified by

calculating the interplanar spacings according to Bragg's law and comparing with data from the JCPDS Powder Diffraction Files [219].

6.1.4. Transmission Electron Microscopy (TEM)

6.1.4.1. Specimen Preparation and Equipment

Both plan view and cross-section TEM specimens were used. A standard procedure [9, 220] for specimen preparation, including gluing (cross-section specimens only), grinding, disc-cutting, dimpling and sputtering, was followed. The procedure is described in Appendix 2 of Ref.[9] in detail. A Gatan ultrasonic disc cutter (Model 601), a Gatan dimple grinder (Model 656), and an ion mill (a Gatan Duo Mill 600CTMP) were used for the disc cutting, dimpling, and sputtering processes respectively during specimen preparation.

Plan view and cross-section specimens were examined by TEM. The TEMs used in this experiment were a Hitachi H-7000, with an accelerating voltage of 125 kV and a JEOL-2010 TEM equipped with a Noran, ultra thin window, Ge x-ray detector, operated with an accelerating voltage of 200 kV.

The techniques applied to examine the specimens included bright field imaging, selected area diffraction (SAD), convergent beam electron diffraction (CBED), and energy dispersive x-ray spectroscopy (EDX).

6.1.4.2. Thickness Measurement Using TEM Micrographs

Bright field images were used to examine the structure of silicide layers formed during the annealing process and to measure the thickness of these layers. The following method was adopted to measure the thickness. For each cross-section specimen, micrographs from three different areas were taken. Layer thicknesses were measured directly on the negatives with a ruler. The initial measuring point was selected randomly and every successive measuring point was chosen at a distance of 100 nm from the last point. Each negative was measured twice with different initial points so that about 30 readings were obtained from each negative and 90 readings from each specimen. Average layer thicknesses, $\bar{x}$, and standard deviations (σ_d) were evaluated from these readings (x_i) using the following formulas:

$$\bar{x} = \frac{\sum_{i=1}^{n} x_i}{n} \quad (6\text{-}1),$$

$$\overline{\sigma_{ij}} = \frac{\sum_{i=1}^{n} (\overline{x} - x_i)^2}{n - 1} \qquad (6\text{-}2);$$

where n is the number of readings from one specimen.

6.1.4.3. Phase Identification

Since the grain sizes of all the silicides investigated were smaller than 1 μm and most of the silicide layers were thinner than 100 nm, several techniques, such as selected area diffraction (SAD), convergent beam electron diffraction (CBED), and energy dispersive x-ray spectroscopy (EDX), were used to identify the phases. Diffract v1.5b software, purchased from Virtual Labortories, was used for simulating the diffraction (SAD and CBED) patterns.

A. Convergent Beam Electron Diffraction

CBED patterns were obtained from the H-7000 TEM and the smallest incident beam size obtained was 300nm in the H-7000 TEM. An internal standard calibration method was adopted to minimize the systematic error. Since the crystal structure of Si is well known and large thin areas of Si were always available in cross-section samples, it was very convenient to use Si as the internal standard sample. Whenever a CBED diffraction pattern from a silicide was taken, a CBED pattern from Si was obtained at the same operating condition. The same method was also applied to SAD patterns. Therefore, the camera constant could be exactly determined throughout all the experiments.

B. Energy dispersive x-ray spectroscopy (EDX)

The JEOL-2010 TEM was used for EDX to analyze the composition of individual layers and phases. The composition in a given phase can be determined by the following formula [221]:

$$\frac{X_{Si}}{X_{Ni}} = K_{Ni/Si} \frac{I_{Si} \times W_{Ni}}{I_{Ni} \times W_{Si}} \qquad (6\text{-}3),$$

where X_{Si} and X_{Ni} are the concentrations (atomic percent) of Si and Ni, W_{Si} and W_{Ni} are the atomic weights of Si and Ni, I_{Si} and I_{Ni} are the intensities from Si and Ni in the EDX spectra from the phase of interest, and $K_{Ni/Si}$ is the proportionality constant, often referred

to as the Cliff-Lorimer factor. This factor is independent of specimen composition and thickness, but dependent on instrumental conditions [221]. In this experiment, approximate compositions were determined using appropriate Cliff-Lorimer "K" factors. These were determined using a standardless approach or from appropriate standards [222].

6.2. Experimental Results

6.2.1. Multiple Phase Growth in Thin Ni Film-Si Diffusion Couples

When cold substrate samples are annealed at 300°C up to 120 min., only two nickel silicides are observed. They are identified as Ni_2Si and NiSi, respectively. An example of phase identification is shown in Fig.6-1. Fig.6-1a is a plan view TEM micrograph from a cold substrate sample annealed at 300°C for 10 min. The sample was ion milled from both the surface side and Si side to remove the unreacted Ni film and Si, keeping the Ni_2Si layer only. The large grains in the micrograph are Ni_2Si while the small grains in a very thin layer are the remaining Ni film. Fig.6-1b is an SAD pattern from the sample, showing a typical polycrystalline SAD pattern of δ-Ni_2Si, without preferred orientation. Fig.6-1c is an EDX spectrum from the same layer in a cross-section TEM specimen of the same sample, indicating the layer's composition, $X_{Ni}/X_{Si} \cong 2$.

In the samples annealed for 5, 10, and 20 min., respectively, only a Ni_2Si layer forms, while a second layer, i.e., NiSi, is observed in the samples annealed for 40 and 120 min. Two cross-section TEM micrographs from samples annealed for 10 and 40 min., respectively, are shown in Fig.6-2. It is evident that Ni_2Si forms a uniform layer at the Ni/Si interface initially (Fig.6-2a) and that a second silicide layer (NiSi) starts to grow at the Ni_2Si/Si interface (Fig.6-2b). The multiple phase growth sequence in the thin film Ni-Si diffusion couples is summarized in Fig.6-3. These results lend strong support to the prediction of multiple phase growth in a Ni-Si system shown in Table 5-2. It is worth mentioning that a previous study on thin film Mn-Si couples reported that when the couples were annealed at 380°C, the initial phase was Mn_3Si which formed a uniform layer at the original Mn/Si interface and a second silicide layer, i.e., MnSi, started to grow only after annealing for more than 15 min. In order to show the formation sequence in a Mn-Si system, two cross-section TEM micrographs from Mn-Si couples annealed at 380°C for 10 and 40 min. are given in Fig.6-4a and 6-4b, respectively. Since Mn_3Si had not been reported to be the initial phase in the Mn-Si system before that study was carried out, these results provide experimental support for the predictions of both initial silicide and multiple phase growth in the Mn-Si system (see Table 5-2).

6.2.2. Direct Deposition Reactions between Ni and Si Substrates

TEM micrographs from cross-section specimens of samples deposited at 300°C with deposition rates of 0.1 nm/s and 2 nm/s, are shown in Figs.6-5 and 6-6 respectively. It can be seen that only one silicide, identified as $NiSi_2$ (Fig.6-7), is formed when the nominal Ni film thicknesses are less than and equal to 5 nm (Figs.6-5a, 6-5b, 6-6a, and 6-6b). The orientation relationship between the epitaxial $NiSi_2$ and the Si substrates is $NiSi_2$ [001] // Si [001] and $NiSi_2$ (110) // Si (110) (Fig.6-7b). The $NiSi_2$ shows an island growth behavior and those small crystals have a pyramid shape that is believed to stem from preferential growth along {111} planes of Si crystal. The smallest island observed is about 3 to 4 nm at the base of the pyramid, which indicates that the critical size for $NiSi_2$ nucleation should be no larger than 3 nm. As more Ni is deposited on the substrates more and more islands form, while the islands already nucleated continue to grow until the islands meet and form a continuous layer.

Figs.6-5c and 6-6c show that a second continuous layer, identified as δ-Ni_2Si (Fig.6-8), is formed at a nominal Ni thickness of 10 nm. The growth of the δ-Ni_2Si layer shows strong preferred orientation. Fig.6-8 shows selected area diffraction patterns (SAD), from a plan view sample with the Ni deposited at 300°C and a rate of 2 nm/s. The strong reflections in Fig.6-8 are from $NiSi_2$ (ZA=[102]), i.e., the spiking like layer in Fig.6-5c and 6-6c. The weak reflections are from δ-Ni_2Si (orthorhombic structure, a=0.739 nm, b=0.99 nm, c=0.703 nm, and ZA=[$12\bar{2}$]) and from δ-Ni_2Si crystals with ZA=[$\bar{1}\bar{2}2$]. The Ni_2Si and $NiSi_2$ have the following orientation relationships: $NiSi_2$ [102] // Ni_2Si [$12\bar{2}$] and $NiSi_2$ (020) // Ni_2Si (022); $NiSi_2$ [102] // Ni_2Si [$\bar{1}\bar{2}2$] and $NiSi_2$ (020) // Ni_2Si (022).

When the nominal Ni thickness reaches 30 nm, three layers are visible in the micrographs from cross-section specimens (Figs.6-5d and 6-6d). The first layer, spiking-like and adjacent to Si, is $NiSi_2$. The second is identified as NiSi (orthorhombic structure, a=0.518nm, b=0.334nm, c=0.562nm). The top layer appears to be a Ni-rich solid solution because the diffraction pattern from this polycrystalline layer matches best with a ring pattern of Ni. However, EDX analysis shows that the layer contains about 15-20 at.% Si which is higher than the solubility (about 10 at.% Si) of Si in Ni . Therefore, the existence of some Ni-rich silicide, possibly Ni_2Si, cannot be ruled out. According to an SAD pattern from a plan view specimen deposited at 300°C and a rate of 0.1 nm/s (Fig.6-9), the growth of NiSi has strong preferred orientation with NiSi [010] // $NiSi_2$ [010] and NiSi (200) // $NiSi_2$ (200) as well as NiSi (002) // $NiSi_2$ (200).

TEM micrographs from cross-section specimens, deposited at 250°C and a rate of about 0.1 nm/s, are shown in Fig.6-10. It is found that only one continuous layer is

formed up to 5 nm of deposited Ni. This layer is identified as epitaxial $NiSi_2$ for 3 nm of Ni, and as epitaxial $NiSi_2$ plus Ni, (which are not distinguishable layers from the micrograph (Fig.6-10b) although a SAD pattern does show a ring pattern matched best with that of Ni), for 5 nm of Ni. A second layer is formed when the nominal Ni thickness reaches about 10 nm. This layer is δ-Ni_2Si (Fig.6-11), which also has preferred orientation with respect to the underlying $NiSi_2$.

All of the experimental results from this study are summarized in Table 6-1. There is no significant difference between the reactions using different deposition rates (0.1 to 6 nm) and the same temperature. However, the difference in the morphology between the $NiSi_2$ formed through island growth and that showing layered growth behavior is significant. The reason for this is not known at this point. The overall silicide formation sequence, during direct deposition reactions at temperatures ranging from 250 to 300°C, can be summarized as follows: $NiSi_2$ forms initially, which is followed by Ni_2Si, and then NiSi grows. In this study, the starting point for NiSi formation is not observed. But, it is likely that, when the Ni_2Si thickness reaches a certain value, NiSi begins to nucleate and grow at the $NiSi_2/Ni_2Si$ interface.

6.3 DISCUSSION

6.3.1. Critical Diffusion Flux for NiSi Formation

It is very interesting to compare the present results from the cold substrate samples with those obtained by Scott *et al.* [49] for samples with oxygen doped Ni films on Si substrates. In that experiment, Ni films were implanted with 1.6×10^{16} cm^{-2} O^+ ions and the samples were then annealed in a vacuum furnace at 290°C. A Ni_2Si growth kinetic plot from Ref.49 is shown in Fig.6-12a. Using this plot, the relationship between Ni_2Si thickness, x, and the annealing time, t, can be determined as

$$x = 2.71\sqrt{t} \qquad (6\text{-}4),$$

where the units for x and t are nm and seconds respectively. The data from this work are also used to plot Ni_2Si thickness as a function of annealing time which is shown in Fig.6-12b. The expression for this function, obtained from linear regression analysis, has the same form as Eq.(3-8),

$$x = 4.02 + 2.33\sqrt{t} \qquad (6\text{-}5),$$

where x and t have the same units as those in Eq.(6-4). It is evident that the two curves in Figs.6-12a and 6-12b have similar shapes. The main difference is the kinetic curve deviates from parabolic behavior (i.e., deviates from the straight line in the figures) earlier in Fig.6-12b than in Fig.6-12a, which implies a faster decrease in Ni diffusion flux encountered in this experiment. Using Eqs.(6-4) and (6-5) combined with Eq.(3-6), the initial diffusion fluxes (i.e., that at $t = 0$) and the diffusion fluxes at the times when the kinetic curves deviate from the straight lines in Figs.6-12a and 6-12b are calculated and the results are listed in Table 6-2 (as in Sec.3.4.1, t_1 in this table indicates the times when the deviation starts). In addition, the fluxes, corresponding to the annealing times 40 and 120 min for this experiment and that of Scott *et al*, are also estimated by directly inserting the observed thicknesses into Eq.(3-6). The results are also listed in Table 6-2. These last two points are chosen because NiSi formation is observed only after 40 min annealing in this experiment and this point is considered as starting point for NiSi formation. According to Scott *et al*'s results, NiSi formation can be observed only after annealing for 169 minutes. Considering that the backscattering technique used by these authors usually has a depth resolution of 20 nm and that the NiSi first observed in the present experiment is only about 17 nm thick, it is likely that the time for initiating NiSi formation in Scott *et al*'s experiment is earlier than reported. Therefore, the point corresponding to 120 minutes of annealing is used as the actual starting point for NiSi formation in their experiment. As in Section 3.4.1, t_2 is used to indicate the approximate times when NiSi starts to form. From Table 6-2, it is obvious that the initial diffusion fluxes, the fluxes corresponding to t_1, and, in particular, the critical fluxes for NiSi formation to start (at t_2), obtained by both experiments are very close, although the diffusion flux in the present experiment decreases at a faster rate than in the other. These results provide further evidence for the new kinetic model, i.e., in addition to kinetic factors such as diffusivity and nucleation barriers, some other factors also play an important role in controlling silicide formation processes. These factors have been defined as release rate and formation rate respectively and have been examined in Chap.3 to Chap.5.

6.3.2. Explanation of Silicide Formation Sequence during Direct Deposition Reactions

It is noteworthy that the Ni deposition rates used in this study are very close to the diffusion fluxes for Ni_2Si or NiSi formation during annealing of a thin Ni film-Si diffusion couple around 300°C. From the point of view of transportation rates of Ni atoms to the reactive interface, the deposition rates are equivalent, at least for the initial stages of the reactions, to the diffusion fluxes if their values are same. Then , a question arising from

these experimental results is if similar fluxes of Ni to Si are used with the same substrate temperature, why are different initial phases formed and the formation sequence completely changed. In particular, the silicide, $NiSi_2$, which usually cannot form at such low temperatures (250-300°C) by thermal annealing, can be epitaxially grown by direct deposition reaction. This phenomena may be explained by the new model and an RPP.

During a direct deposition reaction, latent heat will be released when metal atoms in the vapor are held onto or in the substrate, so that they can be considered as atoms in a solid. This energy can make the Ni-Si reactions much easier by either helping Si atoms break their chemical bonds or heating up the local crystal lattice. In the former case, the driving force for the reaction will increase according to

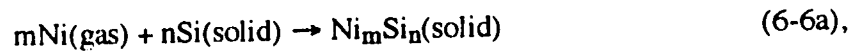

$$mNi(gas) + nSi(solid) \rightarrow Ni_mSi_n(solid) \quad (6\text{-}6a),$$

so that
$$\Delta G^{o}_{ir} = G_{Ni_mSi_n}(solid) - nG_{Si}(solid) - mG_{Ni}(gas) \quad (6\text{-}6b).$$

Comparing Eq.(6-6b) with that for common thermal reaction at the same temperature, it is easy to find that the last term in right hand side of Eq.(6-6b) will result in larger negative ΔG^{o}_{ir} due to the atoms in vapor phase having a much higher potential energy (a few eV per atom). Consequently, the Arrhenius activation energy for the release process will be decreased substantially (recall Eq.(4-38)).

$$r_{imax} = n^* \nu \exp\left[-\frac{\alpha' \Delta G_{ir} + E}{k_B T}\right] \quad (4\text{-}38).$$

In the latter case, the temperature near the reaction region would be increased significantly. Whichever occurs, according to Eq.(4-38), the result is a much larger r_{imax} than in normal thermal annealing at the same substrate temperature. This effect can be schematically shown for the Ni-Si SRPP, i.e., the stepped curve shifts up to the right, which is represented by the dashed curve. Consequently, a different silicide may form at the same diffusion flux. For example, when a Ni-Si diffusion couple is annealed at 300°C and the diffusion flux is J_0 in Fig.6-13, NiSi forms. But, in the case of direct deposition reactions at a substrate temperature of 300°C and at the same diffusion flux (or deposition rate), $NiSi_2$ will form because of the latent heat release. In order to understand why the second phase that forms is Ni_2Si, one has to consider the reaction between incoming Ni atoms and $NiSi_2$ (also, an SRPP for the reaction region between $NiSi_2$ and Ni, instead of that for Ni-

Si, has to be used). In this case, the barrier energy, E, for releasing one unit formula of $NiSi_2$ is much larger than that for Si atoms, because eight Ni-Si bonds have to be broken to release one $NiSi_2$ "molecule" (which has a CaF_2 structure) whereas only two Si-Si bonds are to be broken. Therefore, the maximum release rates, r_{imax}, for Ni-$NiSi_2$ reactions would be much lower than those for Ni-Si reactions. During direct deposition reactions, although the latent heat release can increase r_{imax} significantly, the values of r_{imax} for the silicides, e.g., NiSi and Ni_2Si, formed from Ni-$NiSi_2$ reactions are still much lower than those for the same silicides to form from Ni-Si reactions. Therefore , at the deposition rates used in this study, only the reaction with the highest release rate, i.e., Ni_2Si formation, can actually occur.

From the discussion in this section it is seen that the new model and the RPP plot is also capable of explaining the complex experimental phenomena encountered in direct deposition reaction processes which cannot be explained by other models and theories from the literature. This provides additional support for the model.

Table 6-1. Summary of direct deposition reactions

Nominal Ni Thickness	3 nm	5 nm	10 nm	30 nm
300°C 0.1 nm/s	epitaxial $NiSi_2$ islands	epitaxial $NiSi_2$	$NiSi_2$, δ-Ni_2Si continuous layer	$NiSi_2$, NiSi, Ni-rich alloy layer
300°C 2 nm/s	epitaxial $NiSi_2$ islands	epitaxial $NiSi_2$	$NiSi_2$, δ-Ni_2Si continuous layer	$NiSi_2$, NiSi, Ni-rich alloy layer
250°C 0.1 nm/s	epitaxial $NiSi_2$ continuous layer	epitaxial $NiSi_2$, Ni-rich alloy layer	$NiSi_2$, δ-Ni_2Si continuous layer	

Table 6-2 Comparison of diffusion fluxes in two experiments

Experiments	$J (t = 0)^{a}$ $\times 10^{14}$	$J (t = t_1)$ $\times 10^{14}$	$J (t = t_2)$ $\times 10^{14}$
Scott *et al*	17	1.1 $t_1 = 4800s$	0.24 $t_2 = 7200s$
This work	14	2.0 $t_1 = 1200s$	0.30 $t_2 = 2400s$

[a] the units for diffusion fluxes in this table are atoms/cm^2s.

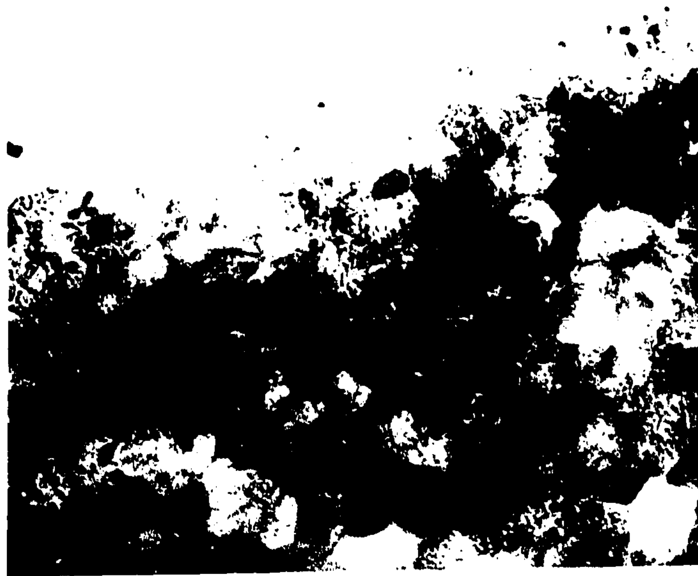

(a)

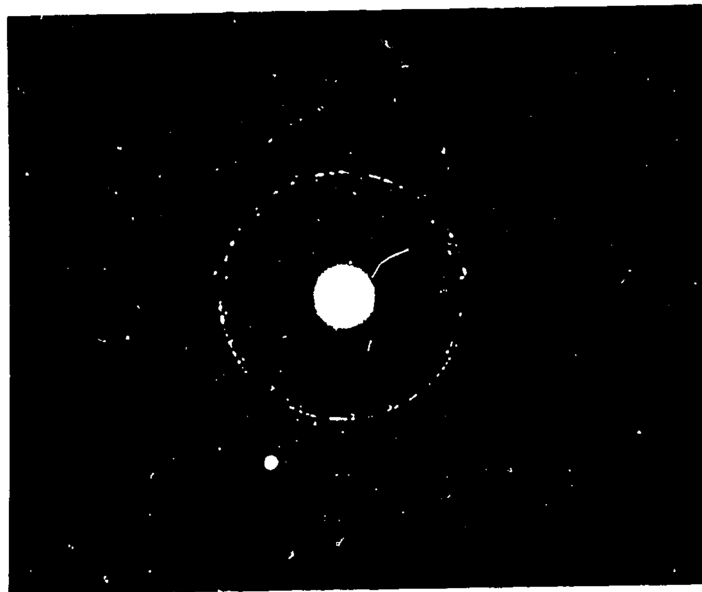

(b)

Fig.6-1 a) Planview TEM micrograph showing a Ni_2Si layer in a cold substrate sample annealed at 300°C for 10 min. The large grains are Ni_2Si and the small grains are the remains of the sputtered Ni film. b) SAD pattern from a) showing a typical ring pattern of δ-Ni_2Si without preferred orientation.

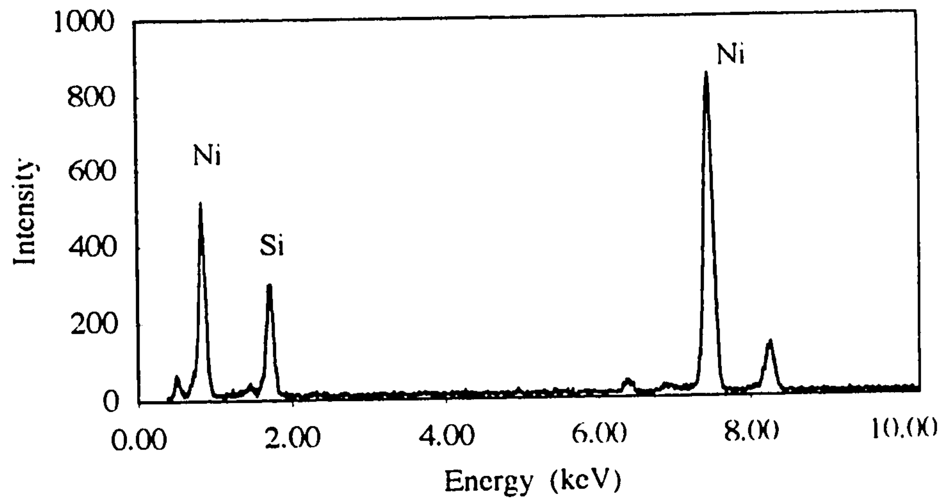

Fig.6-1c EDX spectrum from the same layer in a cross-section TEM specimen of the same sample.

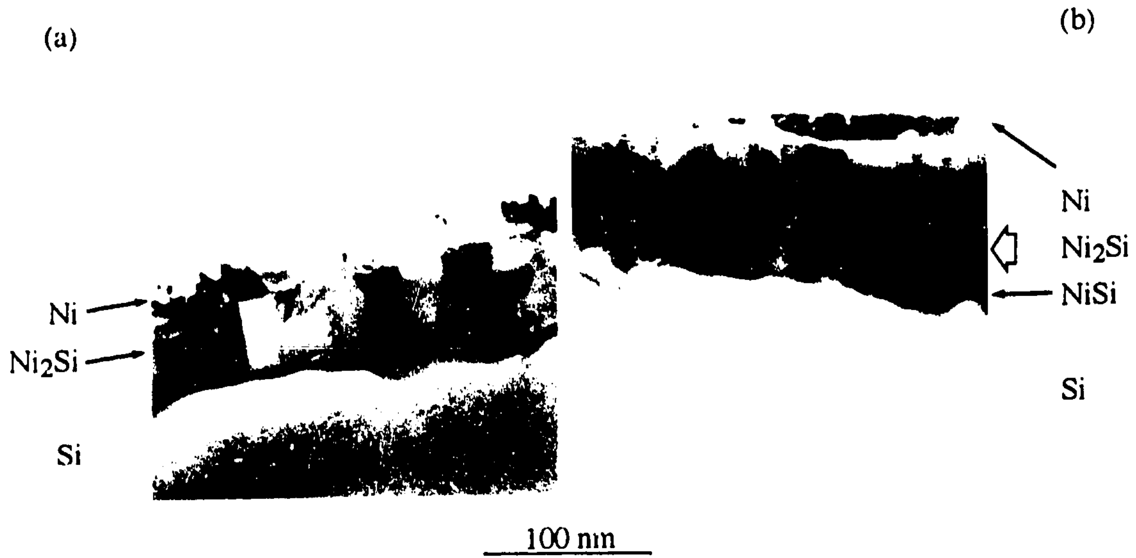

Fig.6-2 Cross-section TEM micrographs from cold substrate samples annealed at 300°C. a) The sample is annealed for 10 minutes. Only a uniform Ni_2Si layer about 42 nm thick forms at the Ni/Si interface. b) The sample is annealed for 40 minutes. The NiSi layer starts to grow at the Ni_2Si/Si interface.

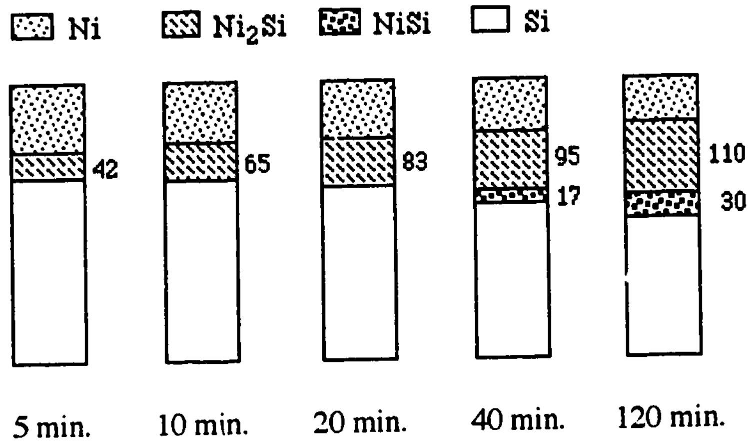

Fig.6-3 Schematic summary of the multiple phase growth sequence in thin Ni film-Si diffusion couples annealed at 300°C. The number at right side of each layer indicate the thickness of the layer in nm.

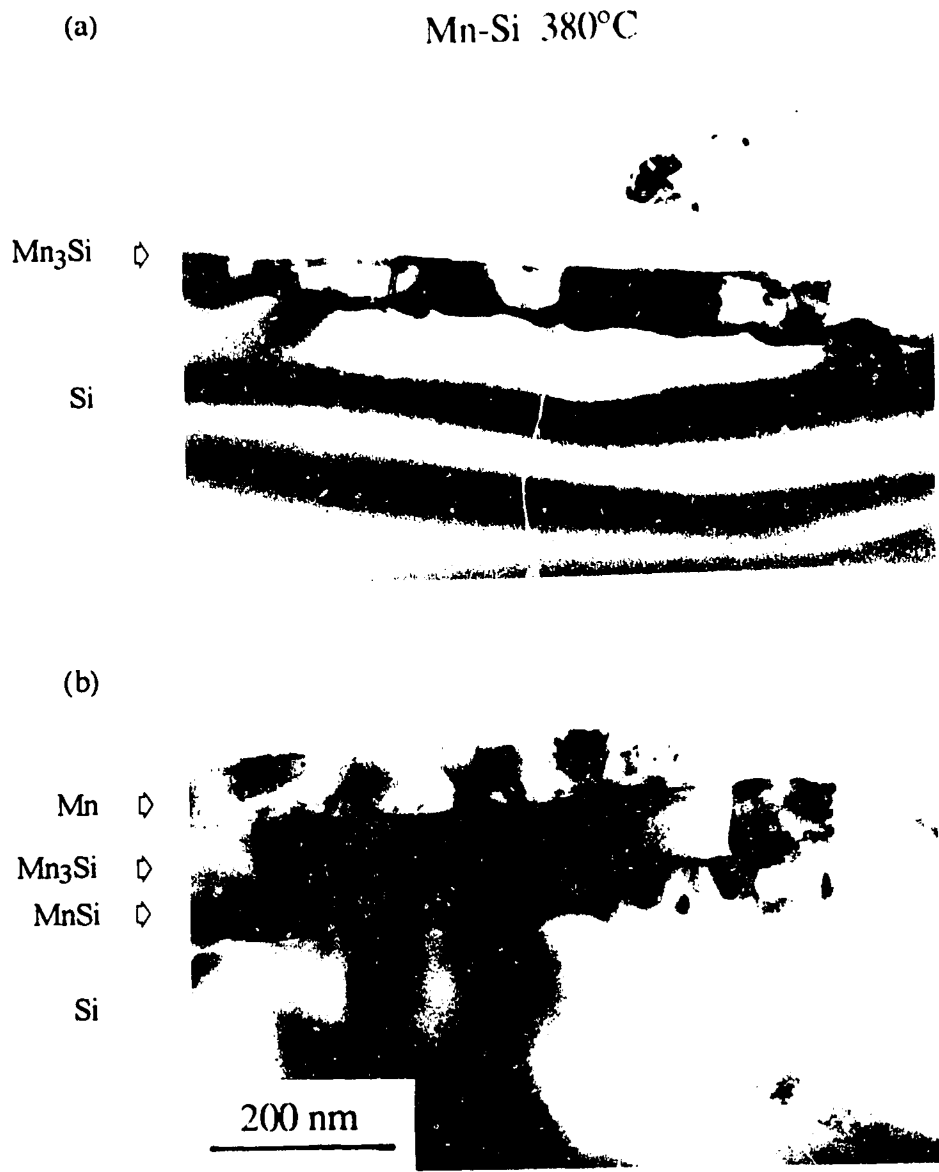

Fig.6-4 Cross-section TEM micrographs from thin film Mn-Si couples annealed at 380°C for 10 minutes (a) and 40 minutes (b) respectively.

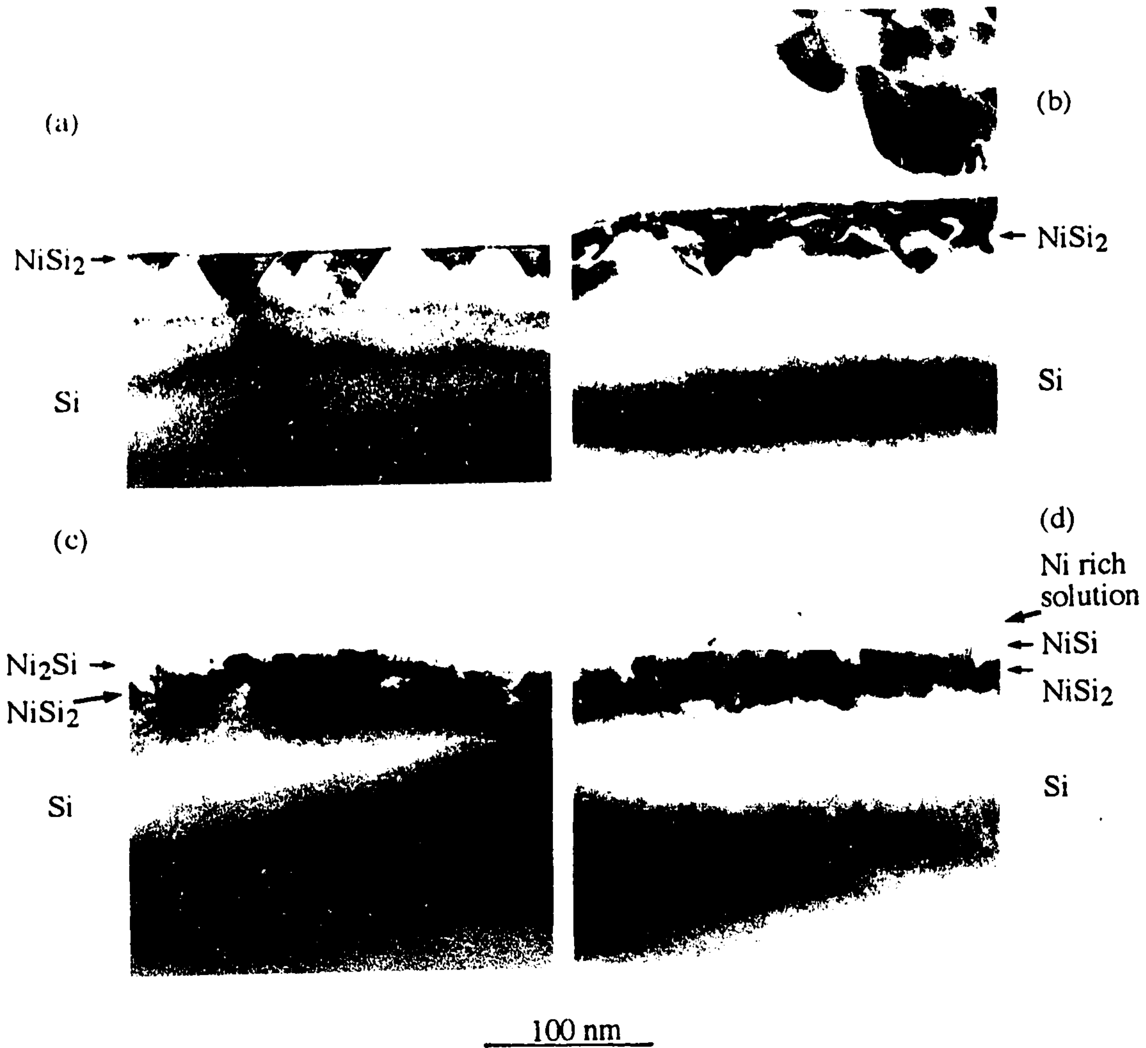

Fig.6-5 TEM micrographs from cross-section specimens deposited at a rate of 0.1 nm/s with the Si substrates heated to 300°C. The nominal Ni layer thicknesses are a) 3nm, b) 5nm, c) 10nm and d) 30 nm respectively.

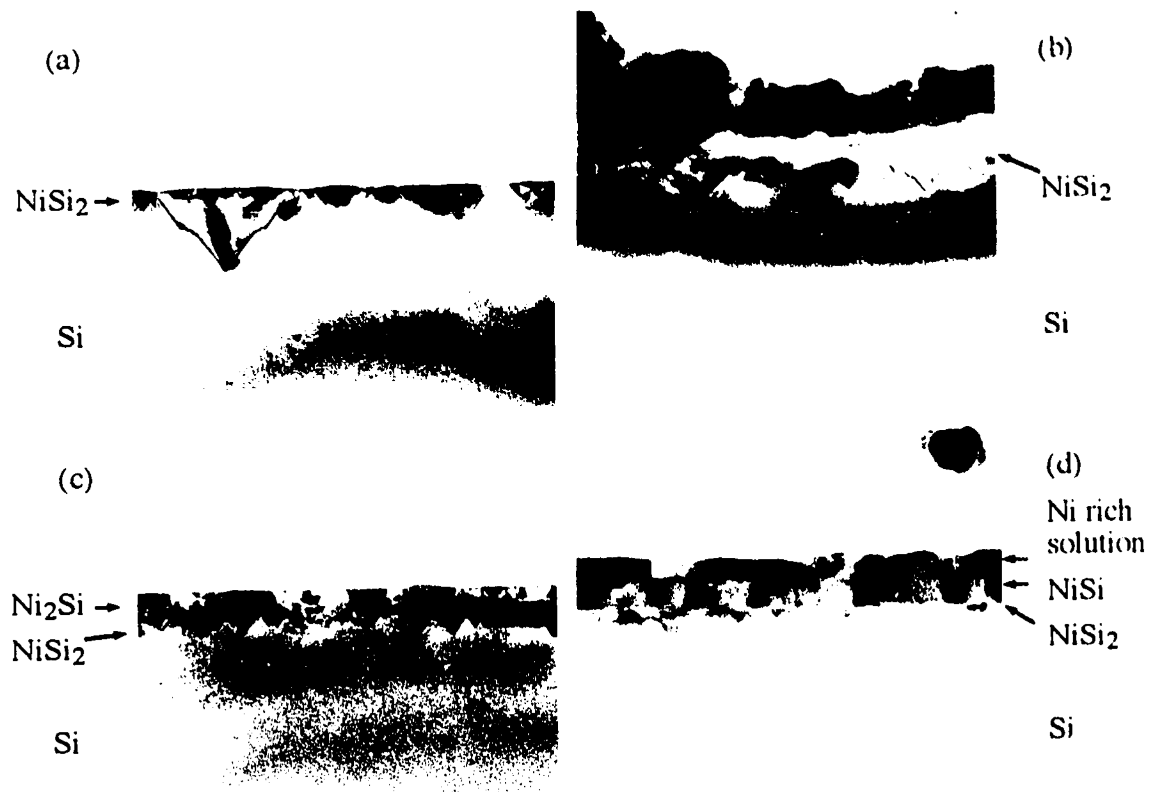

Fig.6-6 TEM micrographs from cross-section specimens deposited at 2nm/s with the substrates heated up to 300°C. The nominal Ni thicknesses are a) 3nm, b) 5nm, c) 10nm and d) 30nm, respectively.

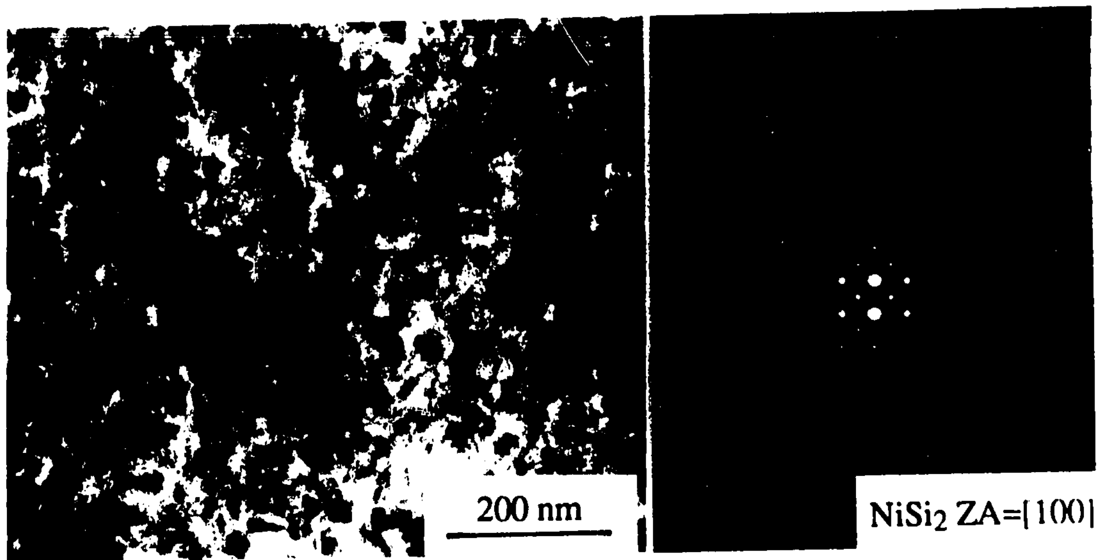

Fig.6-7 Plan view of TEM micrograph from a specimen shown in Fig.6-5b, showing $NiSi_2$ overlapping with Si. SAD pattern from the silicide layer. It is $NiSi_2$; ZA=[100].

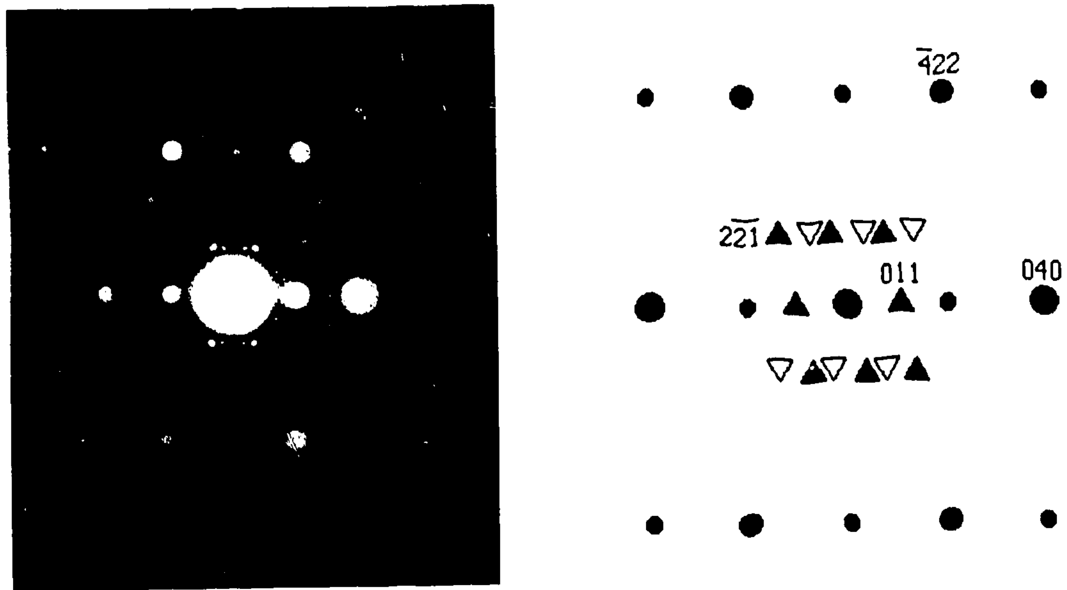

Fig.6-8 SAD pattern from a plan view specimen. Its cross-section micrograph is shown in Fig.6-6c. The strong diffracted spots (closed circles in the indexed pattern) are from $NiSi_2$ ZA=[102] and the weak diffracted spots, indicated by closed and open triangles in the indexed pattern, are from Ni_2Si ZA= $[12\bar{2}]$ and ZA= $[\bar{1}\bar{2}2]$.

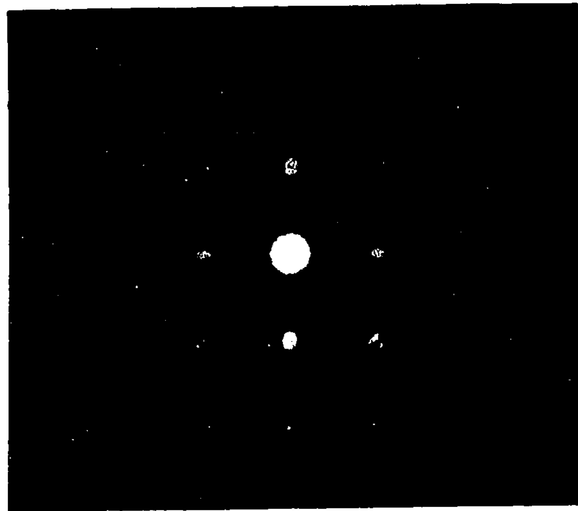

Fig.6-9 SAD pattern from a plan view sample deposited at 300°C and 0.1 nm/s, showing an orientation relationship between $NiSi_2$ [010] and NiSi [010].

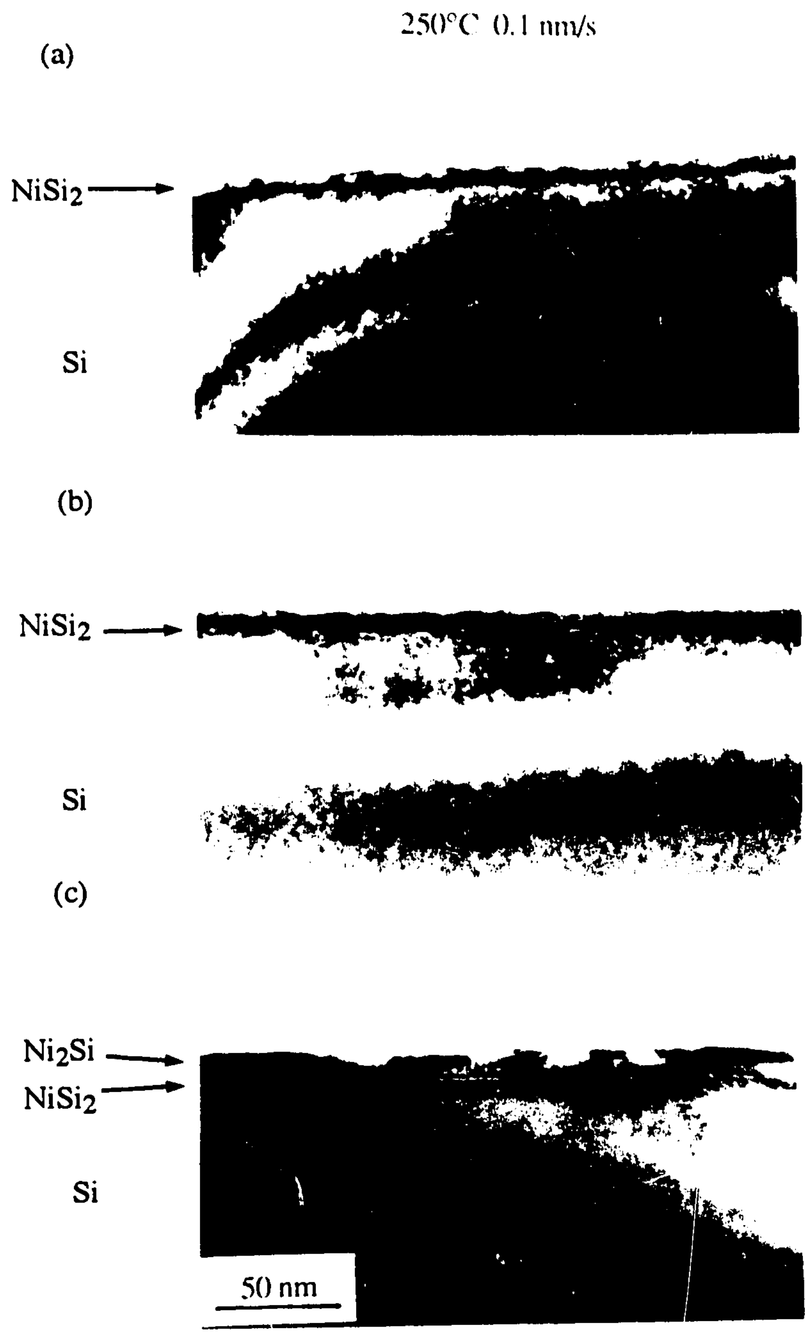

Fig.6-10 TEM micrographs from cross-section specimens deposited at 0.1 nm/s with the substrates heated up to 250°C. The nominal Ni thicknesses are a) 3nm, b) 5nm, and c) 10nm.

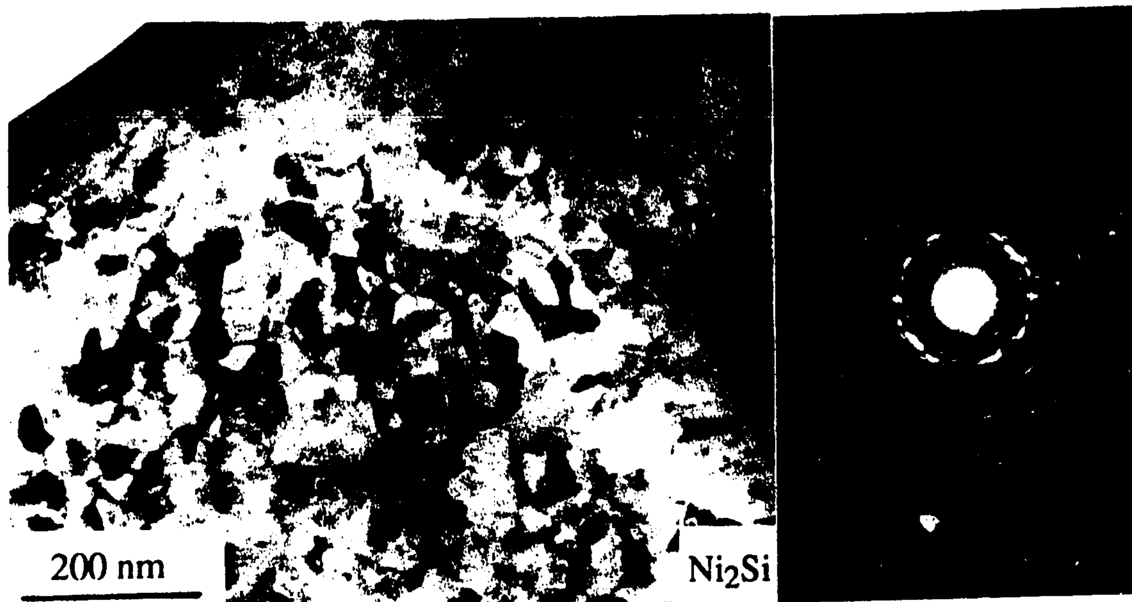

Fig.6-11 Micrograph and SAD pattern from a plan view specimen deposited at 250°C and a deposition rate of 0.1 nm/s, showing polycrystalline Ni_2Si. The SAD pattern shows δ-Ni_2Si growth with preferred orientation.

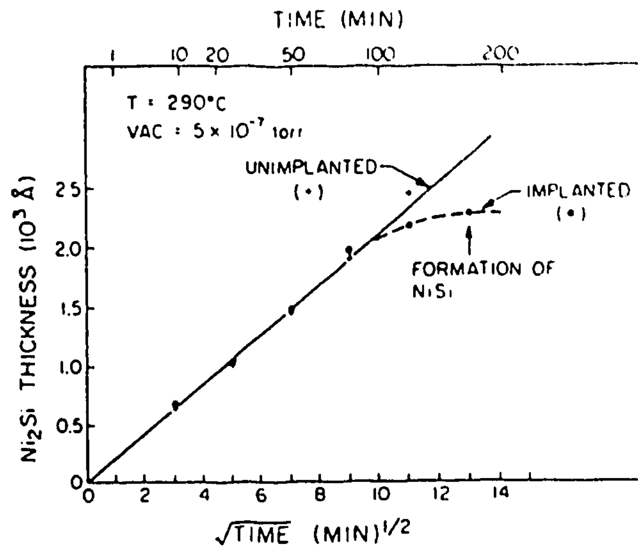

Fig.6-12 a) Kinetic plot showing thickness of Ni_2Si as a function of annealing time from Ref.[49].

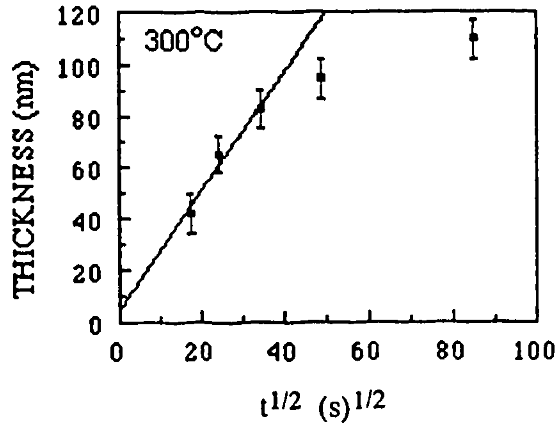

Fig.6-12 b) Kinetic plot showing thickness of Ni_2Si as a function of annealing time drawn using the data from this work.

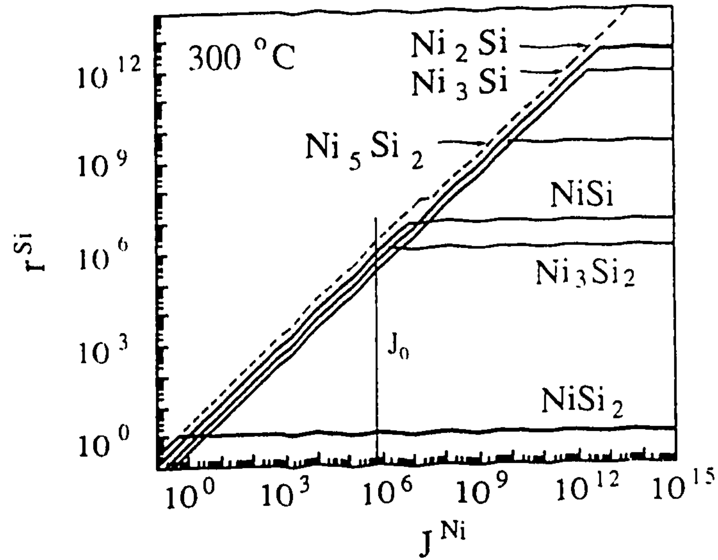

Fig.6-13 Semiquantitative reaction process plot (SRPP) for Ni-Si reactions in a reaction region adjacent to Si substrate, calculated using Eq.(5-1). The dashed curve indicates, schematically, that for a direct deposition reaction the stepped curve will shift up to the right due to the latent heat release. The step on the dashed curve indicates schematically the RMR rate for $NiSi_2$ during direct deposition reaction.

Chapter 7 Conclusions and Recommendations

7.1. Conclusions

Silicide formation mechanisms have been studied with the following conclusions being drawn:

1) A mathematical method for handling kinetic data for silicide formation has been developed. The calculation and analysis of the data from 5 published papers have shown that this method is useful and can provide important information.

2) According to the results of the calculations and analysis of the data, a kinetic model has been proposed. In the new model, a Type II process in a reaction region is divided into three steps. Several physical quantities are defined to describe each of these steps. They are diffusion flux of moving reactant to the reaction region, J, release rate of nonmoving reactant, r, and formation rate of growing phase, F.

3) The relationship between these physical quantities has been discussed and a reaction process plot (RPP) has been developed to demonstrate this relationship.

4) In the discussion of the results of 5 experiments, it has been shown that the new model can explain these complex results very well.

5) The free energy degradation rate (FEDR) in a reaction region can be expressed as a sum of three contributions. Each contribution is a product of a thermodynamic flux and a driving force corresponding to a particular reaction step. The expressions for the fluxes and the forces have been derived.

6) From these expressions and RPPs, it has already been shown that at a given diffusion flux in a reaction region, there exist competitions, such as those among release rates for various silicides to form and those between formation rates for various phases of a given silicide to grow. Among all possible release rates, the largest release rate will result in the largest FEDR. Of all possible formation rates, the largest formation rates usually cause the largest FEDR. If the largest formation rate is for a metastable phase to grow, when the formation rate for the metastable phase decreases as the reaction proceeds and becomes close to or equal to the conditional maximum formation rate of the stable phase of the particular silicide, the formation of the stable phase will lead to the largest FEDR.

7) According to the results (summarized in points 5 and 6), criteria for solid state reactions in metal-Si diffusion couples have been proposed. The general criterion is that during silicide reaction in a reaction region, there are always a number of possible reactions competing with one another. The reactions which can result in the largest FEDR will actually occur. The criterion is also called the largest FEDR criterion. When the criterion is applied to a release process, it can be translated to a simple kinetic criterion: Among all

possible release process at any diffusion flux, the largest release rate will actually take place, which is called the release rate criterion. For formation processes at a given release rate for ith silicide, the phase with the largest ($-F_{ik}\Delta G_{ik}$) will form. The last criterion is called formation rate criterion.

8) According to the kinetic model and the release rate criterion, the stepped curve in the RPP plot for a reaction region adjacent to an elemental nonmoving reactant represents the actual reaction path of release process in that R region. Therefore, the stepped curve can be used to predict silicide formation sequence in the region.

9) A method for calculating relative maximum release (RMR) rates and constructing semiquantitative reaction process plot (SRPP) has been proposed. Using this method, calculations of RMR rates have been done for 15 metal-Si systems and a few typical semiquantitative reaction process plots have been drawn using the resulting data. Predictions of first silicide formation and multiple phase growth sequence have been done using the semiquantitative reaction process plot (SRPPs) for these systems. Comparison of the predictions with experimental results from the literature shows very good agreement, which suggests that the model and the SRPPs are capable of successfully predicting and explaining silicide formation phenomena in metal-Si systems.

10) Multiple phase sequential growth in thin film Ni-Si couples (cold substrate samples) and deposition reactions of Ni on Si substrates have been investigated by means of TEM, EDX and electron diffraction. The multiple phase growth sequence in cold substrate samples is Ni_2Si followed by NiSi. Experimental results from a previous study using thin film Mn-Si couples are also given, which indicate a formation sequence of Mn_3Si followed by MnSi. The results in the two systems provide experimental evidence for the predictions of silicide formation sequences in these systems.

11) For the deposition reactions of Ni and Si substrates, the observed silicide formation sequence is $NiSi_2$, Ni_2Si, then NiSi and Ni-rich solid solution layers. Most of the observed phenomena in this study can be explained by SRPPs and the new kinetic model.

7.2. Recommendations

1) In order to obtain more experimental evidence for the new model and the reaction criteria proposed in this study, experimental observations of different initial silicides in a given metal-Si system are recommended, especially in refractory metal-Si systems. As mentioned in Secs.5.2 and 5.3, this type of experiment may require diffusion barriers to be introduced, in order to decrease the initial diffusion flux. In addition, multiple phase

growth experiments in bulk couples, or lateral couples, or the couples with thick metal films on Si substrates are recommended to observe silicide formation sequences.

2) It has been shown that an RPP (which is a combination of an r vs. J plot and an F vs. r plot) is able to demonstrate the relationship between the physical quantities J, r, and F for all possible reaction processes in a given R region. In particular, SRPPs (which show r vs. J relationships only) for R regions adjacent to the elemental nonmoving reactants in 15 metal-Si systems have been calculated and been used to successfully predict silicide formation sequences in each of these systems. In order to apply RPP to practical processing control and to provide further test of the new kinetic model, experimental determination of quantitative r vs. J plot is recommended. This work can be done by determining growth kinetic curves of silicides through either single phase or multiple phase sequential growth experiments and then by calculating critical diffusion fluxes and corresponding maximum release rates from the kinetic curves, using the method proposed in Chap.3.

3) As discussed in Sec.4.2.2.1 (also see Table 5-1), it is likely that there exist linear free energy relationships (LFERs) correlating maximum release rates to free energy changes of the release processes. Since the LFER method is a useful tool, in chemical kinetic studies, for classifying chemical reactions and exploring reaction mechanisms, it is recommended that the empirical LFERs between maximum release rates and free energy changes of release processes be determined from multiple phase sequential growth experiments. From the resulting LFERs, the activation energy E for breaking chemical bonds of nonmoving reactant and the proportionality coefficient α can also be determined and used for further mechanistic studies.

4) Some new experimental phenomena have been found from deposition reactions of Ni with Si substrates, i.e., the silicide formation sequence during the deposition and the local epitaxial growth of Ni_2Si and NiSi on $NiSi_2$. The former can be explained by the new model, which provides additional support for the model. The latter suggests that direct deposition reaction technique may be useful to obtain epitaxial growth of thin film silicides that cannot be obtained by conventional thermal reaction. Therefore, further study on direct deposition reactions in Ni-Si and other metal-Si systems at various substrate temperatures is also recommended.

REFERENCES

[1] K. N. Tu and J. W. Mayer, Chap.10 in *Thin Film-Interdiffusion and Reactions*, ed. J. M. Poate, K. N. Tu, and J. W. Mayer, Wiley, New York, (1978) p.359.

[2] G. Ottaviani, *J. Vac. Sci. Technol.* **16**, (1979) 1112.

[3] M-A Nicolet and S. S. Lau, Chap.6 in *VLSI Electronics Microstructure Science, V6*, ed. Norman G. Einsprunch and Graydon B. Larrabee, Academic Press, New York, (1983) p.329.

[4] S. P. Murarka, *Silicides for VSLI Applications*, Academic Press, New York, (1983).

[5] F. M. d'Heurle and P. Gas, *J. Mater. Res.* **1**, (1986) 205.

[6] G. Ottaviani, *Thin Solid Films* **140**, (1986) 3.

[7] F. M. d'Heurle, *J. Mater. Res.* **3**, (1988) 167.

[8] G. Ottaviani and C. Nobili, *Thin Solid Films* **163**, (1988) 111.

[9] Lin Zhang, *M.Sc. Thesis*, University of Alberta, 1990.

[10] R. M. Walser and R. W. Bené, *Appl. Phys. Lett.* **28**, (1976) 624.

[11] B. Y. Tsaur, S. S. Lau, J. W. Mayer, and M.-A. Nicolet, *Appl. Phys. Lett.* **38**, (1981) 922.

[12] U. Gösele and K. N. Tu, *J. Appl. Phys.* **53**, (1982) 3252.

[13] K. N. Tu, *Ann. Rev. Mater. Sci.* **15**, (1985) 147.

[14] K. N. Tu, Chap.7 in *Advances in Electronic Materials*, ed. B. W. Wessels and G. Y. Chin, American Society for Metals, (1986) p.147.

[15] A Hiraki, in *Layered Structures and Interface Kinetics*, ed. S. Furukawa, KTK Scientific Publishers, Tokyo, (1985) p.47.

[16] R. W. Bené, *J. Appl. Phys.* **61**, (1987) 1826.

[17] Y. I. Dybkov, *J. Mater. Sci.* **22**, (1987) 4233, and *J. Phys. Chem. Solids* **53**, (1992) 703.

[18] L. Borucki, R. Mann, G. Miles, J. Slinkman, and T. Sullivan,"*1988 IEEE International Electron Devices Meeting*, San Francisco, Dec. 14-16, (1988) p.348.

[19] U. Gösele and K. N. Tu, *J. Appl. Phys.* **66**, (1989) 2619.

[20] F. M. d'Heurle, *J. Vac. Sci. Technol.* **A7**, (1989) 1467.

[21] R. Pretorius, *Mater. Res. Soc. Symp. Proc.* Vol.**25**, (1984) 15.

[22] R. Pretorius, *Vacuum* **41**, (1990) 1038.

[23] R. Pretorius, A. M. Vredenberg, F. W. Saris, and R. de Reus, *J. Appl. Phys.* **70**, (1991) 3636.

[24] V. V. Tokarev, A. N. Likholet and B. N. Zon, *Mater. Res. Soc. Symp. Proc.* Vol.**181**, (1990) 151.

[25] J. Philibert, *Appl. Surf. Sci.* **53**, (1991) 74.
[26] C. V. Thompson, *J. Mater. Res.* **7**, (1992) 367.
[27] A. I. Barg, B. S. Bokstein, and L. M. Klinger, *J. Appl. Phys.* **72**, (1992) 1356.
[28] Wolfgang Losch, *Thin Solid Films* **216**, (1992) 225.
[29] G. V. Kidson, *J. Nucl. Mater.* **3**, (1961) 21.
[30] C. Wagner, *Acta Metall.* **17**, (1969) 99.
[31] A. J. Hickl and R. W. Heckel, *Metall. Trans.* **6A**, (1975) 431.
[32] S. R. Shatynski, J. P. Hirth, and R. A. Rapp, *Acta Metall.* **24**, (1976) 1071.
[33] A. Hiraki, M-A. Nicolet, and J. W. Mayer, *Appl. Phys. Lett.* **18**, (1971) 178.
[34] C. Canali, C. Catellani, M. Prudenziati, W. H. Wadlin and C. A. Evans, Jr., *Appl. Phys. Lett.* **31**, (1977) 43.
[35] C. A. Crider and J. M. Poate, *Appl. Phys. Lett.* **36**, (1980) 417.
[36] K. N. Tu, W. K. Chu, and J. W. Mayer, *Thin Solid Films* **25**, (1975) 403.
[37] J. O. Olowolafe, M-A. Nicolet, and J. W. Mayer, *Thin Solid Films* **38**, (1976) 143.
[38] D. J. Coe and E. H. Rhoderick, *J. Phys. D: Appl. Phys.* **9**, (1976) 965.
[39] M. Costato, *Nuovo Cimento Lett.* **32**, (1981) 219.
[40] K. E. Sundström, S. Petersson, and P. A. Tove, *Phys. Status Solidi* **A20**, (1973) 653.
[41] M. Eizenberg and K. N. Tu, *J. Appl. Phys.* **53**, (1982) 6885.
[42] K. N. Tu, G. Ottaviani, U. Gösele, and H. Foll, *J. Appl. Phys.* **54**, (1983) 758.
[43] K. N. Tu, G. Ottaviani, R. D. Thompson, and J. W. Mayer, *J. Appl. Phys.* **53**, (1982) 4406.
[44] Hiroki Muta and Daizaburo Shinoda, *J. Appl. Phys.* **43**, (1972) 2913.
[45] J. M. Poate and T. C. Tisone, *Appl. Phys. Lett.* **24**, (1974) 391.
[46] G. J. van Gurp and C. Lagnereis, *J. Appl. Phys.* **46**, (1975) 4301.
[47] S. S. Lau, J. W. Mayer, and K. N. Tu, *J. Appl. Phys.* **49**, (1978) 4005.
[48] P. Joubert, P. Auvray, A. Guivarch and G. Pelores, *Appl. Phys. Lett.* **31**, (1977) 753.
[49] D. M. Scott, P. J. Grunthaner, B. Y. Tsaur, M-A. Nicolet, and J. W. Mayer, in *Proceedings of the Symposium on "Thin Film Interfaces and Reactions"*, ed. John E. E. Baglin and John M. Poate, The Electrochemical Society, Inc., Princeton, 1980, p.148.
[50] C. A. Crider, J. M. Poate, and J. E. Rowe, in *Proceedings of the Symposium on "Thin Film Interfaces and Reactions"*, ed. John E. E. Baglin and John M. Poate, The Electrochemical Society, Inc., Princeton, 1980, p.135.

[51] F. Nava, S. Valeri, G. Majni, A. Cembali, G. Pignatel, and G. Queirolo, *J. Appl. Phys.* **52**, (1981) 6641.
[52] C. D. Lien, M-A. Nicolet, C. S. Pai, and S. S. Lau, *Appl. Phys.* **A36**, (1985) 153.
[53] Lin Zhang and Douglas G. Ivey, *J. Mater. Res.* **6**, (1991) 1518.
[54] S. Petersson, R. Anderson, J. E. E. Baglin, J. Dempsey, W. Hammer, F. M. d'Heurle and S. LaPlaca, *J. Appl. Phys.* **51**, (1980) 373.
[55] L. R. Zheng, L. S. Hung, and J. W. Mayer, *J. Vac. Sci. Technol.* **A1**, (1983) 758.
[56] J. C. Barbour, J. W. Mayer, and L. R. Zheng, *Inst. Phys. Conf.* Ser. No. **76**, (1985) 163.
[57] J. C. Barbour, P. E. Batson, and J. W. Mayer, *Mat. Res. Soc. Symp. Proc.* Vol.**54**, (1986) 29.
[58] H. Föll, P. S. Ho and K. N. Tu, *J. Appl. Phys.* **52**, (1981) 250.
[59] *Binary Alloy Phase Diagrams*, ed. T. B. Massalski, J. L. Murray, L. H. Bennett, H. Baker, American Society for Metals, 1986.
[60] M. H. Wang and L. J. Chen, *Appl. Phys. Lett.* **58**, (1991) 463.
[61] W. Y. Hsieh, J. H. Lin and L. J. Chen, *Appl. Phys. Lett.* **62**, (1993) 1088.
[62] R. W. Bené and R. M. Walser, *J. Vac. Sci. Technol.* **14**, (1977) 925.
[63] R. W. Bené, *Appl. Phys. Lett.* **41**, (1982) 529.
[64] R. Pretorius, R. de Reus, A. M. Vredenberg, and F. W. Saris, *Mater. Lett.* **9**, (1990) 494.
[65] R. Pretorius, T. K. Marais, A. E. Nlulles and D. Knoesen, *Mater. Res. Soc. Symp. Proc.* **238**, (1991) 475.
[66] Jian Li, J. W. Strane, S. W. Russell, S. Q. Hong and J. W. Mayer, *J. Appl. Phys.* **72**, (1992) 2810.
[67] R. W. Bower and J. W. Mayer, *Appl. Phys. Lett.* **20**, (1972) 359.
[68] R. Beyers and R. Sinclair, *J. Appl. Phys.* **57**, (1985) 5240.
[69] Harrie J. W. van Houtum and Ivo. J. M. M. Raaijmakers, *Mat. Res. Soc. Symp. Proc.* Vol.**54** (1986) 37.
[70] S. P. Murarka and D. B. Fraser, *J. Appl. Phys.* **51**, (1980) 342.
[71] R. W. Bené and H. Y. Yang, *J. Electron. Mater.* **12**, (1983) 1.
[72] L. S. Hung, J. Gyulai, J. W. Mayer, S. S. Lau, M-A. Nicolet, *J. Appl. Phys.* **54**, (1983) 5076.
[73] R. Butz, G. W. Rubloff, T. Y. Tan, and P. S. Ho, *Phys. Rev.* **B30**, (1984) 5421.
[74] K. N. Tu, J. F. Ziegler, and C. J. Kircher, *Appl. Phys. Lett.* **23**, (1973) 493.
[75] B. I. Fomin, A. E. Gershinskii, E. I. Cherepov, and F. L. Edelman, *Phys. Stat. Sol.* **A36**, (1976) K89.

[76] P. A. Psaras, M. Eizenberg and K. N. Tu, *J. Appl. Phys.* **56**, (1984) 3439.

[77] R. J. Schultz and L. R. Testardi, *J. Appl. Phys.* **50**, (1979) 5773.

[78] M. Nathan, *J. Appl. Phys.* **63**, (1988) 5534.

[79] J. O. Olowolafe, M-A. Nicolet, and J. W. Mayer, *J. Appl. Phys.* **47**, (1976) 5183.

[80] M. Nathan and S. W. Duncan, *ThinSolid Films* **123**, (1984) 69.

[81] R. Pretorius, in *Proceedings of the Symposium on "Thin Film Interfaces and Reactions"*, ed. John E. E. Baglin and John M. Poate, The Electrochemical Society, Inc., Princeton, 1980, p.481.

[82] S. S. Lau, J. S. Y. Feng, J. O. Olowolafe and M. A. Nicolet, *Thin Solid Films* **25**, (1975) 415.

[83] J. Alvarez, J. J. Hinarejos, E. G. Michel, J. M. Gallego, A. L. Vazquez de Parga, J. de la Figuera, C. Ocal, and R. Miranda, *Appl. Phys. Lett.* **59**, (1991) 99.

[84] K. Radermacher, S. Mantl, C. Dieker, H. Lüth and C. Freiburg, *Thin Solid Films* **215**, (1992) 76.

[85] R. J. Schreutelkamp, P. Vandenabeele, B. Deweerdt, W. Coppye, C. Vermeiren, A. Lauwers and K. Maex, *Mat. Res. Soc. Symp. Proc.* Vol.**260**, (1992) 145.

[86] C. Zaring, B. G. Svensson and M. Ostling, *Mat. Res. Soc. Symp. Proc.* Vol.**260**, (1992) 157.

[87] C. D. d'Anterroches, *Surf. Sci.* **168**, (1986) 751.

[88] F. Mahmood, H. Ahmed, C. Jeynes, and W. P. Gillin, *Appl. Surf. Sci.* **59**, (1992) 55.

[89] F. Hong, B. K. Patnaik and G. A. Rozgonyi, *Mat. Res. Soc. Symp. Proc.* Vol.**238**, (1992) 587.

[90] F. Hong, B. K. Patnaik and G. A. Rozgonyi, *Mat. Res. Soc. Symp. Proc.* Vol.**260**, (1992) 187.

[91] N. Setton and J. van der Spiegel, *Appl. Surf. Sci.* **38**, (1989) 62.

[92] S. Q. Wang and J. W. Mayer, *J. Appl. Phys.* **65**, (1989) 1957.

[93] S. L. Hsia, T. Y. Tan, P. Smith and G. E. Mcguire, *J. Appl. Phys.* **70**, (1991) 7579.

[94] Fann-Mei Yang and Mao-Chieh Chen, Japanese *J. Appl. Phys.* **31**, (1992) 1004.

[95] G. Majni, F. Della Valle, and C. Nobili, *J. Phys. D: Appl. Phys.* **17**, (1984) L77.

[96] F. M. d'Heurle, C. S. Petersson, J. E. E. Baglin, S. J. La Placa, and C. Y. Wong, *J. Appl. Phys.* **55**, (1984) 4208.

[97] L. R. Zheng, L. S. Hung, and J. W. Mayer, *Mat. Res. Soc. Symp. Proc.* Vol.**54**, (1986) 45.

[98] A. Appelbaum, M. Eizenberg and R. Brener, *J. Appl. Phys.* **55**, (1984) 914.

[99] R. S. Rastogi, V. D. Vankar and K. L. Chopra, *J. Appl. Phys.* **67**, (1990) 6369.

[100] G. A. Rozgonyi, J. H. Lee, D. Knoesen, D. Adams, B. Patnaik, N. Parikh, A. S. M. Salih and P. Balducci, *Appl. Phys. Lett.* **58**, (1991) 729.

[101] R. de Reus, H. C. Tissink and F. W. Saris, *J. Mater. Res.* **5**, (1990) 341.

[102] J. T. Mayer, R. F. Lin and E. Garfunkel, *Surf. Sci.* **265**, (1992) 102.

[103] Y. Igarashi, T. Yamaji, S. Nishikawa and S. Ohno, *Appl. Surf. Sci.* **41/42**, (1989) 282.

[104] C. A. Sukow and R. J. Nemanich, *Mat. Res. Soc. Symp. Proc.* Vol.**260**, (1992) 251.

[105] J. Y. Cheng and L. J. Chen, *Appl. Phys. Lett.* **56**, (1990) 457.

[106] J. Y. Cheng and L. J. Chen, *J. Appl. Phys.* **68**, (1990) 4002.

[107] J. Baglin, J. Dempsey, W. Hammer, F. d'Heurle, S. Petersson, and C. Serrano, *J. Electron. Mat.* **8**, (1979) 641.

[108] A. Guivarc'h, P. Auvray, L. Berthou, M. Le Cun, J. P. Boulet, P. Henoc, G. Pelous, and A. Martinez, *J. Appl. Phys.* **49**, (1978) 233.

[109] K. Holloway, K. B. Do and R. Sinclair, *Mat. Res. Soc. Symp. Proc.* **103**, (1988) 167.

[110] R. J. Schultz and L. R. Testardi, *Appl. Phys. Lett.* **34**, (1979) 797.

[111] N. Cheung, S. S. Lau, M-A. Nicolet and J. W. Mayer, in *Proceedings of the Symposium on "Thin Film Interfaces and Reactions"*, ed. John E. E. Baglin and John M. Poate, The Electrochemical Society, Inc., Princeton, 1980, p.494.

[112] M. O. Aboelfotoh, A. Alessandrini and F. M. d'Heurle, *Appl. Phys. Lett.* **49**, (1986) 1242.

[113] R. Anton and U. Neukirch, *Appl. Surf. Sci.* **29**, (1987) 287.

[114] J. F. Ziegler, J. W. Mayer, C. J. Kircher, and K. N. Tu, *J. Appl. Phys.* **44**, (1973) 3851.

[115] F. C. T. So, C.-D. Lien, and M-A. Nicolet, *J. Vac. Sci. Technol.* **A3**, (1985) 2284.

[116] S. Rigo, A. Turos, and G.Velasco, *Proc. 7th Intern. Vac. Congr. & 3rd Intern. Conf. Solid Surface (Vienna 1977)*, 1977, p.1109.

[117] C. S. Petersson, J. E. E. Baglin, F. M. d'Heurle, J. J. Dempsey, J. M. E. Harper, C. M. Serrano, and M. Y. Tsai, in *Proceedings of the Symposium on "Thin Film Interfaces and Reactions"*, ed. John E. E. Baglin and John M. Poate, The Electrochemical Society, Inc., Princeton, 1980, p.290.

[118] J. Baglin, F. d'Heurle, and S. Petersson, *Appl. Phys. Lett.* **33**, (1978) 289.

[119] A. K. Sinha and T. E. Smith, *J. Appl. Phys.* **44**, (1973) 3465.

[120] J. A. Borders and J. N. Sweet, in "*Applications of Ion Beams to Metals*", ed. S. Picraux, E. Eernisse and F. Vook, Plenum Press, New York, 1973, p.179.

[121] K. N. Tu, W. N. Hammer, and J. O. Olowolafe, *J. Appl. Phys.* **51**, (1980) 1663.

[122] M. Eizenberg and K. N. Tu, *J. Appl. Phys.* **53**, (1982) 1577.

[123] S. Herd, K. N. Tu and K. Y. Ahn, *Appl. Phys. Lett.* **42** (1983) 597.

[124] J. M. M. De Nijs and A. Van Silfhout, *Appl. Surf. Sci.* **40**, (1990) 349.

[125] J. M. M. De Nijs and A. Van Silfhout, *Appl. Surf. Sci.* **40**, (1990) 359.

[126] I. J. M. M. Raaijmakers, and Ki-Bum Kim, *J. Appl. Phys.* **67**, (1990) 6255.

[127] K. Holloway and R. Sinclair, *Mat. Res. Soc. Symp. Proc.* Vol.**77**, (1987) 357.

[128] I. J. M. M. Raaijmakers, A. H. Reader, and P. H. Oosting, *J. Appl. Phys.* **63**, (1988) 2790.

[129] I. J. M. M. Raaijmakers, P. H. Oosting, and A. H. Reader, *Mater. Res. Soc. Symp. Proc.* Vol.**103**, (1988) 229.

[130] A. E. Morgan, E. K. Broadbent, K. N. Ritz, D. K. Sadana, and B. J. Burrow, *J. Appl. Phys.* **64**, (1988) 344.

[131] Karen Holloway and Robert Sinclair, *Journal of the Less Common Metals* **140**, (1988) 139.

[132] R. Sinclair, K. Holloway, K. B. Kim, D. H. Ko, A. S. Bhansali, A. F. Schwartzman, and S. Ogawa, *Inst. Phys. Conf.* Ser. No.**100**, (1989) 599.

[133] W. Lur and L. J. Chen, *Appl. Phys. Lett.* **54**, (1989) 1217.

[134] Amol Kirtikar and Robert Sinclair, *Mat. Res. Soc. Symp. Proc.* Vol.**260**, (1992) 227.

[135] Karen Holloway, Robert Sinclair, and Menachem Nathan, *J. Vac. Sci. Technol.* **A7**, (1989) 1479.

[136] E. Ma, W. J. Meng, W. L. Johnson and M. A. Nicolet, *Appl. Phys. Lett.* **53**, (1988) 2033.

[137] J. Y. Cheng and L. J. Chen, *Appl. Phys. Lett.* **58**, (1991) 45.

[138] J. Y. Cheng and L. J. Chen, *J. Appl. Phys.* **69**, (1991) 2161.

[139] J. C. Hensel, J. M. Vandenberg, L. F. Mattheiss, F. C. Unterwald, and A. Maury, *Mat. Res. Soc. Symp. Proc.* Vol.**77**, (1987) 737.

[140] H. Jeon, C. A. Sukow, J. W. Honeycutt, T. P. Humphreys, R. J. Nemanich, and G. A. Rozgonzi, *Mat. Res. Soc. Symp. Proc.* Vol.**181**, (1990) 559.

[141] Y. L. Corcoran, A. H. King, N. de Lanerolle, and B. Kim, *J. Elect. Mater.* **19**, (1990) 1177.

[142] R. J. Nemanich, H. Jeon, C. A. Sukow, J. W. Honeycutt, and G. A. Rozgonyi, *Mat. Res. Soc. Symp. Proc.* Vol.**260**, (1992) 195.

[143] L. A. Clevenger, J. M. E. Harper, C. Cabral, Jr., C. Nobili, G. Ottaviani, and R. Mann, *J. Appl. Phys.* **72**, (1992) 4978.

[144] J. Y. Cheng, H. C. Cheng, and L. J. Chen, *J. Appl. Phys.* **61**, (1987) 2218.

[145] J. M. Gibson, D. Loretto, and D. Cherns, *Mat. Res. Soc. Symp. Proc.* Vol.**181**, (1990) 91.

[146] H. Föll, P. S. Ho, and K. N. Tu, *Philos. Mag.* **A45**, (1982) 31.

[147] A. L. Vazquez de Parga, J. de La Figuera, C. Ocal, and R. Mirasda, *Ultramicroscopy* **42-44**, (1992) 845.

[148] C. H. Jan, C. P. Chen, and Y. A. Chang, *J. Appl. Phys.* **73**, (1993) 1168.

[149] W. L. Johnson, *Prog. in Mater. Sci.* **30**, (1986) 81.

[150] B. M. Clemens and R. Sinclair, *MRS Bull.* **No.2**, (1990) 19.

[151] R. B. Schwarz and W. L. Johnson, *Phys. Rew. Lett.* **51**, (1983) 415.

[152] R. T.-Tung, J. M. Gibson, and J. M. Poate, *Phys. Rev. Lett.* **50**, (1983) 429.

[153] K. L. I. Kobayashi, S. Sugaki, A. Ishizaka, Y. Shiraki, H. Daimon and Y. Murata, *Phys. Rev.* **B25**, (1982) 1377.

[154] Fabio Comin, *J. Vac. Sci. Technol.* **A3**, (1985) 930.

[155] P. A. Bennett, B. N. Halawith, and A. P. Johnson, *J. Vac. Sci. Technol.* **A5**, (1987) 2121.

[156] J. F. van der Veen, A. E. M. J. Fischer, and J. Vrijmoeth, *Appl. Surf. Sci.* **38**, (1989) 13.

[157] R. T. Tung, *J. Vac. Sci. Technol.* **A7**, (1989) 598.

[158] H. von Känel, J. Henz, M. Ospelt, J. Hugi, E. Müler, N. Onda, and A. Gruhle, *Thin Solid Films* **184**, (1990) 295.

[159] R. T. Tung, *Mater. Chem. Phys.* **32**, (1992) 107.

[160] C. Pirri, J. C. Peruchetti, G. Gewinner, and J. Derrien, *Phys. Rev.* **B29**, (1984) 3391.

[161] J. Y. Veuillen, J. Derrien, P. A. Badoz, E. Rosencher, and C. d'Anterroches, *Appl. Phys. Lett.* **51**, (1987) 1448.

[162] J. M. Gibson, J. L. Batstone, and R. T. Tung, *Appl. Phys. Lett.* **51**, (1987) 45.

[163] H. B. Ghozlene and P. Beaufrere, *J. Appl. Phys.* **49**, (1978) 3999.

[164] J. R. Abelson, K. B. Kim, D. E. Mercer, C. R. Helms, R. Sinclair, and T. W. Sigmon, *J. Appl. Phys.* **63**, (1988) 689.

[165] P. S. Ho, T. Y. Tan, J. E. Lewis, and G. W. Rubloff, *J. Vac. Sci. Technol.* **16**, (1979) 1120.

[166] G. W. Rubloff, *Mat. Res. Soc. Symp. Proc.* Vol.**54**, (1986) 3.

[167] M. Del Giudice, J. J. Joyce, F. Boscherini, C. Capasso, and J. H. Weaver, *Mat. Res. Soc. Symp. Proc.*, **77**, (1987) 277.

[168] K. Konuma, J. Vrijmoeth, P. M. Zagwijn, J. W. M. Frenken, E. Vlieg, and J. F. van der Veen, *J. Appl. Phys.* **73**, (1993) 1104.

[169] J. Alvarez, J. J. Hinarejos, E. G. Michel and R. Miranda, *Surf. Sci.* **269/270**, (1992) 1011.

[170] E. Horache, J. van der Spiegel and J. E. Fischer, *Thin Solid Films* **177**, (1989) 263.

[171] R. W. Balluffi and J. M. Blakely, *Thin Solid Films* **25**, (1975) 363.

[172] R. D. Thompson, and K. N. Tu, *Thin Solid Films* **93**, (1982) 265.

[173] M. Diale, C. Challens and E. C. Zingu, *Appl. Phys. Lett.* **62** (1992) 943.

[174] R. Pretorius, W. Strydom, and J. W. Mayer, *Phys. Rev.* **B22**, (1980) 1885.

[175] A. P. Botha, and P. Pretorius, *Thin Solid Films* **93**, (1982) 127.

[176] W. K. Chu, S. S. Lau, J. W. Mayer, H. Muller, and K. N. Tu, *Thin Solid Films* **25**, (1975) 393.

[177] T. G. Finstad, *Phys. Status. Solid.* **A63**, (1981) 223.

[178] M. Bartur and M.-A. Nicolet, *J. Appl. Phys.* **54**, (1983) 5404.

[179] J. E. Mcleod, M. A. E. Wandt, R. Pretorius, and C. M. Comrie, *J. Appl. Phys.* **72**, (1992) 2232.

[180] C. M. Comrie and J. M. Egan, *J. Vac. Sci, Technol.* **A7**, (1989) 1492.

[181] K. T. Ho, C. D. Lien, U. Shreter, and M. A. Nicolet, *J. Appl. Phys.* **57**, (1985) 227.

[182] J. E. E. Baglin, F. M. d'Heurle, and C. S. Petersson, *J. Appl. Phys.* **52**, (1981) 2841.

[183] F. M. d'Heurle, *Thin Solid Films* **151**, (1987) 41.

[184] Marc Wittmer, *J. Appl. Phys.* **54**, (1983) 5081.

[185] P. Gas, *Appl. Surf. Sci.* **38**, (1989) 178.

[186] V. G. Weizer and N. S. Fatemi, *J. Elec. Mater.* **18**, (1989) 7.

[187] M. P. Siegal and J. J. Santiago, *J. Appl. Phys.* **65**, (1989) 760.

[188] H. S. Lee and G. J. Wolga, J. Electrchem. Soc. **137**, (1990) 2619.

[189] H. Heintze, A. Catana, P. E. Schmid, F. Levy, P. Stadelmann, and P. Weiss, *J. Phys. D: Appl. Phys.* **23**, (1990) 1076.

[190] A. R. Sitaram and S. P. Murarka, *Mat. Res. Soc. Symp. Proc.* Vol.**181**, (1990) 185.

[191] R. Beyers, D. Coulman and P. Merchant, *J. Appl. Phys.* **61**, (1987) 5110.

[192] H. K. Park, J. Sachitano, M. McPherson, T. Yamaguchi, and G. Lehman, *J. Vac. Sci. Technol.* **A2**, (1984) 264.

[193] J. Torres, J. C. Oberlin, R. Stuck, N. Bourhila, J. Palleau, G. Göltz and G. Bomchil, *Appl. Surf. Sci.* **38**, (1989) 186.

[194] H. Jiang, H. J. Whitlow, M. Ostling, E. Niemi, F. M. d'Heurle, and C. S. Petersson, *J. Appl. Phys.* **65**, (1989) 567.

[195] K. Maex and L. van den Hove, *Mater. Sci. Eng.* **B4**, (1989) 321.

[196] F. M. Ross and J. M. Gibson, *Inst. Phys. Conf.* Ser. No.**117**, (1991) 187.

[197] F. M. Ross and J. M. Gibson, *Appl. Phys. Lett.* **68**, (1992) 1782.

[198] F. M. d'Heurle, in *Solid State Devices 1985*, ed. P. Balk and O. G. Folberth, Elsevier Science Publishing Inc., (1986), 213.

[199] J. Lajzerowicz, Jr., J. Torres, G. Goltz, and R. Pantel, *Thin Solid Films* **140**, (1986) 23.

[200] G. Goltz, J. Torres, J. Lajzerowicz, Jr., and G. Bomchil, *Thin Solid Films* **124**, (1985) 19.

[201] E. Ma, B. S. Lim, and M.-A. Nicolet, *J. Electron. Mater.* **17**, (1988) 207.

[202] J. E. Baglin, F. M. d'Heurle, and C. S. Petersson, *Appl. Phys. Lett.* **36**, (1980) 594.

[203] R. D. Thompson, B. Y. Tsaur, and K. N. Tu, *Appl. Phys. Lett.* **38**, (1981) 535.

[204] C. S. Petersson, R. Anderson, J. E. Baglin, J. Dempsey, W. Hammer, F. M. d'Heurle, and S. J. Laplaca, *J. Appl. Phys.* **51**, (1980) 373.

[205] G. Ottaviani, G. Majni, and C. Canali, *Appl. Phys.* **18**, (1979) 285.

[206] C. W. Allen and G. A. Sargent, *Mat. Res. Soc. Symp. Proc.* Vol.**54**, (1986) 97.

[207] S. M. Sze, *VLSI Technology*, 2nd ed. McGraw-Hill, New York, 1988, p111.

[208] O. F. Devereux, Chap.13 in *Topics in Metallurgical Thermodynamics*, John Wiley and Sons, Inc., New York, 1983.

[209] I. Prigogine, *Introduction to Thermodynamics of Irreversible Processes*, third edition, John Wiley and Sons, Inc., New York, 1967.

[210] G. Nicolis and I. Prigogine, Part I in *Self-Organization in Nonequilibrium Systems*, John Wiley and Sons, Inc., New York, 1977.

[211] H. J. Kreuzer, *Nonequilibrium Thermodynamics and its Statistical Foundations*, Oxford University Press, New York, 1981.

[212] J. W. Cahn and J. E Hilliard, *J. Chem. Phys.* **28**, (1958) 258.

[213] S. Wold and M. Sjöström, Chap.1 in *Correlation Analysis in Chemistry*, ed. N. B. Chapman and J. Shorter, Plenum Press, New York, 1978.

[214] R. P. Bell, Chap.2 in *Correlation Analysis in Chemistry*, ed. N. B. Chapman and J. Shorter, Plenum Press, New York, 1978.

[215] C. D. Ritchie, Chap.2-4, 7 and 9 in *Physical Organic Chemistry*, Marcel Dekker, Inc., New York, 1975.

[216] E. S. Lewis, Chap.XIII in *Investigation of Rates and Mechanisms of Reactions Part I*, forth edition, ed. C. F. Bernasconi, John Wiley and Sons, Inc., New York, 1986.

[217] I. N. Levine, Chap.23 in *Physical Chemistry*, third Edition, McGraw-Hill, Inc., New York, 1988.

[218] G. V. Samsonov and I. M. Vinitskii, *Handbook of Refractory Compounds*, IFI/Plenum Press, New York, (1980).

[219] *Powder Diffraction Files*. JCPDS-internationalCenter for Diffraction Data.

[220] D. G. Ivey and G. R. Piercy, *J. Electron Microscopy Technique* **8**, (1988) 233.

[221] D. B. Williams, Chap.4 and 6 in *Practical Analytical Electron Microscopy in Materials Science*, by D. B. Williams, Philips Electronic Instruments, Electron Optics Publishing Group, Mahwah, (1984).

[222] J. I. Goldstein, D. B. Williams and G. Cliff, Quantitative X-Ray Analysis, from "*Principles of Analytical Electron Microscopy*", D. C. Joy, A. D. Romig and J. I. Goldstein, eds., Plenum Press, New York, (1986).